IAEA TECDOC SERIES

IAEA-TECDOC-1767

IAEA-TECDOC-1767

The Contribution of Palaeoseismology to Seismic Hazard Assessment in Site Evaluation for Nuclear Installations

IAEA
International Atomic Energy Agency

IAEA SAFETY STANDARDS AND RELATED PUBLICATIONS

IAEA SAFETY STANDARDS

Under the terms of Article III of its Statute, the IAEA is authorized to establish or adopt standards of safety for protection of health and minimization of danger to life and property, and to provide for the application of these standards.

The publications by means of which the IAEA establishes standards are issued in the **IAEA Safety Standards Series**. This series covers nuclear safety, radiation safety, transport safety and waste safety. The publication categories in the series are **Safety Fundamentals**, **Safety Requirements** and **Safety Guides**.

Information on the IAEA's safety standards programme is available at the IAEA Internet site

http://www-ns.iaea.org/standards/

The site provides the texts in English of published and draft safety standards. The texts of safety standards issued in Arabic, Chinese, French, Russian and Spanish, the IAEA Safety Glossary and a status report for safety standards under development are also available. For further information, please contact the IAEA at PO Box 100, 1400 Vienna, Austria.

All users of IAEA safety standards are invited to inform the IAEA of experience in their use (e.g. as a basis for national regulations, for safety reviews and for training courses) for the purpose of ensuring that they continue to meet users' needs. Information may be provided via the IAEA Internet site or by post, as above, or by email to Official.Mail@iaea.org.

RELATED PUBLICATIONS

The IAEA provides for the application of the standards and, under the terms of Articles III and VIII.C of its Statute, makes available and fosters the exchange of information relating to peaceful nuclear activities and serves as an intermediary among its Member States for this purpose.

Reports on safety and protection in nuclear activities are issued as **Safety Reports**, which provide practical examples and detailed methods that can be used in support of the safety standards.

Other safety related IAEA publications are issued as **Radiological Assessment Reports**, the International Nuclear Safety Group's **INSAG Reports**, **Technical Reports** and **TECDOCs**. The IAEA also issues reports on radiological accidents, training manuals and practical manuals, and other special safety related publications.

Security related publications are issued in the **IAEA Nuclear Security Series**.

The **IAEA Nuclear Energy Series** consists of reports designed to encourage and assist research on, and development and practical application of, nuclear energy for peaceful uses. The information is presented in guides, reports on the status of technology and advances, and best practices for peaceful uses of nuclear energy. The series complements the IAEA's safety standards, and provides detailed guidance, experience, good practices and examples in the areas of nuclear power, the nuclear fuel cycle, radioactive waste management and decommissioning.

THE CONTRIBUTION OF PALAEOSEISMOLOGY TO SEISMIC HAZARD ASSESSMENT IN SITE EVALUATION FOR NUCLEAR INSTALLATIONS

The following States are Members of the International Atomic Energy Agency:

AFGHANISTAN
ALBANIA
ALGERIA
ANGOLA
ARGENTINA
ARMENIA
AUSTRALIA
AUSTRIA
AZERBAIJAN
BAHAMAS
BAHRAIN
BANGLADESH
BELARUS
BELGIUM
BELIZE
BENIN
BOLIVIA, PLURINATIONAL STATE OF
BOSNIA AND HERZEGOVINA
BOTSWANA
BRAZIL
BRUNEI DARUSSALAM
BULGARIA
BURKINA FASO
BURUNDI
CAMBODIA
CAMEROON
CANADA
CENTRAL AFRICAN REPUBLIC
CHAD
CHILE
CHINA
COLOMBIA
CONGO
COSTA RICA
CÔTE D'IVOIRE
CROATIA
CUBA
CYPRUS
CZECH REPUBLIC
DEMOCRATIC REPUBLIC OF THE CONGO
DENMARK
DJIBOUTI
DOMINICA
DOMINICAN REPUBLIC
ECUADOR
EGYPT
EL SALVADOR
ERITREA
ESTONIA
ETHIOPIA
FIJI
FINLAND
FRANCE
GABON
GEORGIA
GERMANY
GHANA
GREECE
GUATEMALA
GUYANA
HAITI
HOLY SEE
HONDURAS
HUNGARY
ICELAND
INDIA
INDONESIA
IRAN, ISLAMIC REPUBLIC OF
IRAQ
IRELAND
ISRAEL
ITALY
JAMAICA
JAPAN
JORDAN
KAZAKHSTAN
KENYA
KOREA, REPUBLIC OF
KUWAIT
KYRGYZSTAN
LAO PEOPLE'S DEMOCRATIC REPUBLIC
LATVIA
LEBANON
LESOTHO
LIBERIA
LIBYA
LIECHTENSTEIN
LITHUANIA
LUXEMBOURG
MADAGASCAR
MALAWI
MALAYSIA
MALI
MALTA
MARSHALL ISLANDS
MAURITANIA
MAURITIUS
MEXICO
MONACO
MONGOLIA
MONTENEGRO
MOROCCO
MOZAMBIQUE
MYANMAR
NAMIBIA
NEPAL
NETHERLANDS
NEW ZEALAND
NICARAGUA
NIGER
NIGERIA
NORWAY
OMAN
PAKISTAN
PALAU
PANAMA
PAPUA NEW GUINEA
PARAGUAY
PERU
PHILIPPINES
POLAND
PORTUGAL
QATAR
REPUBLIC OF MOLDOVA
ROMANIA
RUSSIAN FEDERATION
RWANDA
SAN MARINO
SAUDI ARABIA
SENEGAL
SERBIA
SEYCHELLES
SIERRA LEONE
SINGAPORE
SLOVAKIA
SLOVENIA
SOUTH AFRICA
SPAIN
SRI LANKA
SUDAN
SWAZILAND
SWEDEN
SWITZERLAND
SYRIAN ARAB REPUBLIC
TAJIKISTAN
THAILAND
THE FORMER YUGOSLAV REPUBLIC OF MACEDONIA
TOGO
TRINIDAD AND TOBAGO
TUNISIA
TURKEY
UGANDA
UKRAINE
UNITED ARAB EMIRATES
UNITED KINGDOM OF GREAT BRITAIN AND NORTHERN IRELAND
UNITED REPUBLIC OF TANZANIA
UNITED STATES OF AMERICA
URUGUAY
UZBEKISTAN
VENEZUELA, BOLIVARIAN REPUBLIC OF
VIET NAM
YEMEN
ZAMBIA
ZIMBABWE

The Agency's Statute was approved on 23 October 1956 by the Conference on the Statute of the IAEA held at United Nations Headquarters, New York; it entered into force on 29 July 1957. The Headquarters of the Agency are situated in Vienna. Its principal objective is "to accelerate and enlarge the contribution of atomic energy to peace, health and prosperity throughout the world".

IAEA-TECDOC-1767

THE CONTRIBUTION OF PALAEOSEISMOLOGY TO SEISMIC HAZARD ASSESSMENT IN SITE EVALUATION FOR NUCLEAR INSTALLATIONS

INTERNATIONAL ATOMIC ENERGY AGENCY
VIENNA, 2015

COPYRIGHT NOTICE

All IAEA scientific and technical publications are protected by the terms of the Universal Copyright Convention as adopted in 1952 (Berne) and as revised in 1972 (Paris). The copyright has since been extended by the World Intellectual Property Organization (Geneva) to include electronic and virtual intellectual property. Permission to use whole or parts of texts contained in IAEA publications in printed or electronic form must be obtained and is usually subject to royalty agreements. Proposals for non-commercial reproductions and translations are welcomed and considered on a case-by-case basis. Enquiries should be addressed to the IAEA Publishing Section at:

Marketing and Sales Unit, Publishing Section
International Atomic Energy Agency
Vienna International Centre
PO Box 100
1400 Vienna, Austria
fax: +43 1 2600 29302
tel.: +43 1 2600 22417
email: sales.publications@iaea.org
http://www.iaea.org/books

For further information on this publication, please contact:

International Seismic Safety Centre
International Atomic Energy Agency
Vienna International Centre
PO Box 100
1400 Vienna, Austria
Email: Official.Mail@iaea.org

© IAEA, 2015

Printed by the IAEA in Austria
June 2015

IAEA Library Cataloguing in Publication Data

The contribution of palaeoseismology to seismic hazard assessment in site evaluation for nuclear installations. — Vienna : International Atomic Energy Agency, 2015.
p. ; 30 cm. — (IAEA-TECDOC series, ISSN 1011–4289 ; no. 1767)
ISBN 978–92–0–105415–9
Includes bibliographical references.

1. Nuclear facilities — Location. 2. Nuclear facilities — Safety measures. 3. Earthquake hazard analysis. 4. Paleoseismology. I. International Atomic Energy Agency. II. Series.

IAEAL 15–00976

FOREWORD

IAEA Safety Standards Series No. SSG-9, Seismic Hazards in Site Evaluation for Nuclear Installations, published in 2010, covers all aspects of site evaluation relating to seismic hazards and recommends the use of prehistoric, historical and instrumental earthquake data in seismic hazard assessments. Prehistoric data on earthquakes cover a much longer period than do historical and instrumental data. However, gathering such data is generally difficult in most regions of the world, owing to an absence of human records.

Prehistoric data on earthquakes can be obtained through the use of palaeoseismic techniques. This publication describes the current status and practices of palaeoseismology, in order to support Member States in meeting the recommendations of SSG-9 and in establishing the necessary earthquake related database for seismic hazard assessment and reassessment.

At a donors' meeting of the International Seismic Safety Centre Extrabudgetary Project in January 2011, it was suggested to develop detailed guidelines on seismic hazards. Soon after the meeting, the disastrous Great East Japan Earthquake and Tsunami of 11 March 2011 and the consequent accident at the Fukushima Daiichi nuclear power plant occurred. The importance of palaeoseismology for seismic hazard assessment in site evaluation was highlighted by the lessons learned from the Fukushima Daiichi nuclear power plant accident. However, no methodology for performing investigations using palaeoseismic techniques has so far been available in an IAEA publication.

The detailed guidelines and practical tools provided here will be of value to nuclear power plant operating organizations, regulatory bodies, vendors, technical support organizations and researchers in the area of seismic hazard assessment in site evaluation for nuclear installations, and the information will be of importance in support of hazard assessments in the future.

The contributions of all those who were involved in the drafting and review of this report are greatly appreciated. The valuable contributions from L. Guerrieri (Italy) in the development of this publication is acknowledged. The IAEA officer responsible for this publication was Y. Fukushima of the Division of Nuclear Installation Safety.

EDITORIAL NOTE

This publication has been prepared from the original material as submitted by the contributors and has not been edited by the editorial staff of the IAEA. The views expressed remain the responsibility of the contributors and do not necessarily represent the views of the IAEA or its Member States.

Neither the IAEA nor its Member States assume any responsibility for consequences which may arise from the use of this publication. This publication does not address questions of responsibility, legal or otherwise, for acts or omissions on the part of any person.

The use of particular designations of countries or territories does not imply any judgement by the publisher, the IAEA, as to the legal status of such countries or territories, of their authorities and institutions or of the delimitation of their boundaries.

The mention of names of specific companies or products (whether or not indicated as registered) does not imply any intention to infringe proprietary rights, nor should it be construed as an endorsement or recommendation on the part of the IAEA.

The IAEA has no responsibility for the persistence or accuracy of URLs for external or third party Internet web sites referred to in this publication and does not guarantee that any content on such web sites is, or will remain, accurate or appropriate.

CONTENTS

1. INTRODUCTION 1

1.1. CONTENT, OBJECTIVES AND SCOPE OF THE PUBLICATION 1

1.2. BACKGROUND 1

1.2.1. Key definitions 1

1.2.2. Paleoseismology applied to NPP site evaluation 4

1.2.3. Limitations of paleoseismology for SHA of NPP sites 5

2. PALEOSEISMOLOGY: STATE OF THE ART 7

2.1. PALEOSEISMIC CHARACTERIZATION OF CAPABLE FAULTS: ASSESSING SEISMIC SOURCE POTENTIAL FROM PALEOSEISMOLOGY 7

2.1.1. General remarks 7

2.1.2. Paleoseismic analyses in the site vicinity, near regional and regional area 7

2.1.3. Factors controlling trench site selection 11

2.1.4. Trench logging, stratigraphic and structural interpretation 15

2.1.5. Understanding maximum earthquake magnitude from capable faults: the Seismic Landscape 18

2.1.6. Case histories: interplate settings 22

2.1.7. Case histories: intraplate settings 35

2.2. PALEOSEISMIC CHARACTERIZATION OF DIFFUSE SEISMICITY 38

2.2.1. Introduction 38

2.2.2. Paleoliquefaction Investigations 41

2.2.3. Paleolandslide investigations 50

2.2.4. Investigation of lacustrine-marine sediments and cave sediments 60

2.2.5 Geomorphic, micro-geomorphic and other techniques 65

2.2.6 Summary of capabilities and limitations of paleoseismic investigations to characterize diffuse seismicity 65

2.3 TSUNAMI GEOLOGY IN PALEOSEISMOLOGY 66

2.3.1 Significance of tsunami geology 66

2.3.2. Tsunami effects on coastal geology 71

2.3.3. Identification of buried tsunami deposits 74

2.3.4. Paleotsunami investigations 77

2.3.5 Use of tsunami deposits in assessing tsunami and earthquake hazard at nuclear installations 81

2.4. DATING TECHNIQUES IN PALEOSEISMOLOGY 82
2.4.1 Introduction 82
2.4.2 Most prominent methods 86
2.4.3 Other dating methods 90
2.4.4 Dating strategies in the field 92
3. PALEOSEISMIC DATA AND ITS CONTRIBUTION TO AN IMPROVED SEISMIC HAZARD ASSESSMENT. 95
3.1. EMPIRICAL RELATIONSHIPS BETWEEN FAULTING PARAMETERS AND MAGNITUDE 95
3.1.1. Empirical relationships: some examples and critical issues 96
3.1.2. Uncertainties in empirical relationships 105
3.1.3. Empirical relationships and paleoseismology 106
3.2. THE ESI INTENSITY SCALE AND THE EEE GLOBAL CATALOGUE: TOOLS TO COMPARE PALEO, HISTORICAL AND MODERN EARTHQUAKES 108
3.2.1 Environmental Seismic Intensity scale - ESI 2007 108
3.2.2 The EEE Catalogue: a global database of Earthquake Environmental Effects 111
3.3. PALEOSEISMIC AND FAULT DATABASES 114
3.3.1 Introduction 115
3.3.2 Active and capable fault databases 115
3.3.3 Neotectonic Features Database 117
3.3.4. Seismogenic sources databases 118
3.3.5 Composite databases 119
3.3.6. Guidelines for building a Paleoseismic Database: structure and content 120
4. THE APPLICATION OF PALEOSEISMOLOGY TO NPP SEISMIC HAZARD ASSESSMENT 122
4.1 APPLICATIONS OF PALEOSEISMOLOGY TO NPP SEISMIC AND TSUNAMI HAZARD ASSESSMENT IN JAPAN 122
4.1.1 Onagawa NPP's Investigations 122
4.1.2 Paleotsunami Investigations around the Fukushima area 136
4.2. APPLICATION OF PALEOSEISMOLOGY TO SEISMIC HAZARD ANALYSIS IN THE CENTRAL AND EASTERN UNITED STATES (CEUS) 137
4.3. PREHISTORIC SEISMIC RUPTURES REVEALED BY PALEOSEISMIC STUDIES IN THE SIERRAS PAMPEANAS, ARGENTINA 141
4.3.1. Nature of the problem 141

4.3.2. Paleoseismic studies at El Molino fault 143
4.3.3. Some lessons learned from the Sierras Pampeanas case 145
APPENDIX 1 - SEISMIC VS. ASEISMIC FAULTS (CREEPING): SOME CRITERIA FOR DISCRIMINATION 147
APPENDIX 2 - ENVIRONMENTAL SEISMIC INTENSITY SCALE - ESI 2007 150
DEFINITIONS 157
REFERENCES 168
CONTRIBUTORS TO DRAFTING AND REVIEW 193

1. INTRODUCTION

1.1. CONTENT, OBJECTIVES AND SCOPE OF THE PUBLICATION

In the framework of site evaluation/re-evaluation procedures for nuclear power plants and other nuclear installations, this publication aims at encouraging and supporting Member States, especially from newcomer countries, to include paleoseismic investigations into the geologic database.

In fact, paleoseismology is not just a crucial discipline for Fault Displacement Hazard Assessment (FDHA) but also an indispensable tool for Seismic Hazard Assessment (SHA), as recommended in the reference IAEA Safety Guide (IAEA SSG-9 [1]).

Within this scope, this document provides an updated review of the state of the art of paleoseismology, integrated with practical recommendations addressed to Member States, aiming to emphasize the value of earthquake geology studies for nuclear safety.
Paleoseismic investigations in the context of site evaluation of nuclear installations, as described in the IAEA SSG-9 [1], have the following main objectives:

- Identification of seismogenic structures based on the recognition of effects of past earthquakes in the region;
- Improvement of the completeness of earthquake catalogs, through the identification and dating of ancient moderate to large earthquakes, whose trace has been preserved in the geologic record;
- Estimation of the maximum seismic potential associated with an identified seismogenic structure/source, typically on the basis of the amount of displacement per event (evaluable in paleoseismic trenches), as well as of the geomorphic and stratigraphic features interpretable as the cumulative effect of repeated large seismic events (concept of 'seismic landscape');
- Rough calibration of probabilistic seismic hazard assessment (PSHA), by using the recurrence interval of large earthquakes detectable by paleoseismic investigations, and providing a 'reality check' based on direct observations of earthquake environmental effects.

1.2. BACKGROUND

1.2.1. Key definitions

Paleoseismicity
Paleoseismicity is any geologic evidence of seismicity that has occurred in the past, generally found in the stratigraphic and geomorphic record, while Paleoseismology is the study of Paleoseismicity. In this sense, Paleoseismology may be considered a subdiscipline of much broader fields of the Earth Sciences: according to IAEA SSG-9 [1], the term 'paleoseismicity' is defined as *the evidence of a prehistoric or historical earthquake* (i.e. past) *manifested as displacement on a fault or secondary effects such as ground deformation (i.e. liquefaction, tsunami, landslides).'*

Thus, the IAEA definition considers a longer time window in comparison to classical definitions (e.g. *"Paleoseismology is the study of the timing, location, and size of prehistoric earthquakes"* of McCalpin, 2009 [2]; or *"the subdiscipline of geology that employs features of the geological record to deduce the fault displacement and age of individual, prehistoric earthquakes",* NRC, 2003 [3]). In fact, based on the IAEA definition, Paleoseismology also includes, for instance, the study of historical events not included in the seismic catalog due to a lack of written information or the characterization of surface ruptures induced by historical events in order to determine their magnitude.

Capable fault
According to IAEA SSG-9 [1], a 'capable fault' is *a fault that has a significant potential for displacement at or near the ground surface.* A capable fault is different from an active fault. Comparing its definition with available definitions of active fault (e.g. *"a tectonic structure that is expected to move within a future time span of concern to society"* Wallace in 1986 [4]) it is possible to state that capable faults are only those active faults that can produce a significant and permanent deformation at or near the surface.

By this definition, a capable fault represents an 'engineering' hazard that must be considered when designing nuclear installations. The attention is, therefore, focused on the potential dislocation/deformation of the topographic surface, especially in the near regional and site vicinity areas (see subsequent text). In this sense, even shallow blind thrusts may be classified as capable faults if they produce, for instance, significant deformation of the ground surface, i.e. differential uplifting or subsidence at a scale relevant for the foundation stability of a nuclear installation. Evidently, a creeping fault is also capable.

However, a capable fault also has a direct link to SHA, since it can be considered as primary or secondary evidence of a seismogenic structure. In this regard, it is important to note that fault capability due to creeping phenomena falls beyond the scope of the pertinent IAEA Safety Guide [1] (para. 8.2), and also this publication. As it might be difficult to demonstrate the seismic or aseismic behavior of a capable fault (see Annex 1 for some details), in most cases it is also recommended to conservatively include creeping faults in SHA.

The time window for the latest movement to be considered in the definition of a capable fault cannot be fixed 'a priori' since it strongly depends on the local tectonic environment (for instance, interplate vs. intraplate), which significantly influences deformation rates. *In highly active areas, where both earthquake data and geological data consistently reveal short earthquake recurrence intervals, periods of the order of tens of thousands of years (e.g. Upper Pleistocene–Holocene, i.e. the present) may be appropriate for the assessment of capable faults. In less active areas, it is likely that much longer periods (e.g. Pliocene–Quaternary, i.e. the present) are appropriate (IAEA SSG-9,* [1]*, 8.4).*

Seismogenic structure/source
According to SSG-9, a seismogenic structure is *"a structure that displays earthquake activity or that manifests historical surface rupture or the effects of paleoseismicity, and that is considered likely to generate macro-earthquakes within a time period of concern".*

In practice, seismogenic structures are only identifiable sources that are taken into account in the SHA for the NPP site. Usually, these sources are represented by tectonic structures which, includes capable faults; however, tectonic structures not containing capable faults (usually

located within near region) should also be considered, in case they are of interest for the site due to the potential of significant ground shaking.

There are also seismogenic sources not directly linked to a well identified fault or seismotectonic regions, which exhibit seismic activity. This is often the case for seismicity attributed to volcanic activity, mining, fluid injection and fluid extraction. The most relevant sources from the hazard viewpoint are the very deep ones, such as those related to deep subduction processes: a typical example of this is the Vrancea region in Eastern Europe.

Zone of diffuse seismicity
Zones of diffuse seismicity are areas where seismogenic structures cannot be clearly identified because geomorphic and/or structural evidence is absent and, therefore, it is difficult or even impossible to correlate between seismicity and the causative structures.
This situation is typical of geologically stable areas, i.e. intraplate areas; however, some interplate areas can also be characterized by a low/moderate level of seismicity.

As recommended by SSG-9, it is essential to gain a comprehensive set of indirect (e.g. geophysical) data, of any type appropriate, to characterize the tectonic situation of a zone of diffuse seismicity. The lack of this database will necessitate more conservative assumptions in the selection of SHA model parameters.

More details about investigations aimed at characterizing zones of diffuse seismicity, including case studies, are reported in Section 2.2.

Scales of investigations
Geologic and geophysical investigations should be conducted at four spatial scales with increasing detail of data: regional, near regional, site vicinity and site area (SSG-9, [1]; 3.6 – 3.19).

The size of the *regional area* may vary, depending on the geologic and tectonic setting, and its shape may be asymmetric in order to include distant significant seismic sources of earthquakes. Its radial extent is typically 300 km. In intraplate regions, and in the particular case where the potential for tsunamis is being investigated, the investigations may need to consider seismic sources at very great distances from the site as the investigations may need to consider seismic sources of far-field tsunamis. If it can be demonstrated that there are major tectonic structures closer to the site than the radius indicated, then studies should concentrate on this part of the region. The purpose of obtaining data on a regional scale is to provide knowledge of the general geodynamic setting of the region and the current tectonic regime, as well as to identify and characterize the geologic features that may influence or relate to the seismic hazard at the site. The most relevant among these geologic features are structures that show potential for displacement and/or deformation at or near the ground surface (i.e. capable faults).

Near regional studies should include a geographic area typically not less than 25 km in radius, although this dimension should be adjusted to reflect local conditions. The objectives of these studies are to: (i) define the seismotectonic characteristics of the near region on the basis of a more detailed database than that obtained from the regional study; (ii) determine the latest movements of faults; and (iii) determine the amount and nature of displacements, rates of activity and evidence related to the segmentation of faults.

Site vicinity studies should cover a geographic area typically not less than 5 km in radius. In addition to providing a yet more detailed database for this smaller area, the objective of these investigations is to define in greater detail the neotectonic history of the faults, especially for determining the potential for and rate of fault displacement at the site (fault capability), and to identify conditions for potential geologic instability within the site area.

The *site area* investigations are mainly aimed at developing the geotechnical database, but may also provide valuable data to help identify past seismicity (e.g. paleoliquefaction features).

1.2.2. Paleoseismology applied to NPP site evaluation

Earthquakes occur on faults. However, it is not always possible to associate an earthquake to a fault in a given region.

Earthquake geologists in charge of the identification of seismogenic structures usually evaluate the severity of expected earthquakes (Magnitude or Intensity), based on the fault rupture parameters (e.g. rupture length, rupture width, maximum displacement). In case of smaller earthquakes with little rupture lengths and negligible surface effects, some impacts on natural environment may exist. Such relations have been considered in the Intensity scales, for exaples, Mercalli Cancani Sieberg (MCS), Modified Mercalli (MM), Medvedev Sponheuer Karnik (MSK), and are well represented in the Environmental Seismic Intensity (ESI) scale, 2007 (see Appendix 2).

What is the magnitude/intensity threshold between the potential recognition and the lack of recognition of seismogenic structures at surface? According to the current state of the art in Earth Sciences, and also considering the limits of existing geological/geophysical technologies, it is very difficult to detect crustal seismogenic structures that can only generate earthquakes $M_w < 5.5–6.0$ or Io = VIII-IX (e.g. list of references of the above intensity scales). Only in exceptional cases (e.g. very shallow earthquakes with focal depths in the order of 2–3 km such as in volcanic environments) can detectable ground effects occur which are associated with a lower M_w (small associated fault ruptures). Below this magnitude/intensity threshold, in a suitable geologic environment, it is possible to infer the existence of a seismogenic structure based on secondary effects induced by past earthquakes. Nevertheless, using only secondary effects it may not be possible to define the seismogenic structure's exact location.

Although the so-called 'random in space' earthquake has not a physical and geological sense, during seismic hazard analysis, an earthquake may be treated as random-in-space if there is lack of sufficient data to constrain the future locations of earthquakes. To define adequately the seismogenic structures for an accurate representation of areas prone to future seismic activity (concept of 'background earthquake') might be impossible. This is especially important for regions where the expected larger earthquakes are in the magnitude range of 5.5–6.0. Therefore, the introduction of a non-identified earthquake of M > 5.5–6.0 for seismic hazard assessment purposes, must indeed be well justified.

In case, evidence of fault capability is absent on a crustal seismogenic structure, which is well-studied by geological/geophysical investigations, the maximum magnitude of a potential earthquake associated with this structure may not have a magnitude larger than 6. Larger values are possible based on a substantial database (e.g. the 2000 Tottoriken-seibu, Japan

earthquake), especially if the structure is located in the near region of the NPP site, as well as, in case it is not possible to increase the quality and completeness of the geological/geophysical database for the whole regional area.

It is important to remark here that the surface faulting data now available are still insufficient for a well consolidated relation with magnitude and intensity. To avoid misleading interpretations (e.g. lack of data = no surface faulting), for future events it is, therefore, recommended that all the coseismic effects (primary and secondary) are mapped and described and the collected data should be used for seismic intensity evaluation through the recently developed ESI 2007 intensity scale (Section 3.2).

When dealing with SHA, it is generally assumed that the geodynamic setting will not change during the NPP lifetime, since it is related to mechanisms that commonly evolve through time spans in the order of hundreds of thousands (often millions) of years. Of course, some natural phenomena (such as glaciation and volcanism) may induce significant variations on the rate of tectonic movements, but in a time period much longer than the NPP's lifetime. Conversely, some human activities near the NPP site (including the construction of large hydraulic facilities and filling of extensive reservoirs, fluid injection and fluid extraction, also gas injection in exhausted reservoirs) may theoretically induce some changes that are not negligible, even during the NPP's lifetime, altering the validity of the above statement.

Taking into account what is said above, it is also possible to state that tectonic reactivation of faults (including secondary and sympathetic faulting) can occur only on existing capable faults located in the area between primary and secondary ruptures (see Section 2.1). As a consequence, if the closest trace of the potential surface faulting is located far away from the site, it is realistic to conclude that fault displacement hazard is not relevant at the site, and therefore it will not be necessary to perform a Probabilistic Fault Displacement Hazard Analysis (PFDHA) for already existing sites. Of course, this assessment has to be based on robust geologic information from the area surrounding the NPP site. In particular, detailed paleoseismic investigations, especially in the near region and site vicinity areas must be available. If not, it is recommended to perform the PFDHA considering the traces of the mapped faults in these areas.

1.2.3. Limitations of paleoseismology for SHA of NPP sites

Assessing the uncertainties

Paleoseismologists are required to provide reliable quantitative data on past earthquakes, derived from field investigations, for input into SHA models. In this process, the assessment of uncertainties becomes a very challenging issue, as field data supporting the assessment is affected by an intrinsic uncertainty. The problem is particularly evident for the evaluation of recurrence intervals and slip rates when it is based on dating of samples and offsets measured by paleoseismic methods.

Every attempt should be undertaken to obtain the most complete and robust database to reduce the epistemic uncertainties as much as possible. Obviously, only where surveyed data are complete and sampling procedures very accurate will the amount of uncertainty be reasonable and acceptable, as indicated by SSG-9: *the most sophisticated methods will not yield good (seismotectonic) models if the database is poor or insufficient.*

Earthquakes clustering: a problem in the extrapolation of paleoseismic results
Historical and paleoseismic data show the occurrence of clustered earthquakes, i.e. seismic events can be more frequent during certain periods and rarer in others. In fact, the recurrence history is cyclically characterized by long (inter-cluster) intervals alternated by short (intra-cluster) intervals; paleoseismic studies have also shown that there are faults that exhibit variable recurrence times between large earthquakes. However, paleoseismic investigations cannot always reveal such behavior: in fact, a paleoseismic history that is long and detailed enough to show if the events on a given fault are truly temporally clustered, or simply have a large variability around a single-mode recurrence, is rarely achievable.

The extrapolation of the paleoseismic history that is only focused on a series of clustered earthquakes may cause the recurrence interval estimate to be too short (if single events can be discerned) or a larger slip per event than the true one to be assumed (by taking the summation of slips caused by two or more events closely spaced in time for a single event). Clearly, this would cause an overestimation of the seismogenic structure under investigation. This is a limit for paleoseismology, but also for PSHA, especially when applying Poisson methods.

Magnitude assessment from paleoseismic data
Several empirical relationships between magnitude (M_w) and surface faulting parameters have been developed in the last decades (see Section 3.1). By using these relationships it is possible to evaluate the magnitude range expected along the fault under investigation.

However, magnitude evaluation could be misleading because the paleoseismic interpretation is not always univocal: for example, the same paleoseismic feature may be produced by one single large paleoearthquake as well as by several more moderate paleoearthquakes closely spaced in time (see above). Similar limitations are derived from the use of other secondary effects, such as liquefactions, landslides, etc., in absence of a consolidated relationship with magnitude.

A suitable approach that may help to overcome this type of uncertainties is the application of the 'seismic landscape' concept for the assessment of maximum magnitude. Details are reported in Section 2.1.

Earthquake magnitude, as well as fault location and geometry, may also be estimated using the combination of the spatial distribution of paleotsunami deposits and inundation modeling (see Section 2.3). This approach works better if historical/recent data exist for comparison. However, the likely incomplete paleotsunami deposit record and the uncertainties in model parameters leave substantial doubts in the estimates.

Completeness of stratigraphic record
The stratigraphic record used for the paleoseismic characterization of a potential capable fault is often incomplete, mainly due to erosional processes or lack of sedimentation. Pedogenesis and root disruption can obscure the original stratigraphy. These effects may cause an underestimation or overestimation of the paleoseismic history of the investigated area.

Furthermore, even if the stratigraphy is complete, the absence of datable material or landforms could affect the completeness of the paleoseismic characterization. These issues are discussed within greater detail in the classic textbooks of paleoseismology (e.g. McCalpin, [2]).

2. PALEOSEISMOLOGY: STATE OF THE ART

2.1. PALEOSEISMIC CHARACTERIZATION OF CAPABLE FAULTS: ASSESSING SEISMIC SOURCE POTENTIAL FROM PALEOSEISMOLOGY

2.1.1. General remarks

As shown in IAEA SSG-9 [1], paleoseismology is the study of the ground effects of past earthquakes as preserved in the geologic and geomorphic record. Possibly the main goal of paleoseismology is the identification of capable faults and seismogenic structures. Paleoseismic analyses also provide constraints on the assessment of local rates of active tectonics in the study area (e.g. [2, 5–7]). In this way we can also understand the influence of this activity on the local landscape, stratigraphy and geological structures (e.g. [8–14]).

Within the conceptual framework defined by the IAEA SSG-9 [1] and according to the definitions given in this publication (see Section 1.2.1 and Glossary), with the term 'capable fault' we refer to faults that show both primary and secondary/sympathetic relations with the main seismogenic structure (e.g. [15]). These include faults that are able to generate strong to large earthquakes with surface rupture or other primary deformation at the ground surface; secondary faults that are not directly connected with the seismic source at depth are also included as they may be very important from the engineering point of view (Fault Displacement Hazard).

This section particularly focuses on the characterization of source parameters from paleoseismic analyses of capable faults. In the following, several examples are shown in onshore interplate and intraplate settings in order to illustrate the advantages and limitations of paleoseismology for understanding the hazards posed by capable faults to a specific site in terms of both surface faulting and ground shaking. Examples of offshore capable fault characterization are given in Section 4.

2.1.2. Paleoseismic analyses in the site vicinity, near regional and regional area

Paleoseismic analyses are typically based on investigations conducted at the site scale, such as exploratory trenching, GPR and high resolution seismic surveys and stratigraphic drilling. In the site vicinity area (5 km radius), paleoseismic trenching is applied with the purpose of characterizing the potential for surface faulting at the site. However, as clearly stated in the IAEA SSG-9 [1], these analyses are by no means limited to the site vicinity area. In fact, paleoseismic investigations at the site scale might also be of critical value for the identification and characterization of seismogenic structures located in the near regional and regional area, and relevant for the seismic hazard at the site. This point is illustrated in Figure 1.

FIG. 1. (a). Paleoseismic research type-investigations according to the SSG-9 (Case Zero). The figure illustrates the typical cases of fault capability expected in the entire regional area (and adjacent zones) linked to satellite study-cases needing of complementary investigation at near-regional and site-vicinity scales. (b) According to the type of evidence it is possible to distinguish six cases in which complementary investigation will be necessary in order to establish the fault capability level. Blue and pink circles show respectively the near-regional and site vicinity research scale areas centered on the faults, tectonic structures and/or identified geological anomalies under investigation (radius size is not in scale).

Figure 1 schematically illustrates some cases of fault capability that are typically expected in the regional area (300 km) and outside of it, for a site under investigation (advised from SSG-9 guidelines; Case Zero). According to the type of evidence it is possible to distinguish six cases. As a consequence, near regional and site vicinity type-research scale zones might be identified along different structural elements within the *regional area* (300 km) under investigation or even in the surrounding zone. In coastal areas located in subduction zone margins, hazardous seismotectonic structures can be located far away (>300 km), but they must be subject to detailed investigation at site vicinity and site type-research scales, since dangerous secondary earthquake environmental effects (e.g. tsunamis, liquefaction, landslides) can be triggered.

CASE ZERO - RECOMMENDATION ACCORDING TO SSG-9 (Mandatory): This case is focused on the selected site for nuclear installation. Thus, research areas (circles) are centered on the site at the mandatory research scales (Fig. 1(a). During the investigations, paleoseismic evidence/anomalies (e.g. paleoliquefaction features) may appear within the regional research area indicating previously-unknown strong motion in the area adjacent to the proposed/selected nuclear site.

This means additional detailed research in these zones or on tectonic structures could be necessary at *near regional* and *site vicinity* scales (Fig. 1(b), if the structures are significant for the estimation of earthquake hazards (SHA and FDHA). These additional research zones will from herein be referred to as '*satellite case studies*'. The areal extent of these satellite research cases must be defined according to the size of the detected evidence (e.g. fault length, lake extension, mountain front, area of strong historical damage, etc.). From these studies, it will be possible to establish different levels of fault capability according to the identified evidence (Fig. 1): 1) Capability one (red faults in Fig. 1) indicates the record of well-documented historical surface faulting on the fault trace and not complementary investigation is necessary (capable fault); 2) Capability two (orange in Fig. 1) indicates the occurrence of on-fault primary Earthquake Environmental Effects (EEEs), surface faulting, and on-fault paleoseismic investigations are necessary in order to establish fault capability; 3) Capability three (green in Fig. 1) indicates the identification of clear evidence on off-fault secondary EEEs (e.g. paleoliquefaction features, landslides, etc.) and on-fault and off-fault paleoseismic investigations are necessary; 4) Capability four (grey in Fig. 1) indicate the occurrence of geological and geomorphological anomalies evidencing suspect recent tectonic activity (e.g. drainage deflections or similar cases to capability three) but complementary investigation demonstrate no capability. Additionally, a wide range of bedrock faults and other tectonic structures may occur at the regional scale but displaying clear no capability (light grey in Fig. 1). All the necessary complementary investigations will follow the guidelines for on-fault trenching analyses and the on-fault/off-fault application of the ESI-07 scale, provided in this technical document for the paleoseismic characterization of diffuse seismicity (section 2.2).

Satellite case studies requiring additional detailed investigations can be summarized as follows (Fig. 1(b)):

CASE A: *Well documented historical reports indicate the occurrence of past seismic events*. The example shows a capable fault located south of the site under investigation close to the external boundary of the *regional* research area, but due to the length of the fault, it is also located in the *near-regional* area of the site. The historical events caused surface faulting, but also affected an ancient city causing widespread structural damage. Primary EEEs also

supported by well preserved EAEs (Earthquake Archeological Effects) demonstrate the capability of the fault. In this case, additional paleoseismic research is not necessary to demonstrate fault capability. However, exploratory trenching along the documented trace of historical surface faulting might be planned in order to identify previous surface rupturing events. This will complement the existing seismic catalog and characterize the fault behavior (e.g. paleoearthquake magnitudes, return periods).

CASE B.1: *Well exposed fault displaying surface faulting throughout its entire length affecting alluvial deposits of presumed Holocene age but undated*. Fresh earthquake fault scarps are preserved in the southern segment, but are practically buried/eroded in the northern one. *Near regional* scale research is necessary along the entire fault, and in northern segment site vicinity scale investigations (boreholes, trenching) are also needed. Investigations at *near regional* scale in the north identify disturbed lake-sediments. Fault trenching at both fault segments, lake investigations (including seismic survey, coring, and dating) and dating is necessary to evaluate fault capability.

CASE B.2: *Historical epicenter located outside the regional area with well-supported documentation on coseismic surface faulting*. Since the fault trace length reaches the site *regiona*l area, additional *site vicinity* scale paleoseismic research around the reported macroseismic epicenter could be necessary. Furthermore, near-regional type research along the fault in order to characterize the fault behavior and capability could be also required.

CASE C: *Range-front fault with well-preserved triangular facets and bedrock fault scarps which also partially affects the apex zone of Late Quaternary untrenched alluvial fan surfaces*. Investigation at *near regional* scale is necessary and bedrock fault scarps have to be dated (e.g. using cosmogenic dating). *Near regional* research identifies some paleolandslides probably triggered by a Holocene event and a *near regional*-scale area has to be engaged in order to investigate other paleolandslides (e.g. sackungen). Fault trenching is necessary on alluvial fan surfaces. Complementary trenches are also needed in the detected sackung and paleolandslide scars in order to characterize the seismic history of the zone and fault capability. Ancient moderate seismic events with negligible or no surface faulting (M_w in the order of 5.5 to 6.0) can be recorded in the landslide history of the faulted range-front and adjacent valleys. Likewise, if any existing lake or paleolake sediments are in the *vicinity* of the zone under investigation, these moderate events can also be recorded in the geologic record as paleoliquefaction horizons.

CASE D: *Geomorphic lineament associated to apparent drainage offsets of several hundred meters. Near-regional* type-research is necessary, but investigations conclude that the lineament is an ancient pre-Pliocene fault and the apparent offsets are only drainage deflections (false offsets), caused by shutter ridges of structural relief (not tectonic landforms) generated by differential erosion on the fault line. Thus, there is no evidence of the fault being capable, and therefore, no complementary paleoseismic investigations are necessary.

CASE E: *Earthquake epicenter (commonly historical ones) apparently not linked to any mapped fault in the area under investigation ('floating' earthquake case)*. This is a common case in areas of diffuse seismicity where tectonic structures are buried, but are capable of generating strong ground motion. This motion is linked to seismic events in the range of M_w 5.5 – 6.0. At these magnitudes surface faulting may or may not occur, which is mainly a function of local tectonic style and crustal stress environment. Detailed investigations at the *near regional* scale have to be undertaken over the damaged area in order to identify and

characterize potential seismogenic structures. In this case the review of existing geophysical information, acquisition of new geophysical data and geomorphic research are all necessary to identify potential seismogenic structures and to understand the existing seismic landscape which has recorded past seismic events in the required geologic time-span (Plio-Quaternary to Pleistocene-Holocene period depending on the seismotectonic context – SSG-9-3.12). The *Baelo Claudia* case study in southern Spain, related with a suspect 'floating' earthquake of intensity ≥ VIII in AD 365–390, illustrates the set of paleoseismic, geophysical and archeoseismic (if relevant) investigations to be developed to identify potential seismic sources and recognize their capability for this type of case (e.g. [16–18]).

2.1.3. Factors controlling trench site selection

Trenching is the most common paleoseismic technique, although it is not the only one. In addition or in replacement of trenching, may be considered paleogeodetic techniques used from near-fault as well as off-fault in the footwall or hangingwall of thrusts or normal faults (e.g. techniques using marine terraces and coral microatoll abandonments or alluvial terraces abandonments).

Success in trench evaluation relies 90% on trench site selection. In turn, this selection is entirely dependent on both the quality and accuracy of prior neotectonic mapping of the fault zone and detailed understanding of the trench site geology. In fact, as clearly illustrated in IAEA SSG-9 [1], the identification of capable faults must be based on a complete and coherent geologic and geophysical database, collected through specific field investigations at the site vicinity and near regional scale.

Figure 2 shows the pertinent logic framework during the siting process, i.e. how the investigation of capable faults is related to all the necessary study of the Muzaffarrabad earthquake surface faulting summarized in Section 2.1.6.2 is a clear example of the problems arising from a very incomplete database due to the difficulty in accessing the epicentral area; this situation is typical of most of the seismically active regions in the world. This so-called 'developing nation' situation, where there is a lack of complete and reliable geologic databases (topographic maps at detailed scales, geologic maps at detailed scales, geophysical data, seismic reflection coverage, and so on) is in fact the rule and not the exception in many areas.

The most effective tool for the paleoseismic analysis of capable faults is most likely the excavation of exploratory trenches across the fault trace. The length of the trench is usually in the order of 20–30 m, and its depth in the order of 3m. However, length and depth might vary according to the local conditions. Figure 2 also points out that the selection of a site suitable for trench excavations across capable faults is a process which requires special consideration.

In fact, choosing a trench site for capable fault characterization is a complex task since several favorable conditions have to be met at a single location along the fault's trace [2, 19]. These conditions can be classified into two main categories: geographic/administrative and geologic/geomorphic. The first one includes factors like site accessibility and topography, water table depth, vegetation, environmental impact, possibility for machine maneuvering and land ownership. The second category involves the clear definition of the fault trace, the presence of a continuous sedimentary record and the availability of datable material (see Section 2.4).

Moreover, it is possible to use other techniques or methods in combination with trenching in order to better define the trench location and aid in interpretation, thus reducing cost. Ground-Penetrating Radar (GPR) has been successfully used in the Rhine graben, in combination with other more classical geophysical methods (e.g. shallow high-resolution seismic profiling, geoelectrical tomography from light electromagnetic geophysical survey) to increase the precision of locating faults whose surface expression is obscured in a setting of subtle, smoothed or anthropogenically-modified surface morphology including fault-related landforms [20–22].

Also, a few shallow (up to 20 m deep) boreholes might assist in the trench site selection, as the three-dimensional geometry of faulted sedimentary sequences can then be visualized. A relatively recent and powerful technique for detecting surface faulting features is the use of airborne LIDAR (e.g. [23]). This is extremely useful, in particular, in densely forested areas, because the LIDAR technology allows vegetation cover to be filtered out and subtle topographic features can be mapped beneath the forest canopy.

Deformation needs to be both quantified and dated in order to characterize the fault's seismogenic behavior and potential (potential magnitude deduced from unitary co-seismic offset, return period, event(s) dating(s), return period and slip rate). This makes up the fundamental information as input parameters for seismic hazard assessment.

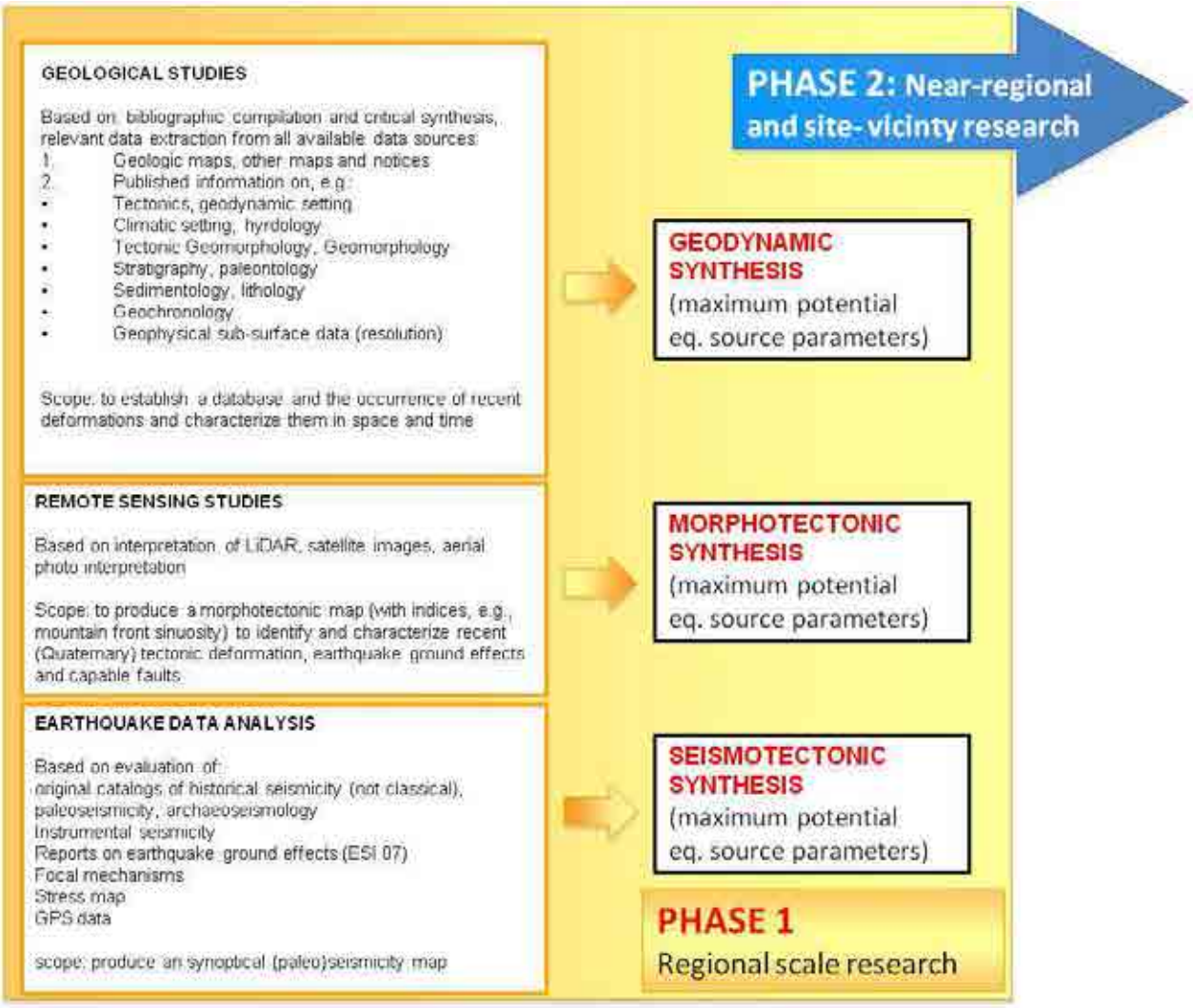

FIG. 2. (a) Flow-chart of proposed paleoseismic methodologies for capable fault characterization and seismic hazard assessment (Phase I).

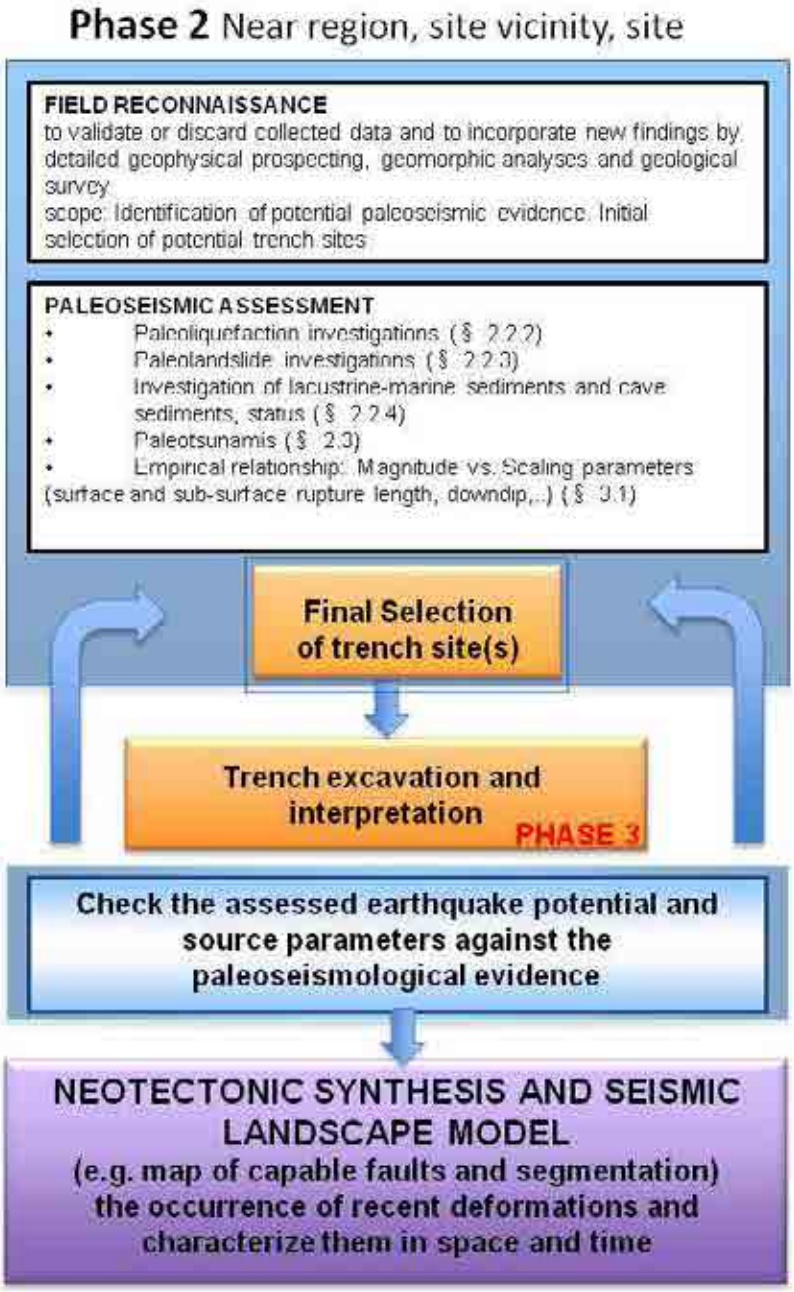

FIG. 2. (b) Flow-chart of proposed paleoseismic methodologies for capable fault characterization and seismic hazard assessment (Phase II).

2.1.4. Trench logging, stratigraphic and structural interpretation

Paleoseismic analysis of trench walls is based on the identification of stratigraphic features that record the occurrence of past surface faulting earthquakes. The first step is trench-wall logging, which is usually done by hand. A colored-string square reference grid is typically laid out on both trench walls for ease of drawing. The spacing of the grid squares depends on the structural and sedimentary complexity exposed on walls. Typical spacing is 1 m x 1 m. It can be more closely spaced where many details are present. Complex features can be also highlighted with nails or drawing pins. Conversely, for simple structures a wider grid spacing will suffice.

Trench photographing might also be useful, especially when presenting the findings; however, direct logging at the trench-wall allows the viewer to record detail more thoroughly.
A diagnostic stratigraphic feature of earthquake surface faulting occurs at places where differential uplift has created a fault scarp on which erosion produces sedimentation at its foot on the down-thrown block, which can be interpreted as evidence for individual seismic events (like in case 5 of Fig. 3). This is known as a colluvial wedge and constitutes an important and frequently used criterion in paleoseismology (Fig. 4). Other diagnostic features are illustrated in Fig. 3. Likewise, McCalpin in 2009 [2], Grant in 2002 [24] and Yeats et al. in 1997 [25], among others, have described a number of typical stratigraphic indicators of paleo-earthquakes in strike-slip environments.

Interpretation of paleoseismic surface faulting along trench walls often requires retrodeformation techniques, such as in the case illustrated in Fig. 4. Dates of paleo-earthquakes have been bracketed from stratigraphic evidence preserved in the sedimentary sequence ruptured by the fault (Fig. 4).

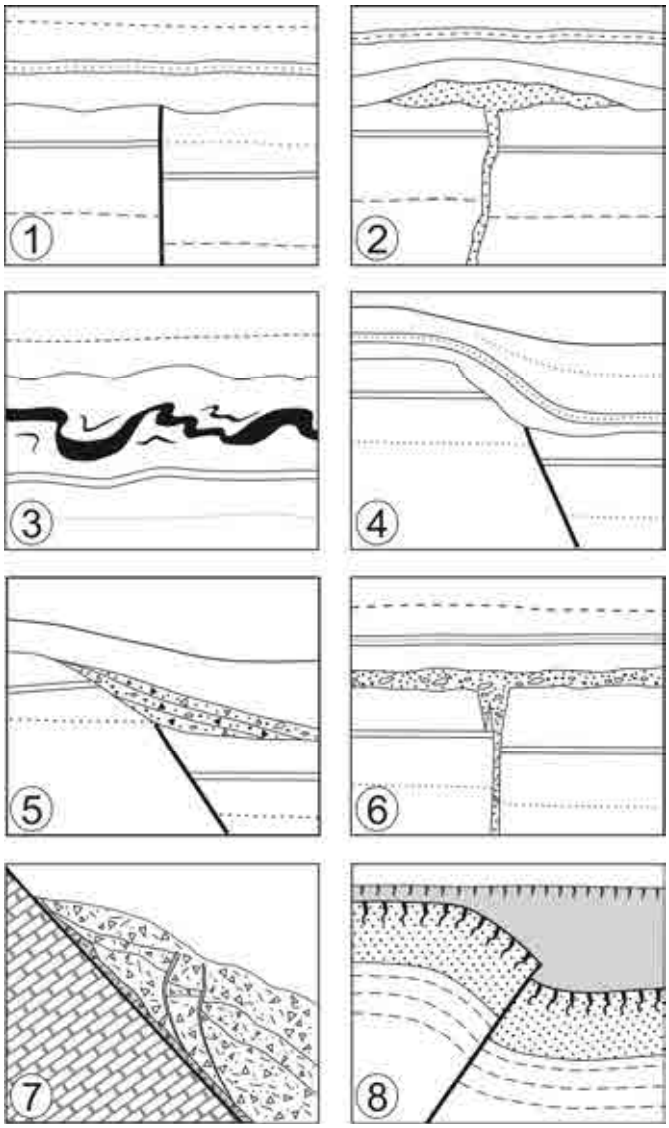

FIG. 3. Diagrams illustrating stratigraphic and structural criteria used to identify the occurrence and timing of paleoearthquakes in the paleoseismic analysis of trench walls: (1) Vertical fault offset sealed by a levelling sedimentation episode; (2) Liquefaction along a fault offset sealed by subsequent sedimentation episodes; (3) Soft-sediment deformation sealed by subsequent sedimentation episodes; (4) Fault-scarp eroded and sealed by subsequent sedimentation; (5) Colluvial wedge derived from scarp degradation on normal fault offset; (6) Filling of open surface fissures along a vertical fault plane, sealed by a levelling sedimentation episode; (7) Normal bedrock fault scarp with offset slope deposits, typical of carbonate fault plane in the Mediterranean Region; (8) Reverse fault offset sealed by a levelling sedimentation episode. This figure is based on Audemard in 2005 [19] and Grant in 2002[24].

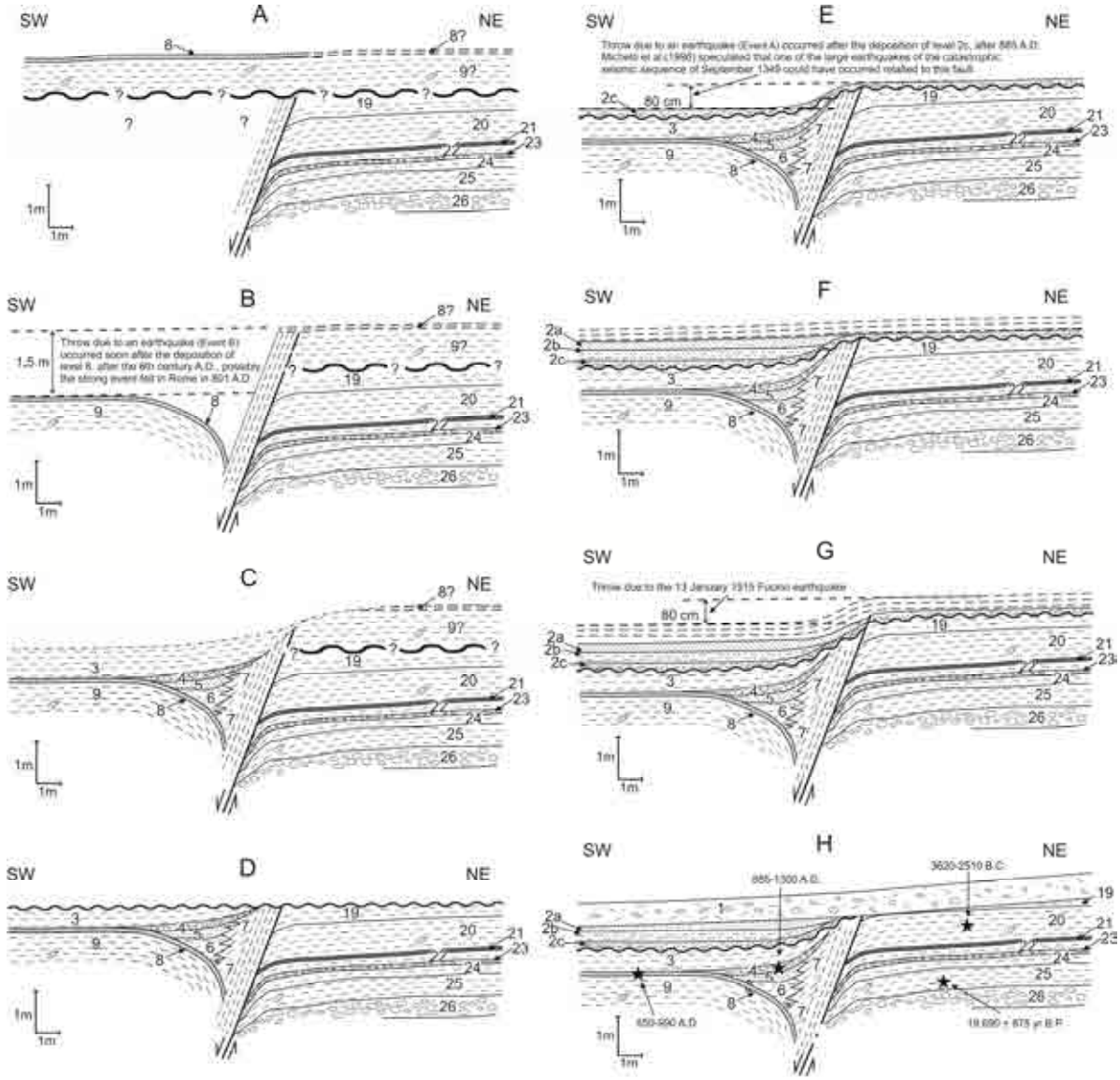

FIG. 4. Retrodeformation of the trench log, through a sequence of simplified cross sections showing the interpreted evolution of the fault zone exposed in the trench wall at the San Benedetto site (Fucino Basin): (A) scarp configuration immediately before event B; dashed thin lines show thickness of units 8 and 9 in the footwall, which is estimated from the exposure in the hanging-wall; sinuous dashed bold line with question marks represents the possible geometry of an old unconformity inferred to explain the stratigraphic gap between unit 19 and unit 9; (B) scarp configuration immediately after event B; the throw hypothesized as due to this event is also indicated; this was estimated using the thickness of the colluvial wedge mapped in C; (C) scarp configuration after the deposition of the colluvial wedge (Units 3 to 7) that fill the trench and smooth the fault scarp caused by event B; (D) scarp configuration immediately before the beginning of unit 2 deposition; the sinuous line at the top represent an unconformity i.e. an erosional episode that occurred just before the deposition of unit 2; (E) scarp configuration immediately after event A; (F) scarp configuration before the 1861–1875 drainage; dashed lines show hypothetical thickness of fluvio-lacustrine units that were deposited after unit 2; (G) scarp configuration immediately after the 13.01.1915, M7 earthquake; dashed lines show units removed or mixed up by subsequent agricultural activity; and (H) present-day configuration of the fault scarp. Immediately before or during the deposition of the sandy subunit 2c an earthquake reactivated the fault plane producing a broad monocline on the lake floor, similar to the one generated in a sub-aerial environment by the 1915 event. Units 3 to 7 form a prism of lacustrine and debris sediments. This prism reaches a maximum thickness of about 2 m against the fault plane. This indicates an earlier episode of fault rejuvenation associated with a scarp free face higher than 2 m. The full discussion of this paleoseismic analysis is presented in [26].

2.1.5. Understanding maximum earthquake magnitude from capable faults: the Seismic Landscape

Trench investigations on capable faults, and also most studies on all categories of seismites [5]; see also Section 2.2 for the description of other evidence of paleoseismicity such as paleoliquefaction), aim to determine the seismic nature of the features under observation, and also the magnitude and date of the causative earthquake.

A proper understanding of the local seismic and geologic setting (the 'Seismic Landscape'; Michetti et al., [27], see subsequent text), in terms of recent tectonic and climatic evolution, crustal stress environment (e.g. [28, 29]), style of faulting, fault slip rates, and Quaternary geomorphic-stratigraphic framework, are crucial requirements for achieving these goals. The resulting data on location, magnitude, and recurrence of large earthquakes form the basic input for seismic hazard analyses, with the goal of characterizing the threat to the nuclear installations from earthquakes.

Moreover, we have to keep in mind that the 'capable fault' issue also needs to be investigated in order to mitigate the effect of displacement and deformation of the topographic surface (irrespective of vibratory ground motion) with respect to nuclear installations. Where present, various solutions from engineers are proposed (typically, site rejection for new projects, Probabilistic Fault Displacement Hazard Analysis (PFDHA) for an existing nuclear installation).

The main point to be addressed here is that the process of deriving source parameters from the paleoseismic evidence of surface faulting, as identified along trench exposures of capable faults, is not simple and straightforward. In few cases are capable faults directly representative of the seismogenic source at depth. Therefore, the collected paleoseismic evidence must be compared and contrasted with the whole geologic, geophysical and seismologic database collected according IAEA SSG-9 [1], in order to obtain a reliable interpretation of the causative earthquake source magnitude, style of faulting, geometry and rates of activity. For instance, an example of paleoseismic interpretation of secondary surface faulting along a capable buried thrust is illustrated below for the Monte Netto site in N Italy (see Section 2.1.6.3).

The most reliable approach for the effective use of paleoseismic data is to use them in the framework of the local seismic landscape. Michetti et al., in 2005 [27] defines the *'seismic landscape'* as

> "the cumulative geomorphic and stratigraphic effect of the signs left on an area's physical environment by its past earthquakes over a geologically recent time interval".

In this definition, the term 'landscape' it is not necessarily linked with an existing geomorphic expression. Seismic landscapes might be represented, for instance, by buried geological landscapes [6]. For instance, in the New Madrid seismic zone of the Central US the erosion and sedimentation rates of the Mississippi River are much greater than the slip rate of the local capable faults. Therefore, the study of the seismic landscape at this location should be based essentially on the widespread evidence for paleoliquefaction, and on the understanding of the buried paleolandscapes as preserved in the Holocene stratigraphic record [30, 31]; see also Section 2.2.2.

The notion of 'seismic landscape' is based in fact on the observation of the consistency existing between A) the erosional and depositional processes, the landforms, and the late Quaternary geological record existing in an area, and B) the earthquake magnitude assessed from the analysis of earthquake ground effects, for instance from a colluvial wedge along a fault scarp exposed through exploratory trenching. If the rates of surface faulting are very high compared with the local rates of deposition and erosion, typically it is not very difficult to obtain paleoearthquake magnitudes coherent with the local geologic and geomorphic environment. This is because in this case the cumulative effect of repeated strong surface faulting events will generate characteristic morphologies and stratigraphic features that will continue to grow over a geological time interval. This is due to the repetition at the same location of coseismic environmental phenomena (such as landslides, liquefaction, fault scarps, coastline uplift or subsidence) of similar size.

The Quaternary geological evidences strongly suggest that significant earthquakes (typically Mw 5.5 – 6.0 or greater) repeat themselves along a specific seismic source [6, 32, 33]. In other words, from the paleoseismological point of view strong earthquakes are not 'random' phenomena. This implies that over a certain time-interval the local landscape and stratigraphy will be characterized by certain earthquake-controlled features, which define a specific seismic landscape. The study of these features enables us to assess the source parameters (including earthquake magnitude, style of faulting, slip-rates) of the reference seismic event for the studied region.

Figure 5 illustrates an example of seismic landscape, in a region where tectonic rates exceeds erosional and depositional rates, resulting in a characteristic geomorphic signature (the classic intermountain basins of the Central Apennines). The dimensions and structures of each intermountain basin show a clear relation with the earthquake magnitude of the local causative normal faults [11].

Using the flow-chart described in Fig. 2 is therefore possible to properly assess the seismic potential of an area using paleoseismic analyses coupled with the definition of seismic landscapes. Michetti et al. in 2005 [27] describe this methodological approach as follows:

> "First, the location, geometry and seismic potential (magnitude/intensity and rate of occurrence of the 'characteristic' earthquakes, also based on fault slip rates and recurrence interval) of possible relevant earthquake sources in the region should be analyzed.
> Second, according to the assessed seismic potential, the expected assemblage of paleoseismic features should be defined.
> Third, the resulting hypotheses should be tested against the paleoseismic evidence in the field, near each outlined source and also in the subsurface (for instance, through exploratory trenching). If the paleoseismic evidence does not fit the assessed earthquake magnitude/intensity and recurrence, the adopted seismic landscape is wrong, and the described methodological steps should be reconsidered until a proper calibration of the source parameters is obtained. This approach guarantees that the assessed magnitude and recurrence is consistent with the geologic, geomorphic and paleoseismic features existing around the causative earthquake source(s)."

In order to appreciate the variability of seismic landscapes as a function of the plate tectonic setting, in Section 2.1.6 and 2.1.7 several case studies are described from normal faulting in Central Italy, and reverse faulting in Po Plain in Italy, Central Andes, Pakistan and in the

Alpine Region of France (this latter in a reverse-strike slip environment). For major strike slip environments, McCalpin [2] and Yeats et al. [25], among others, provide a comprehensive review of the available literature. Examples of offshore compressional environments are given in Section 4.

It should be taken into account that the occasional and extreme variability of the tectono-sedimentary response to earthquake(s) along the same scarp increases the limitations of paleoseismic studies in SHA. An exploration of this variability, when possible, is important for Seismic Hazard Analysis applications. The case histories illustrated below provide suitable illustrations from this perspective.

Examples of the use of paleoseismic data for SHA are also given in Section 4.

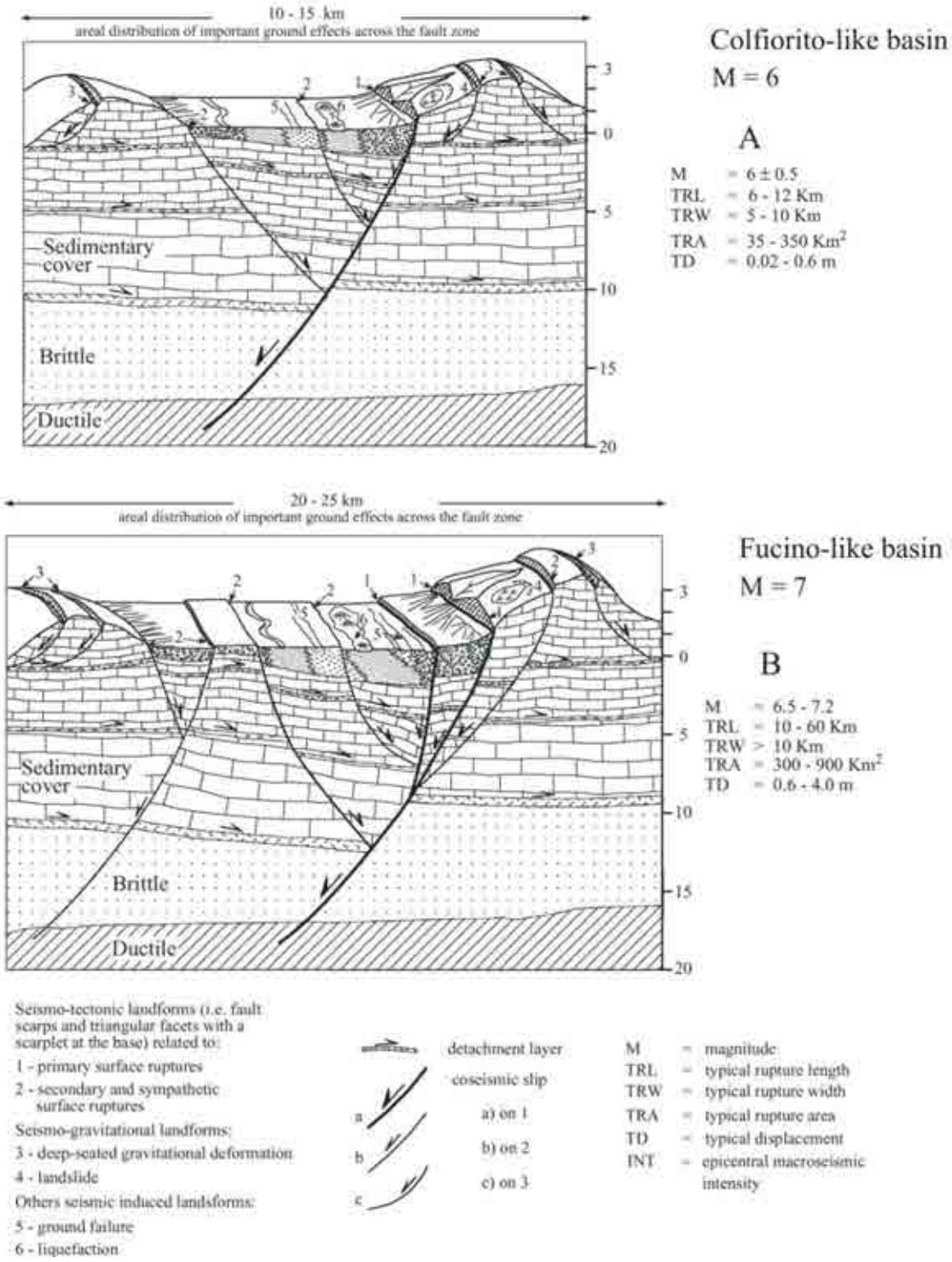

FIG. 5. Seismic landscape of two intermountain basins in Central Italy, A) the Colfiorito basin, affected by the September 26, 1997, M 5.6 and 6.0 earthquakes [34] and B) the Fucino basin, affected by the January 13, 1915, MS 7.0 earthquake [26]; see also the specific illustration of this case history later in this Section). The differences in the geomorphology and geologic structure of the two basins are consistent with the repeated occurrence of similar earthquakes of different magnitude and rupture length over the Quaternary, so that it is possible, within the extensional setting of the Apennines, to define A) as a M6-type seismic landscape, and B) as a M7-type seismic landscape This figure is reproduced with the permission of editor from Serva et al. in 2002 [11].

2.1.6. Case histories: interplate settings

2.1.6.1. The belt of capable normal faults in the Apennines, Italy: emphasis on the Fucino basin

The seismic landscape of the Italian Apennines is a suitable example to show the importance of a complete and reliable geologic database when assessing source parameters from paleoseismic evidence along capable faults. Strong normal faulting earthquakes from the extensional provinces of Italy and Greece typically only reactivate some of the numerous Holocene fault scarps developed during the growth of the causative seismogenic structure (e.g. [35–42]). The Irpinia-Lucania area in Italy is a very clear example of how important event timing is in capturing a full understanding of fault behavior for hazard analysis. This area was hit by a M_S 6.9, intensity X (MCS scale) earthquake on November 23, 1980, and by an intensity X earthquake on September 8, 1694 (Serva, [43]; Galli and Peronace, [44]). The reported damage, ground effects and isoseismal maps for the two earthquakes are nearly identical, which demonstrates that they were generated by the same seismogenic source [40].

However, trench investigations along the surface ruptures that accompanied the November 23, 1980, M 6.9, Irpinia-Lucania normal faulting earthquake in Italy show that surface faulting apparently did not occur at these sites during the 1694 earthquake as the penultimate event is constrained to have occurred at least 1500 to 2000 years before present [45, 46]. Evidence for the 1694 surface rupture is likely preserved along other Holocene scarps that did not break during the 1980 event [40, 44, 47], or at other locations along the 1980 ruptures. Coseismic surface faulting during the 1980 earthquake was quite extensive, including an over 40-km-long main rupture [36, 46], a 7-km-long, cross-fault rupture in the Senerchia area within the footwall of the main rupture [48], and at least two parallel, ca. 8-km-long, antithetic ruptures in the Muro Lucano area [40, 49].

Fault trenching investigations are critical in paleoseismic analysis because they have the potential to provide a direct assessment of the amount and timing of fault movement. However, the experience from the Apennines of Italy shows that trench investigations along a fault segment are in fact not always able to capture all recent surface faulting events that occurred along that segment. For instance, the earthquake rupture may not occupy exactly the same trace every time. Several capable faults might be associated within prominent, composite tectonic structures such as the Quaternary extensional intermountain basins, especially when viewed at the scale of a trench excavation site (tens to a few hundreds of meters; e.g. the Fucino basin, see Fig. 5). Also, the April 6th 2009, L'Aquila earthquake ruptured the Paganica Fault, a relatively minor capable fault within the large L'Aquila Quaternary basin (Vittori et al., [50]; Fig. 6). Typically fault zones are wider and more complex at bends of the fault trace in map view, or within stepovers. Their surface expression might be distributed along strike over a significant fault width, and often includes a set of second-order surface ruptures, such as antithetic, en-echelon and release faults.

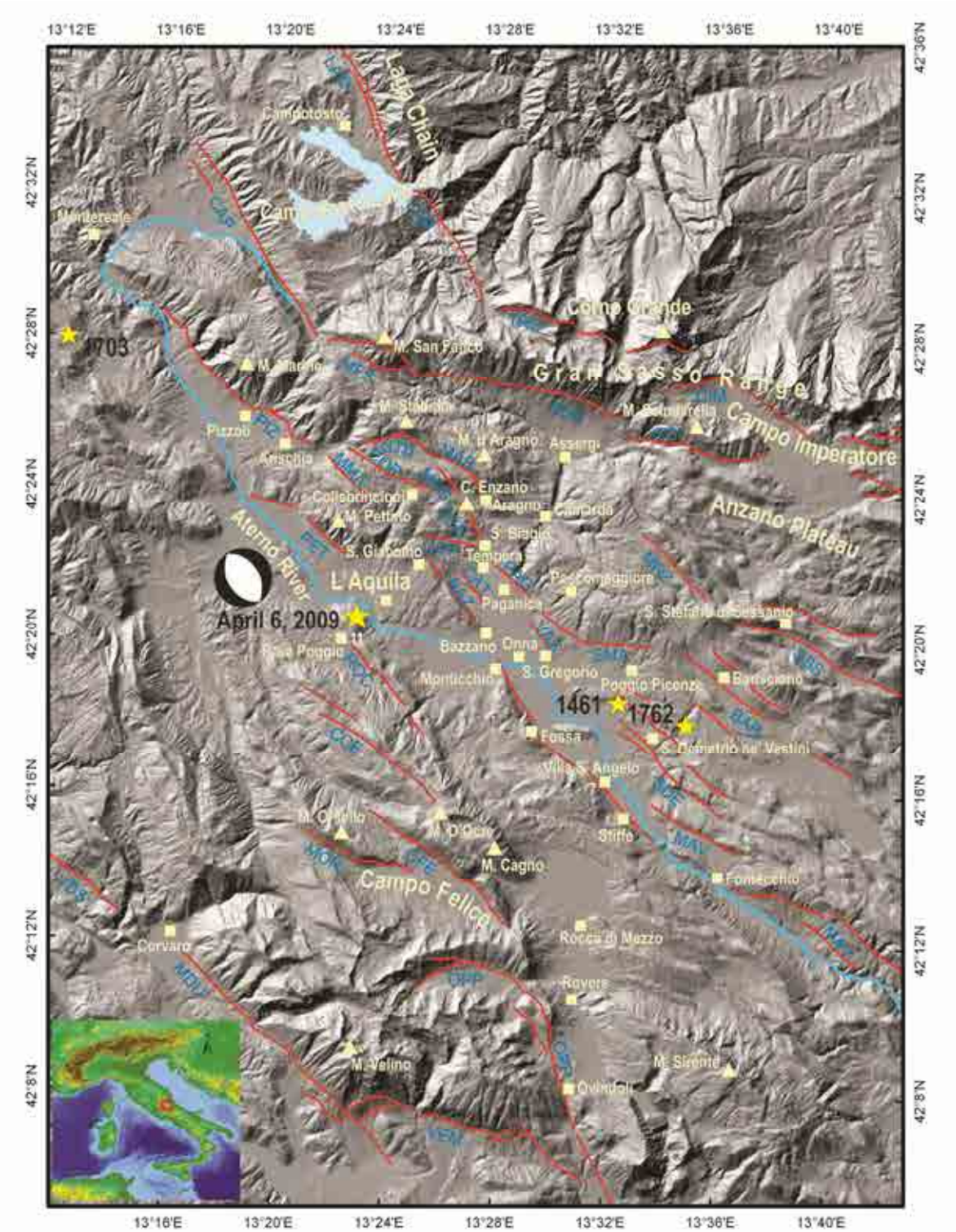

FIG. 6. Map of faults capable of surface rupturing known for the L'Aquila basin and nearby region (from the ITHACA catalogue) and epicenters of the main historical earthquakes (stars). The Paganica Fault (PAG) ruptured during the April 9, 2009, M_w 6.3 earthquake. ASG, Assergi fault; BAR, Barisciano fault; BAZ, Bazzano fault; CAP, Capitignano fault; CAT, Colle Caticchio fault; CCE, Colle Cerasitto fault; CEN, Colle Enzana fault; CFE, Campo Felice fault; CIM, Campo Imperatore fault; CLB, Collebrincioni fault; COC, Colle Cocurello fault; COF, Colle Frolla fault; COP, Colle Praticciolo fault; MAV, Middle Aterno valley fault system; MCS, Monte Castellano fault; MDU, Monti della Duchessa fault; MFS, Monticchio-Fossa-Stiffe fault system; MMA, Monte Macchione fault; MOR, Monte Orsello fault; MRZ, Monte Ruzza fault; MSF, Monte San Franco fault; OPP, Ovindoli-Piani di Pezza fault; PET, Monte Pettino fault; PIZ, Pizzoli fault; ROC, Roio–Canetre fault; SDE, San Demetrio faults system; SCI, Scindarella fault; SMA, San Martino fault; SSS, Santo Stefano di Sessanio fault system; STB, Stabiata fault; TRS, Tre Selle fault; VAS, Valle degli Asini fault; VDS, Valle del Salto fault.This figure is based on Guerrieri et al. [51]. Source for Digital Elevation Model is http://www.pcn.minambiente.it/GN/.

One particularly interesting case regarding the paleoseismic characterization of capable faults in interplate settings is the Fucino basin, whose seismic landscape is sketched in Fig. 5. Here it has been possible to document the interaction between normal faults in a large extensional basin, due to the large amount of available paleoseismic analyses, allowing reliable correlation between different trenches.

The Fucino basin has been extensively studied in the past decades. The seismic landscape of the Fucino basin is arguably one of the best studied examples worldwide (Figs. 5 and 7). It is a typical Quaternary intermountain normal-fault-bounded structure, and the largest tectonic basin of the Apennines. Its central part, which was hydrologically closed during the Late Glacial and Holocene, previously contained the third largest lake in Italy (ca. 150 km^2). In the 2nd century AD, Emperor Claudius prompted the drainage of Lake Fucino through the excavation of a 6-km long tunnel mostly carved in the Mesozoic limestone, one of the most remarkable engineering projects in the Roman history (Fig. 8). More recently a serious drainage effort achieved the complete emptying of the lake by the end of the 19th century.

This area was struck by an earthquake on 13th January 1915 with XI (MCS) of I_0, which caused 30,000 casualties. In Avezzano, the biggest town of the area, only one house was still standing after the earthquake. It is remarkable that the seismic history of the basin did not register other events. This was the reason why Italian researchers chose this zone to carry out pioneering paleoseismic studies in the late 1980s [52, 53], and successively a large amount of paleoseismic investigations were carried across the individuated fault scarps [26, 54–59].

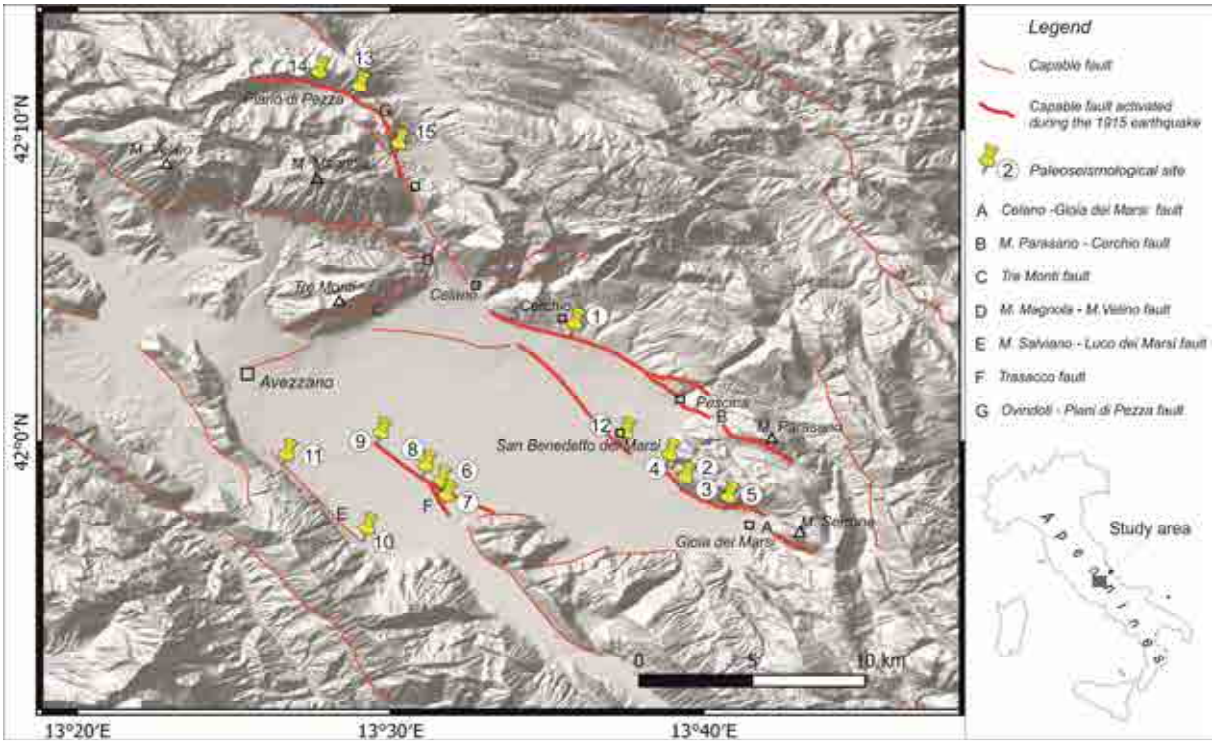

FIG. 7. The system of capable normal faults in the Fucino area. Yellow nails show sites where paleoseismic investigations have been carried out (numbers like in Table 1). Red lines are capable faults from ITHACA database (http://sgi1.isprambiente.it/geoportal/catalog/content/project/ithaca.page); Source for Digital Elevation Model is http://www.pcn.minambiente.it/GN/.

TABLE 1. SYNOPSIS OF PALEOSEISMIC ANALYSES IN THE FUCINO BASIN AND NEARBY AREAS (SITE NUMBERS AS IN FIG. 7. DATA FROM THE GEOLOGICAL SURVEY OF ITALY ITHACA CATALOGUE - ITALY HAZARDS FROM CAPABLE FAULTS, AVAILABLE AT THE WEBPAGE HTTP://SGI.ISPRAMBIENTE.IT

Trench site	Locality	Strike	Dip	Holocene vertical offset (m)	Holocene horizontal offset (m)	Vertical slip-rate (mm/yr) and time-window(yr)	Recurrence time and time window (yr)	Total events	Paleoearthquake ages	Vertical slip per event (m)
1	Strada Statale Marsicana	NW-SE	SW	> 5	none	0.4–0.5 (last 20000)	4500–5000 (20000)	5	1915 AD; 6500–3700 BP; 7300–6100 BP; 13600–12300 BP; 19100–18500 BP	Event 1: 0.8
2	Colle delle Cerese	N50W	SW	>3	none	0.35–0.40 (last 7000)	1000–1800	3	1915 AD; 1100–1500 AD; 7200–6540 BP	Event 1: 0.7
3	Colle delle Cerese (Cave)	NW-SE	SW	10–15	none	0.35–0.40 (last 4200)	1400–2100	3	1915 AD; 150–1349 AD; 3760 BP-150 AD	Event 1: 0.7
4	Molini di Venere	NW-SE	SW	>3	none	0.35–0.40 (last 10000)	1200–1500 (2000)	4	1915 AD; 1300–1500 AD; 7120–5340 BP; 10400–7120 BP	Event 1: 0.7
5	Casali D'Aschi	NW-SE	SW	5	none	0.35–0.40 (last 20000)	800–1000 (3000); 3300–5500 (33000)	7	1915 AD; 1200–1400 AD; 2783 BP-1300 AD; 4700–2800 BP; 10400–7120 BP; 20000–10000 BP; 32520–20000 BP	Event 4: 2
6	Trasacco (Fosso 41)	N22W	WSW	>3	none	0.3–0.4 (last 7000)	1500–1800 (2000)	2	1915 AD; 1000–1349 AD	0.5; 0.6
7	Trasacco (Strada 37)	NW-SE	SW	>3	none	0.3–0.4 (last 7000)	1800–2000 (7000)	5	1915 AD; 1000–1349 AD; 3700–3500 BP; 7120–5000 BP; 10790–7120 BP	Event 1: 0.5
8	Trasacco (Strada 38)	N60W	SW	>3	none	0.3–0.4 (last 7000)	1600–1800 (10800)	7	1915 AD; 1000–1349 AD; 3700–3500 BP; 7120–5000 BP; 10790–7120 BP (2 events); >12000 BP	Events 1,2,3,4: 0.55; Events 5,6,7: 0.15;
9	Trasacco (Strada 10)	NW-SE	SW	>3	none	0.3–0.4 (last 7000)	1800–2000 (12000)	8	1915 AD; 1000–1349 AD; 3700–3500 BP; 7000–5000 BP; 10790–7120 BP (3 events); >10790 BP	Event 1: 0.1
10	Luco dei Marsi (Strada 42)	NW-SE	NE	>3	none	0.8 (last 1500)	1000–1800 (1500)	2	1915 AD; 500–1500 AD	0.1; 0.15
11	Luco dei Marsi (Strada 45)	NW-SE	NE	>3	none	0.8 (last 1500)	(s.a.a.)	2	1915 AD; 500–1500 AD	0.1; 0.15
12	San Benedetto dei Marsi	NW-SE	SW	>3	none	1.0–1.6 (last 2000)	500–800	3	1915 AD; 885–1349 AD; 550–885 AD	ca.0.5; ca.0.5; >1
13	Piano di Pezza	N120E	SW	3.5	none	0.7–1.2 (Holocene)	800–3300 (5000)	2	860–1300 AD; 1900 BC	2–3.4; 1.2–2.5
14	Vado di Pezza	N135E	SW	12–16	none	(s.a.a.)	(s.a.a.)	3	860–1300 AD; 1900 BC; 3300–5000 BC	2–3.4; 1.2–2.5; 2.0
15	Campo Porcaro	N165E	W	6.5–11	5.5–8.5	(s.a.a.)	(s.a.a.)	2	860–1300 AD; 1900 BC	2–3.4; 1.2–2.5

Seismic reflection profiles (e.g. Cavinato et al., [60]) indicate that the Fucino structure is a half *graben* controlled by a master fault along the NE border of the basin, and parallel

subsidiary faults. The range fronts bounding the Fucino basin are fault escarpments and the whole geomorphic setting of the basin shows a clear tectonic control. In particular, the Quaternary activity of the master normal fault zone at the NE border generated several orders of lacustrine terraces. Over the Quaternary, these were progressively uplifted, tilted and faulted and younger terraces repeatedly developed in the down-thrown block. Therefore, sedimentation is mostly influenced by tectonics. In Fig. 8, the Quaternary terraces are grouped into three major orders, namely «upper», «intermediate» and «lower terraces» separated by prominent fault scarps.

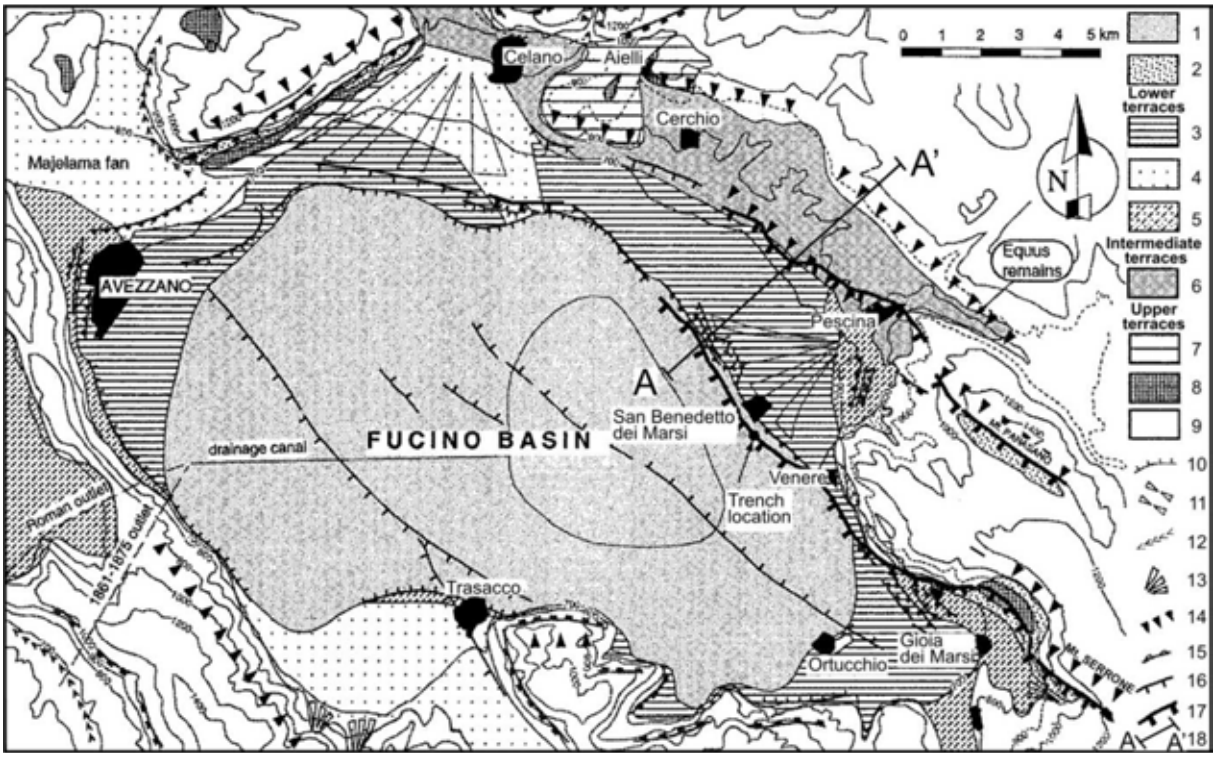

FIG. 8. Geologic map of the Fucino Basin, displaying the surface faulting associated with the January 13, 1925, M7 earthquake. The location of the Equus cf. Altidens site is also shown. Legend: 1) Historical lake; 2) talus deposits (late Glacial and Holocene); 3) alluvial deposits (Holocene); 4) alluvial fan deposits (late Glacial); 5) fluvio-lacustrine deposits (late Glacial); 6) fluvio-lacustrine deposits (middle Pleistocene); 7) fluvio-lacustrine deposits (late Pliocene-lower Pleistocene); 8) breccias (late Pliocene-middle Pleistocene); 9) sedimentary bedrock (Meso-Cenozoic); 10) fluvio-lacustrine terrace edge; 11) Gorge; 12) V-shaped valley; 13) alluvial fan; 14) fault scarp; 15) fault scarp within the lower terraces; 16) Holocene normal fault; 17) Holocene normal fault reactivated during the 1915 earthquake; 18) Cross section trace. Data are from Michetti et al. [26],.Serva et al. [52] and Blumetti et al. [53].

The interpretation of seismic reflection lines (Fig. 9) provides an estimate of ca. 1.6 mm/yr for the Quaternary slip-rate for the master fault of the basin. More locally, the total throw between a layer within the «intermediate terraces», dated ca. 1 Ma to 0.45 Ma through mammal remains (an *equid* of the latest Villafranchian to latest Galerian in terms of Mammal Age) found at 830 m a.s.l. and a tephra found at a depth of 100 m in the center of the basin dated to ca. 540 ka B.P (39Ar/40Ar age), constrain the long term slip rate across the section A-A' of Figure 8 to 0.3– 0.6 mm/yr (Fig. 10).

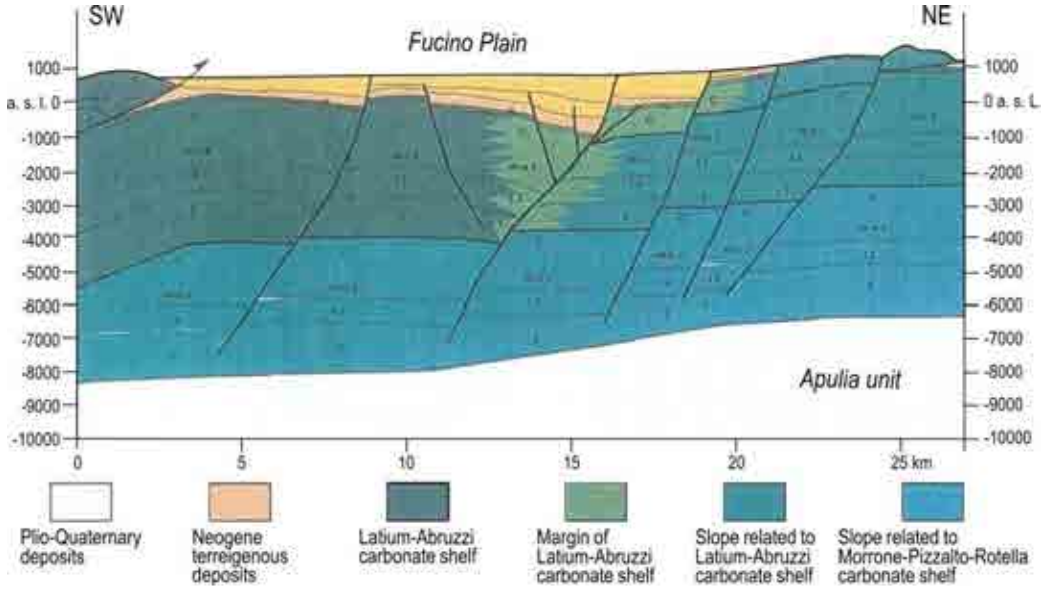

FIG. 9. Geologic cross section of the Fucino basin interpreted from seismic reflection profiles. Based on Cavinato et al. [60].

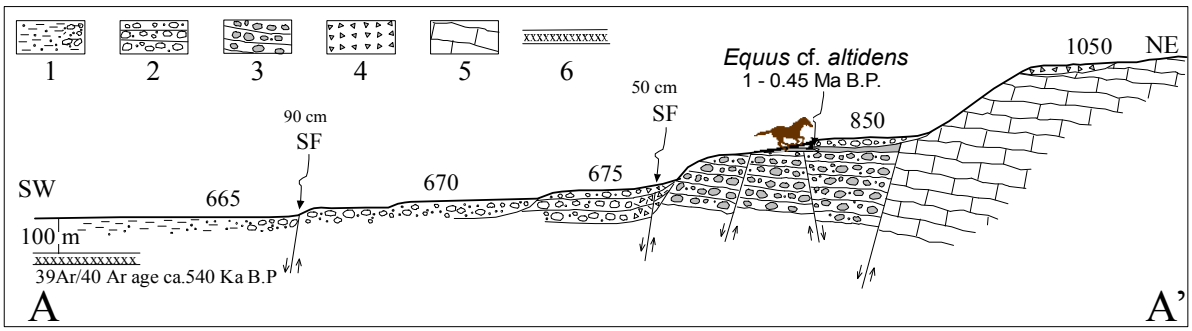

FIG. 10. Synthetic geologic profile across the Quaternary terraces at the NE border of the Fucino Basin (location in Fig. 8). The «intermediate» and «lower terraces» deposits are shown, whereas the «upper terrace» is represented here by an erosional surface with only a thin layer of overlying deposits. Legend: 1) Holocene deposits of the Fucino Lake; 2) Late Pleistocene to Holocene alluvial fan deposits; 3). Middle Pleistocene fluvial and lake deposits; 4). Pliocene?- Early Pleistocene? breccias; 5) Mesocenozoic pelagic limestone sequence; 6) Dated tephra layer; SF). Surface faulting occurred during the January 13, 1915 earthquakes. Reproduced with the permission of Serva et al. [11].

In the following section the results of several paleoseismic investigations carried out in the Fucino Basin and surrounding areas are summarized. This will lead to some considerations regarding the growth of the Fucino tectonic structures by repeated strong earthquakes.

Along the eastern border of the Fucino basin and its NW extension in the Ovindoli and Piano di Pezza area [54, 61], the Holocene paleoseismology and deformation rates have been investigated at several sites along the trace of the Celano–Gioia de' Marsi fault (sites 2, 3, 4, 5, and 12 in Fig. 1; Michetti et al., [26]; Galadini et al., [55]; Galadini et al., [57]), the Parasano–Cerchio fault (site 1 in Fig. 1; Galadini et al., [55]; Galadini et al., [57]) and the Ovindoli–Pezza fault (sites 13, 14 and 15 in Fig. 1; Pantosti et al., [54]) as described in Table 1.

It is possible to view these paleoseismic results in terms of variation in deformation rates and earthquake recurrence along a single tectonic structure. For instance, the extension rates vary with distance from Fucino basin's center. In fact, as already pointed out, most of the eastern part of the basin is bounded by two parallel normal faults, the Parasano–Cerchio fault (or

Marsicana Fault of Galadini et al., [57]) and the Celano–Gioia de' Marsi fault, both reactivated during the 1915 earthquake [52, 55, 62] and showing Holocene displacement. If extension rates observed along these two traces using the San Benedetto trenches (1.0 to 1.6 mm/yr; site 12 in Fig. 7; Michetti et al., [26]) and the Marsicana trenches (0.4 to 0.5 mm/yr; site 1 in Fig. 7; Galadini et al., [57]) are summed up, the cumulative value near the center of the segment is 1.4 to 2.1 mm/yr for a 45° dipping fault. This is significantly higher than the value at the NW termination of the Fucino structure in the Ovindoli–Piano di Pezza area, where a maximum extension rate of 1.0 to 1.2 mm/yr can be derived for a 45° dipping fault plane. Data in Table 1 also indicate that the variation in extension rates is probably due to a higher frequency of earthquakes per unit time at the center of the fault compared to its NW termination.

It is important to note that the NW lateral termination of the Fucino tectonic structure occurs within a high mountain area where Mesozoic carbonates outcrop in the hanging-walls of the Quaternary faults. The Quaternary throws on the faults are lower than a few hundred meters at this location [61, 63]. In contrast, the faults at the center of the Fucino basin are characterized by Mesozoic carbonates juxtaposed against Neogene - Quaternary sediments. As already pointed out, Quaternary fault throws at this location are in the order of 1–2 km. Therefore, the pattern of coseismic Holocene (short term) deformation recorded at the trench sites indicated above is consistent with the Quaternary (long term) geologic and geomorphic setting of the Fucino structure and its NW termination in the Ovindoli–Piano di Pezza area. This observation strongly suggests that the growth of the Fucino extensional structure can be interpreted as the cumulative effect of repeated earthquake rupture sequences throughout the Quaternary.

Other capable faults have also ruptured during Holocene earthquakes in the Fucino basin. Galadini et al. [57] have performed paleoseismic studies on two other faults in addition to the Celano–Gioia and Parasano–Cerchio Faults, and assuming that the faults dip at 45°, the implied rates of horizontal extension are ca. 0.4–0.5 mm/yr across the Trasacco and Luco de' Marsi faults. Therefore, the overall extension rate in the Fucino tectonic structure during the Holocene might be in the order of 3 to 3.5 mm/yr.

The following evolutionary model for the Fucino Basin can be proposed. The southern and western margins of the ancient lake that occupied the Fucino basin before the latest glacial are not known. High continental terraces at elevations up to 1050 m a.s.l. are stranded in the footwall of the Celano–Gioia dei Marsi normal fault. Most likely lacustrine sediments of the same age are buried below the modern deposits in the hanging-wall of this master fault. Seismic reflection data from Cavinato et al. [60] clearly show that continental deposits are several hundreds of meters thick toward the Celano–Gioia dei Marsi Fault. On the southern and western borders of Fucino Basin only the main younger terrace (at ca. 720 m a.s.l.) can be observed, forming a narrow *banquette* (i.e. abrasion lacustrine platform) at the foot of the mountain slopes. Since all the available data indicate that Fucino basin was an endorheic, closed depression over the whole Quaternary, it is very difficult to think that erosional processes could have obliterated any trace of the previous terraces. We can conclude that the Fucino Basin extended progressively to the west and to the South following the continuing Quaternary hanging-wall subsidence of the Celano–Gioia dei Marsi normal fault segment. The most spectacular evidence of this process was the geomorphic change observed during the Jan. 13, 1915, Avezzano earthquake. Therefore, (a) the sequence of lakes that occupied this depression, (b) their size and (c) the related landforms (fault scarps, flights of terraces)

and deposits, all appear to be mostly controlled by active extensional tectonics capable of producing strong seismic events, with a maximum magnitude in the order of M_w 7.

Of course, during the site evaluation for nuclear installations, typically it is not possible to obtain a similar amount of paleoseismic data as is now available for the Fucino basin. However, this case history can be used as a test site for understanding the value and limitations of paleoseismic analyses. It also shows how the accurate mapping of Quaternary deposits and landforms at the near regional scale, which is clearly recommended in IAEA SSG-9 [1], provides the basic information for a proper characterization of the local seismic potential.

2.1.6.2. The Muzaffarabad earthquake fault, Pakistan: Paleoseismology problems for geologists in developing nations, and the lack of a complete and reliable geologic database

In the field of paleoseismology, the basic short comings being faced by the geologists of developing nations are due to the lack of appropriate knowledge, inadequate experience and fewer opportunities to share their knowledge and experience.

Generally, science and technology are not priorities of developing nations' governments particularly when it does not contain short term material benefits. Keeping in view these conditions, this publication addresses the basics of paleoseismology and provides a simple and clear guideline for such studies. The regulatory bodies in developing nations have either not been formulated or they are inefficient, and therefore, the methodologies, standards and minimum requirements may not be available or not well defined. Although the publication is not intended for such purposes, the content and its arrangement may indirectly provide such information in generalized form.

Instrumental and historical seismicity data are generally used and relied upon for seismic hazard assessment in developing countries, as this office-based activity is far cheaper than fieldwork campaigns. The devastating October 8, 2005, M_w 7.5 Muzaffarabad earthquake (e.g. Kaneda et al., [64]; Ali et al., [65]; Fig. 11) occurred along a fault which had no previous record of instrumental or historical seismicity, although it was suspected to be capable on the basis of the structural setting. The tectonics, dynamics, distribution and direction of stress and local structural framework are essential elements of paleoseismic studies. They provide the basis to discriminate between coseismic and non-tectonic deformation features and allow intensities to be loosely assigned to blind seismogenic faults.

As observed by many workers (e.g. Avouac et al., [66]), during the 2005 earthquake the majority of the landslides occurred on the hanging-wall in the close vicinity of the rupture (Fig. 11). Similarly, the frequency and intensity of fractures/cracks are high on the hanging-wall along the rupture. In active fold and thrust belts, the hanging-wall generally constitutes topographic fronts i.e. linear high land along the thrust. Consequently, the preservation of paleoseismic evidence is poor due to the higher degree of erosion on the hanging-wall. The preservation is, however, relatively better on the footwall. The majority of environmental effects are also modified soon after the event. Is the paleoseismic evidence collected from the footwall representative of actual intensity? If not it could lead to underestimation of intensity and hazard. It should be possible to discriminate the environmental effects on hanging-wall and footwall and to assign an according intensity with respect to their location, position, degree and size of deformation.

It is also very difficult to assign an intensity when the seismite is either partially preserved or has been modified. In the case when thrust and fold belts are marked by closely spaced stacked thrusts, it becomes difficult to relate the seismites with a particular thrust. It is also hard to decide whether the seismite is of the hanging-wall of one thrust, or the footwall of another. The amount of slip associated with rupture, along which successive events have occurred, is also difficult to ascertain. Precise dating of events is also another issue, particularly in arid or semi-arid areas where organic matter is poor. These two difficulties were partially overcome, unfortunately only after the 2005 earthquake, in Muzzafarabad thanks to Kondo et al. [67]. Who determined a net slip of 5.4 m and 5.0 m for the last and penultimate earthquakes, constraining this latter event between 500 and 2200 BP. Furthermore, discrimination of coseismic paleo-landslides from normal landslides on the basis of their modified scars and down-slid materials is also very difficult.

There are other difficulties which are being faced in paleoseismic studies. Some communication gaps among geologists, seismologists and engineers have also been noticed. One of the important lessons learned from the study of the Muzaffarabad earthquake is the large uncertainty still existing today in the identification of distribution and amount of surface faulting, even for large magnitude earthquakes, when the epicentral area is located in remote mountain regions, or with difficult political situations. The assessment of surface rupture length in the literature, for instance, varies from ca. 60 to more than 100 km (e.g. Ali et al., [65]). It should be remarked that the NW sector of the epicentral area was only surveyed in the field by a few aftershock teams due to the difficult logistic setting. This is more the rule than the exception in most seismically active regions worldwide. Existing databases of surface faulting should, therefore, be regarded as largely incomplete, and the associated wide epistemic uncertainty must always be taken into account when using empirical relations between earthquake rupture length/displacement and source parameters.

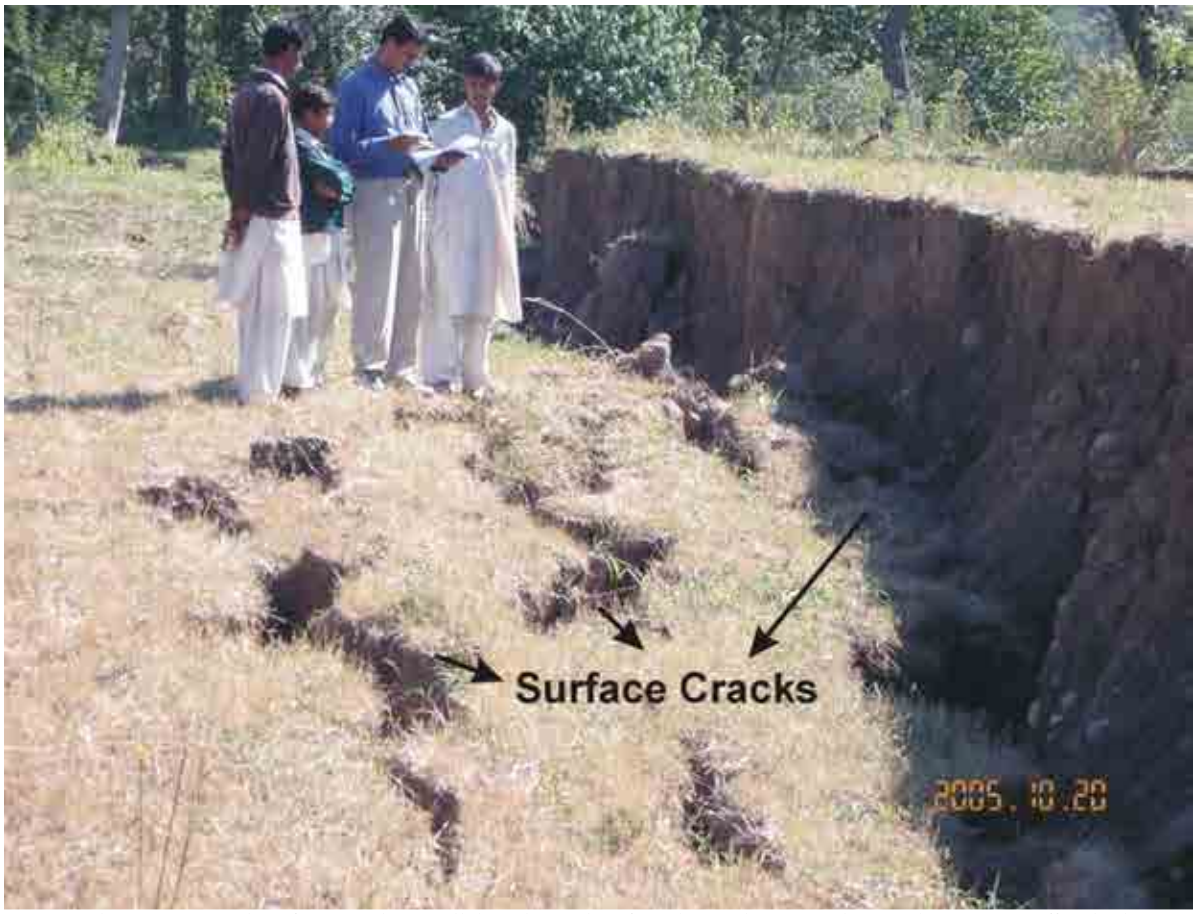

FIG. 11. Thrust-generated surface cracks parallel to the strike of Kashmir Thrust in Chatter Jhatian, Muzaffarabad region, most likely related to deep-seated slope gravity deformation triggered by the coseismic surface rupture. Photo taken by the Micro Seismic Studies Programme Team, Islamabad, on October 20, 2005, 12 days after the October 8, 2005, M_w 7.6 earthquake main shock.

2.1.6.3. The Quaternary thrust faults near Brescia, Northern Po Plain, Italy, and the issue of secondary surface faulting along capable structures

This case history provides clues on how to use secondary surface faulting and liquefaction for constraining source parameters in a tectonic setting characterized by 'blind' thrust faults.
A belt of segmented 10 to 20 km long fault-propagation folds with evidence of Quaternary activity, sitting above S- and N-verging out-of-sequence thrusts, have been identified in the frontal sector of the Southern Alps beneath the Po Plain. The formation of this belt is mostly related to the Oligo-Miocene Alpine tectonics (e.g. Fantoni et al., [68]). However, displacement along these thrust can be observed to grow even during the Pliocene and Pleistocene, as shown by available high-quality seismic reflection industrial data (Fig. 12; [69–71]). A typical example of the recent activity along these structures is illustrated by the Capriano del Colle fault-propagation fold (e.g. [72, 73]).

The surface expression of the late Quaternary growth of this structure is the Monte Netto hill. This is an 'isolated relief' in the piedmont belt of the Brescia Southern Alps, which was already interpreted by Desio [74] as evidence of active tectonics and strong local seismic events. Based on the analysis of syn-growth depositional architecture observed on the seismic reflection data and on the outcropping mid Pleistocene to Holocene fluvial and loess sequence, Livio et al. [72] assessed an uplift rate at Monte Netto of 0.1 mm/yr in the last 200 kyr.

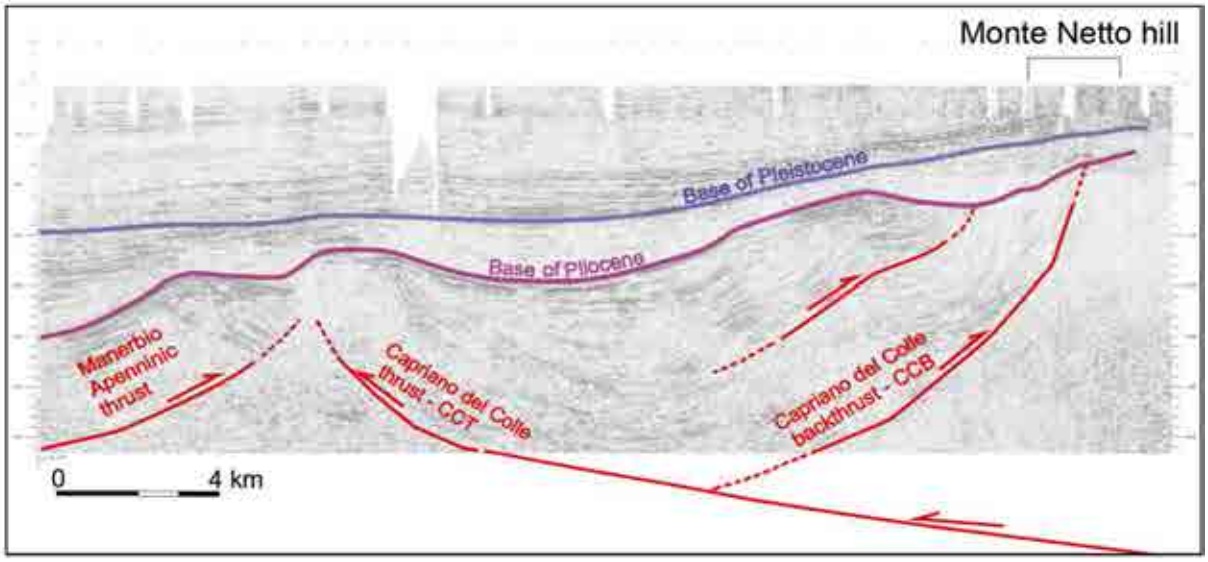

FIG. 12. Interpreted seismic section (courtesy of ENI E&P) along the Capriano del Colle structure; the Capriano del Colle N-verging thrust affects the whole succession, with displacement of the Oligo-Miocene strata and folding in the Plio-Quaternary sequence; the S-verging thrust is also interpreted to fault the Oligo-Miocene and fold overlying Plio-Quaternary strata. The Capriano del Colle hill is located on the surface projection of the N-verging thrust. Based on Michetti et al. in 2012 [75].

At the summit of the Monte Netto hill quarry excavations exposed recent continental sedimentary units, clearly folded and faulted (Fig. 13). Evidence of paleoseismicity has been observed along the quarry walls. The alluvial horizons in the core of a decametric anticline in the Northern border of the quarry are characterized by well-preserved paleoliquefaction features. Moreover, the crest of the anticline is affected by bending-moment faults, along which it is possible to observe the stratigraphic signature of several earthquake surface faulting events.

The stratigraphic and structural characteristics of the secondary surface faulting and liquefaction observed at the Monte netto site clearly show that these features were generated during strong local earthquakes. Similar environmental effects are typically associated with a macroseismic intensity > IX in the MCS, MM and MSK scales (e.g. [40, 76, 77]) and are, therefore, consistent with the environmental effects of an earthquake like the Dec. 25, 1222, Brescia event (Fig. 14).

Maximum expected magnitudes for compressional structures that are deforming at such low strain rate can be derived from an analysis of several scenarios of reactivation, including uncertainties related to each fault's geometry. Considering subsurface fault length, width, fault area and net dip-slip rates, the range of derived M_w for these structures can be estimated based on scalar relationships between fault parameters and the maximum expected magnitude (e.g. Wells and Coppersmith, [78]).

FIG. 13. Details of the paleoseismic surface faulting (left) and liquefaction (right) exposed at Monte Netto site, in a quarry site.

Taking into account the source complexity which is typical of similar compressional structures, the Michetti et al. [75] interpreted for the causative events a magnitude interval of M_w = 5.9– 6.8.

These values are consistent with the maximum expected magnitude (Mexp) derived for these structures by Serva [79]; Mexp = 6.8 for his 'Sistema Verona – Brescia', in the framework of the NPP siting research conducted in Northern Italy. Historical data show in fact a similar seismic potential, as illustrated in Figure 14.

It should be emphasized that no evidence of surface rupture during the Salò, earthquake, whose epicenter was located ca. 35 km NE of the Capriano del Colle site, has been observed. More recently, there was no surface faulting documented during the Emilia earthquake sequence. This sequence included two major shocks with M_w 5.9 and 5.8 on May 20 and 29, 2013, respectively [80], whose epicentral areas were both located ca. 150 km SE of the Monte Netto site. This supports the notion that the observed secondary surface faulting at Monte Netto is indicative of earthquakes with M_w greater than 6.0.

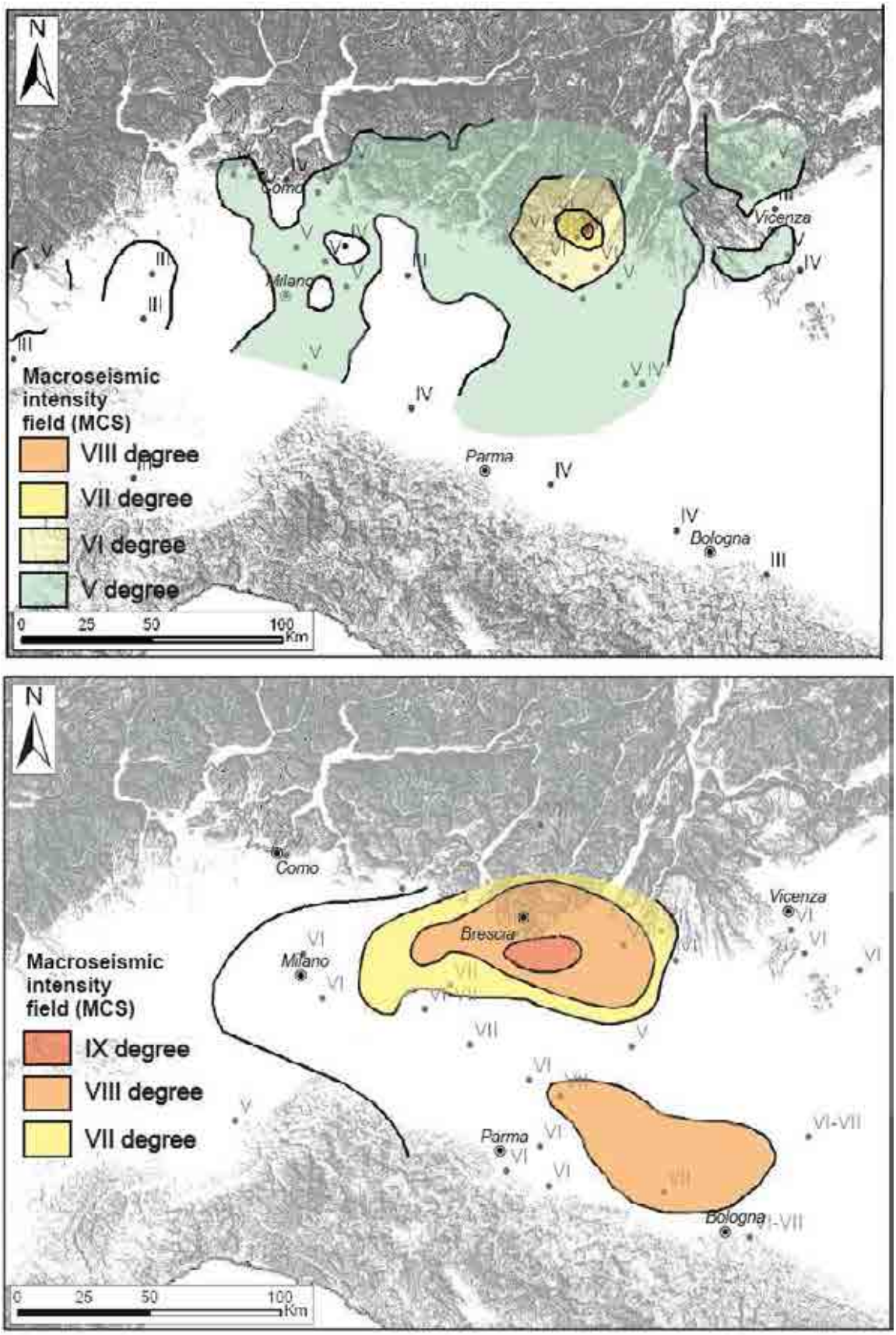

FIG. 14. Intensity map (MCS scale) for the (a) Nov. 24, 2004, Salò earthquake (INGV 2004) and (b) Dec. 25th, 1222, Brescia earthquake. Reproduced with the permission from Livio et al. [70].

2.1.7. Case histories: intraplate settings

2.1.7.1 The hazardous faults in the Central Andes: Challenges for understanding their seismogenic capability through paleoseismic studies

Only a few examples of historical primary coseismic surface ruptures are known along the Central Andes [81–84] and most of them do not reasonably match the common empirical relationships used worldwide for estimating the size of paleoearthquakes (i.e. coseismic displacement, rupture length). Therefore, there are few proxies for understanding the correspondence between the seismogenic potential of capable structures at these crustal settings and their surface signatures.

Parameters which have proved to be useful for well-studied interplate faults (i.e. slip rate, recurrence interval, and so on) are often difficult to gather at medium- to low-slip rate structures within these intraplate settings, even if their seismogenic potential is significant. Most of the already known Quaternary structures have not been studied using modern paleoseismic methods. Accordingly, their characterization as seismogenic sources in a suitable format for the seismic hazard model is commonly inadequate or implies considerable epistemic uncertainties.

Requirements established by regulatory agencies in many countries for defining the hazard related to a specific structure or area have commonly been imported from the experience arising from studies along interplate faults in other regions. For instance, definitions widely used such as ´active´, ´capable´, ´potentially active´, etc., are often merely based on the age of the last movement and/or on the number of events during a certain time span without a clear appreciation of the local seismic landscape. In fact, in intraplate settings `activity` and `hazard` may not be equivalent concepts; they may even have an opposite meaning (i.e. the most ´active´ fault may not be the most hazardous), due to clustering of paleoseismic events. Thus, results arising from paleoseismic investigations under ´standard formats´ could be inappropriate or even misleading for users; although continued studies in this setting will provide a longer time window which will make paleoseismology a mandatory input for SHA applied to nuclear installations. This is particularly the case in America where the seismic catalog covers a time span much shorter than the seismic cycle of most crustal seismogenic sources.

In paleoseismic studies there are many challenges that must be met in order to provide the data required by SHA as described in the IAEA SSG-9 [1]. This is because in order to document a suitable number of events for deriving parameters such as slip rate and recurrence interval, the excavation of deep trenches and/or a significant number of them may have to be carried out - a situation not always affordable. Another aspect even more difficult is to understand is whether a certain structure is significantly late or `overdue` in its seismic cycle. However, even if reliable and complete paleoseismic records are difficult to obtain, the definition of the ´threshold earthquake´ (the minimum earthquake magnitude to produce surface rupture at a certain crustal setting), based on a proper assessment of the local seismic landscape, can provide better insights on the reliability of the seismic catalog and, therefore, can assist in the SHA.

On the other hand, at the interplate boundary along the Pacific region where the main seismic threat is posed by subduction earthquakes, foundations are designed to withstand a M_w 9.0 event, but the ‘capable fault’ issue, or the probability of surface ruptures (either primary ones or triggered by passive slip), is usually not taken into account.

Because some upcoming siting studies for nuclear installations might be characterized by the lack of suitable neotectonic background studies or by the critical revision of studies done decades ago, it is considered necessary to: i) provide guidelines encompassing these complexities in different tectonic settings, with clear statements about scope, limitations and uncertainties carried by paleoseismic studies for SHA, and ii) encourage the training of professionals and the involvement of multidisciplinary teams throughout siting studies; here, neotectonic practitioners should learn how to upgrade the traditional neotectonic data into seismogenic sources, making sure that the full range of paleoseismic evidence is used for a better characterization of capable faults.

2.1.7.2. Shallow, capable and seismogenic faults in Alpine region of France (the Middle Durance and the Vuache faults)

The Middle Durance Fault (MDF) is an 80-km-long fault system in Provence, southeastern France. This fault system has a moderate and recurring historical seismicity [85], Quaternary tectonic activity [86] and some paleoseismic evidence of large events [87, 88]. The major fault line is a NE-SW oblique ramp with a sinistral-reverse slip, structurally connected with E-W folds and reverse faults (Luberon and Trévaresse thrusts).

The fault system has been extensively studied with complementary methods and techniques [89], from geomorphology to deep geophysics, space geodesy and Quaternary geology. The MDF is also one of the rare slow capable faults in Europe that has been monitored with a dedicated and dense seismometric network. The fault system is segmented in map and cross section views; it consists of staircase basement faults topped by listric faults deep seated in Triassic evaporitic beds. Seismic sections allowed the construction of a 3-D structural model used to accurately locate microseismicity [89]. According to microseismicity records, the southern part of MDF seems to be slipping mainly above a depth of 5 km. In this part, the fault can typically be considered as a shallow-depth fault, which moves above a decollement level which uncouples sedimentary cover from its basement. In its northern part close to the Subalpine nappes, seismicity deeper than 8 km was also recorded, meaning that this seismogenic structure might involve deep-seated fault segments within the crust.

Paleoseismic trenches were performed and analyzed for two segments of the MDF. During the early ‘90s a trench was excavated near Manosque city (segments 3–4) and results were published by Sébrier et al. [87]. These authors interpreted a knee-fold in recent deposits (26 ka) as evidence of a reverse-type paleoearthquake along this transpressive segment of the MDF. The undeformed Holocene deposits (9 ka) unconformably overly the inferred fault branch. Despite the scarcity of information the authors then suggested the occurrence of one big earthquake of a magnitude greater than 6.5.

More recently, the paleoseismic history of the Trévaresse fault, one of the E-W reverse structures associated with the MDF, has been investigated. This structure is actually a ramp anticline developed above a reverse fault active during the Neogene. Even if this seismogenic source is only 10 km long, it has been suspected to be the source of the most damaging earthquake in France during the 20th century, the so-called M≈6 Lambesc earthquake [90, 91] and, thanks to a detailed geomorphic analysis of the Trévaresse ridge, Chardon et al., [88] evidenced the existence of a cumulative fault-scarp caused by repeated earthquake activity. After trenching, they also proved the occurrence of surface ruptures caused by several successive earthquakes, including the M≈6 1909 event. The slip rate on that southernmost

segment of the MDF system is low and estimated to be between 0.05 and 0.3 mm/a. The recurrence time period for characteristic M≥6 events is then between 700–5000 yr.

The seismogenic potential of the MDF system can be assessed thanks to the source size and segmentation, and also its estimated slip rate. These imply that the upper bound magnitude ranges between 6.0 and 6.5, with a return period of a few thousand years [89]. Aochi et al., [92], thanks to dynamic rupture simulations, estimated probable scenarios with rupture lengths up to 45 km implying magnitudes up to 7 in scenarios where the basement is involved in faulting. The (scarce) available paleoseismic data seem more consistent with the seismic potential assessment from the former authors. The available mapping and neotectonic/paleoseismic data allow a rather precise trace of this capable fault to be defined.

Further north, another typical Quaternary fault of 'peri-alpine' France is the Vuache fault (VF). This left-lateral fault recently generated a shallow, low magnitude (M_s≈5) but damaging earthquake in 1996 close to Annecy, Eastern France [93]. This fault has not been extensively studied like the MDF fault system; however, the 1996 seismic event and a recent neotectonic study [94] contributed to the seismic hazard assessment of this particular structure. The VF segments can be mapped over 60 km from the subalpine front west to the Jura range. During the 1996 earthquake, surface cracks and even small left-lateral offsets were observed along the fault trace in alluvial deposits [93]. Thanks to its geomorphic expression, it is possible to observe the cumulated sinistral throw of the fault as it has regularly displaced the Quaternary drainage network. According to stratigraphic correlations, a mean slip rate of 0.15–0.4 mm/a has been inferred. Evidences of Quaternary deformation and paleoliquefaction have also been observed along the fault, but until now the investigations have not revealed any recurrent activity or sizable paleoearthquakes. Like the MDF, the VF is recognized thanks to shallow (2 to 4 km) industrial seismic lines in the sedimentary cover above a decollement level, and even though not proven a structural connection with a basement fault cannot be ruled out [94].

The seismic potential of the Vuache fault has not been completely identified. Historical and instrumental seismicity in the nearby area is concentrated within the very-shallow part of the crust, and thus tends to minimize the magnitude of possible earthquakes to M≈5. However, the possibility of a connection between the surface and deep-seated faults might drastically increase the possible magnitude to M≈6.5. The capability of the fault to rupture the surface is particularly prominent here despite the severe erosional capacity during recent cold periods.

Paleoseismology was largely used to obtain compelling evidence of large past earthquake along rapid faults (slip rate over 1 mm/a). The aforementioned examples show that the seismic hazard of slow capable faults can be assessed using 'classical' methods. Despite their low slip rates and the actions of climatic forcing (erosion/sedimentation), cumulative throws over long periods can be evaluated thanks to detailed geomorphic indices of fault activity and/or geophysical studies, and on-fault earthquake-related offsets or soft-sediment deformations can also be observed. These two examples also highlight the basic and crucial role of deep geophysical prospection to constrain the seismic hazard of a fault, which is particularly striking for buried capable faults (for example, the accurate knowledge of capable faults at the northern Apennines front would not be so acute beneath the Po plain without the seismic lines' tight mesh). For instance, the coupling of 3-D fault geometry imaging and accurate location of microseismicity provided a robust model of the MDF sources, and consequently its seismic hazard assessment could be refined. The examples also clearly show the suitability of a comprehensive 'paleoseismic' approach to explore the two seismotectonic issues of nuclear siting, i.e. surface faulting and ground motion. With respect to fault

capability, the available data in these examples from France are too sparse and scarce to feed a probabilistic evaluation of fault displacement hazard for an existing nuclear installation (PFDHA). However, according to SSG-9, the available knowledge is sufficient to define avoidance perimeters for future sites. With respect to the ground motion issue, the available data can be exploited to define the fault parameters in order to be included in a fault-source model for PSHA or DSHA (slip rate, Mmax, geometry, 1st order mapping).

2.2. PALEOSEISMIC CHARACTERIZATION OF DIFFUSE SEISMICITY

2.2.1. Introduction

Seismicity which cannot be attributed to specific faults or seismogenic structures must be regarded as dispersed activity. This is referred to as 'diffuse seismicity'. By this definition, only off-fault types of geologic environmental earthquake effects (EEE) considered in the ESI-07 Macroseismic Scale [77] should be used for the characterization of diffuse seismicity, and they should be regarded as special kinds of paleoseismic evidence. The most important indicators of diffuse seismicity are:

- Paleoliquefaction features;
- Disturbance of certain sediments and sedimentary layers from lacustrine and cave environments;
- Paleolandslides;
- Geomorphic and microgeomorphic evidence.

Geologic evidence comes mainly in the form of paleoseismic indicators known as 'seismites' as first suggested in the pioneering publication of Seilacher [95] and subsequently analyzed by Montenat et al. [96].

As a consequence, investigations of such effects will only deliver indirect constraints and assessments of earthquake processes in comparison with the on-fault investigations discussed in Section 2.1. The different methodological approaches and investigative techniques regarding off-fault effects will be discussed in this Section, including their restrictions and pitfalls. A summary of the specific dating techniques suitable for each type of investigation will be explained in Section 2.4. The specific consequences of possible misinterpretations of EEE features will also be discussed.

In areas where surface faulting is absent or unclear (diffuse seismicity), the best approaches come for the study of multiarchive paleoseismic records provided by a variety of secondary earthquake effects (EEE) as mentioned above (lake seismites, speleoseismites and slope movements). In the case of multiple paleo-earthquake evidence being present in a specific area, an integrated paleoseismic research study is feasible from lake, cave and geologic slope records (e.g. [97]). Following these criteria and depending on the size of the earthquake (magnitude), the attenuation/amplification effects (intensities), and the geographic distribution with respect to the suspected macroseismic epicenter, the same geologic archive or several different ones can be affected by a given event. Furthermore, these archives can contain evidence for repeated events from the same seismogenic source or from different sources existing in the same area (Fig. 15).

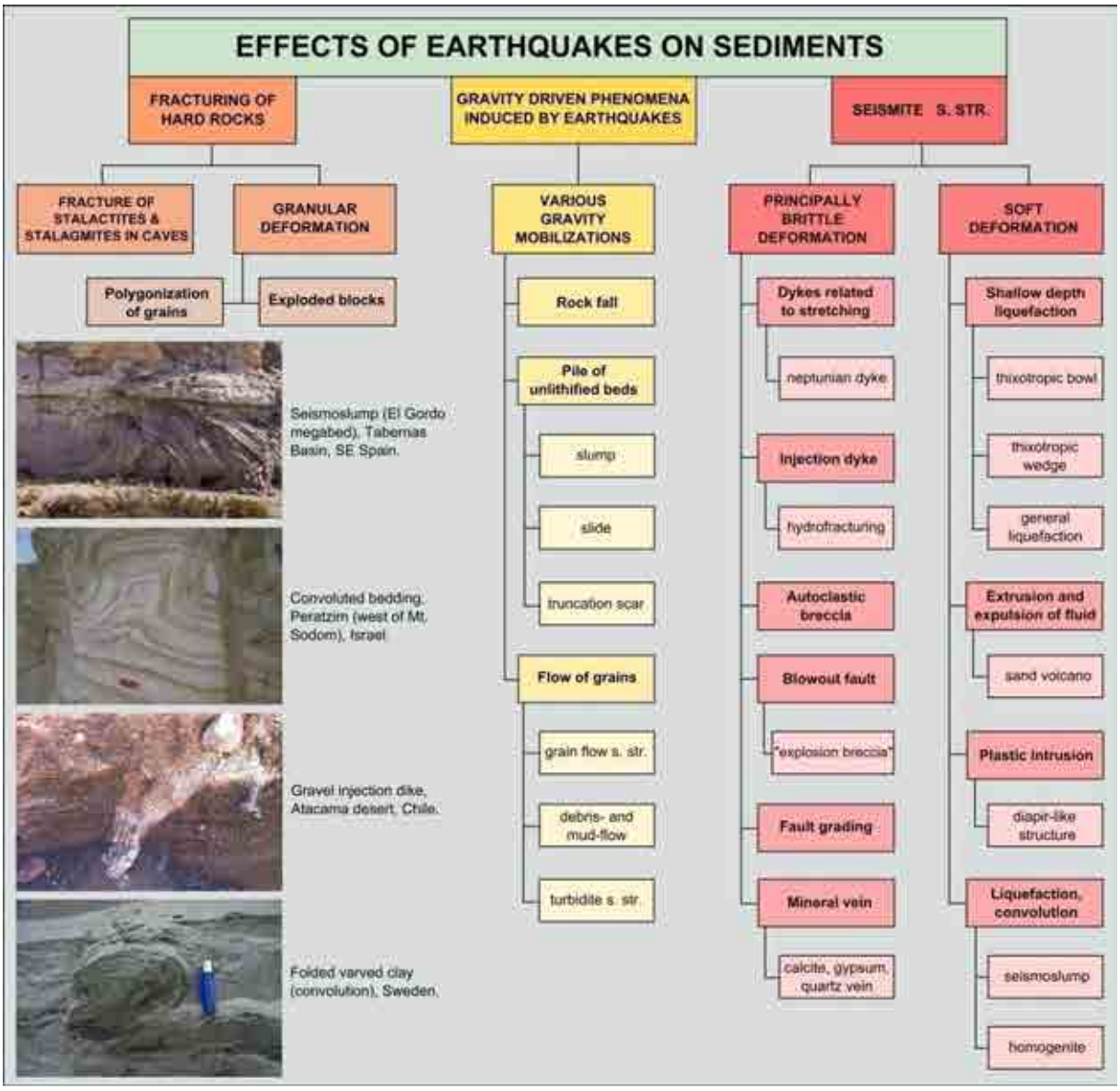

FIG. 15. Attempt of a classification of seismites and related earthquake-induced features (Based on Montenat et al. in 2007 [96]).

In areas where surface faulting occurs, a combination of primary and secondary earthquake effect analyses will offer the best scenario for the reconstruction of the area's seismic history. This will provide the most accurate image for calculation of the potential seismic hazard based on ground motion history and size during single or multiple paleoseismic events evidenced in the geologic record (Fig. 16).

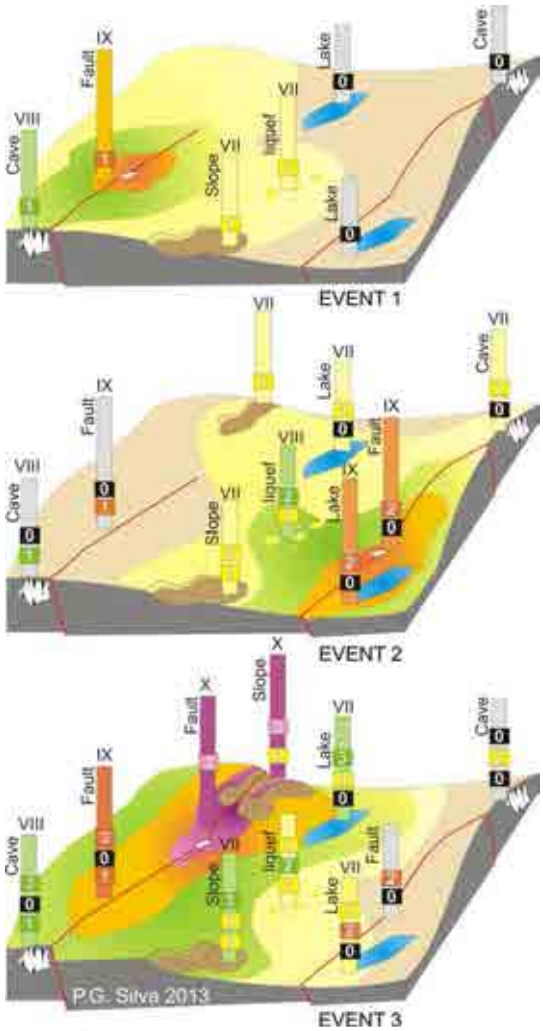

FIG. 16. Sketch illustrating the concept of integrated paleoseismology using the lake, cave, slope, and active fault geologic archives. The chance to achieve a complete record of pre-historic strong earthquakes in a region is highest if the evidence from different geologic archives and different sites is combined. In absence of fault surface ruptures the illustrated archives of secondary earthquake environmental effects can be used in a similar way. Based on Becker et al. in 2005 [97].

In any case, if paleoseismic activity is recorded in the area of interest the bracketed ages of the dated EEE (i.e. seismites) have to be coeval, or at least within the error range of the dated on-fault seismic events [97]. When on-fault paleoseismic evidence is absent, the coeval occurrence of a variety of secondary earthquake environmental effects in a restricted area between 10 to 100 km^2 is sufficient to determine paleo-earthquake occurrence (e.g. Michetti et al., [77]). These events are commonly shallow (< 10–15 km depth), of moderate-strong intensity (VII–VIII) and have associated magnitudes of ca. 5.0–6.5 M_s as documented in recent seismic events worldwide (e.g. 2011 Lorca, 2011 Canterbury and 2012 Emilia-Romagna earthquakes). Finally, it is necessary to note that far-field ground shaking from strong earthquakes can trigger relevant mass movements in susceptible areas, even at distances of some hundreds of kilometers from the epicenter [98].

This section does not refer to any specific tectonic setting: in fact, in all tectonic settings it is not possible to relate all paleoseismic evidence to specific active faults or seismogenic structures, which means that in every tectonic setting it is necessary to address part of the seismic activity as diffuse seismicity.

2.2.2. Paleoliquefaction Investigations

Liquefaction is a phenomenon that mainly occurs in saturated, loosely packed and relatively cohesionless sediment. When subjected to strong ground shaking the structure of the sediment is distorted and may break down resulting in an increase in pore water pressure, a decrease in shear strength, and sediment mobilization. An increase of pore pressure and loss of cohesion can, however, also be induced by processes like rapid sediment loading, ice-loading and -carving, deloading of ice, as well as by thawing of ice masses and disturbance of sedimentary layering. Other possible causes of liquefaction are volcanic eruptions and impacts.

Generally, the most common grain or particle sizes prone to overpressure of pore water, and hence liquefaction, are sands (Fig. 17). Other grain sizes are, however, also potentially liquefiable or susceptible to liquefaction. These range from gravel to clay, and an important factor for liquefaction potential is the sorting of the deposits [2]. Gravel venting has been frequently observed, e.g. during post-glacial rebound earthquakes in Scandinavia [99] or during the Borah Peak earthquake of Idaho/US in 1983 (in McCalpin, [2]). Galli, [100] provides a database on liquefaction in Italy and frequently observed 'mud volcanoes' associated with earthquakes. Another process to mention here is the injection of clays into open fissures, or into materials of larger grain size from below, due to differential loading. Reicherter et al. [101] observed clay dikes in silty material in the foundation of Aachen Cathedral, probably injected during a medieval earthquake with a magnitude higher than 5.5. This is the threshold magnitude where liquefaction generally occurs (Obermeier, [102]; see also ESI 2007 intensity scale in Appendix 2 of this volume).

Further important factors to be considered for the evaluation of ground failures in clays and silts during earthquakes are the Liquid Limit and Plasticity Index [103]. There is a vast amount of geotechnical publications on liquefaction potential which must be consulted and considered [103–107] when materials other than liquefiable sands are encountered. Liquefiable sands are described here in detail.

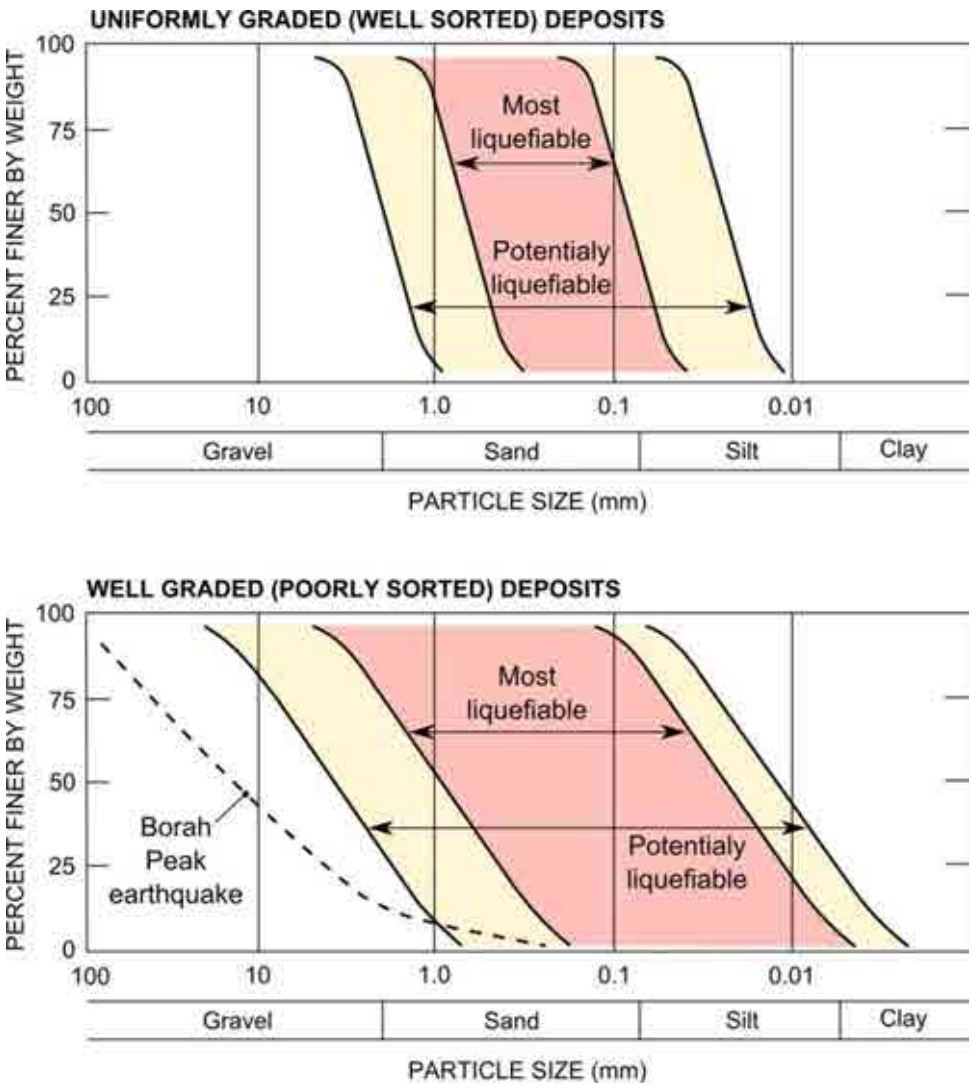

FIG. 17. Gradation curves showing grain sizes and gradations generally most susceptible to liquefaction (Based on McCalpin in 2009[2]).

Telltale signs of earthquake-induced liquefaction include intrusive sand dikes and sills, and extrusive sand blows or sand deposits vented on the ground surface. These all occur at the time of the event. Figure 18 is a schematic illustrating these relationships. Soft-sediment deformation features such as sand diapirs may also result from an earthquake-induced liquefaction event.

Paleoliquefaction (PL) features serve as evidence of past strong ground motion. Studying these features preserved in the geologic record can help estimate ages, source locations, magnitudes, and recurrence intervals of large earthquakes. In some cases, PL features may be the only evidence of significant seismic activity in a region. Information collected from PL features can greatly improve knowledge of regional seismic hazards, leading to reduced uncertainties in hazard estimates.

This section on PL investigations is largely excerpted from Appendix E of the 2012 technical report, Central and Eastern United States Seismic Source Characterization for Nuclear Facilities (hereafter referenced as Technical Report [108]). Appendix E of this report, written by M. Tuttle and R. Hartleb and titled CEUS Paleoliquefaction Database, Uncertainties Associated with Paleoliquefaction Data, and Guidance for Seismic Source Characterization

(hereafter referenced as Tuttle and Hartleb [109]), provides a compilation of PL data in the CEUS, a review of each major dataset, discussion of uncertainties related to collecting and interpreting PL data, and guidance for use of PL data in seismic hazard analyses. Appendix E is available at http://www.ceus-ssc.org/Report/AppendixE.html, and it should be consulted prior to embarking on a study of PL features for use in seismic hazard analysis.

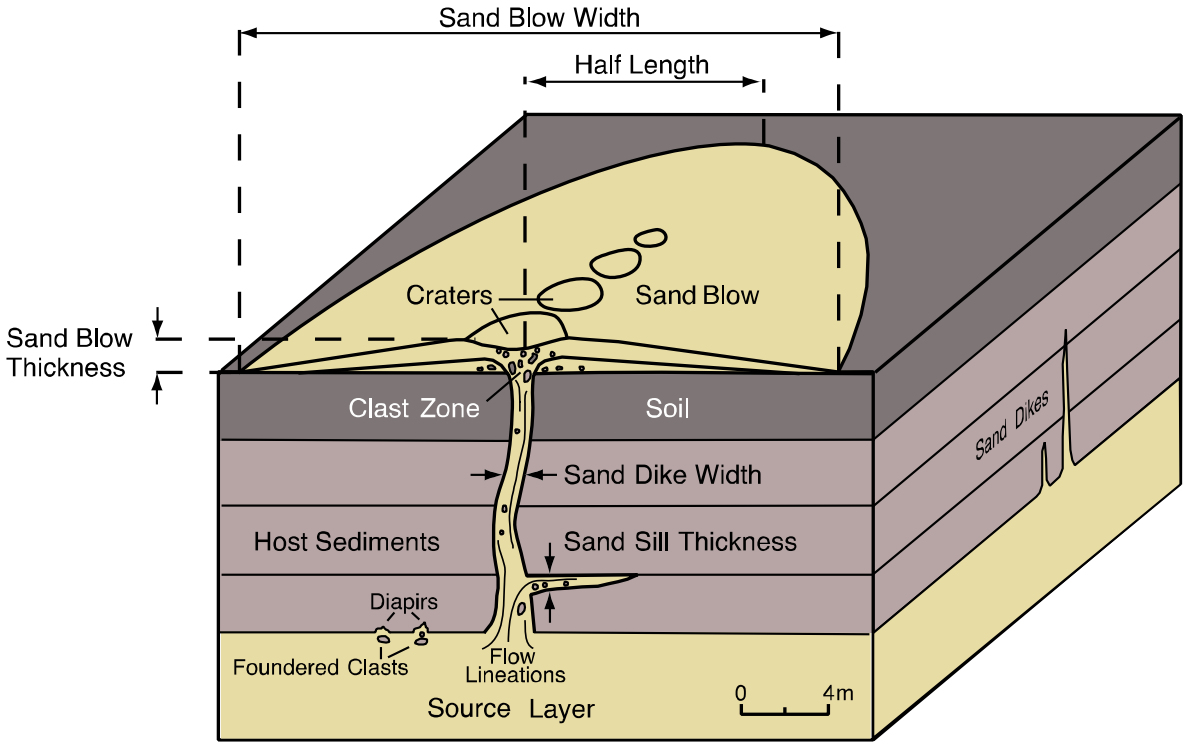

FIG. 18. Diagram illustrating size parameters of liquefaction features including sand blow thickness, width, and length, sand dike width, and sand sill thickness, as well as some of the diagnostic characteristics of these features (Reproduced with permission from Tuttle and Hartleb in 2012 [109]).

2.2.2.1 Detection

PL features form and are preserved in certain sedimentary and groundwater conditions. Liquefaction of sand is herein described as an example. First, a loose to moderately dense, sandy sediment at shallow depth must be water-saturated. A relatively impermeable confining layer, normally a fine silt or clay, is not required but will promote an increase in pore water pressure in the sandy layer during ground shaking. In order for PL features to be preserved, they must occur in an environment of sediment accumulation or relative stability, not in an environment of active erosion [31, 102, 110].

PL studies should be assigned to and conducted by investigators with experience locating and identifying PL features, and also the subsequent evaluation of the seismic hazard arising from those findings. If geologic conditions are favorable for the formation of PL features, aerial photographs and satellite images can be examined for light-colored elliptical to linear patterns indicative of sand blows. Landforms that are often underlain by sediments susceptible to liquefaction, such as river floodplains and old lake beds, are often productive agricultural lands, so aerial evidence of prehistoric sand blows may be obscured by modern agricultural activity unless the liquefaction features are large. Figure 19 shows how multiple sand blows can be expressed at the surface.

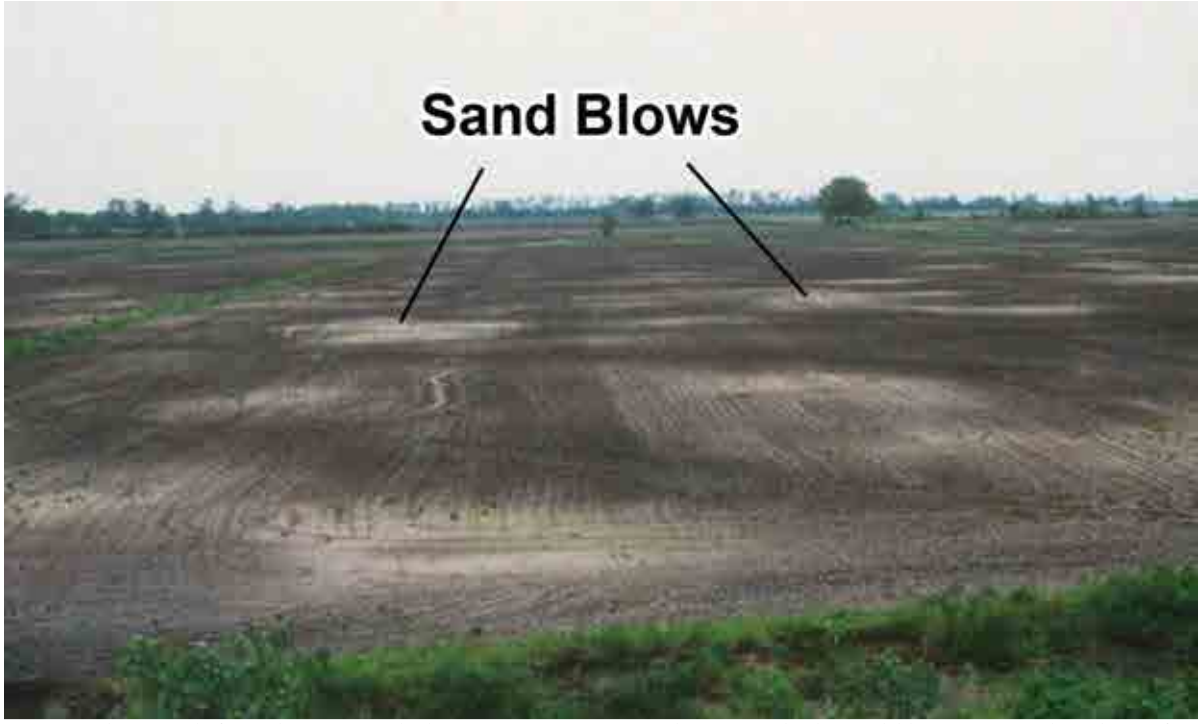

FIG. 19. Photograph from the New Madrid Seismic Zone, U.S.A., showing multiple sand blows expressed at the surface. Light areas are sands that were ejected onto overlying, darker silts and clays during liquefaction from a seismic event. These sand blows likely formed during earthquake sequences in A.D. 1811–1812, A.D. 1450, A.D. 900, and 2350 B.C. Reproduced with permission from M. Tuttle.

Possible sand blows identified on aerial photos and satellite images must be verified on the ground by excavating soil pits or trenches and may provide excellent targets for site investigations. Geophysical methods, especially electrical resistivity and ground penetrating radar, can be used to locate feeder dikes below a sand blow and to define a sand blow's thickness and lateral extent [111, 112]. This information is useful for siting trenches. Trenches are required in order to verify the presence of PL features, to collect samples for dating the PL features and estimate the timing of the causative earthquake, and to gather other information used to interpret the location and magnitude of the causative earthquake. PL features can also be identified through reconnaissance surveys on exposures of Quaternary deposits that include sediment susceptible to liquefaction. These surveys often focus on natural exposures provided by rivers, lakes, or ocean cut-banks. A stream bank exposure of an ancient sand dike and sand blow is shown in Figure 20.

Ground surveys should be planned with consideration of seasonal and tidal variations in water level (lower water provides more bank exposure) and the presence of vegetation or snow cover.

FIG. 20. River cut-bank revealing a sand dike, sand blow deposit, and buried soil beneath the sand blow. Reproduced with permission from M. Tuttle.

2.2.2.2 Dating strategy for PL features

Dating multiple PL features in an area is important for estimating the timing of the paleoearthquake that led to their formation. Organic material in a soil buried by a sand-blow can provide a close maximum age constraint. Organic material washed into a crater in the top of a sand blow, or organic material developed in a soil within a sand blow, can provide a close minimum age constraint. Organic material in sedimentary layers below and above a sand blow also provides maximum and minimum constraining ages. Some of these stratigraphic relationships are illustrated in Figure 21.

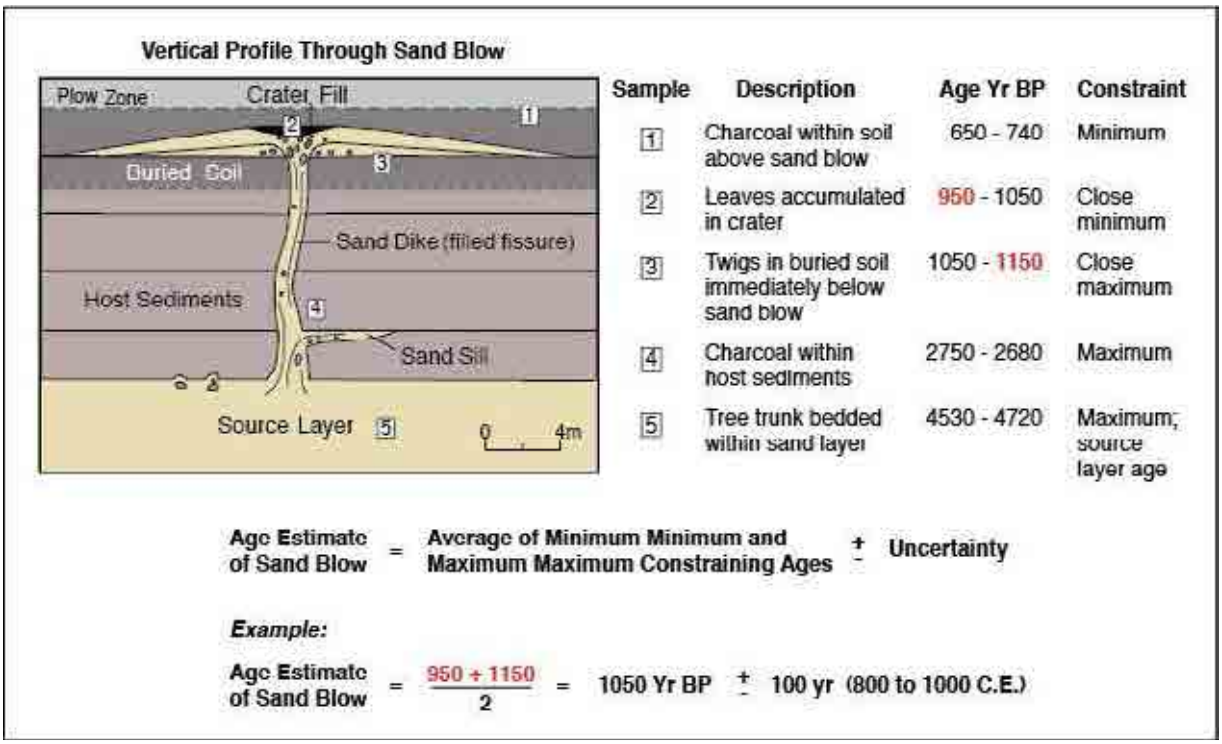

FIG. 21. Diagram illustrating sampling strategy for dating liquefaction features, as well as age data, such as 14C maximum and 14C minimum, used to calculate preferred age estimates and the related uncertainties of liquefaction features (reproduced with permission from Tuttle and Hartleb in 2012 [109]).

Dating of sand dikes that did not breach the paleosurface to form a sand blow can also provide age information about the timing of the causative paleoearthquake, but often with much greater uncertainty [31]. The maximum age constraint for a sand dike can be derived by dating stratigraphic units cut by the sand dike. Even in the best of circumstances, however, the highest stratigraphic unit cut by the sand dike may predate the formation of the dike by hundreds to tens of thousands of years. The minimum age constraint can be determined by dating a plant root, animal burrow, or cultural feature that intrudes the dike, as well as a sedimentary deposit that overlies an unconformity truncating the dike [31]. Such relationships are, however, rarely found.

Caution must always be exercised in examining stratigraphic relationships and selecting material for quantitative age analysis. All of the above mentioned techniques have potential pitfalls. A highly experienced Quaternary geologist should be consulted to identify and date PL features.

2.2.2.3 Interpreting liquefaction features

Most PL features are fairly easy to interpret in the field so long as they exhibit common diagnostic characteristics (see Tuttle and Hartleb, [109]). Chief among the diagnostic characteristics are sand dikes with subparallel sidewalls that usually widen downward, but may also broaden upward, into a vent structure at the (paleo) ground surface; sand blow deposits that are elliptical or linear and sometimes circular in plain view, and are connected to feeder dikes below, are also considered to be key diagnostic characteristics. Inexperienced geologists may, however, misinterpret ordinary sedimentary features and deposits as PL features. Several criteria have been developed by Obermeier [102] and Tuttle [31], as listed in Tuttle and Hartleb [109], to identify earthquake-induced liquefaction features:

1. Features have sedimentary characteristics consistent with case histories of earthquake-induced liquefaction. In other words, the features look similar to those that were observed following modern and historic earthquakes;
2. Features have sedimentary characteristics indicative of sudden, strong, upwardly directed hydraulic force of short duration;
3. More than one type of liquefaction feature is found and liquefaction features occur at multiple locations;
4. Features occur in geomorphic settings where the hydraulic conditions noted in 2) above are unlikely to develop in the absence of strong ground motion;
5. Age estimates of features support both contemporaneous and episodic formation of features over a large area.

Sand blows are the most commonly observed and useful PL features. These features result from the venting of over-pressurized pore water and entrained sediment onto the ground surface. They are often elliptical in plain view, reflecting the elongated shape of the fissure from which water-entrained sediment vented [113]. Sand blow deposits are usually thickest and coarsest near their vent, and they often contain clasts of the underlying strata. The ground beneath a sand blow may subside due to venting or removal of sediment from the layer that liquefied, so buried soil layers may dip toward the sand-filled vent structures and feeder dikes below. Ground failures may be symmetrical or asymmetrical. The structural relationships between sand blows and feeder dikes are observed in vertical sections provided by natural exposures or trenches. These characteristics help distinguish sand blows from fluvial deposits

such as overbank sediments or crevasse splays that also bury soils [109]. Figure 22 is a trench cross-section showing several PL features.

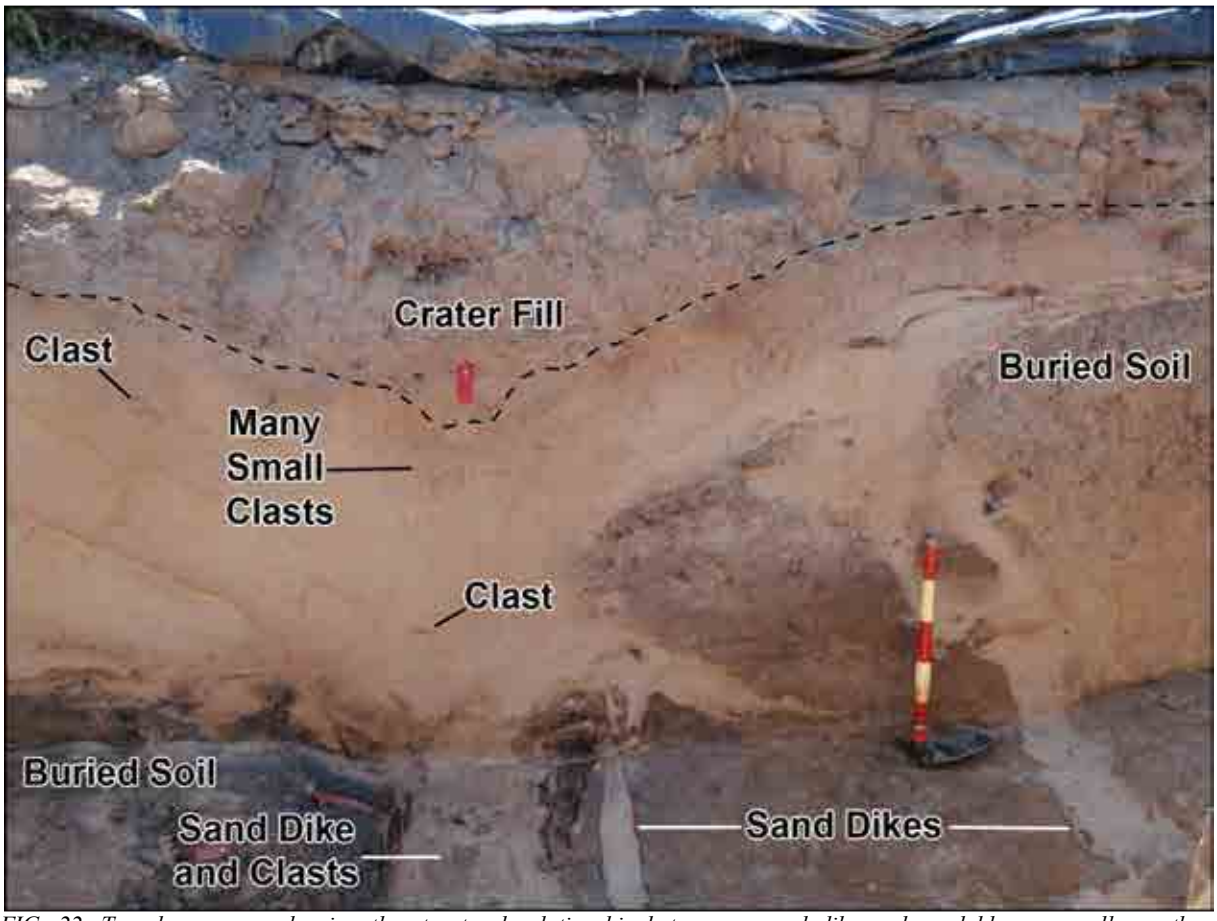

FIG. 22. Trench exposure showing the structural relationship between a sand dike and sand blow, as well as other characteristic PL features, such as entrained clasts, buried soil, and sand blow crater fill. Reproduced with permission from Tuttle and Hartleb in 2012 [109].

2.2.2.4 Derivation of characterizing parameters

If PL features are sufficiently abundant, and they have been adequately characterized and correlated across a region, the data can be used to estimate the ages, locations, magnitudes, and in some cases recurrence intervals of prehistoric earthquakes.

The comparison of the age ranges of multiple features is most useful to reduce the age uncertainty of an earthquake. A single PL feature is likely to have an age uncertainty of 100 years or more (and if considering the Finale Emilia earthquake in 2011, which occurred within 9 days of the first and had a similar magnitude of around 6, the spatial extent of liquefaction could easily be interpreted as larger due to irresolvable time resolution of the two events, and hence lead to larger paleomagnitude estimates). The intersection of overlapping age ranges from several PL features across a region, if they are believed to result from the same event, can provide a better estimate of an earthquake's timing. In addition to correlative age ranges, PL features assigned to a single earthquake should demonstrate a compatible distribution of feature size and stratigraphic setting. For example, a collection of PL features suspected to result from a single earthquake will, in general, show decreasing size away from the largest observed features, reflecting lower levels of ground shaking with increasing distance from the earthquake source. There may, however, be variations in the spatial

distribution and size of features related to site-specific sedimentary, hydrologic, and topographic conditions.

Analysis of multiple sand blows believed to result from a single earthquake can allow the source area of the earthquake to be estimated. Modern and historical earthquakes have demonstrated that sand blows generally decrease in size and frequency with increasing distance from an epicentral area [e.g. 100, 114, 115]. Therefore, the spatial distribution of contemporaneous PL features can point to a likely epicentral area of a paleoearthquake. In particular, the area where the largest features are concentrated is often interpreted as the epicentral area of paleoearthquakes, although with an uncertainty of several tens of kilometers or more. Such an analysis must consider that the spatial distribution and size of PL features induced by a single earthquake can have an asymmetric distribution based on a number of factors. These factors include the style of faulting, the directivity of the seismic energy, and the distribution of liquefiable sediments. If paleoliquefaction features can be directly related to a fault, as has been done with the Reelfoot fault in the New Madrid seismic zone, uncertainty in the location of the paleoearthquake may be reduced to just a few kilometers (e.g. [116, 117]). Despite the high uncertainty in locating paleoearthquake locations with paleoliquefaction features alone, even approximate source areas of large prehistoric earthquakes can be valuable additions to seismic hazard analyses.

The spatial and size distribution of contemporaneous PL features can not only provide estimates of epicentral locations, but also provide estimates of paleoearthquake magnitudes (e.g. [31, 102]). In general, larger PL features, and a broader spatial distribution of features caused by a given earthquake, indicate a larger earthquake magnitude. Such estimates have large uncertainties, perhaps as high as a full magnitude unit [109]. Uncertainties can be reduced by conducting comparative studies, using empirical relations and analyzing geotechnical properties of liquefied strata [31]. Several empirical relations using a worldwide database of earthquakes that caused surface manifestations of liquefaction, or sand blows, have been developed [e.g. 100, 114, 115]. These earthquake magnitude-liquefaction distance relations have been used in paleoliquefaction studies to estimate magnitudes of paleoearthquakes using the farthest observed sand blow locations. Earthquake magnitudes estimated using these relations will usually be lower bound values, as the actual distance from epicenter to the most distant sand blow is unlikely to be known and the most distant small and sparse sand blows are likely to remain undiscovered [31, 115]. Note that this technique is suitable for use with sand blows, not sand dikes.

The timing of a particular paleoearthquake is determined by selecting an age range common to multiple PL features in a region. If multiple generations of PL features occur in a region, and the features and ages can be reasonably well correlated, a paleoearthquake chronology or space-time diagram, can be constructed (Fig. 23 [117, 118]). If there is confidence that the paleoearthquakes were centered in the same source area, they can be used to estimate a rate of recurrence for significant earthquakes in the area. The precision of the recurrence estimate depends on the precision of the estimated timing of the paleoearthquakes [31]. A recurrence rate of large earthquakes for a source area, even with high uncertainty, is a significant contribution to a seismic hazard analysis.

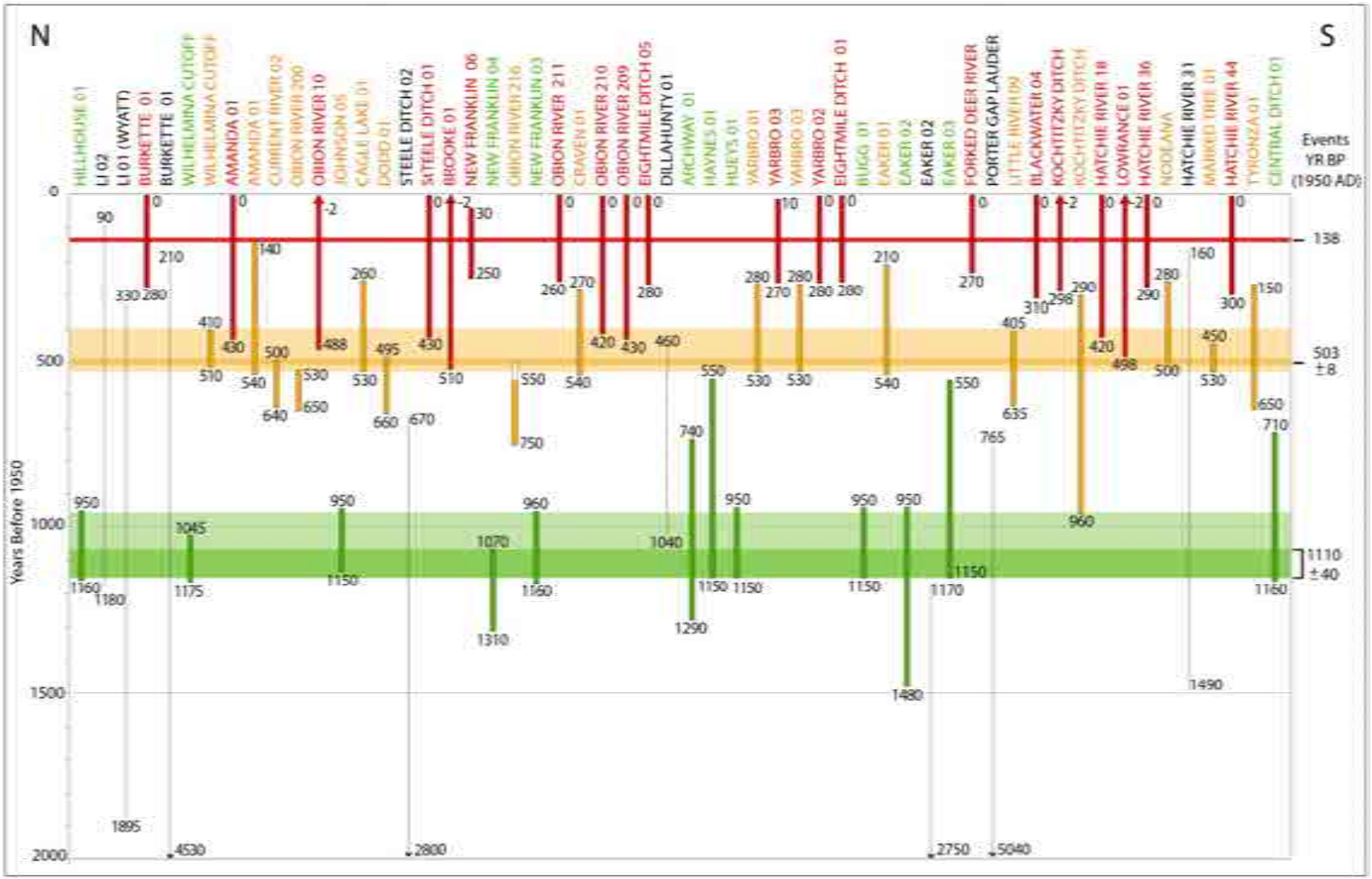

FIG. 23. Earthquake chronology of the New Madrid seismic zone for the past 2,000 years based on paleoliquefaction studies. Vertical bars represent age estimates of individual sand blows, and horizontal bars represent inferred event times based on intersection of overlapping age estimates: 138 yr BP (AD 1811–1812); 500 yr BP ± 150 yr; 1,050 yr BP ± 100 yr. Statistical analysis resolved event times with narrower uncertainty ranges of 503 yr BP ± 8 yr and 1,110 yr BP ± 40 yr, as indicated by darker portions of the horizontal bars reproduced with permission from Tuttle and Hartleb in 2012 [109].

An estimate of a regional recurrence rate must consider the completeness of the paleoseismic record and use judgment when using the rate in a seismic hazard analysis [109]. A recurrence rate based on observed PL features is likely to be a minimum rate, as some features may be at unobservable depths or have been removed during periods of erosion, and some earthquakes may go unrecorded at times of low groundwater conditions. The susceptibility of sediments to liquefaction may vary through time due to water table fluctuations, so some large earthquakes may not generate PL features. Furthermore, some earthquakes may have occurred in an area with few liquefiable deposits. Older earthquakes may have occurred before liquefiable deposits were formed, or their PL evidence may be too deeply buried to be discovered. Consider that months of data collection and analysis of numerous PL features, conducted over the course of several years across a broad area, are usually required to estimate an earthquake recurrence rate based on paleoliquefaction.

2.2.3. Paleolandslide investigations

Seismic induced mass movements cover a wide range of typologies (rock-falls, avalanches, landslides and submarine slumps) over a wide range of earthquake magnitudes (rockfalls from > 4.0 MS on, the others from > 5.0 MS) and intensities (>VI–VII). As noted in the ESI-07 Macroseismic scale [77] and previous relevant compilation works (e.g. [119–121]) affected areas and the total volume of mobilized materials increase with earthquake magnitude/intensity around the epicentral area, where steep slopes are more susceptible to gravitational movements. However, significant landslides can also be produced as far-field effects of large earthquakes over epicentral distances of about 300–350 km; an example of this is the Güevejar landslide in southern Spain triggered by the 1755 Lisbon earthquake [122–123].

Large-scale seismically induced mass movements are recognizable from conventional aerial-photos, satellite imagery and existing geologic or geomorphic maps. Landslides reported during historical and recent earthquakes are generally accessible, and therefore an accurate investigation can be undertaken (e.g. [124–131]). Also, regional/worldwide databases contain landslides induced by different earthquakes (e.g. [95, 119, 121, 132] and references therein). These compilations serve as the base documents for the analysis of seismic-induced landslide hazards [133]. Most of the studies offer regression equations for earthquake magnitude/affected area [118, 119] or earthquake intensity/affected area [77, 132], as well as empirical relationships between maximum epicentral distance and landslide occurrence. Most of the cases are valid for events of $M \geq 6.5$, but the dataset of induced landslides for events of lower magnitude (in the lower bound of the ESI Scale) remains scarce. The associated landslide hazard of moderate earthquakes was illustrated by the 2011 Lorca earthquake (Mw 5.2) in SE Spain [129]. According to recent statistics the number of landslides induced by large onshore earthquakes at plate boundaries is three times than those triggered by strong offshore earthquakes at subduction zones (e.g. Yamada et al., [134]).

Studies on seismically induced slope movements normally consider two broad categories of events following the classification proposed by Keefer et al in 1984 [119]: ‘disrupted (D)’ and ‘coherent (C)’ mass movements. D-type movements include rock falls, and rock/earth avalanches, which generate a disorganized mass of mobilized material. C-type movements normally consider larger slope movements such as complex composite landslides. Both typologies of slope movements generate characteristic landforms and/or landform assemblages susceptible to identification by geomorphic analysis. Additionally, flow slides

and lateral spread cases (FSL-type) are also common gravitationally-driven processes that occur during earthquakes [132].

Seismically induced paleolandslides, out of the temporal limits of the historical seismicity, are difficult to identify and to discriminate from those triggered by extreme climatic conditions in a particular area (e.g. heavy rainfall, storms, large flood events, etc.). Other natural processes linked to volcanic activity, glaciated and periglacial areas, etc., are also sources of landslide hazards, especially when these processes occur together in mountain chains (e.g. Andes; Alps), large volcanoes or high volcanic islands. In tectonically active areas, slope movements will also be concentrated in zones with high susceptibility to this kind of gravitational processes, such as steep slopes, cliffs, and canyons of varying and composite lithology. Only regional surveys on landslide susceptibility can identify areas prone to gravitational mass wasting. Once identified, past events have to be cataloged and accurately dated. This will allow temporal clustering of landslide occurrence, assignable to known historical events or to the activity of existing seismic sources, to be identified.

Paleoseismic landslide analyses differ from fault studies and those for seismites. According to Jibson in 2009 [135],

> They aim to "characterize the shaking history of a site or entire region irrespective of the seismic source",

even in areas where surface faulting is rare or absent. Paleoseismic landslide studies involve three steps: (a) identification of paleolandslide(s) from the geologic or geomorphic record; (b) dating the main landsliding event; and (c) correlation of the landslide with the seismic record and/or fault activity history of the area.

2.2.3.1 Detection

Seismically induced slope movements are generated in zones where normal gravitational processes occur. Geologic and geomorphic mapping can detect the occurrence of characteristic landforms associated to landslides, rock avalanches, etc. The occurrence of fresh scarps (or scars) on landslide heads are related to recent slope-movements. In order to detect paleolandslides, large and continuous, apparently inactive, smoothed and vegetated topographic scarps need to be identified (e.g. Jibson, [135]). Special attention should be drawn to landslide bodies which have an extended area over 10 km2. These are commonly associated with earthquakes of magnitude up to 7 Mw and intensities ≥ VIII as described in the ESI-07 Scale [77]. On forested slopes, disturbed, disrupted and over-toppled tree trunks may also provide additional evidence for landslide occurrence. Dendrochronological ages of the oldest undisrupted trees can provide reliable minimum ages for the last movement [135]. The geomorphology revealed by LIDAR is a useful tool in densely vegetated areas or zones subject to active erosion.

According to Hammond et al. in 2009 [136]:

> "LIDAR image interpretation can be used to detected ancient landslide boundaries including head scarps, toes, and lateral and basal shear zones".

In many cases the oldest slides are not visible and most of their boundaries have been removed or masked by surficial processes. This gives rise to landslide segmentation of giant landforms [137].

Areas with proven historical and/or instrumental landslides triggered by earthquakes must be checked in order to determine their susceptibility to gravitational movements around epicentral areas. This is because the areas which are commonly affected by mass wasting processes will also be the areas prone to activation by future earthquake events.

Deterministic and probabilistic approaches based on linear regression equations and/or non-linear logistic regressions can be used to estimate earthquake landslide hazards in regional and more detailed studies (e.g.[138, 139]). Based on GIS, estimations can be carried out using the most common factors for landslide susceptibility and hazard combined with seismic triggering factors such as peak ground acceleration and topographic amplification (e.g. Fig. 24, [139]). In Figure 24, case A shows that no previous events are known to have triggered landslides in the studied area; therefore, only landslide susceptibility is used in order to identify susceptible sites to be analyzed at near-regional and site-vicinity scales. Using some seismic assumptions such as peak-levels of seismic ground acceleration, slope stability analysis in the study area can then be undertaken.

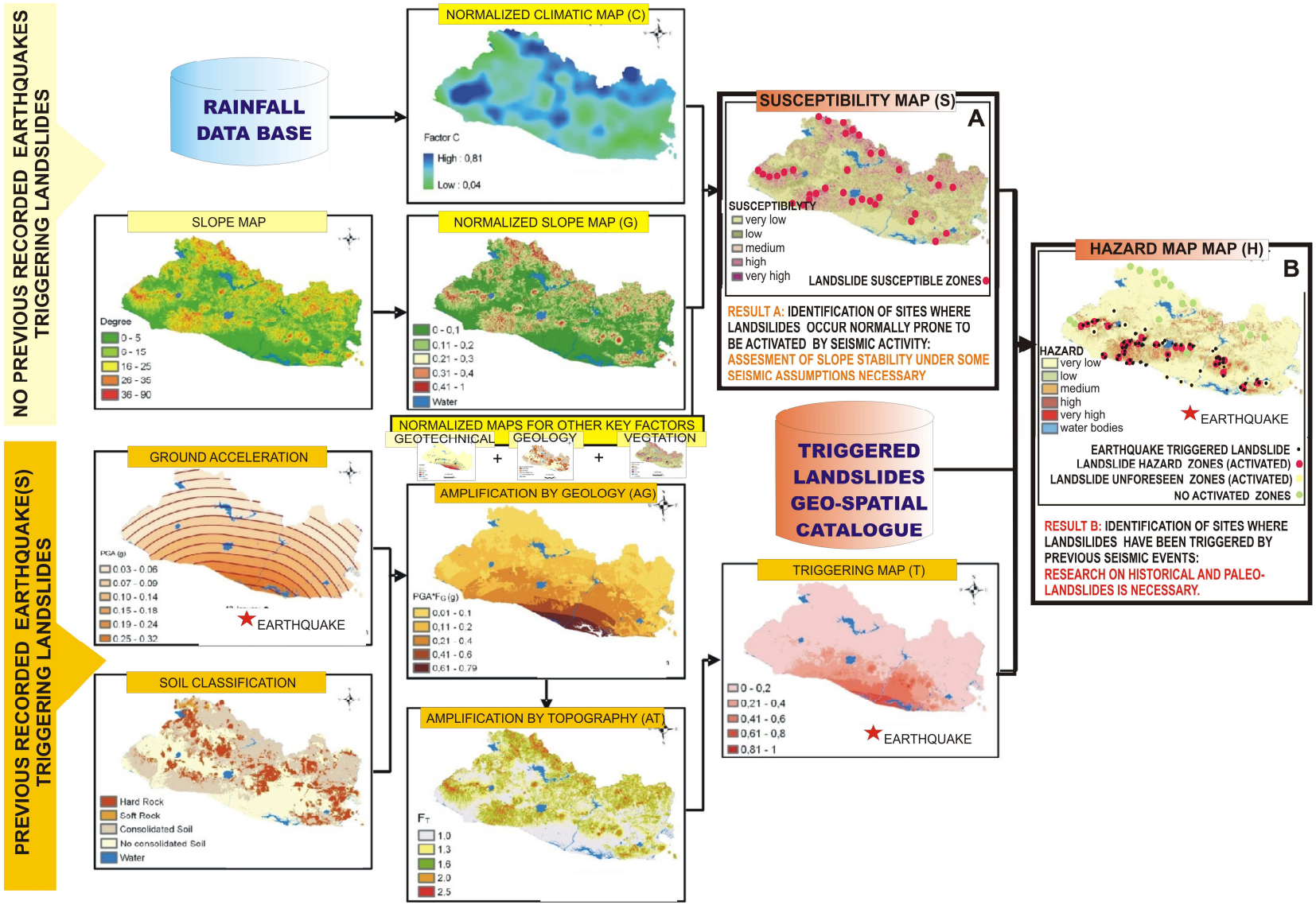

FIG. 24. Example of the compilation and processing of cartographic information necessary for the hazard assessment of earthquake-induced landslides using the GIS methodology. Probabilistic approach for El Salvador 2001 Earthquake. Based on data from García Rodríguez et al. in 2008 [139]

In case B, previous earthquake triggering landslides in the studied area are known, and seismic parameters and amplification factors (geology, topography, etc.) are combined to obtain a landslide triggering map (Fig. 24). The combination of the susceptibility and the triggering map then result in a hazard map (H). This map will illustrate those zones activated (red) and not activated (green) during previous earthquakes. Additionally, this hazard map will highlight zones in which triggered landslides have occurred but are unforeseen from susceptibility predictions (orange). These zones have to be investigated in detail if they are either in the site-vicinity region of a nuclear installation, or at a scale which is adjacent to critical facilities linked to energy production or maintenance.

A more difficult task is to identify buried or hidden paleolandslides which are embedded within the geologic record. In this case, geomorphic research needs to be carried out to identify characteristic features generated by large landslides and/or related geomorphic anomalies. Large-scale mass wasting can be identified in the geologic record by the occurrence of normal faults with curved or circular geometry. The identification of chaotic breccia or slumped levels linked to discrete blind faults within the geologic record is clear evidence that paleolandslides have occurred.

Holocene to Late-Pleistocene lacustrine sedimentary sequences in mountainous areas, range-front piedmonts, ponded zones close to scarps, valley slopes, and fluvial terrace sequences may provide better paleoenvironments to preserve and subsequently detect ancient landslides. This is because interbedded homogenites, anomalous/uncommon breccia-levels and sin-sedimentary deformation features can commonly be detected in these settings (rock/debris avalanches and slumps). In regions affected by present periglacial environments, 'sackung' and 'sackung-like' slope features can provide excellent locations for paleoearthquake detection (McCalpin, [2]). In all these cases additional geomorphic and/or geologic evidence for paleoearthquakes are necessary in order to provide a consistent and logical seismotectonic framework (e.g. Strom, [140]).

In ancient populated areas, geo-archeological records of colluvial formations at cave entrances and rock-shelter sites can offer valuable information for the occurrence of sudden and repeated rock collapses. These can then be linked to paleoseismic activity (e.g. Sánchez Gómez et al., [141]).

In summary, detection of paleolandslides from geologic investigations is relatively easy when the associated landforms have been well preserved and geomorphic techniques and analysis can be applied (generally from Holocene to mid-Pleistocene times). In areas where surficial processes and/or vegetation cover, mask or smooth the characteristic landform features, LIDAR-imaging can help in their analysis, which can cover Lower Pleistocene and even Pliocene cases. In any case, geophysical subsurface imaging methods (GPR, ERT) are in most cases obligatory in order to obtain key parameters such as the total displacement and the total volume of mobilized materials (e.g. Jibson, [135]). Once the landslide(s) or landslide area has been detected, trenching analysis is recommended in order to identify the master sliding plane and to obtain both slip and age data following the procedures for fault trenching [2]. In the case of preserved rock-falls, data on block-size dimensions and associated run-out can offer relevant data on the earthquake size. Buried landslides embedded within the geologic record (paleolandslides) are commonly not detectable and, hence, are difficult to unravel by geomorphic analyses. If a logical relation to a coseismic origin of the landslide(s) is evident, complementary studies of contemporary earthquakes and near-fault studies are necessary. It is recommended to implement an experienced landslide specialist in the study.

2.2.3.2 Possibility of misinterpretation due to non-tectonic processes

Gravitational processes and landforms occur in a variety of scales and environments and are not necessarily linked to earthquakes. The unambiguous identification of mass movements triggered by ancient earthquakes is a difficult task and additional complementary data on earthquake occurrence are helpful. Mass movements triggered by instrumental and historic earthquakes need to be investigated in order to provide data for their further parameterization. Historical reports of earthquakes can provide sufficient data to locate and evaluate the affected areas and/or sites.

Paleolandslides only evidenced from geologic and/or geo-archeological records need additional data on earthquake triggering, since they could also have been induced by many other processes. In the case of known historical events, if the ages provided by the dated evidence match the event date, this is normally sufficient to assign the dated evidence to a seismic event. In the case of paleolandslides only witnessed using geologic or geomorphic records, contemporary evidence of earthquakes (e.g. surface ruptures or seismites, i.e. ≥ M 5.5) is necessary.

In volcanic areas, gravitational collapse of volcanoes, volcanic cones and large sloped areas in shield volcanoes are commonly linked to seismo-volcanic activity. On volcanic islands (Hawaii, Canary Islands, parts of Sicily), Quaternary sea-level changes may also promote giant landslide events during sea-level low-stands [142]. In all these cases, a detailed analysis of seismic and volcanic activity (for historic events) can help put constraints on landslide triggering factors.

In coastal areas, landslides can also occur due to other high-energy events (e.g. large storms, storm surges) or secondary earthquake environmental effects, such as large tsunamis. Cliff and/or mountainous coasts can experience large landslides due to the impact of tsunami waves. In these areas, additional evidence on earthquake environmental effects and tsunami deposits are necessary in order to link landslides to tsunami events of seismic origin. A wide variety of examples have been studied by Ugai et al., [131]. Uplifted marine and/or coral terraces can provide a very good framework to detect Holocene to Late Pleistocene clusters of varied-size slumps, rock slides or rock avalanches in raised beach sequences. These geologic features can be associated with recurrent meter-scale coseismic uplift (e.g. Ota et al., [143]).

In areas where surface faulting is absent, the best approaches come from multiarchive paleoseismic records provided by a variety of secondary earthquake effects, such as lake seismites, speleoseismites and slope movements (see also Section 2.2.3). In the case of multiple paleo-earthquakes, evidence will be present in the specific area. An integrated paleoseismic study is feasible from lake, cave and geologic slope records (e.g. Becker et al., [97]). Following these criteria and depending on the size of the earthquake (magnitude), the attenuation/amplification effects (intensities), and the geographic distribution with respect to the suspected macroseismic epicenter, the same geologic archive, or several different ones, can be affected by a given event. Also, these archives can contain evidence for repeated events from the same seismogenic source or from different sources existing in the area. In areas where surface faulting occurs, the combination of primary and secondary earthquake effects may offer the best scenario in order to reconstruct the seismic history of the area. The study of these effects will provide a reasonable image of the potential seismic hazard on the basis of the ground motion history and size during single or multiple events (Fig. 24).

In any case, if seismic activity is recorded in the area, the bracketed ages of the dated mass movements have to be coeval, or at least within the error range of the dated seismic event or events. Finally, it is necessary to note that far-field ground shaking from strong earthquakes can trigger relevant mass movements in susceptible areas, even at distances of some hundreds of kilometers from the epicenter [98].

2.2.3.3 Derivation of characterizing parameters

The key data for further seismic parameterization of earthquake-triggered landslides are the individual landslide size (m^2 and/or m^3), the total mobilized volume (m^3), maximum area affected by coseismic mass wasting (km^2), and epicentral distance (km). Several worldwide data sets (e.g. [119, 120]) and regional data sets (see Table 2) have been used to establish empirical relationships between earthquake magnitude/intensity and landslide parameters.

TABLE 2. LIST OF DATASETS PUBLISHED IN INTERNATIONAL LITERATURE ON SEISMICALLY TRIGGERED LANDSLIDES. MAGNITUDES ARE USUALLY MS FOR EVENTS < 7.0 AND MW FOR THOSE >7.0. (UPDATED FROM DELGADO ET AL. IN 2011 [132]; REFERENCES FOR THE CITED DATABASES CAN BE FOUND IN THE REFERENCES LIST OF THIS PUBLICATION).

Geographical area	*Period covered*	*Magnitude range*	*Source (year)*
Worldwide	1811–1980	5.2–9.2	Keefer (1984) [119]
Costa Rica	1888–1993	5.2–7.5	Mora and Mora (1994) [144]
Worldwide	1980–1997	5.3–8.1	Rodríguez et al. (1999) [120]
Greece	1650–1995	3.8–7.9	Papadopoulos and Plessa (2000) [145]
Italy	461 BC–1980	4.5–7.5	Prestininzi and Romeo (2000) [146]
Central America	1902–2001	4.6–8.0	Bommer and Rodríguez (2002) [121]
New Zealand	1848–1995	4.9–8.2	Hancox et al. (2002) [147]
USA	1988–1994	4.6–5.7	Keefer (2002)[98]
Colombia	1644–1999	5.0–8.1	Rodríguez (2006); CEREIS (2010) [148]
Spain	1504–2005	4.2–8.7	Delgado et al. (2011b) [132]

These data are implemented in specific regression equations in order to obtain the estimated earthquake magnitude or intensity. An overall revision and updating of the existing databases can be consulted in Delgado et al. [132]. These authors perform different empirical approaches for coherent (C-type) and disrupted (D-type) landslides, but also for associated cases of earthquake induced earth-flows and lateral spreading (FSL-type). Also, the authors classify the nature of the mobilized rock mass.

The macroseismic intensity for seismic hazard studies takes into account possible variations in the intensity of shaking that could occur within a certain distance [121]. Analyses need to consider the local site intensity at landslide locations, and also the maximum macroseismic intensity [149]. These approaches take into account possible site-effects triggering ground motion amplification in terms of peak ground acceleration or Arias Intensity [132, 149, 150].

This fact is of special interest in the analysis of seismically induced landslides which have occurred in the far-field of strong earthquakes. In these cases, disrupted landslides may occur

at lower local-site intensities (i.e. V) and further away (> 700 km) than the coherent types [132]. Most of the empirical approaches developed from the datasets listed in Table 2 normally generate logarithmic regressions for the upper bound curve of landslide occurrence with the following functional forms:

$$\ln D = -a(\pm n) + b(\pm n) \times \ln I_0 \quad (1)$$

Where D is the distance in km for both coherent and disrupted landslides, a and b are constant coefficients, $\pm n$ the corresponding errors of the coefficients, and I_0 the maximum intensity generally applicable to the MM, MSK and MSC macroseismic scales (Fig. 25).

These relationships express the maximum epicentral distance at which landslides can occur for different intensity levels in the Macroseismic scales MM, MSK, MCS, and therefore the ESI-07 Scale, and also for Magnitude (M_s/M_w) estimations (Fig. 25). When using historical or paleolandslide data where the causative faults are unknown or unclear, epicentral distances instead of fault-rupture distance must be used. Similar regression equations are applied for relationships between total affected areas and earthquake intensity/magnitude.

The analysis of terrestrial or aerial LIDAR imagery can provide a good basis in order to obtain numerical data on landslide areas and/or volume [136, 151]; octo-copter flights and stereo-images can also be helpful for this purpose. Using aerial imagery, the ESI-07 scale provides a double entry to estimate the earthquake size (intensity) taking into account the maximum mobilized volume of materials for individual cases, the total area affected by landslides, and also other secondary earthquake effects [77]. In this sense, isoseismal mapping on recent earthquakes has been developed using the ESI-07 scale [152].

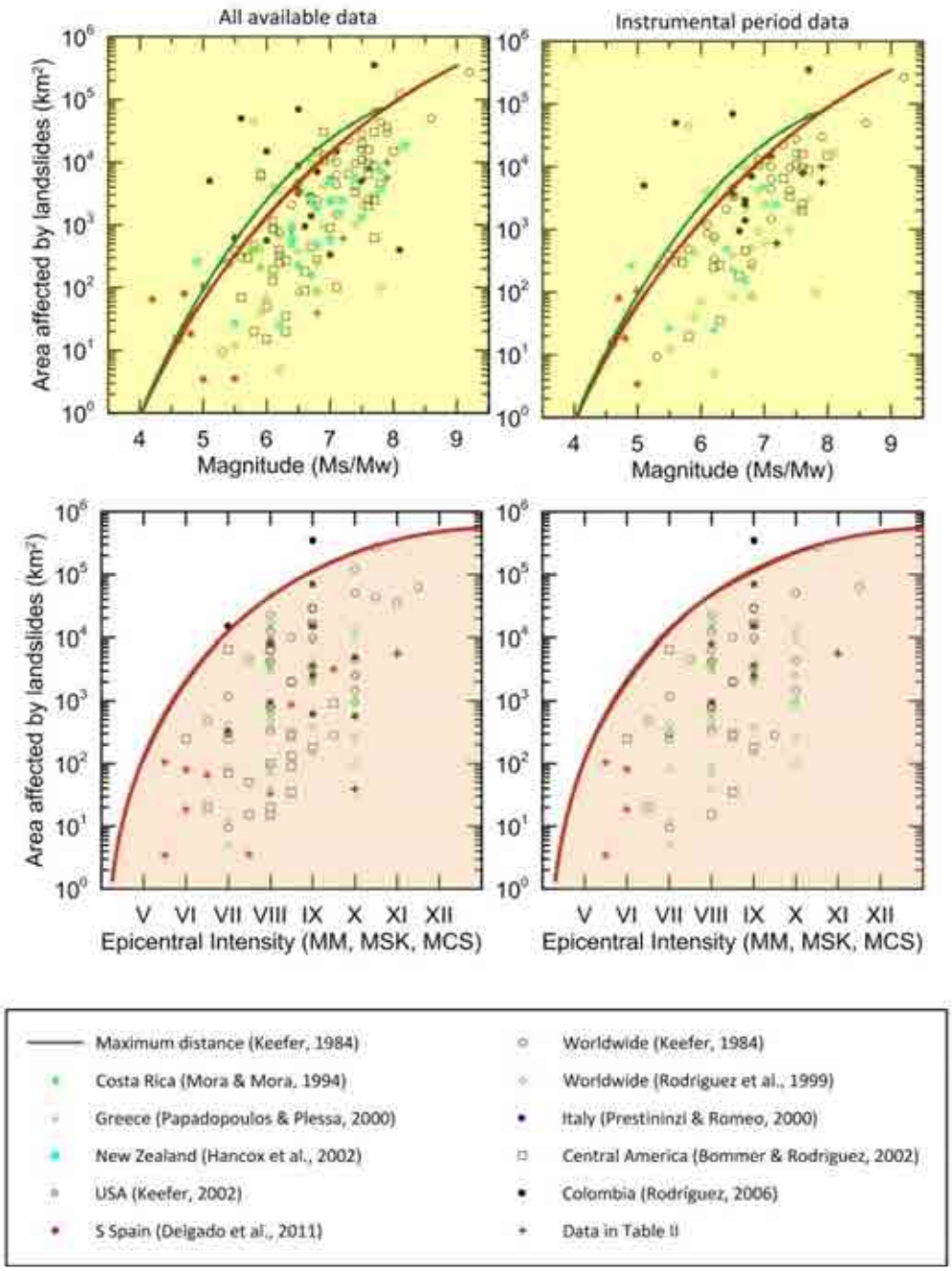

FIG. 25. Distribution of maximum affected areas by seismic induced landslides as a function of magnitudes (up) and macroseismic intensity (down) of events. All available data refer to all historic and instrumental events considered in the world-wide data used by Delgado et al. [132]. Red regression lines identify maximum distance – event size relationships from Keefer [119].Green regression lines modified in the work of Delgado et al. [132]. Based on Delgado et al. in 2011 [122]

This can then be applied to cases of paleoseismic events in order to give preliminary approaches for earthquake intensity estimations. Ota et al. [152] developed an ESI-07 macroseismic map of the Kobe area and Awaji Island affected by the 1995 Kobe Earthquake (M_w 7.3). They performed an EEE count in areas of 1 km^2, differentiating between intensity levels IV to X, depending on the size and density of EEE (mainly landslides and liquefaction features) in each 1 km^2 box.

In the case of landslides only evidenced from the geologic record (slumped, deformed and/or chaotic breccia levels), empirical relationships can be used in an 'inverse' way. Giving the location of the evidence the empirical relationships can be used to estimate the maximum distance (radius) at which the causative fault can be located. If evidence of fault surface rupture is located within the search radius, a preliminary approach for earthquake intensity can be estimated. Whatever the case, complementary evidence of contemporary earthquake occurrence is necessary to confidently estimate an earthquake magnitude.

Parameterization of earthquake induced landslides can also be performed by the use of the Newmark's sliding block method [153], which estimates the coseismic displacements affecting a sliding mass subject to a given seismic loading. The method has undergone several modifications and improvements and several relations between seismic ground motion parameters and computed slide displacements have been proposed for several regional databases [e.g. 149, 150, 154]. In these models, seismic slope stability is measured in terms of critical acceleration, which depends on the mechanical soil properties, pore-pressure distribution, and slope geometry. Conversely, the triggering seismic forces are investigated in terms of energy radiation from the source, propagation and site effects for different earthquake magnitude cut-offs. The results are

> "an inverse function of the distance from the fault rupture, and the computed block displacements provide criterion to predict the occurrence of slope failures" (Romeo in 2002 [149]).

This method can also be applied to individual cases of historical earthquake-induced landslides or paleolandslides by performing slope stability analyses [e.g. 154], which provide additional constraints on the size and location of pre-instrumental seismic events.

2.2.3.4. Case study on paleolandslides

The example of the analysis of EEE triggered by the AD 1356 Basel earthquake is one of the best approaches using paleolandslides for earthquake assessments [97]. This study combines the use of earthquake evidence on caves and lake paleo-slumps together with the previous analysis on rockfalls developed by Becker and Davenport [124]. These authors investigated the epicentral region of the Basel event in which thick-bedded Jurassic limestones develop large cliffs subject to active slope movements in the form of multiple rockfall blocks. The basic assumption to use fallen blocks as indicators of past strong events is that such earthquakes would instantaneously trigger many rockfalls in a region of limited extent (up to 100 km^2 [124]). Therefore, contemporary multiple rockfalls together with other EEE evidence of a similar age may indicate a seismic origin of these particular slope processes. Becker and Davenport [124] used big fallen blocks up to 10–15 m^3 in favorable zones where blocks were resting on clayey-marly substratum. This allowed the preservation of organic matter within the soil which developed before the block emplacement. The procedure used was to drill through the blocks from their top surfaces to their bases in order to reach the underlying organic matter within the soil (e.g. charcoal, wood fragments, pine needles, etc.) for radiocarbon dating. The Authors proved the contemporaneity of 11 out of 20 blocks sampled, giving calibrated 14C dates within the range of the AD 1356 Basel event. Combining this technique with dated paleo-slump records in nearby lakes, Becker et al. [97] developed a catalog of historic and prehistoric earthquakes from AD 1774 to about 8000 BC, most of them with estimated magnitudes between 5.9 and 6.5 M_w, and none evidenced by surface faulting.

This case study illustrates how the use of paleolandslide investigations, combined with other paleoseismic evidence, can support the analysis of moderate-strong seismic events not observed using paleoseismic fault-trenching. However, the confident discrimination of paleolandslides triggered by earthquakes from those of different origins is still one of the most controversial paleoseismic issues, especially when paleolandslides are only witnessed in the geologic and geomorphic record. For thoughtful analyses on this issue please consult Jibson [135] and Strom [140].

2.2.4. Investigation of lacustrine-marine sediments and cave sediments

2.2.4.1. Subaqueous investigations

Subaqueous research in paleoseismology involves specific methods and techniques, which differ from terrestrial ones, but still relate to on-fault evidence and off-fault secondary markers.

Subaqueous 'on-fault' studies involve the characterization of underwater morphology (sonars), fault geometry together with cumulated and incremental offsets (indirect geophysical techniques like seismic profiling), and finally dating (sediment coring) [155]. Here, we only discuss off-fault investigations that deal with secondary evidence of earthquakes, i.e. seismic shaking effects on sediments.

In subaqueous environments, surficial sediments are loose, unconsolidated and saturated. Effects of earthquake-induced increases in pore-water pressure in unconsolidated sediments have been widely investigated, both for geotechnical needs and as a potential means of recording earthquakes. These investigations concern both subaqueous marine or lacustrine settings.

In subaquatic sediments, seismic vibration, which may or may not be associated with seiches, may induce effects including stratification perturbations (such as liquefaction), total re-homogenization of the sediment layers (called homogeneites; e.g. Beck, [156]), or turbidite currents along delta foreset slopes and their emplacement in the basin. In lakes, underwater landslides may take place along their rims and steep slopes, whereas in the flattest part, turbidites deposits are likely to be deposited (e.g. [157, 158]). Soft-sediment deformation or liquefaction features, like the ones described in the Annecy lake, France [156] or in the Dead Sea Rift Zone [159–161] are mostly expected to occur in the shallow and flat areas of lakes. On the shorelines of large lakes, seiches may leave sedimentary traces such as tsunami deposits (e.g. Garduño-Monroy et al., [162]); however, such perturbations may also be induced by external events such as landslides, glacio-tectonic deformation, block falls or dam ruptures. Slope and delta failures may be related to huge rainfall events and associated sediment loading.

Detection

Lacustrine sedimentation generally offers more continuous sedimentation and higher chronological resolution than deep and shelf marine environments.
In lakes (or paleolakes) as well as in shallow marine basins, subaqueous deposits should be identified and inventoried. At a regional and near regional scale (cf. Section 1 for definition), specific studies on (paleo)-lakes and basins should be undertaken. To identify perturbation in lacustrine sediments, high resolution seismic reflection profiles are needed. These allow the sedimentary structure and particular reflection interfaces to be imaged. With respect to other techniques, seismic profiling for paleoseismic purposes need to focus on the shallowest

deposits, in order to image the reflector geometry and continuity with a high resolution. For this, the use of high-frequency systems (typically 3–20 kHz) would be preferred. Sedimentologic (texture, granulometry) investigations and dating are to be done on the lacustrine sediments by coring (gravity or piston coring in lakes). Complementary sonar mapping may allow the delineation of mass flow and megaturbidites features.

Deposits which are accessible onshore can be investigated using other sub-surface geophysical investigations (e.g. high-resolution seismic reflection, electrical resistivity tomography: ERT, ground penetrating radar: GPR), prior to trenching and borehole coring/drilling. The main analytical techniques [e.g. 155, 156] involved in sediment analyses are numerous (i.e. texture and grain-size analysis, sediment structures analysis using X-ray tomography; magnetic susceptibility, density, chemistry, isotopic imprint characterization). Many dating techniques may be used (e.g. tephrochronology, deposition rates estimations, isotopic or radiogenic methods; for more details see Section 2.4).

Possibilities of misinterpretation due to non-seismic processes

Processes other than earthquakes, such as sediment or storm wave loading, subaerial rock falls or landslides into the subaqueous environment, as well as tsunamis and hyperpycnal flow, can happen spontaneously and trigger similar sedimentary events (turbidites, landslides, soft-sediment deformation) which can mislead the investigator. Several authors proposed some sedimentologic tools to distinguish seismoturbidites from flood-generated and storm-generated turbidites. For instance, in the marine environment, seismoturbidites are expected to contain minerals from various sources in numerous coarse-grain pulses over wide areas, with a predictable stack pattern due to the distance from the sources, whereas storm-generated deposits may not exhibit such a pattern [163]. In addition, climatic floods are expected to cause turbidite beds richer in 'terrestrial' elements like organic material. Seismic events can also disturb the hydrogeologic conditions and geologic structure of the sea/lake floor, which then lead to potentially measurable perturbations in chemical and biochemical signals [164]. Finally, Goldfinger [155] emphasizes a key aspect to separate between seismic and non-seismic origin, which is to test for the simultaneity of deposition over widely spaced sites. This is the best way to rule out local sources, as also stated by Becker et al. [97].

Derivation of characterizing parameters

Estimations of paleo-intensities of recorded earthquakes have been proposed based on properties and volumes of remobilized sediments (e.g. [77, 165–168]). In several cases, different kinds of evidence such as surface faulting, rockslides and lacustrine sediment disturbances can be used together to characterize the same major event [97] and thus better assess the seismic origin.

Regional correlation of disturbed sediments in a given stratigraphic horizon is a reliable criterion for interpreting coeval seismites [97, 156]. Progressive gathering of new data allow refining empirical relationships between earthquake magnitude or intensity, distance-to-epicenter and sediment texture (e.g. [5, 167, 169–171]). These relationships can therefore be used to infer the historical or paleo-earthquakes characteristics from sediment analyses.
Finally, subaqueous investigations can indicate the following parameters:

- Paleo-intensity (ESI) and magnitude-distance relationships for liquefaction characteristics (see Section 2.2.2.);

- Age of single/multi event(s) with uncertainties (broad bracketing or following Bayesian statistics (e.g. Becker et al., [97]);
- Recurrence interval for significant earthquakes;
- Gutenberg-Richter distribution for complementary information (e.g. Becker et al, [97]).

2.2.4.2. Speleoseismology – characterization of past earthquakes with cave studies

Cave sediments and carbonate concretions are often well preserved against erosion for hundreds of thousands of years. Their study provides information on paleo-environments and, as caves may be a few million years old, it is possible to collect data for very long periods. The vibration from earthquake events may disrupt and deform cave features such as stalagmites, stalactites, soda straws or flowstones. They may also deform or liquefy cave sediments, provoke block falls or fractures, or be the cause of growth anomalies (e.g. [172–174]).

These types of evidence are called speleothem breaks or perturbations, or speleo-seismites (Kagan et al., [175]). They constitute archives of local or regional past earthquakes (e.g. [97, 175–177]). The study of earthquake impacts on cave environments, i.e. speleo-seismology [178, 179] may be generally restricted to karstic areas. However, one could perform this kind of research in any preserved underground or man-made place such as lava caves or archeological voids (e.g. [180, 181]). In such preserved places, only sedimentary features or falling rocks may have been triggered by past earthquakes.

Such perturbation evidence have to be studied very closely to avoid misinterpretations from other causative processes such as in-cave stream flows, in-cave ice flowing or long term a-seismic displacements (tectonic or gravitational). When the analysis is solely based on cave archives, a conclusion about earthquakes often remains tenuous. However, combining 'in-cave' archives with other 'external' paleoseismic evidence (i.e. Earthquake triggered lake deformations, rock falls, landslides) is a powerful tool, which allows extensive regional earthquake effects to be determined.

Detection

The first important issue when studying Earthquake Environmental Effects in caves is the identification of alternative processes which may have caused the deformations.
Affected features can be found in karstic caves, but also in man-made cavities in any geologic context, natural caves in volcanic areas or in some archeological voids (e.g. in aqueducts).
An inventory of cavities with concretion/unstable formations should be undertaken. This inventory should be performed at least at the near regional scale, since damaging effects are expected to occur throughout a large area from strong shaking around fault sources (at least 25 km around the site Case Zero of Fig. 1). It is also useful to perform investigations of speleothem breaks around regional active structures (faults, folds (case B1 and C for off-fault EEE; see Fig. 1). The absence of breaks may be an indicator for low shaking history, especially when there are unstable rocks (e.g. [182, 183] and cited references). However, as mentioned below, this 'negative' evidence must be handled with extreme caution, as these indicators only record large seismic motion and then only a small percentage of damage appears in shaken caves.

It is commonly recognized that seismic motion is attenuated in underground cavities (with respect to ground motion at the surface) according to eye witness accounts [176, 177]. The observed effects of post-earthquake damage confirm this assertion. When situated near steep slopes or in high topographic positions, damage can be more significant [97].

The theoretical strain needed to break speleothems is extreme and a seismic vibration may not able to cause it. Natural resonance frequencies of speleothems are generally higher than the seismic frequency range (0.1 to 30 Hz), generally precluding their rupture during an earthquake [179]. Only very elongated and thin speleothems could undergo such amplification and then rupture. However, the resonance frequencies of stalactites and stalagmites significantly increase the dynamic amplification and applied strain. Moreover, defects in the speleothem's structure increase their vulnerability to vibration. This is why, even if speleothems are not prone to break, earthquakes break some concretions. Finally, the percentage of damage in caves remains very low; maximum of a few percent of the concretion population. Modeling and statistical analysis of broken stalactites/mites showed that soda straws and long/slender speleothems are more likely to break during an earthquake when peak-ground acceleration ranges between 0.3 and 1 g (Lacave et al., [178, 179]).
Features related to earthquakes effects in caves include:

- Stalactite breaks followed by regrowth;
- Growth anomalies as indicators of displacement or tilting (along fractures or faults);
- Changes of texture, color, chemical composition or growth rate of speleothems, flowstone or travertine (Sinter) deposits;
- Fallen rocks from the cave edge or roof (incasions);
- Flowstone embedding broken speleothems features;
- Deformation by liquefaction or convolution of in-cave laminated soft sediments.

Possibility of misinterpretation due to non-seismic processes

To identify one single event, dating (see details in Section 2.4) has to show that collapses, breaks, deformations and perturbations are synchronous in different parts of a cave or in many places, taking in account the dating uncertainties. Other explanations for growth anomalies or breaks have to be eliminated. One important issue when seeking earthquake environmental effects in caves is to discuss and discriminate which alternative process(es) could be the cause of deformations, for instance gravitational processes (e.g. heavy stalactite collapse due to its own weight, base of stalagmite compaction or failure also due to overweight/overloading on loose soil), slope decompression processes, water circulation under flowstones or stalactites, man or animal passage effects, and very close blasting (< 100 m) from quarrying. Even slow tectonic processes can cause speleothem anomalies such as local fault creep. These processes are generally local, do not extended within the whole cave and cannot be shared by multiple caves like seismic events [176].

Other processes remain difficult to link to a local event and require more attention. These are phenomena that may cause perturbations at the whole cave scale or even at the regional scale, such as ice-flow (limited to higher latitudes), sediment fill creeping [177], floods, mud and debris flows, slope movements (e.g. valley-ward sliding along bedding planes), etc.

Derivation of characterizing parameters

Some useful parameters can be derived from speleothem studies. They are listed below, in increasing degree of required information:

- Occurrence of a 'significant' earthquake, where magnitude can only be evaluated with large uncertainties (magnitude M_w >> 5.0 to 6 at short distances; M_w >> 6–7 at larger distances);
- On the contrary, lack of speleo-seismite could also be an indicator for the lack of significant seismic event in the cave area. This may be an important information for SHA but the absence of evidence must be handled with caution;
- Rough estimation of epicenter when no single source is identified around the cave(s) area;
- Broad estimation of underground intensities based on empirical observations (a five degree scale was proposed by Gilli et al. [174]);
- Direction of fall as an indicator of ground motion or source direction (see cited bibliography in Becker et al. [177]);
- Statistical evaluation of the stalactites/mites vulnerabilities [179, 184]) allows an estimation of the probability that a certain level of acceleration was reached;
- Estimation of PGA range parameters from elongated concretions;
- Age of single/multiple event(s) with uncertainties (broad bracketing or following a Bayesian statistics (e.g. [97, 161]);
- Recurrence interval for significant earthquakes;
- Gutenberg-Richter distribution for complementary information (see e.g. [97]).

2.2.4.3 Case Study of lacustrine and cave investigations

An emblematic study of archives based on Earthquake Environmental Effects (EEE), with the aim of completing the seismic hazard assessment, was conducted in Switzerland by Becker et al. [97]. In the early 90's, the AD 1356 Basel Earthquake was already known as a strong historical regional earthquake even though no previous strong seismicity had been evidenced (Case E paragraph 2.1.2). Paleoseismic investigations performed in the framework of academic research and for the purpose of safety assessment enabled the identification of surface fault ruptures, damage in caves, lacustrine sediment deformations and rock fall events. Dating of these effects showed that similar strength earthquakes might have occurred in prehistoric times. By compiling classical on-fault studies (geomorphology, trenches), lake investigations, cave analyses and rock fall data, Becker et al. [97] were able to: 1) determine the occurrence of (previously) unknown significant earthquakes, 2) propose a chronological sequence for prehistoric and historic strong earthquakes in north-western Switzerland, and 3) complete the regional Gutenberg-Richter distribution towards the high magnitudes as 7; this greatly improved the historical earthquake catalog. This regional synthesis is of primary significance in an area where several nuclear installations are located. The results of these combined approaches (so called 'integrated paleoseismology' or 'multiarchive approach') then greatly improved the seismic hazard assessment, especially regarding the recurrence interval for large earthquakes. Thus, the recurrence interval for strong earthquakes was estimated between 2500–3000 years for the Basel region. EEE from lakes [157, 158, 161] or caves [175] are also good examples to use for the production of past 'off-fault' earthquake

calendars, which are able to provide Gutenberg-Richter distributions. These kinds of results should be used as input for PSHA computations and may be very useful to explore the low probabilities, as required by the SSG-9 guidelines to assess the seismic hazard for NPPs.

2.2.5 Geomorphic, micro-geomorphic and other techniques

Apart from the methods discussed above, there are several additional techniques that can be used in certain circumstances and boundary conditions to investigate diffuse seismicity. Obviously, geomorphic evidence can be found directly at faults, if one thinks of scarps in the landscape, triangular facets associated with normal faulting or typical wine glass shaped valleys [2]. But apart from these features observed at faults, more subtle geomorphic evidence may indicate earthquake occurrence.

Illustrative examples of river course anomalies (deflection) are provided by Burrato et al. [69]. The Authors found systematic shifts of river courses in the Po plain due to the convergence of the Appenines and the Alps during the last millennia, and also movements of blind reverse faults below the thick sedimentary cover of the Po plain.

Detection of coseismic subsidence was possible due to the geomorphic determination of sea level changes. For example, using only this evidence, events of large magnitudes (up to M_w=9) could be attributed to the Cascadia subduction zone, as historical and instrumental seismicity does not reveal any larger earthquakes in the region higher than around M_w 7 [185, 186]. A similar approach can be used for diffuse seismicity areas.

2.2.6 Summary of capabilities and limitations of paleoseismic investigations to characterize diffuse seismicity

Paleoseismic investigations can reveal effects which are spatially separated from the faults which caused the earthquakes. If the location of the fault cannot be determined, the inferred seismicity has to be addressed as diffuse seismicity occurring at a certain range of distances from the observed effects. In this Section the methodological approaches for characterization of paleoliquefaction, paleolandslides, and disturbance of lake and cave sediments have been discussed in detail. They are directly related to the occurrence of significant seismic shaking in the past. Geomorphic methods reveal the general behavior at the Earth's surface due to sudden subsidence or uplift, or slow movements.

The aforementioned methods can be used to derive the possible range of paleoearthquake magnitudes and their recurrence rates. The possible range of distances from the observation locations to the epi/hypo-centers can also be specified. It has been demonstrated that uncertainties are higher compared to the case where faults can be accessed and investigated directly; however, these complementary investigation methods addressing off-fault effects or blind fault characterization (i.e. seismic profile investigations, geomorphic analysis) must be performed.

2.3 TSUNAMI GEOLOGY IN PALEOSEISMOLOGY

2.3.1 Significance of tsunami geology

2.3.1.1 Tsunamis and tsunami geology

The 2004 Indian Ocean and 2011 Tohoku-oki disasters dramatically demonstrated the destructiveness and deadliness of tsunamis. For the assessment of future risk posed by tsunamis it is necessary to understand past tsunami events. Recent work on tsunami deposits has provided new information on paleotsunami events, including their recurrence interval and the size of the tsunamis (e.g. [187–189]). Tsunamis are observed not only on the margin of oceans but also in lakes. The majority of tsunamis are generated by earthquakes, but other events that displace water such as landslides and volcanic eruptions can also generate tsunamis. These non-earthquake tsunamis occur less frequently than earthquake tsunamis; it is, therefore, very important to find and study geologic evidence for past eruption and submarine landslide triggered tsunami events, as their rare occurrence may lead to risks being underestimated.

Geologic investigations of tsunamis have historically relied on earthquake geology. Geophysicists estimate the parameters of vertical coseismic displacement that tsunami modelers use as a tsunami's initial condition. The modelers then let the simulated tsunami run ashore. This approach suffers from the relationship between the earthquake and seafloor displacement, the pertinent parameter in tsunami generation, being equivocal. In recent years, geologic investigations of tsunamis have added sedimentology and micropaleontology, which focus on identifying and interpreting depositional and erosional features of tsunamis.

For example, coastal sediment may contain deposits that provide important information on past tsunami events [190, 191]. In some cases, a tsunami is recorded by a single sand layer. Elsewhere, tsunami deposits can consist of complex layers of mud, sand, and boulders, containing abundant stratigraphic evidence for sediment reworking and redeposition. These onshore sediments are geologic evidence for tsunamis and are called ‘tsunami deposits’ (Figs. 26 and 27).

Tsunami deposits can be classified into two groups: modern tsunami deposits and paleotsunami deposits. A modern tsunami deposit is a deposit whose source event is known. A paleotsunami deposit is a deposit whose age is estimated and has a source that is either inferred to be a historical event or is unknown.

FIG. 26. Sheet-like sandy tsunami deposit formed by the 2011 Tohoku-oki tsunami on the Sendai Plain, Miyagi, (1) and cross section of the deposit (2). Buried paleotsunami deposit formed by the 869 Jogan tsunami found on the same plain (3).

FIG. 27. Sandy tsunami deposits found in eastern Hokkaido, Japan.

2.3.1.2 Assessing tsunami and earthquake hazards based on tsunami deposits

Estimates of tsunami heights from earthquake magnitudes are equivocal because of uncertainties about the relationships between seafloor displacement, which vertically moves water that is acted on by gravity and generates a series of tsunami waves, and earthquake magnitude. Tsunami deposits are direct evidence of tsunamis and have been studied in recent years to reconstruct prehistoric tsunami recurrence and magnitude (e.g. [187, 188, 192]). As an example, a remarkable study was done along the northeastern coast of Hokkaido, which faces the Kuril Trench. Time-space distributions of tsunami deposits suggested unusually large earthquakes have occurred on average about every 500 years over the past 2000–7000 years [188]. The last event, which occurred in the 17th century, was determined to be a multi-segment earthquake that had not been known to occur in this area. In 2003, a hazard map based on a source model of a M 8.6 earthquake that generated inundation consistent with the tsunami deposit's spatial distribution and crustal deformation was issued in Kushiro, the largest city in the eastern part of Hokkaido (Fig. 28). This is the first hazard map for the region based on pre-historical events revealed by geologic investigations rather than historical earthquakes. However, subsequent investigations of modern tsunami deposits, such as the 2011 Tohoku-oki tsunami, suggest that the 2003 estimate of inundation limit in northeastern Hokkaido based on paleotsunami data may have been significantly underestimated. In 2011, the magnitude of the potential largest earthquake was revaluated. This resulted in an increase from M 8.6 to 9.0 and a corresponding enlargement of the tsunami inundation area in Kushiro.

FIG. 28. Tsunami hazard map for Kushiro, eastern Hokkaido, Japan. Reproduced with the permission from Kushiro local government.

In Tohoku, uncertainties in tsunami geology hindered an attempt to quantify hazards in the area of the 2011 disaster. The work focused on an unusually large earthquake and tsunami that caused documented damage near Sendai in July AD 869. Independent teams sought geologic clues from AD 869 along 300 km of coast in Iwate, Miyagi, and Fukushima Prefectures. The teams identified the AD 869 tsunami with confidence along the 100 km of coast where volcanic ash from AD 915 provides age control, an extended planar area at the coast allows inundation limits to be estimated, and evidence for subsidence locally brackets the AD 869 sand sheet. Modeling the inundation and subsidence for a 200 km long fault rupture yielded M 8.4 for the AD 869 earthquake. Two of the teams recently reflected on whether these findings could have forewarned the authorities and public of the 2011 M 9.0 event [189, 193]; both teams emphasized that the modeled M 8.4 was a minimum, and that it was limited by geologic unknowns about the coastal extent of coeval rupture. The teams also cited uncertainties in using the inland extent of sandy tsunami deposits to estimate amounts of seismic slip. One of the teams concluded that the inland extent of sandy tsunami deposits was a good proxy for the limit of inundation and the 2011 earthquake may have simply dwarfed its predecessor of AD 869.

Tsunami deposits are recognized in many areas of the world; however, the incorporation of information from tsunami deposits into hazard assessment has only occurred relatively recently. The first report of paleotsunami deposits in U.S. Pacific Northwest was published in 1987 [194], and 52 studies were published from 1987 to 2002 documenting known or potential paleotsunami deposits at 59 sites from northern California to Vancouver Island in British Columbia, forewarning a large tsunami impacting the Pacific Northwest [195, 196]. A hybrid approach of geology, geophysics, and hydrodynamics has been used to produce tsunami-inundation maps at the Cascadia subduction zone since the late 1990s. It is illustrated today by the third generation of tsunami-inundation maps in Oregon [197]. These are based on a 10,000-year history of submarine mass movements that have been interpreted as proxy records of earthquake shaking [198]. While debatable in its estimates of earthquake magnitude and recurrence [199], the inferred history extends uncommonly far, both back in time and along the coast; the modeled inundation is somewhat testable by means of tsunami geology [200–202].

The first tsunami hazard map in the United States (coastal Washington), including locations of paleotsunami deposits showing maximum inundation delimitation, was not published until 2000 [204] (Fig. 29). A new approach to tsunami hazard assessment was used in a joint National Oceanic and Atmospheric Administration (NOAA)/US Geological Survey/Federal Emergency Management Agency (FEMA) pilot study that included a paleotsunami deposit component and applied Probabilistic Tsunami Hazard Assessment (PTHA) methodologies [205] to assess tsunami flooding at Seaside, Oregon, USA [203]. This PTHA, however, only used paleotsunami information to determine the local tsunami recurrence interval and for model validation (Fig. 30). A next step is to explicitly use paleotsunami deposit information to characterize tsunami magnitude in PTHAs.

The subduction slip that generated the 1952 Kamchatka earthquake, the 20th century's third-largest earthquake worldwide, also set off a Pacific Ocean tsunami that was minimally documented in its near field. Geologic fieldwork five decades later uncovered 1952 tsunami deposits on plains and hillsides. The inland limits of these deposits, interpreted as close minimum limits for the inundation, were used in tsunami simulations to compute the distribution of seismic slip in the estimated fault-rupture area [206].

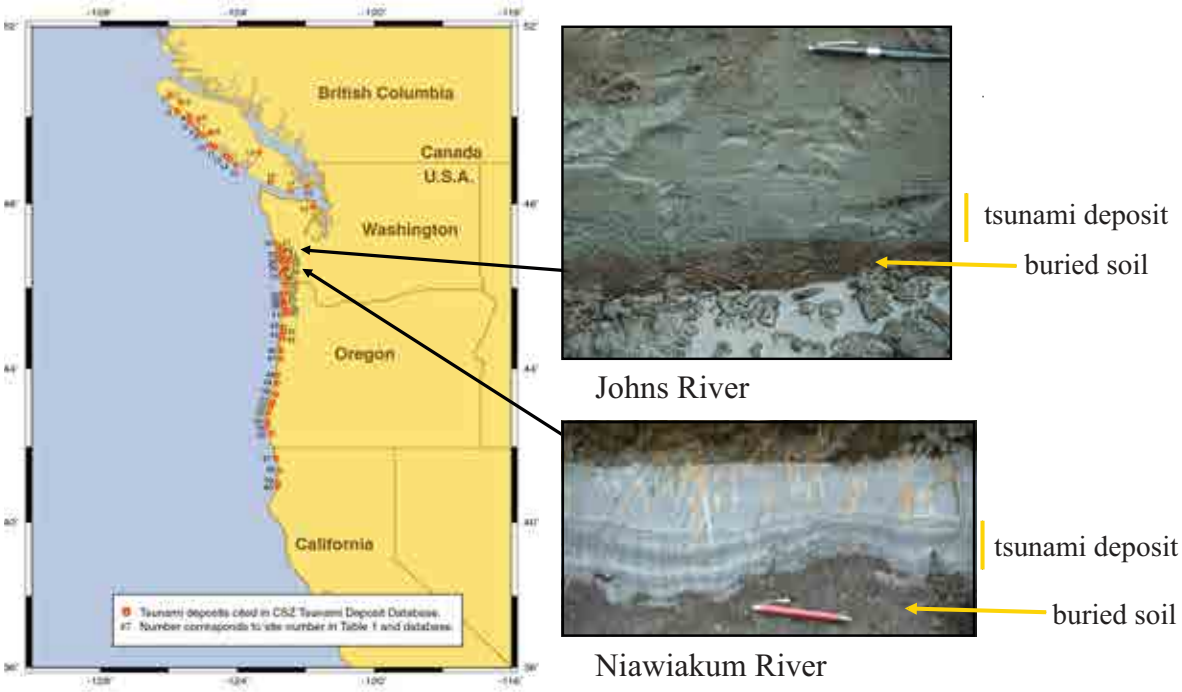

FIG. 29. Locations of tsunami deposits along the Cascadia margin, United States and British Columbia. Based on Peters et al. in 2003 [195].

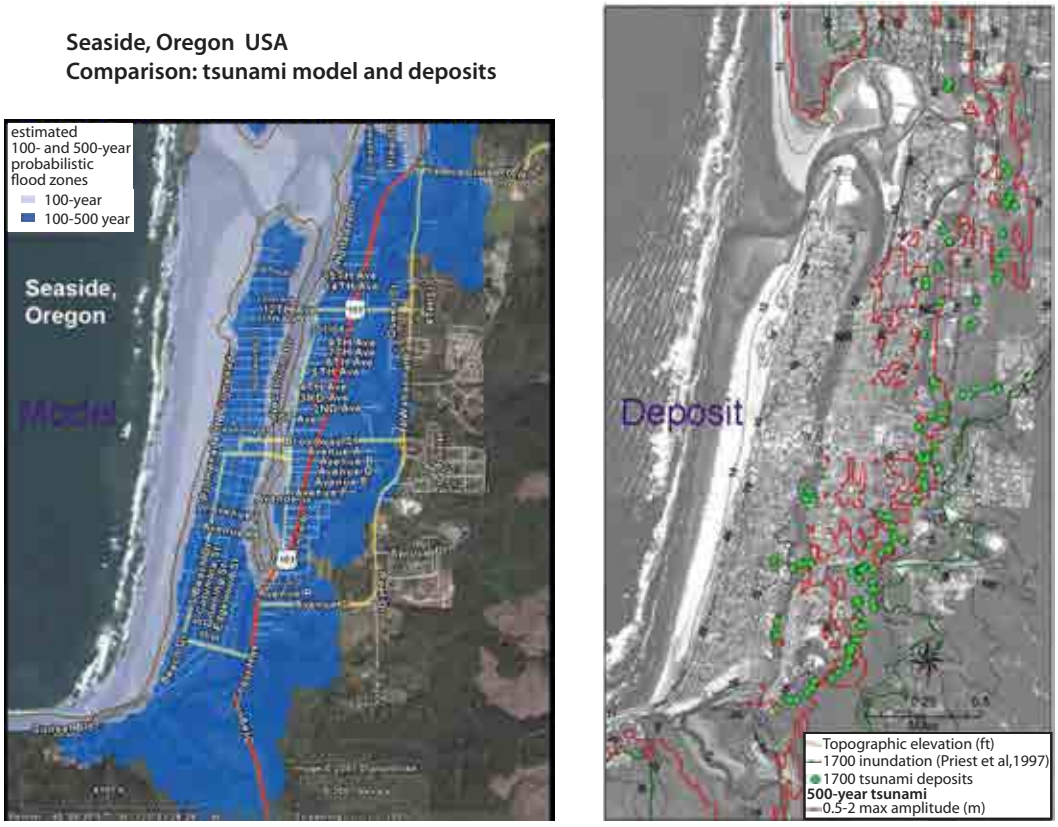

FIG. 30. Comparison of the flood zone from 500-year tsunami PTHA and AD 1700 tsunami deposits at Seaside, Oregon, USA. Based on Gonzalez et al. in 2009 [203].

The 1755 Lisbon tsunami left sand deposits with complex characteristics and also deposited boulders of various sizes. Some of the 1755 tsunami deposit studies have revealed the possible tsunami run-up height; for example in Cadiz, Spain, Reicherter et al. [207] identified the 1755 tsunami deposit up to 700 m inland at 4 m above sea level (asl). Scheffers and Kelletat [208] identified a number of boulders at heights more than 10 m asl to the west of Lisbon. Costa et al. [209] calculated a maximum tsunami run-up height of 10 m asl in the central Algarve coast. These new run-up data from geologic studies are useful, both for assessing tsunami hazard and for tsunami modeling to estimate the source earthquake (e.g. [210–214]).

Ruiz et al. [215] compiled geologic and historical data that revealed the occurrence of at least 20 tsunamis during the last 7000 years in Portugal and southern Spain. Luque et al. [216] identified an event similar to the 1755 tsunami that might have occurred ca. 216–218 BC. Morales et al., [217] identified geologic evidence of five historical tsunamis (1755, 1531, 949, 881, and 395) in the Huelva Estuary, Spain. These studies show that different tsunamis possibly formed the tsunami deposits observed at different sites.

2.3.2. Tsunami effects on coastal geology

It is important to understand characteristics of tsunami deposits to be able to identify paleotsunami deposits in the field. Recent post-tsunami surveys included geologic investigations and they revealed that tsunami deposits are diverse in distribution, sedimentary structure, composition, thickness, and grain size characteristics (e.g. [218–223]). Deposits reflect not only onshore tsunami behavior, but also local topography and the coastal area's environmental setting (Fig. 31). Although tsunami deposits are generally quite complex, there are several commonly observed characteristics of sandy-to-muddy tsunami deposits that are listed below. Figure 32 shows two of the characteristics typical of tsunami deposits, a general landward fining and lightening. Although there is considerable variability in tsunami deposits, a simple explanation for many of their features is that they form during a quasi steady-state flow that slowly decelerates after an erosive pulse of water moves landward, with additional sediment deposited for each successive wave [224].

Geometry
- continuous, sheet-like;
- generally inland thinning.

Composition
- sand from shallow sea, beach, and dune;
- marine biota such as marine diatoms, foraminifera, ostracods;
- mud eroded out from the original surface or lagoon;
- concrete fragments;
- generally inland lightening.

Lithofacies
- one to several layers;
- generally inland fining;
- normal grading (suspended sediment);
- reverse grading and lamination (traction sediment);
- overlain by mud (near the landward limit);
- include rip-up clasts.

FIG. 31. Typical features of tsunami erosion and deposition moving inland from the coast (left side of figure) to the inundation limit (right side of the figure).

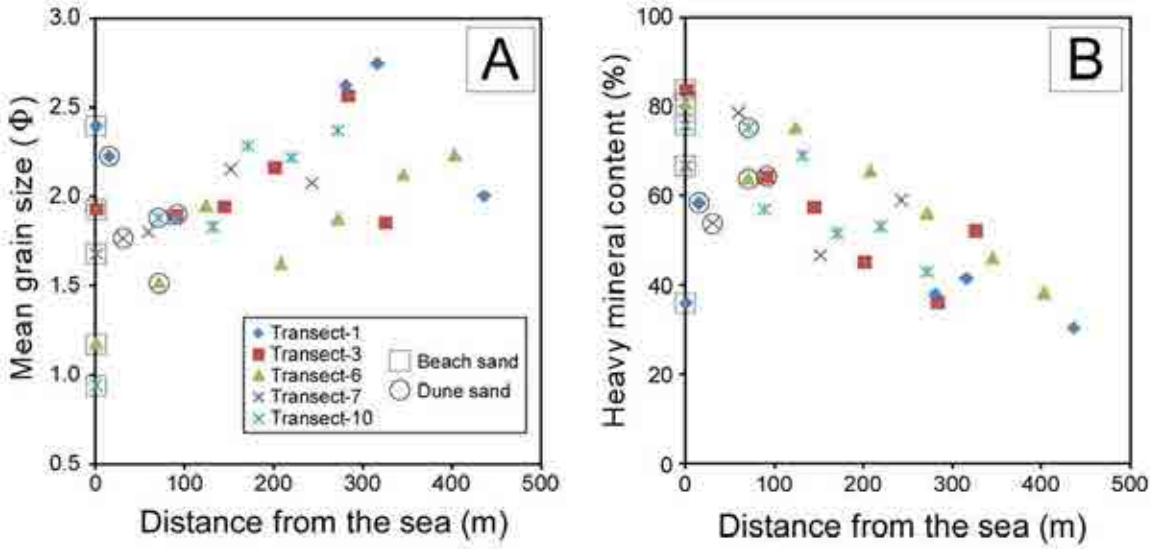

FIG. 32. Relationship between the distance from the shoreline and mean grain size of tsunami deposit (A) and heavy mineral content (B) for the 2011 Tohoku-oki tsunami deposits at Misawa, northern Honshu, Japan.

Research on the identification of tsunami boulder deposits is increasing (e.g. [225–228]). Similar to sandy tsunami deposits, boulder deposits are expected to provide useful information to improve our understanding of recurrence intervals and paleotsunamis size. The pattern of deposition (dispersed vs. concentrated), boulder orientation and inland variation in boulder size have all been used as criteria to determine whether they were formed by a tsunami [225, 227, 229–235].

Information about where and how tsunamigenic erosion and deposition occurred is important for a paleotsunami study. The 2011 Tohoku-oki tsunami impacted various types of coasts and both tsunami behavior and the resultant geologic changes were studied.

Along the irregular coastline of Sanriku, the tsunami invaded into steep coastal valleys. In these valleys, tsunami run-up heights were more than 30 m above the sea level and the inundation distances were more than 1 km from the beach (Fig. 33). On some steep slopes, the surface vegetation and soil were stripped away. Some freshly formed gullies were evident on the surface of the slope. On gently-sloping topography, the tsunami left continuous sand deposits on the surface. The thicknesses of the deposits were typically less than 20 cm, but deposits were thicker where there was a large dune or sandy beach at the valley mouth. In most valleys the deposit thickness tends to decrease with distance from the sea. Near the limit of inundation, the tsunami deposits became patchy sand sheets.

FIG. 33. Tsunami heights (top) and spatial distribution of tsunami erosion and deposition (bottom) of the 2011 Tohoku-oki along a narrow valley at the Sanriku coast, Japan.

In the Sendai Plain, Miyagi, the tsunami inundated areas up to 4.5 km inland. The tsunami flow heights were about 10 m near the coast and about 5 m in the middle of the inundation area. In contrast to the Sanriku coast, continuous sandy deposits formed only to about 60% of the inundation distance [235]. The deposit changed from sand-dominated sediment to mud-dominated sediment with distance from the coast. A muddy tsunami deposit formed farther inland up to the inundation limit. Muddy deposits were also left behind in the large lagoon of Matsukawa-ura, Fukushima. Here, the tsunami height was about 10 m near the coast, and the deposits are mainly composed of well sorted to poorly sorted coarse to very fine sand that is covered by a mud layer. The lagoon is interpreted to be the main source of the sediments.

In tropical countries, such as Indonesia, Samoa, Tonga, and Solomon Islands, tsunami deposits are mainly composed of carbonate grains, with coral and shell fragments making up the bulk of the deposit. Complex characteristics of carbonate grains (high variations in shape, size, and density) may affect sedimentation processes and are responsible for the complexity of the tsunami deposits (e.g. [223–236]). Studies of modern tsunami deposits in carbonate-

dominated environmental settings are important for identification of paleotsunami deposit in tropical countries. This is because our inability to recognize carbonate-dominated tsunami deposits may be responsible for them not being observed rather than poor preservations as suggested by Nichol and Kench, [237].

2.3.3. Identification of buried tsunami deposits

2.3.3.1 Criteria for distinguishing tsunami deposits from the other coastal event deposits

Direct evidence to identify tsunami deposits has not been established. Typically, a buried event deposit is identified as being formed by a tsunami by similarity with modern tsunami deposits and dissimilarity with other coastal event deposits such as a storm surge or flood deposits. Features of unequivocal modern sandy tsunami deposits frequently used to identify paleotsunami deposits are: (1) sheet-like geometry, (2) landward thinning, (3) landward fining, (4) upward fining (normal grading), (5) multiple units or layers (not always present), (6) inclusion of beach materials, (7) inclusion of rip-up clasts (eroded surface material), and (8) a marine geochemical or microfossil signature (not always present). Identification of a muddy tsunami deposit is difficult at present, though new research on geochemical, microfossil, and x-radiograph approaches is promising [238]. The distribution of mud deposits is important because mud deposits typically extend farther inland than sandy deposits and failure to recognize them may result in a significant underestimate of paleotsunami size [239]. Hydrodynamic modeling to explain a deposit's horizontal and vertical sand particle distribution and sedimentary structures also can help to identify tsunami deposits [224, 240–245]). This approach allows evaluation of various tsunami parameters (height, flow velocity and flow direction) from the observed sediment.

Tsunami geology and storm geology can overlap and may do so in confounding ways. Places where this ambiguity has been examined include Australia [226, 246], the Netherlands Antilles [247, 248], and the British Virgin Islands [249].

Progress has been made in attributing coastal boulders to historical tsunamis and storms. In Hawaii, boulders atop historical lava flows can be attributed in some cases to the tsunamis of 1868 and 1975 and in other cases to recent storms [232]. Deposits from the two historical tsunamis are characterized by boulder fields that extend inland over several hundred meters. Many of the boulders are angular to sub-angular and show little evidence of reworking or sorting. In contrast, boulder deposits from large storm and/or swell waves in the same area are generally confined to within 50m (100m maximum) of the shoreline and form prominent shore-parallel ridge complexes and boulders tend to be more rounded, reflecting reworking. In Ireland, an absence of tsunamis in recent centuries leaves only storms to account for boulders that have moved across 19th-century walls [250]. In Japan, an 18th-century tsunami moved coral-reef blocks farther landward than subsequent storms achieved [239]. As with sand deposits, modeling the transport of boulders gives clues to whether they were deposited by tsunamis or storms. Progress has been reported in computing the forces needed to lift the boulders to the tops of sea cliffs, and in relating the repetitive storm waves to the shingled clasts of bouldery ridges [251].

Historical examples also provide a starting point for distinguishing between tsunami and storm evidence, where sand has been washed over beaches or through breaches cut into them. Many of the storm examples come from the U.S. Atlantic and Gulf coasts [220,233, 252]. Conversely, near the equator in areas overrun by the 2004 Indian Ocean tsunami, historical

tracks of tropical cyclones make catastrophic storms as an unlikely explanation for the pre-2004 sand sheets in Sumatra and southwest Thailand [253, 254].

Geologic context provides a simple means of distinguishing between tsunami and storm in estuarine deposits along the Pacific coast of the Cascadia subduction zone [185]. Great Cascadia earthquakes are evidenced most clearly by buried marsh and forest soils that are abruptly overlain by tidal-flat mud; the same sequence produced near Anchorage by abrupt tectonic subsidence that accompanied the 1964 Alaska earthquake [255, 256]. At many Cascadia bays and river mouths the buried soils are locally coated with sand that tapers landward, contains marine fossils, and is coarser grained than the tidal-flat deposits. Such sand provides evidence for landward-directed flows of salt water that shortly followed coseismic subsidence. Such near-coincidence with land-level change can be expected of a near-field tsunami but not of a storm. Land level changes cannot be used to discriminate between tsunami and storm deposits on Cascadia floodplains that lack evidence for coseismic subsidence [257].

2.3.3.2 Evaluation of preservation of tsunami deposits

To identify tsunami deposits, it is necessary to consider possible post-depositional changes. The processes that decrease preservation include physical and chemical weathering and bioturbation [258].

Post-depositional change
- Physical
  - washing out the fine sediment at the surface;
  - redeposition of sediment;
  - leveling of the surface;
  - disruption by frost heaving.
- Chemical
  - removal of salt;
  - dissolution of carbonate materials;
  - oxidation of metalloids.
- Biological
  - bioturbation by roots and animals;
  - human activity.

Deposits from the 2004 Indian Ocean and 2011 Tohoku-oki tsunamis provide opportunities to study the early stage of taphonomic processes for various types of tsunami deposits. For example, Nakamura et al. [259] studied tsunami deposits along the Misawa coast in March 2011 and May 2012 and compared their thickness patterns. One year after deposition, thick deposits were not significantly altered and retained their original structure and thickness (Fig. 34). However, thin tsunami deposits close to the inundation limit were hardly distinguishable as they had been eroded or mixed with humic soil; the geometry and inland extent of deposits, therefore, changed significantly in only one year. Thickness and sedimentary structure of the tsunami deposits were also affected by bioturbation by roots and animals, and human activity (Fig. 35).

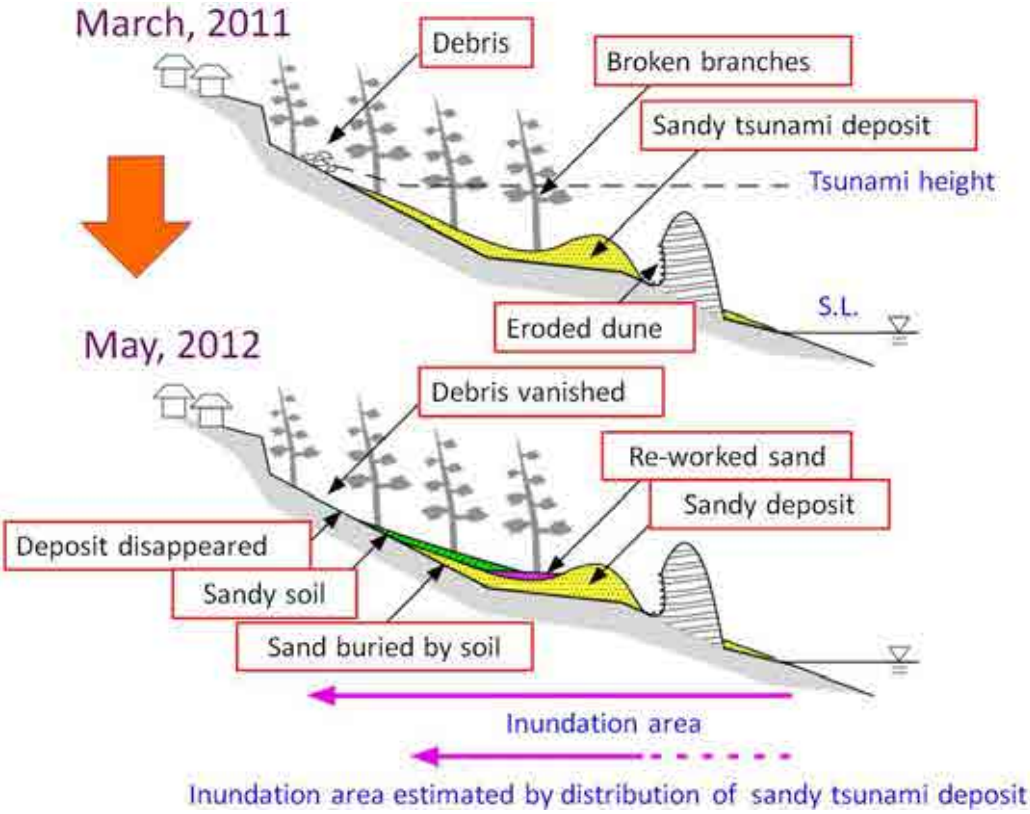

FIG. 34. Schematic cross sections showing the 2011 Tohoku-oki tsunami deposit on March, 2011 and May, 2012 at the Misawa coast, northern Honshu, Japan.

FIG. 35. Examples of complete overturning of tsunami deposits and mixing with pre-tsunami sediments by bioturbation, roots, and animals.

Furthermore, over a longer time period, the composition of a tsunami deposit may change. When sand is deposited on acid peat, the foraminifera and shell fragments in the sand start to dissolve. Jankaew et al. [254] investigated 2004 and pre-2004 tsunami sand sheets in Thailand and mention that the pre-2004 sheets in swales lack diatoms of any kind, while the 2004 tsunami sand includes marine and brackish-water diatoms. They also note that sandy sheets are better preserved in swales where peat had been built up on top of the deposit.

2.3.4. Paleotsunami investigations

2.3.4.1 Methods suited to different environmental settings and expected information

Site and method selection is critical for finding and interpreting tsunami deposits. When we want to know how often a coast is impacted by tsunamis and when it was last impacted, coastal lagoons or ponds where only high-energy washover processes can disturb the bottom sedimentation are suitable. In such settings, the bottom sediment is usually conducive for high-resolution dating and is sometimes old enough to record multiple events. A disadvantage of working in these settings is that it is expensive and requires special techniques for coring. It also it is hard to estimate the size of the tsunami or discriminate between a local and distant source from lagoon or pond deposits.

For cases where we need to know the extent of tsunami inundation as well as recurrence, study sites in flat coastal areas or gently sloping wetlands are needed. In these environments it is advantageous to study as large area as possible because tsunami deposits may not be continuously distributed. It is also necessary to study coastal geologic features, including the location of the shoreline in the past. A series of coastal beach ridge and swale systems is ideal for establishing the position of the shoreline at the times of paleotsunami inundation (Fig. 36).

A large-enough trench or outcrop is required to observe detailed sedimentary structure (Fig. 37). Small trenching or coring on a line perpendicular to the coast allow identification of tsunami deposits and their inland distribution by observing lateral changes in thickness and grain size of deposits relative to microtopography. The disadvantage of this type of study setting is that near-coast young swales are not old enough to record prehistoric events and for tsunami deposits found in inland old swales it is not easy to estimate the coastline position at the time of paleotsunami inundation.

In addition to the spatial distribution of the deposits investigated in the field, the sandy and muddy deposit is sampled and analyzed in laboratory to check for plant microfossils or fossil insects within the deposit. Biological and geochemical marine signatures are used to establish whether the deposit has a marine origin. Mineral composition of the sand and morphological characteristics of sand grains include information on the source and processes that transported the sand.

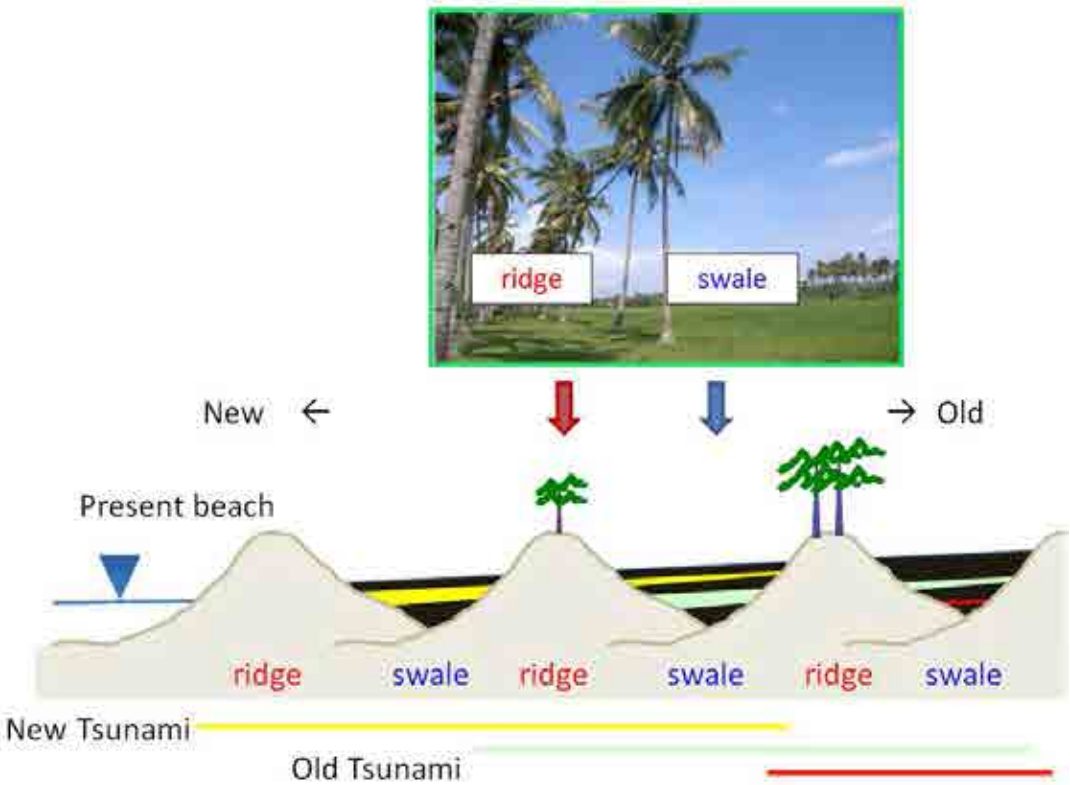

FIG. 36. A series of coastal beach ridge and swale systems is ideal for tracing a series of tsunami deposits and establishing the position of the shoreline at the times of paleotsunami inundation.

FIG. 37. Examples of methods and tools used to observe the spatial distribution and sedimentary structure of buried tsunami deposits. Clockwise from the upper left the methods are: examining an intact small trench, describing slabs from the walls of a large trench, a geoslicer core that limits disturbance in sensitive areas, and a small-diameter push core that penetrates several meters of more into the subsurface.

2.3.4.2 Dating paleotsunami deposits

Identified tsunami deposits can be dated by means of relative and absolute methods, the latter being commonly radiocarbon, lead-210, cesium-137, optically stimulated luminescence (OSL), and tephrochronological methods (see Section 2.4). The most frequently used methods are AMS radiocarbon and tephrochronology. For radiocarbon dating, the time of tsunami inundation is estimated based on the ages of the soil deposited just above and beneath the target tsunami deposit. Where the deposit is found in pure peat, the accuracy of the age determined by AMS radiocarbon dating can be a few decades. However, because tsunami can erode the original surface and redeposit the eroded soil on the layer or within the layer as evidenced by a mud cap and/or rip-up clasts, one should be careful to choose appropriate material for dating. Well characterized and widely-distributed tephra whose age is known are also very useful to estimate the time of deposition, when tephra and tsunami deposits are close to each other in the stratigraphic record. For example, this is sometimes the case in Japan (see section 4.1).

2.3.4.3 Estimating paleotsunami size and earthquake magnitude from tsunami deposits

For assessing tsunami hazard, it is critical to know the size (flow depth, tsunami height, inundation distance, and run-up) of paleotsunamis at each site. As discussed in previous sections, the lateral extent and spatial distribution of tsunami deposits are significantly affected by the local topography of the coastal area, microtopography of the inundated area, and location and type of the source material. Only where a tsunami inundates a flat area and creates a well preserved continuous deposit, traceable from the present shoreline to its inland limit, can the minimum extent of the deposits, and the minimum inundation of the paleotsunami that created them, be correlated. Even for this special case, the minimum extent of the paleotsunami inundation is a valid indicator of the present hazard only when the location of the present and paleo-coastlines can be compared, and the subsidence rate be assessed.

There are some reports indicating that the thickness of tsunami deposits is a good indicator of the original tsunami size, at least in a relative sense (e.g. [260]). However, even in a lagoon, the thickness of deposits interpreted to be formed by one tsunami event and found in multiple cores located near each another can vary significantly [261]. For the 2011 Tohoku-oki tsunami and the 2010 Pagai tsunami, there is no simple relationship between deposit thickness and maximum local tsunami flow depth or tsunami inundation height (Fig. 38). The reasons for the lack of such correlation include: (1) variable deposition by spatial gradients in transport, such as would occur in a spatially decelerating flow, whose thickness depends on the velocity gradients and the duration that they act [245]; and (2) deposition by multiple waves, each one contributing to the final thickness, whose number depends on inland distance, not flow depth [262].

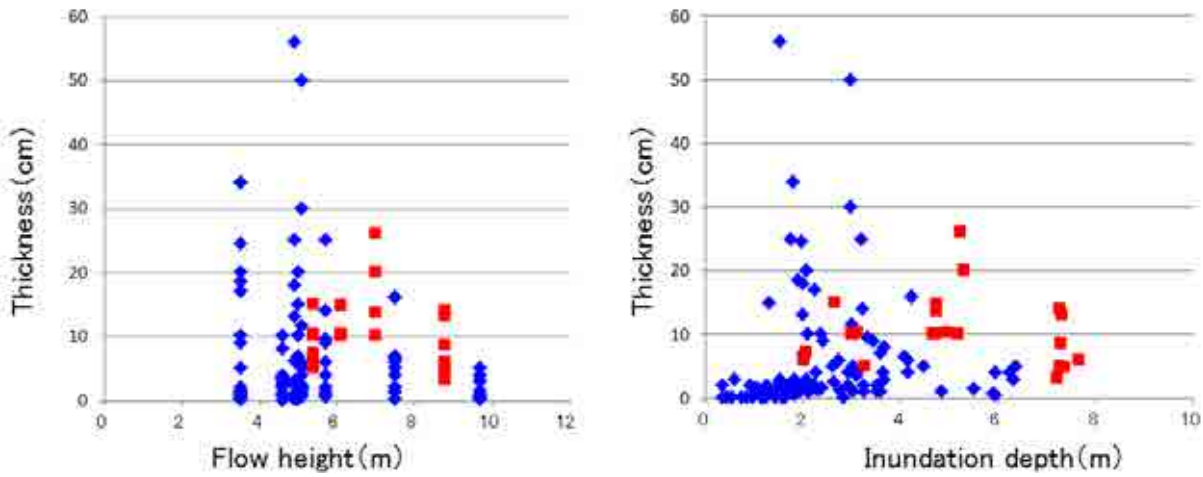

FIG. 38. Relationships between tsunami deposit thickness and tsunami flow height (left) and inundation (flow) depth (right). Data from the 2011 tsunami at the Misawa coast, Aomori, Japan (blue dots), and the 2010 Mentawai tsunami at Pagai Islands, Indonesia (red dots).

A recent research field that holds promise for tsunami hazard assessment is the development of tsunami sediment transport models that estimate tsunami magnitude from observed deposits (Sugawara et al., [263]). Models have focused on estimating two parameters, tsunami flow depth and flow speed. Four approaches have been used thus far: (1) inverse modeling of grain size distribution and tsunami deposit thickness to calculate tsunami flow speeds necessary to suspend the deposit [243], (2) inverse modeling of the largest grains in the deposit to estimate tsunami flow depth at the shoreline [224], (3) forward modeling of simple settling of suspended sediment to obtain tsunami flow depth at the shoreline [244], and (4) forward modeling of flow and sediment transport to estimate tsunami flow depths and speeds consistent with tsunami deposit characteristics [264].

Tsunami sediment transport modeling is a recently developed field of research [263] and, although valuable for tsunami hazard assessment at nuclear power plants, must be applied judiciously. The inverse models require specific conditions to be met, and as a result, are not applicable for all tsunamis in all environments and for all deposits from a given tsunami. For example, the Jaffe and Gelfenbaum [243] model is only applicable for deposits with clearly identifiable portions formed primarily by sediment settling out of suspension [245]. The trajectory models of Moore et al. [224] and Soulsby et al. [244] assume that grains are picked up at the shoreline, are suspended to the full height of the tsunami, and move inland settling to where they are deposited without being resuspended (i.e. simple trajectory instead of a trajectory where the grain touches the bed multiple times). The Apotsos et al. [264] forward model used a single grain size sediment source, and although deposit geometry sensitivity to grain size was explored, a source with a complete grain size distribution has yet to be modeled. Even with these limitations, sediment transport models have been useful for estimating paleotsunami magnitude (e.g. [202]).

To assess earthquake and tsunami hazard where paleotsunami information is not available at a location of interest, it is necessary to construct an earthquake source model and simulate tsunamis (Fig. 39). To inform the source model, tsunami deposits at multiple remote sites must be correlated and the tsunami size estimated for each site for use in matching tsunami size from a tsunami propagation model. However, at sites where tsunamis have hit frequently in the past and consequently multiple paleotsunami layers are preserved, it is sometimes difficult

to estimate tsunami size because of difficulty correlating layers inland (e.g. based only on age dating).

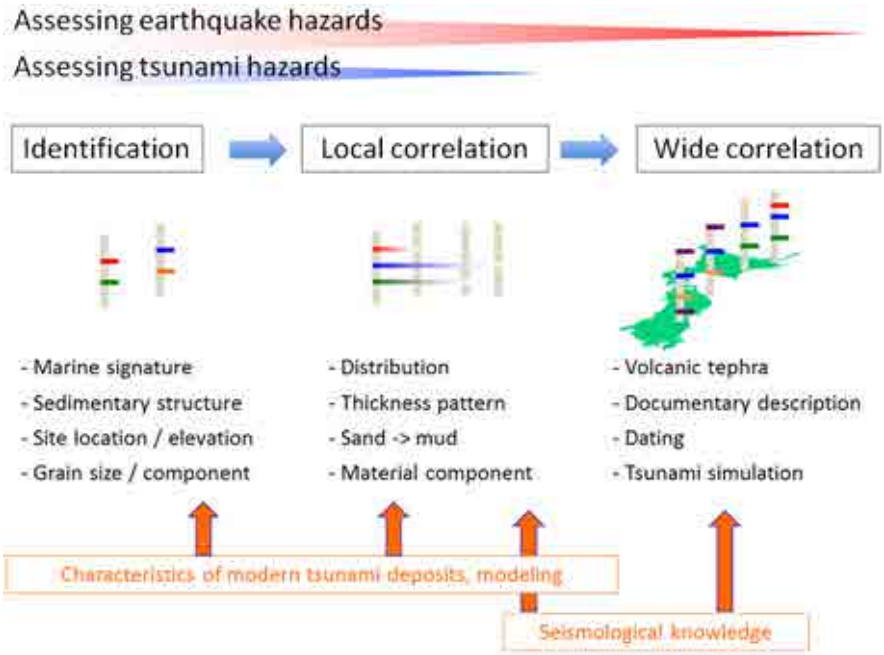

FIG. 39. Required steps to assess earthquake and tsunami hazard from paleotsunami deposits. For sites where paleotsunami information is not available tsunami hazard is assessed using an earthquake source model and inundation modeling. To inform an earthquake source model, tsunami deposits at multiple remote sites must be correlated and the tsunami size estimated for each site. Earthquake hazard is assessed from the regional distribution of paleotsunami deposits and deposit-based tsunami size estimates input into inverse models of tsunami inundation and earthquake source.

2.3.5 Use of tsunami deposits in assessing tsunami and earthquake hazard at nuclear installations

As already discussed, for a paleotsunami survey it is important to choose a study site where a tsunami could leave a deposit and the deposit is likely to be preserved and easily identifiable. For the case where suitable depositional and preservational environments are not found at or near a nuclear power plant (NPP) site, paleotsunami investigations should be performed at multiple remote sites, including sites as close as possible to the NPP, with suitable environments. The information derived from these investigations can be used to both establish recurrence and tsunami size near the NPP [265] and to construct a data-constrained earthquake source to simulate the tsunami at the NPP site.

As tsunami deposits are not spatially continuous in many settings, one must be careful to not report that there are no tsunami deposits at a site based on a limited number of excavations. Absence of evidence is not evidence of absence. There are four possible explanations for no tsunami deposits: (1) no tsunami inundation, (2) tsunami inundated but no deposit was left, (3) a tsunami created a deposit that was subsequently destroyed, and (4) there are tsunami deposits, but they have not yet been found or identified.

2.4. DATING TECHNIQUES IN PALEOSEISMOLOGY

2.4.1 Introduction

The purpose of dating sediments including volcanic ash, charcoal and other organic particles is to reveal an age. This derived 'number' will be highly dependent on the sampler's scientific discipline; the paleoseismology expert would take different samples compared to those taken by a sedimentologist or dating specialist. This is because each expert follows their own research questions and tries to get the best samples for solving their problem. In paleoseismic investigations the area of major interest is usually the timing of the last (several) earthquake event(s) at a certain fault or in a defined area. Additionally, the time interval elapsed since the last event (or between events), the slip rate of the fault and the recurrence period of earthquakes may be obtained by applying the appropriate dating methods on appropriate samples. There is a large variety of dating methods ranging from isotopic, radiogenic and sidereal methods; one can obtain numerical, calibrated, relative or correlated ages, which are related to geomorphic, biological or chemical processes. Table 3 shows a compilation of the most common dating methods used in paleoseismology to establish a faulting history. Two field techniques are the most promising: either dating the event layer directly, i.e. the datum when the fault was active, or, if not possible, bracketing the event layer by dating the first layer below (before) and the first layer above (after) the event horizon.

TABLE 3. COMPILATION OF DATING METHODS APPLIED IN PALEOSEISMOLOGY. NOTE LOGARITHMICAL TIME SCALE, THE COLOR-CODING OF THE BARS REFLECTS THE DATING ERROR IN PERCENT, SEE INSET. COSMOGENIC NUCLIDE DATING RANGE BASED ON WALKER IN 2005 [266], AND ADDITIONAL INFORMATION FROM NOLLER ET AL. IN 2000 [267]

	Method		Age range (10^3 – 10^6 years)	Material	Comments
isotopic	radiocarbon			Terrestrial plant and animal remains (bone), pedogenic material (soil), marine fossils and deposits, ceramics (cultural materials).	Radioactive decay of atmospheric ^{14}C to ^{14}N after stop of exchange (death); data need to be calibrated (calendar years) and corrected for hardwater and marine reservoir effects.
isotopic	K-Ar, Ar-Ar			Mainly young volcanic products, and sediments with e.g. ash layers, also fault gouges.	Range assumes high-K content in minerals, young materials (< 1 My) are more accurately dated with Ar-Ar.
isotopic	U-series			Terrestrial, pedogenic, lacustrine and chemical deposits, young volcanics, marine fossils and marine deposits.	Radioactive decay of U and daughter nuclides in minerals (^{234}U - ^{230}Th, or ^{235}U - ^{231}Pa); pure or biogenic carbonate (coral, shell) has a lower error than impure carbonate (calcrete).
isotopic	^{210}Pb			Mainly young lacustrine and marine deposits, wetland deposits.	Resolution is improved when used with ^{137}Cs; can be used to calculate depositional rates.
isotopic	U-Pb, Th-Pb			Volcanic rocks, carbonates (crystals, speleothems).	Age resolution in a function of $\Delta^{234}U$ /^{204}Pb, normalized Pb isotopes are used to detect radiogenic lead from U and Th decay; usually the host rock/mineral relation must be considered.
isotopic	cosmogenic nuclides	^{3}He		Quartz-rich rocks (granites) or quartz clasts, carbonates and many other rocks. Basically used to date (faulted) landforms or surfaces, like colluvial surfaces and pediment, eolian landforms, alluvial or marine terraces, lake shorelines, glacial depositional or erosional forms, lava and pyroclastic surfaces, fault scarps. ^{10}Be, ^{14}C and ^{26}Al for quartz. ^{36}Cl for limestones and carbonates. ^{21}Ne and ^{3}He in minerals (e.g. olivine, garnet).	The material itself is not dated but how long its has been exposed to cosmic rays. Cosmogenic isotope production is related to its topographic position (altitude) and geographic position (latitude). Generally, production is greatest at high altitudes and high latitudes. Noble gases H and Ne are stable, whereas Be, C, Al and Cl are radioactive and decay to daughter isotopes over time.
isotopic	cosmogenic nuclides	^{10}Be			
isotopic	cosmogenic nuclides	^{14}C			
isotopic	cosmogenic nuclides	^{21}Ne			
isotopic	cosmogenic nuclides	^{26}Al			
isotopic	cosmogenic nuclides	^{36}Cl			
radiogenic	luminescence			Eolian and clastic (fluvial, lacustrine, marine) deposits, artifacts (cultural materials), quartz and feldspar-rich sediments.	Accumulation of electrons in crystal defects of quartz and silicates due to natural radiation, time range and resolution dependent natural radiation and mineralogy; 5-20% resolution.
radiogenic	ESR			Lacustrine and marine biogenic deposits, volcanic rocks and cultural materials, quartz and feldspar-rich sediments.	Accumulation of electrical charges in crystal defects of quartz and silicates due to natural radiation, assuming average level of radioactivity in the host rock.
radiogenic	fission-track	apatite		Apatites.	Accumulation of damage trails in crystals (fission tracks) from natural decay of ^{238}Uranium in minerals; unroofing dating.
radiogenic	fission-track	zircon		Zircons and volcanic glass.	
sidereal	dendrochronology			Trees, which form rings, and cultural material (wood).	Counting annual growth patterns (i.e. tree rings) from living trees, or correlation of a sequence of rings (local variation of ring width, cross dating).
sidereal	varve chronology			Rhythmically layered glacial, lacustrine and marine deposits.	Counting seasonal sediment layers back from present (varves) or sequential control of continuous packages.
sidereal	sclerochronology		50 - 200 %; 10 - 50 %; < 10 %	Marine organisms which produce annual growth patterns (e.g. corals).	Counting annual growth patterns (e.g. rings, bands) of coral or mollusks.

In paleoseismic investigations the considered timeframe is usually between several decades/centuries and approximately the last interglacial period in the Quaternary. This interglacial period known as Marine Isotopic Stage (MIS) 5 (Huybers, [268]) includes the Eemian [269] and refers to the interval between 130 and 85 kyr. This means that paleoseismic surveys must take into account glacial/interglacial variabilities and changes in climate throughout this time, and should cover more than one seismic cycle. The effects of these climatic variabilities include changes in landscape formation, variability in erosion and deposition rates, sea-level changes along coastlines, ice/no-ice cover in glacial and periglacial areas, different weathering agents (more/less precipitation, wind, dew), vegetation cover, river incision rates and so on. Reicherter et al. [101] provided an example for this which is shortly explained in the following:

> "Post-glacial (or Late Pleistocene, after the Late Glacial Maximum) bedrock or soft-rock fault scarps, e.g. those made up of limestone displaced against Quaternary sediments, demonstrate fault activity and are usually very easy to recognize. They offset mountain slopes along mountain fronts, which have been degraded by intense Late Pleistocene weathering and cryogenic processes. The preservation of several meter-high coseismic fault scarps is a function of reduced production and mobility of sediments along the slope, persistent climatic conditions, and cumulative earthquake events along the same fault (tectonic slip rate > erosion rate, Fig. 40). During glacial conditions enhanced sediment mobility was faster than fault slip movement; no or only minor scarps developed (e.g. Papanikoulaou et al., (2002) [40]). This is broadly confirmed by cosmogenic dating of fault scarps in Greece (Sparta Fault, Peloponnesus, Greece, Benedetti et al., (2002) [270]; Kaparelli Fault, Greece, Benedetti et al., (2003) [271]) and Italy (Magnola Fault, Apennines, Palumbo et al., (2004) [272]), where oldest exposure ages of around 20–13 kyrs have been found for the exhumation of limestone fault scarps".

Scarp morphology and preservation are also dependent on uplift/erosion or subsidence/deposition [2]. Reicherter et al. [101] summarized the effects on both bedrock fault scarps and those scarps in unconsolidated sediments; where the deformation rates exceed the rates of these geomorphic processes, paleoseismic landscapes form (Fig. 41). Obviously this process is highly dependent on the climatic conditions, i.e. humid vs. arid conditions or glacial vs. interglacial conditions. Scarps can be eroded and destroyed or buried by sediments (Fig. 41, cases 1 and 4). Only relicts of the fault scarps remain preserved either in the footwall (Fig. 41, case 2) or in sediments of the hanging wall (Fig. 41, case 3). A given constant displacement rate of 0.1 mm/yr (including an error, see Fig. 41 black dot) on a normal fault with erosion rates larger than 0.1 mm/yr (uplift) will lead to the destruction of a fault scarp (sector 1). If erosion rates are smaller than 0.1 mm/yr, partial preservation of a topographic step due to a normal fault (sector 2) is expected. If deposition or subsidence occurs, the hanging wall of the fault contains partially preserved sediments (sector 3). In sector 4 the fault scarp is buried by enhanced sedimentation. As an example, blue and red dots show effects on the scarp preservation if sedimentation rates are accelerated, and are larger than the fault displacement rate. Degraded fault scarps may also be dated using morphological methods (e.g. Nash, [273, 274]).

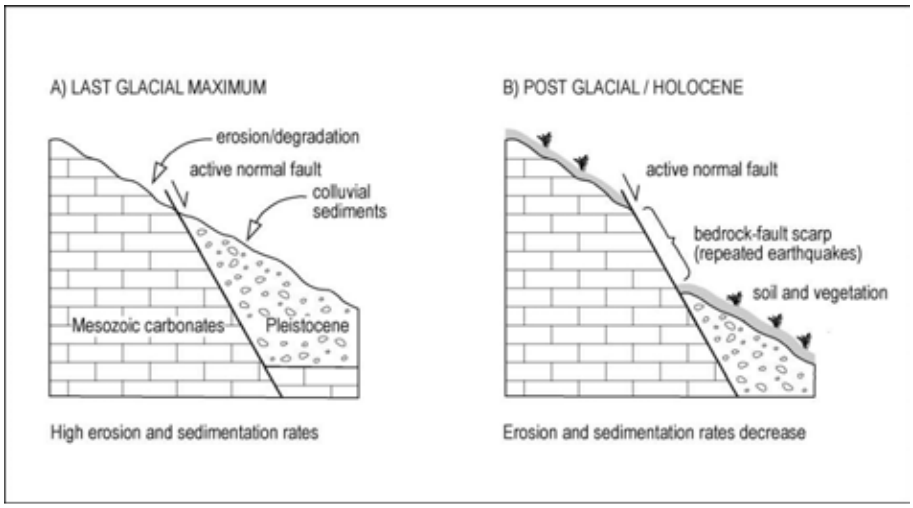

FIG. 40. Geomorphology of fault scarps with respect to the climatic conditions: the model proposed by Papanikolaou et al. in 2005 [40]. Reproduced with the permission of the editor from Reicherter et al. in 2011 [101].

Many commercial institutes and university laboratories offer dating services, the most common being radiocarbon (^{14}C) or Optical Stimulated Luminescence (OSL) dating. Depending on the budget available for the study, a variety of reliable methods should be chosen. Also, archeological remains and artifacts should be considered for dating, as these – at least for the European region – provide a relatively cheap and precise dating opportunity; e.g. Roman remains including buildings, burials or ceramics. If timber is well preserved, dendrochronology may be applied [275, 276]).

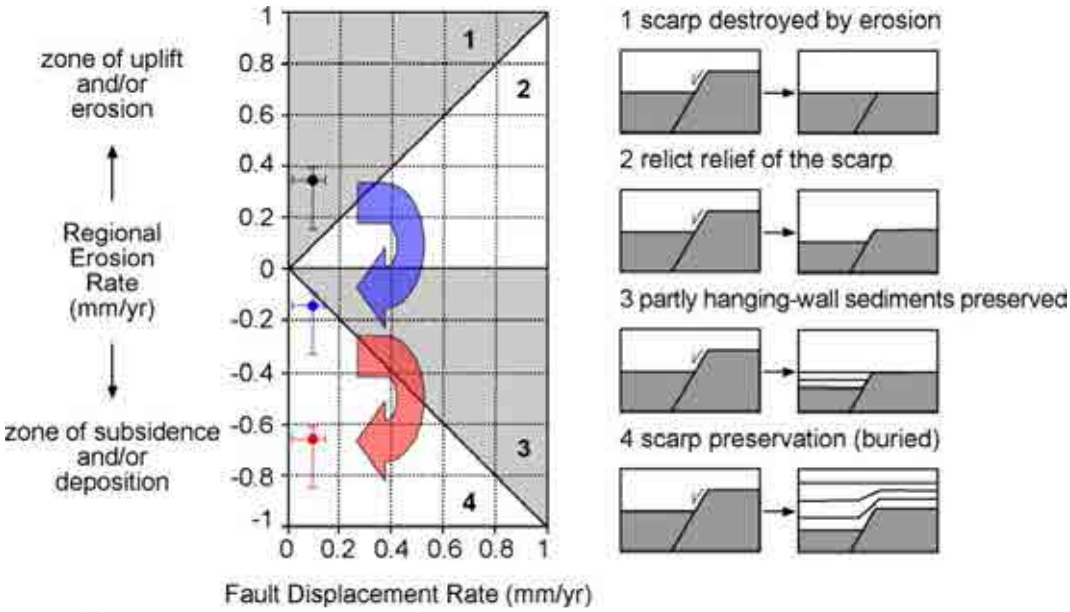

FIG. 41. Plot of fault displacement rate vs erosion/deposition rate and related scarp evolution by McCalpin (2009) [2]; taken from Reicherter et al. in 2011 [101]. A given constant displacement rate on normal faults leads under different erosion rates (uplift) or deposition (subsidence) to the destruction of a fault scarp (sector 1) or to preservation of a topographic step due to a normal fault (sector 2). In sector 3 the fault scarp is buried by enhanced sedimentation. Blue and red arrows show effects if sedimentation rates are accelerated (sector 4), but the fault slip rate remains constant. Further explanation in main text. Reproduced with the permission of the editor from Reicherter et al. in 2011 [101].

It is not the place of this publication to explain all dating methods in detail; furthermore, there is not sufficient space to do this. We will, however, give here an overview of the most common dating methods and techniques used in paleoseismic studies. For further information on dating techniques please refer to the literature, e.g. Walker [266] or the upcoming

'Encyclopedia of Scientific Dating Methods' (to be published in June 2015, Rink and Thompson, eds. [277]). Caution must always be exercised in examining stratigraphic relationships and selecting material for quantitative age analysis for any investigation, especially in paleoseismic studies. All dating techniques have potential pitfalls and large or minor errors (analytical or others) associated with them. A highly experienced Quaternary geologist or paleoseismologist should always be consulted for dating fault-related features.

2.4.2 Most prominent methods

2.4.2.1 Radiocarbon dating

The well-known radiocarbon method is by far the fastest and most-applied dating method in paleoseismology. Since Willard Libby developed the method in 1946 (e.g. [278–279]), many different materials have been used for dating purposes. The radiocarbon method is based on the decay of the radioactive ^{14}C isotope of carbon (half-life of 5,730 years) and reaches back to around 10 half-lives to approximately 60,000 years before present. The classical time interval considered for dating is, therefore, between several 100s of years and 60,000 years. Radiocarbon dates by the laboratories are usually delivered with an uncertainty, which reflects the standard deviation or the variation from a mean age (e.g. 2,000 ± 20 BP). The level of atmospheric ^{14}C has not remained constant over time. The raw data must, therefore, be calibrated to calendar ages (cal yr BP or cal BP) or they are simply given as uncalibrated BP ages (^{14}C yr BP or C14 yr BP); before present (BP) represents time before AD 1950, because since then the amount of atmospheric ^{14}C has almost doubled due to atmospheric atomic bomb tests. There are many calibration methods available; examples are OxCal (https://c14.arch.ox.ac.uk/oxcal/OxCal.html), Calib, IntCal09 and Marine09 (http://calib.qub.ac.uk/calib/), some of which are available online (e.g. Bronk Ramsey, [280–282]).

Datable materials include organic and inorganic remains. These include: charcoal, wood, twigs, leaves, seeds, pollen; peat, lake mud and soil sediments; and also leather, hair, bones, shells, corals, pottery, paper and parchment, resins and textile fabrics. Many of these are used in paleoseismic studies and can be found in excavated trenches across or along faults and fault scarps. Sources of error in radiocarbon dating can result from contamination, which can occur after as well as prior to sampling, e.g. younger roots can penetrate into the layers of interest and this may lead to younger dates. An increase of the sample ages may also occur when incorporating older carbon into the sample, such as wash-in carbon from catchment slopes into lakes [266]. Another source of ageing, or reducing sample dates, is isotopic fractionation where plants or animals produce differing isotopic concentrations (usually the lighter ^{12}C isotope) during their lifetime through natural biochemical processes. When radiocarbon is dated, marine shells are apparently around 400 years older than terrestrial plants of the same age. This anomaly is known as the marine reservoir effect and results from the ocean having two sources of ^{14}C: atmospheric carbon dioxide and deep water carbon dioxide. The ^{14}C from both sources is combined at the surface of oceans leading to higher concentrations in marine organisms. Therefore, as plants only incorporate atmospheric carbon dioxide they have a younger ^{14}C date. The magnitude of the marine reservoir effect does, however, vary from location to location within the oceans and needs to be corrected. The correction factors are available online (http://calib.qub.ac.uk/marine/). Another error source worth mentioning is from the hard-water effect where ^{14}C concentration is diluted by dissolved calcium carbonate. This is particularly evident when dating organic lake deposits, as they are highly susceptible to contamination by older carbon. Significant errors can also arise by dating plant remains

close to active volcanic carbon dioxide sources or sediments from Holocene eruptions. Furthermore, dating samples younger than 250 years can be problematic due to the effects of burning fossil fuels since the industrial revolution.

For more detailed information, please refer to Walker [266] and/or visit radiocarbon.com or radiocarbon.org. A list of laboratories which are specialized in radiocarbon dating is provided (http://www.radiocarbon.org/Info/lablist.html).

2.4.2.2 Radiation exposure dating or luminescence dating

The radioactive decay of ^{40}K, ^{87}Rb, ^{232}Th and ^{238}U contained in the minerals of most sedimentary deposits leads to irradiation of specific components of the sediment (e.g. quartz and feldspar) by the release of α, β and γ particles. Near surface rocks and sediments are also irradiated by cosmic rays. Both of these irradiation processes cause electrons to be trapped in crystal defects until these traps are saturated. The release of the trapped electrons can be stimulated either by heating the sample (thermoluminescence, TL) or by exposing the sample to sunlight (optically stimulated luminescence, OSL or optical dating); different wavelengths of light are used for stimulation - monochromatic green, blue (both for quartz grains), red, infra-red (feldspar), or by using the ultraviolet light of argon lasers. The calculated age is the time since the sample was last exposed to intense heat or sunlight where the luminescence signal was bleached away and reset to zero. Under stimulation, the amount of emitted 'light' (photons) is proportional to the accumulated dose rate at which the sample was irradiated (the environmental radioactivity of the sample) and the paleodose (the amount of radiation needed to generate the luminescence signal subsequent to bleaching or 'zeroing'). By dividing the paleodose by the dose rate, the age of the sample is determined. The dose rate is influenced by groundwater (absorption) and the moisture content of the sample. Effects caused during sampling also need to be taken into account; e.g. possible exposure of the sample to daylight during sampling sets the age of a sample to zero ('zeroing'), which is not representative of the past and will provide a false date.

In general, the different luminescence techniques are dating the time elapsed from the last heating (e.g. lava or pottery) or exposure to sunlight (sediments). If sediments have not been completely bleached or 'zeroed' completely, dating errors arise. Technically, the error of luminescence dating is on the order of 5 to more than 200%. Regardless of this wide range, if no material for radiocarbon dating is available, or the samples are expected to be older than 50 kyrs, TL and OSL provide very helpful dating techniques in paleoseismology for a wide range of different natural materials (Table 4) and artifacts [283].

TABLE 4. DIFFERENT METHODS USED IN LUMINESCENCE DATING (BASED ON PREUSSER ET AL. IN 2008 [284], AND REFERENCES THEREIN)

Abbrev.	Method	Main application	Primary Reference
TL	Thermoluminescence	Dating heated materials	Aitken et al. (1964)
ITL	Isothermal TL	Experimental (quartz)	Jain et al. (2005)
OSL	Optically stimulated lum.	Dating sediments (quartz)	Huntley et al. (1985)
IRSL	Infrared stimulated lum.	Dating sediments (feldspar)	Hütt et al. (1988)
IR-RF	Infrared radiofluorescence	Dating sediments (feldspar)	Trautmann et al. (1999a)
LM-OSL	Linearly modulated OSL	Analytical tool (quartz)	Bulur (1996)
HR-OSL	Spatially resolved lum.	Dating rock surfaces	Greilich et al. (2002)
TT-OSL	Thermally transferred OSL	Experimental (quartz)	Wang et al. (2006 a)

For more detailed information or an overview, please carefully read Preusser et al. [284] or Walker [266]. A list of US laboratories specialized in luminescence dating can be found here: http://crustal.usgs.gov/laboratories/luminescence_dating/index.html, but there are many more luminescence dating laboratories all over the world.

2.4.2.3 Cosmogenic nuclide dating

In earth sciences cosmogenic nuclides are used to date landforms by means of exposure to cosmic rays; applications include dating various exposed surfaces, burial dating and estimation of erosion rates of catchment areas, as well as many others (Fig. 42). Cosmogenic isotope production has significantly varied over the last 10 kyrs and is generally greatest at high altitudes and high latitudes. In contrast to OSL/TL or radiocarbon dating methods where samples are dated, the cosmogenic nuclide technique dates the exposure ages of a surface.

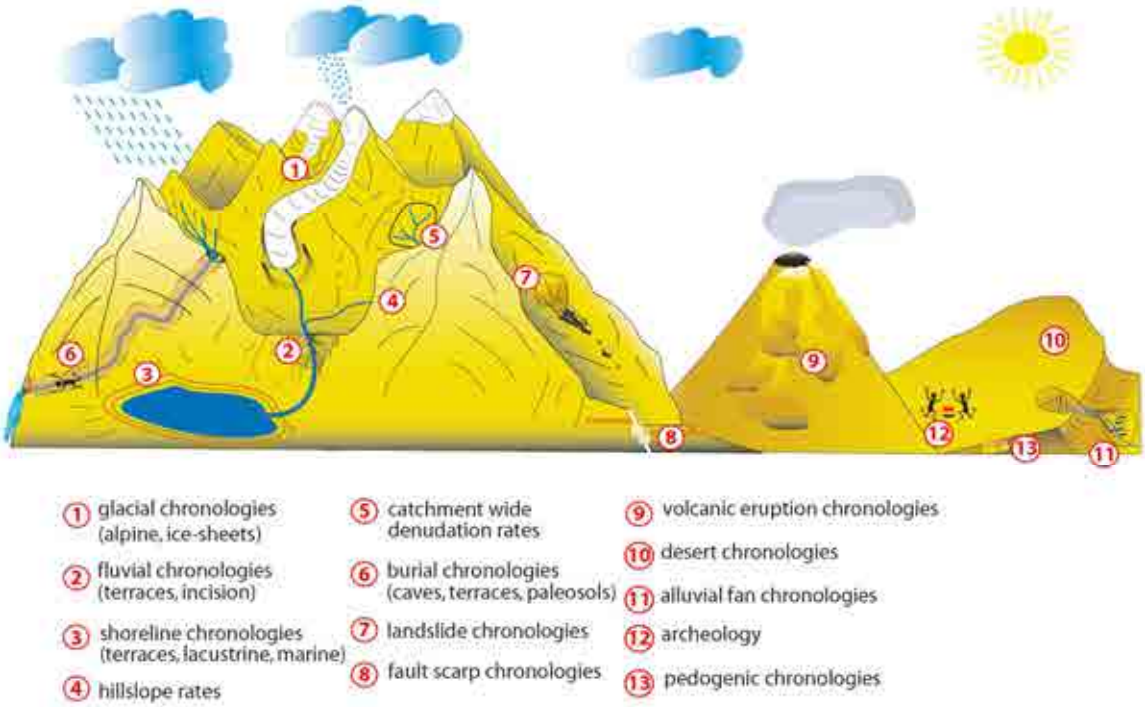

FIG. 42. Various landforms and modifications to landforms (i.e. faulting, sliding, etc.) that can be dated by cosmogenic nuclides (courtesy of S.Ivy-Ochs). Note that in paleoseismic studies faulted geologic features and structures, like landslides, alluvial fans, or shorelines and moraines, can also be indirectly dated.

The six main isotopes that are usually employed and commonly measured with AMS (acceleration mass spectrometry) are ^{3}He, ^{10}Be, ^{14}C, ^{21}Ne, ^{26}Al, ^{36}Cl. This technique is, however, an emerging field and other isotopes are presently being tested. Basic assumptions for dating are: (a) production rate of nuclides are known (Table 5); (b) the surface must have been exposed and not subsequently covered - no erosion; (c) there are no inherited nuclides which have previously been exposed to cosmic rays; and (d) a closed system has been operating since its exposure.

TABLE 5.DIFFERENT MATERIAL USED IN LUMINESCENCE DATING (BASED ON PREUSSER ET AL. IN 2008 [284], AND REFERENCES THEREIN)

Material	Material details	Method	Dated event	Interpreted as time of	Archaeological example
Brick	Quartz, feldspar	TL/OSL	Last firing	Manufacture	Bailiff & Holland (2000)
Brick surface	Quartz, feldspar	OSL	Last exposure	Construction; repair; destruction	Bailiff & Holland (2000)
Ceramic, pottery, tile	Quartz, feldspar	TL/OSL	Last firing	Manufacture; authenticity	Barnett (2000)
Daub (burnt)	Quartz, feldspar	TL/OSL	Last heating	Destruction	Quickert et al. (2003)
Figurine	Quartz, feldspar	TL/OSL	Last heating	Manufacture; authenticity	Zink & Porto (2005)
Hearth stone	Sandstone, limestone, granite (quartz, feldspar)	TL/OSL	Last heating	Last use	Ichikawa & Nagatomo (1978)
Kiln	Quartz, feldspar	TL	Last firing	Last use	Hong et al. (2001)
Lithic artefact (heated)	Flint, chert, quartzite, quartz, silcrete	TL	Last heating	Discard	Richter et al. (2007)
Limestone (heated)	Calcite, quartz	TL	Last heating	Last use	Roque et al. (2001)
Mortar	Quartz, feldspar	TL/OSL	Last light exposure	Building	Goedicke (2003)
Oven	Quartz, feldspar	TL	Last firing	Last use	Roque et al. (2002)
Pit/trench infill	Quartz, feldspar	OSL	Last light exposure	Abandonment; infilling	Lang & Wagner (1996)
Rock surface	Granite, marble, limestone (quartz, feldspar, calcite)	OSL/TL	Last light exposure	Construction; destruction	Greilich et al. (2005, 2006); Liritzis & Vafiadou (2005)
Sediment (burnt)	Quartz, feldspar	TL/OSL	Last heating	Last use	Godfrey-Smith & Shalev (2002)
Sediment, aeolian	Quartz, feldspar	OSL	Last light exposure	Deposition	Jacobs et al. (2003 a,b)
Sediment, colluvial	Quartz, feldspar	OSL	Last light exposure	Deposition	Lang & Hönscheidt (1999)
Sediment, fluvial	Quartz, feldspar	OSL	Last light exposure	Deposition	Folz et al. (2001)
Slag	Quartz	TL	Last firing	Last use	Haustein et al. (2003)
Wasp nest	Quartz, feldspar	OSL	Last light exposure	Building	Yoshida et al. (2003)

In paleoseismic studies a large effort was put into the dating of morphologic fault scarps mainly consisting of carbonates by applying ^{36}Cl methodology after the first attempt of Zreda and Noller in 1998 [285] (e.g. [270, 272, 286, 287]); the results were later correlated to enrichment/depletion of chemical elements, including rare earth elements, on the fault plane [288]. Dating morphological features in non-consolidated alluvial deposits displaced along active faults with in-situ produced ^{10}Be in the Gobi-Altaï (western Mongolia) resulted in the evaluation of slip rates [289]. A combination of ^{10}Be and ^{26}Al from alluvial terrace quartz pebbles constrained the late Holocene slip rate on the Xidatan segment of the Kunlun fault in northeastern Tibet [290]. A major challenge for future cosmogenic nuclide dating are faulted geologic features and secondary structures like landslides, liquefaction, alluvial fans, or shorelines and moraines, which can be indirectly dated to derive a faulting age.

TABLE 6. OVERVIEW OF COSMOGENIC NUCLIDE CHARACTERISTICS (BASED ON IVY-OCHS AND KOBER IN 2008 [291], SEE ALSO REFERENCES THEREIN; *PRODUCTION RATES BASED ON GOSSE AND PHILLIPS IN 2001 [292])

Nuclide	Half-life	Other isotopes	meas. method	Target elements	Production rate (atoms/g.yr*)	Advantages/minerals used	Disadvantages
^{10}Be	1.51 Myr	^{9}Be	AMS	O Si	5	quartz resistant and ubiquitous	low production rate, ^{10}B interference in AMS generally restricted to quartz (no meteoric ^{10}Be)
^{26}Al	716 kyr	^{27}Al	AMS	Si	31	high production rate quartz resistant and ubiquitous	restricted to quartz (low Al) accurate determination of ^{27}Al required
^{36}Cl	301 kyr	^{35}Cl, ^{37}Cl	AMS	Ca K ^{35}Cl	composition dep. e.g. 10 granite e.g. 20 limestone	low detection limit (low AMS Bkgd) any rock type, silicates & carbonates	complicated production, ^{36}S interference in AMS accurate determination of total Cl required determination of rock composition required
^{14}C	5.73 kyr	^{12}C, ^{13}C	AMS	O	16	useful for short timescales quartz resistant and ubiquitous	short half-life atmospheric ^{14}C contamination
^{3}He	stable	^{4}He	static mass spec.	many	120	high production rate useful for long time scales pyroxene, olivine	diffuses out of quartz or volcanic groundmass radiogenic/nucleogenic/magmatic correction beware pre-exposure
^{21}Ne	stable	^{20}Ne, ^{22}Ne	static mass spec.	Mg Si	20	useful for long time scales, > 50 kyr quartz, olivine, pyroxene	nucleogenic /magmatic correction high air background possible beware pre-exposure

For more detailed information or an overview, please carefully read Dunai [293], Ivy-Ochs and Kober [291] or Walker [266] and/or visit http://www.ams.ethz.ch/research/ams/insitu or http://www.cologneams.uni-koeln.de/. There are more cosmogenic dating laboratories located all over the world (e.g. http://cnef.earthsciences.dal.ca/**).**

2.4.3 Other dating methods

Further isotopic dating methods use radioactive decay with relatively long half-lives such as argon-isotope or uranium-series dating (Table 3). Shorter half-life isotopes like ^{210}Pb (half-life: 22.26 yrs), ^{137}Cs (hl: 30.17 yrs) or ^{32}Si (hl: 170 yrs) are used to date sediments, especially of young lacustrine and marine deposits, at much shorter timescales and with a high resolution (tens of years). Bioturbation and reworking may lead to problems when using shorter half-life isotopes for dating.

The argon-isotope or uranium-series dating as well as apatite/zircon fission track methods are not discussed here, but for an overview and more detailed information please consult Walker [266]. All these methods need suitable sample material for dating (e.g. volcanic ashes, carbonates, speleothems or calcretes, mollusk shells, teeth or bones). Sample preparation is time consuming, dating is expensive and not many laboratories are specialized in these techniques. Long half-life isotopes are generally not applied in paleoseismic studies and are better used to constrain long term regional uplift or exhumation rates. Some exceptions may be useful in paleoseismic investigations; if volcanic ashes are encountered in Holocene/Late Pleistocene deposits, and if they yield sanidine phenocrysts, good results can be obtained with the ^{40}Ar/^{39}Ar technique as the dating error is around 5% [294]. Volcanic ash in lake deposits can significantly help dating paleoseismic features or secondary earthquake effects like mass wasting in tectonically active areas. A good example of this is the Mediterranean region where the eruption history and geochemical fingerprints of Italy's volcanoes, as well as the historical seismicity, are well known and documented (Wagner et al., [295]).

In arid or semi-arid environments, larger clasts in coarse-grained alluvial deposits are often coated with a thin pedogenic carbonate rind (calcretes). The carbonate rind usually forms at the bottom of the gravel or cobble and can be dated with the ^{230}Th/U dating technique [296]. A prerequisite is always that the mineral phase within the sample represents a 'closed system' and has not been contaminated [266].

Sidereal methods use annual-banded sediments or organisms and include dendrochronology, varve chronology, lichenometry, annual banding of speleothems, and sclerochronology of corals or mollusks.

Dendrochronology or the study of tree-ring growth may help to date an earthquake with some precision if the regional growth chronology of an affected tree species is available. Through the annual growth of rings in tree trunks, a seasonal banding is present in most softwood species (coniferous). Hardwood or deciduous trees can also be used for chronology; oak (*Quercus*) or pine (*Pinus*) trees are usually used [297]. Timber incorporated in historical buildings or old drainages can also help with dating if a sufficiently long sequence of rings is encountered. Dendrochronology is directly linked to dendroclimatology, as the annual ring variability is strongly dependent on climatic conditions [298]. A number of studies validated tree-ring application to paleoseismology, but mainly concentrated on disturbed growth patterns of trees after large earthquakes (e.g. [299]). Up to now, the contribution of dendrochronology in enhancing the paleoseismic record along individual faults or dating individual earthquakes is still an emerging field in paleoseismology [2].

Varve chronology has been established in 1912 by De Geer [300] in Sweden. It is based on annual sedimentary accumulations which generally consists of a couplet: a 'white' summer layer and a 'black' winter layer (clastic-organic varves); or alternations of coarse- and fine-grained layers (clastic varves). Varves are found in lacustrine and marine environments, best examples are preserved in glaciolacustrine or glaciomarine deposits that lack bioturbation. The thickness of the individual varves may vary. Disturbances of varves, like folding, warping, faulting, liquefaction, unconformities or intercalation of turbidites, can indicate tectonic activities like earthquake shaking, and is regarded as 'off-fault' evidence [301].

Lichenometry uses the growth patterns of lichen (a symbiosis of algae and fungi). It was Austrian scientist Beschel in 1950 [302] who pioneered studies on the colonization of lichen on bare rock faces by their progressive increase in size by marginal growth. Requirements of lichenometry are: (a) growth rates have to be known, and (b) no significant time span has elapsed since the surface exposure and lichen colonization [266]. Not all lichens are suitable for dating; however, some species are relatively long-lived (*Rhizocarpum geographicum*). Some case studies in paleoseismology have applied lichenometry, e.g. dating rockfalls associated with earthquakes (e.g. [303, 304]).

Speleothems are cave deposits of hard carbonates and form stalactites, stalagmites or flowstones (see 2.2.4). Some of those are annual banded —like tree trunks— because of changing conditions during formation and are, therefore, used also in paleoclimate studies. If these growth patterns are disturbed or entire groups of stalagmites or stalactites have collapsed, sometimes a paleoseismic event seems likely. To identify one single event dating has to show that collapses, breaks, deformations and perturbations are synchronous in different parts of a cave, they occur in many places, and/or additional earthquake evidence has been found taking in account the dating uncertainties. Other explanations for growth anomalies or breaks must be excluded. As an example, the top layer or band of a fallen

stalagmite and the oldest layer of the in-place stalagmite should be sampled. This may allow the breaking event to be bracketed. Also, growth anomalies can be investigated for paleoseismic studies. Combining paleoseismicity with speleothem growth and anomalies is, however, not an easy task [175] and should be carried out with experts.

Corals and mollusks of tropical shallow oceans produce aragonite skeletons with relatively fast annual growth rates of several mm to cm. The habitat of corals is closely tied to sea level; sudden uplifting or drowning leads to the death of the colony. The corals can, however, regrow if the coral remains can re-adjust to the favored sea level conditions. The remnants of these animals can be well dated by radiocarbon. Coral skeletons implement trace-elements and stable oxygen and carbon isotopes, which serve as proxy data for salinity, temperature, precipitation, evaporation, and river-run off for paleoclimate investigations. Growth bands of corals can be visualized by X-ray or luminescence techniques. The study of coral growth as a dating method is called sclerochronology and has an annual resolution of 1–2 years per century. In paleoseismology, large subduction earthquakes and associated uplift of coastal coral mini-atolls, and their subsequent death, has been used to detect ancient earthquakes (e.g. [305]). It is even possible to decipher individual stages of the seismic cycle (e.g. [306]).

Relative dating and archeological methods
Relative dating methods include rock-surface weathering, obsidian hydration dating when volcanic material is present, pedogenesis, fossil bone dating, and amino-acid geochronology [266]. In contrast to absolute age estimates for the paleoseismic features, relative dating will likely have large uncertainties, although these uncertainties will decrease with improved accuracy of age estimates for the reference strata. Soil development considers the qualitative development of soil horizons to estimate the age of deposits [307], and the stratigraphic relationship of paleoseismic features to these deposits bounds the age of the paleoseismic feature. Amino-acid racemization (AAR) is a chemical dating technique based on the transformation of the L-amino-acids found in all living organisms to their mirror image molecules. After death, L-amino-acids are gradually transformed into D-amino-acids until equilibrium level is reached. This dating method does not provide ages in years, but only a relative age assignment [266].

Relative dating also encompasses archeological remains for which a relatively precise date can be obtained, at least in the parts of Europe that was colonized by ancient Greeks and Romans 2,500 years ago. The archeological context offers and considers the relation of a paleoseismic feature to an identified archeological horizon. Other methods like oxygen isotope chronostratigraphy or paleomagnetism are not explained here.

2.4.4 Dating strategies in the field

Dating is fundamental in paleoseismic studies. Often the strongest argument for a seismic event is the synchroneity of on-fault and off-fault paleoseismic evidence in a defined region. A combination of different dating methods on different features, like coeval landsliding or rock falls, coastal uplift, liquefaction phenomena and colluvial wedge formation can be helpful to constrain a paleo-earthquake. In case of absolute dating, however, the standard deviation of the results has to be considered in data interpretation.

2.4.4.1 Dating on-fault layers

In trenching studies the first aim is to establish the stratigraphy of the deposits encountered. This includes retro-deformation analysis of the layers and individual event identification (e.g. faulting, folding, sliding, erosion, deposition). Then, samples of key horizons should be taken, either using the bracketing strategy, dating the last deformed layer and the first not-deformed layer, or event dating where samples are taken from the layer associated with earthquake-related deformation. Contamination whilst sampling must be avoided. Finally, other ways and methods of dating the paleoseismic event(s) should be considered.

2.4.4.2 Dating liquefaction features

Deriving an age for liquefaction features (see Section 2.2) can provide an age estimate of the earthquake that caused its formation. A narrow age constraint will help correlate features across a region and differentiate features that resulted from distinct but closely timed earthquakes. Liquefied strata and surface-piercing sand blow deposits are most helpful for constraining an event's age. Organic material or sediment (radiocarbon dating) that immediately underlies/overlies a liquefaction feature can provide reliable maximum/minimum age estimates for the timing of disruption. Furthermore, stratigraphic relationships can help establish relative dating, i.e. maximum age for a sand dike can be derived from the age of the highest stratigraphic unit cut by the sand dike [31]. Such features are, however, rarely preserved and found. Inorganic material in fine-grained sediments yielding quartz and feldspar grains can possibly be dated by OSL and/or TL techniques.

Abrupt changes in soil moisture due to a liquefaction event, burial by a sand blow, or disruption of tree root systems by lateral spreading can affect tree growth and possibly lead to death [308]. Comparison of an affected tree's ring pattern (dendrochronology) against a known regional baseline can pinpoint the time of growth disruption or death, and thus the time of an earthquake. Three other dating techniques that may be helpful for dating liquefaction features involve archeological methods, stratigraphic methods and soil development.

Caution must always be exercised in examining stratigraphic relationships and selecting material for quantitative age analysis. All of these techniques mentioned have potential pitfalls. A highly experienced Quaternary geologist or paleoseismologist should be consulted for dating liquefaction features.

2.4.4.3 Dating paleo-landslides associated to earthquakes

Deriving an age for mass-wasting features triggered by earthquakes (see Section 2.3) can provide an age estimate of the earthquake that caused its formation. An age constraint and evidence for coeval mass wasting (which could point to an active fault in the vicinity) will help correlate features across a region and differentiate them from features that resulted from distinct processes, i.e. heavy rain fall.

Trenching analysis of recognized landslides can provide samples of buried soils and strata containing organic material for radiocarbon dating [136] or, if absent, fine-grained sediments for OSL and/or TL techniques. The same dating methods apply for dating sediments of quake-lakes, which are formed by landslides damming of valleys during earthquakes. In coastal areas, fossils contained in marine terraces can be used for Th/U series dating [143]. Lichenometric techniques and cosmogenic dating have successfully been used for dating the free faces of landslide scars and/or single fallen blocks (e.g. [303, 304]). Individual huge

fallen blocks can be dated with samples of the soil beneath the blocks [124]. Archeological data from historic structures (castles, temples, etc.) damaged by landslides can be used to put constraints on the timing and extent of the affected area (e.g. Silva et al., [309]). If paleolandslides, paleoshorelines, sackungen, etc. still demonstrate a geomorphic expression, the preservation of the features within the regional landforms can provide a rough estimate of the relative age of the landform or landform assemblage (e.g. Late Holocene, Late Pleistocene, postglacial, etc.). Mass movement deposits due to slope failures caused by earthquakes have been found and studied extensively in Lake Lucerne (Switzerland) by Strasser et al. [157].

Caution must always be exercised in examining stratigraphic relationships and selecting material for quantitative age analysis. All techniques mentioned have potential pitfalls. A highly experienced Quaternary geologist or landslide specialist should be consulted for dating mass movement features and events.

2.4.4.4 Dating lacustrine-marine sediments and cave sediments in paleoseismology

Young faulted sediments in lakes [110] or shallow marine settings, or even caves deposits, can be successfully dated; best results are generally obtained by radiocarbon dating, $^{234}U/^{230}Th$ ratio and using shorter half-life isotope methods. For sampling soft sediments, hand-digging or coring techniques can be undertaken. For caves in carbonates, the material should be hard concretionary speleothems (stalactite, stalagmite, flowstone, soda straws) or cored samples of these. Sometimes the lamination pattern in speleotherm cross sections can yield evidence for any kind of interruption of carbonate precipitation. The detailed analysis of the crystalline structure of speleothems is crucial to avoid samples with geochemical openings, dissolution-crystallization, diagenetic processes, or pollution of samples by clay or detrital material (dead carbon), which could alter dates (e.g. [173, 310]). Clay pollution is characterized by an increase in thorium content that can be evidenced by the ^{232}Th signature (e.g. [177]). Other dating methods applied in dating cave deposits are: stable isotopes $\delta^{18}O$ and $\delta^{13}C$ (Genty et al., [311]); $^{238}U/^{206}Pb$ ratio by thermal ionization mass spectrometry (TIMS, see [312]); and $^{226}Ra/^{230}Th$ ratio excess dating [313].

Caution must always be exercised in examining stratigraphic relationships and selecting material for quantitative age analysis. All techniques mentioned have potential pitfalls. A highly experienced Quaternary geologist or speleothem/cave specialist should be consulted for dating young sediments or cave deposits and related earthquake events.

3. PALEOSEISMIC DATA AND ITS CONTRIBUTION TO AN IMPROVED SEISMIC HAZARD ASSESSMENT.

3.1. EMPIRICAL RELATIONSHIPS BETWEEN FAULTING PARAMETERS AND MAGNITUDE

In the SHA, the predicted maximum earthquake size should be credible for the study area, i.e. its physical characteristics and its recurrence rate must be compatible with the local geologic setting. In other words, the prevailing tectonic and geodynamic setting in a region intimately influences the approach to be used for estimating its seismic hazard.

The ultimate goal of all current approaches is to establish the seismic history in order to arrive at estimates of the repeat time (recurrence interval) of maximum credible earthquakes for each individual fault or segment of a given fault or fault system. This means that it seeks to ascribe every individual earthquake to its causative fault (seismotectonic association) in order to determine its seismic cycle.

The experience gained in the past decades indicates that an approach exclusively based on instrumental and historic seismicity data is insufficient in most cases for any of the following reasons: (1) the region under assessment is structurally complex and its seismicity is widely scattered making reliable seismotectonic associations almost impossible; (2) the time span of the instrumental seismicity (less than 100 years long even for the very best cases) worldwide is shorter than the seismic cycle of most faults thus making it impossible to know the return period of destructive or large earthquakes; (3) there are many countries where the written tradition covers less than 500 years - this applies to the African, American and Australian continents with only a number of countries in Middle and East Asia having a historical record of a few thousand years - whereas large earthquakes recur in terms of several thousand years and occasionally tens of thousands of years, making the contribution of the historical seismicity usually too short; and (4) some faults have shown that they do not follow the Gutenberg-Richter relationship for large earthquakes, although being perfectly valid for events of magnitude smaller than m_b 5.5.

To overcome the time limitations posed by both the instrumental and historical seismicity records, together with frequent uncertainties on the seismotectonic associations, a different SHA approach is needed, relying on the geologic deformation associated with strong earthquakes, known as paleoseismology. The state of the art of paleoseismology has been already discussed (Section 2). Paleoseismology is, therefore, at present a standard technique, and following IAEA SSG-9 [1] it shall be used for the characterization of seismic hazards at nuclear installations. Here we focus on the interpretation of paleoseismic features, essentially the evidence of past surface faulting earthquakes, in terms of magnitude. Earthquake magnitude in most cases is derived from paleoseismic surface displacement or surface rupture length by the application of empirical relationships that exist between net slip per event measured in trench walls (as discussed above in Section 2.1) and magnitude data for capable faults available in the literature, always assuming that the total segment length would rupture at once. In the following we will analyze fault scaling parameters related only to surface faulting. Secondary coseismic effects like liquefaction, landslides, markers on sediments, tsunamis and other effects that might also be very important in the interpretation of the actual occurrence and extent of primary surface faulting and in the characterization of the ‘seismic

landscape' (see Section 2.1), are fully explained in the previous paragraphs (Section 2.2 and 2.3).

Consideration will be given regarding the use of these effects in empirical relations through the compilation of worldwide set of regressions, and as to their applicability in the range of tectonic regimes and fault slip types in existence around the world.

3.1.1. Empirical relationships: some examples and critical issues

As previously stated, by studying the effects caused by moderate to large earthquakes on the environment it is possible to define a series of correlations and models that allow us to constrain source parameters, starting with observations recorded in the field (good examples of paleoseismic field studies on capable faults are reported in Sections 2.1.6.1 and 4.1.1).

Over the years, various authors have developed empirical correlations in order to perform an evaluation of the potential seismic risk within an area.

The most used fault scaling parameters are:

- surface or sub-surface rupture length;
- down-dip rupture length;
- average and maximum displacement;
- fault geometry;
- slip rate;
- shear modulus;
- stress drop;
- depth of seismogenic zone;
- seismic moment.

In paleoseismology, the most used parameters in performing regressions are the surface displacement and the surface rupture length.

3.1.1.1 Wells and Coppersmith in 1994 [78]: the most used relationships worldwide

The empirical relationships between magnitude and the direct effect on the Earth's surface which is most well-known and used in the scientific sphere are certainly those presented in the study by Wells and Coppersmith [78].

The parameters related to the source or to the seismic event of 244 historical earthquakes throughout the world which had a magnitude of 4.5 or higher, were compiled by the authors in a database including shallow-focus (hypocentral depth less than 40 km), continental interplate or intraplate earthquakes. Earthquakes associated with subduction zones, both plate interface earthquakes and those occurring within oceanic slabs, are excluded.

These studies show that a high correlation, in general $r > 0.7$, characterizes all the regressions, indicating that a strong correlation exists between moment magnitude (M) and various rupture parameters (e.g. Fig. 43). This enables the use of these relations to confidently estimate dependent variables.

The authors developed a series of correlations between moment magnitude (M), surface rupture length, sub-surface rupture length, down-dip rupture length, area of the rupture and the average displacement per event.

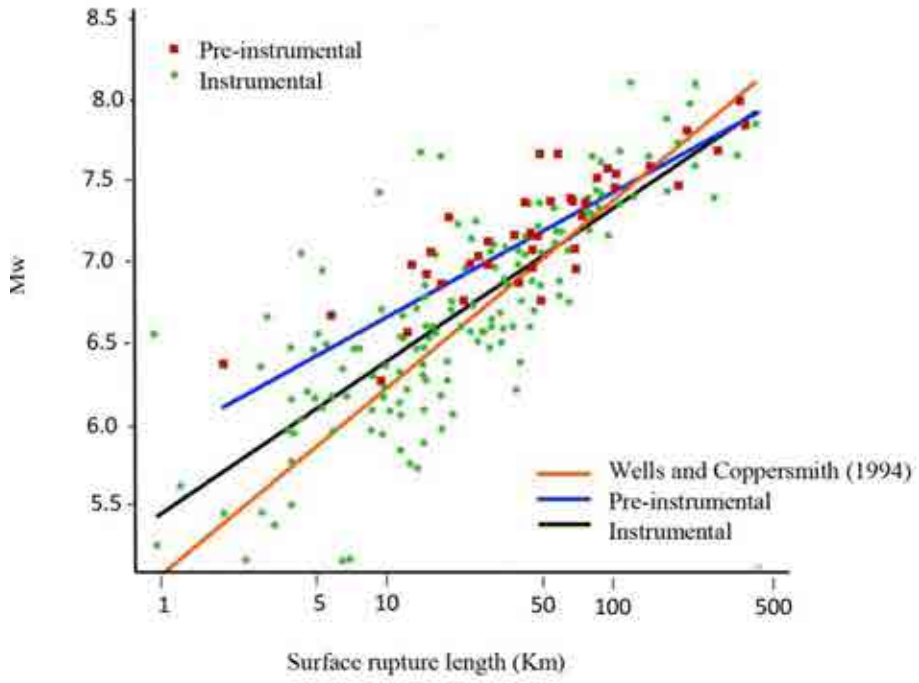

FIG. 43. Regression lines of surface rupture length on moment magnitude (a) and rupture area on moment magnitude (b) Based on Wells and Coppersmith (1994) [78] and Stirling et al. (2002) [314].

Each regression can be applied to a specific range defined by minimum and maximum magnitude values, within which the obtained results can be considered reliable (see Tables 7 and 8). The correlations which have proved the most consistently reliable are those which combine the magnitude and surface rupture length, sub-surface rupture length, down-dip rupture width and rupture area, whereas those between displacement and rupture length or magnitude correlate less well.

TABLE 7. RELATIONS BETWEEN RUPTURE LENGTH, RUPTURE WIDTH, RUPTURE AREA AND MOMENT MAGNITUDE (M) [78]

Equation*	Slip Type†	Number of events	Coefficients and Standard Errors		Standard Deviation s	Correlation Coefficient r	Magnitude Range	Length\Width Range (km)
			a(sa)	b(sb)				
M= a+b × log(SRL)	SS	43	5.16(0.13)	1.12(0.08)	0.28	0.91	5.6 to 8.1	1.3 to 432
	R	19	5.00(0.22)	1.22(0.16)	0.28	0.88	5.4 to 7.4	3.3 to 85
	N	15	4.86(0.34)	1.32(0.26)	0.34	0.81	5.2 to 7.3	2.5 to 41
	All	77	5.08(0.10)	1.16(0.07)	0.28	0.89	5.2 to 8.1	1.3 to 432
log (SRL) = a+b × M	SS	43	-3.55(0.37)	0.74(0.05)	0.23	0.91	5.6 to 8.1	1.3 to 432
	R	19	-2.86(0.55)	0.63(0.08)	0.20	0.88	5.4 to 7.4	3.3 to 85
	N	15	-2.01(0.65)	0.50(0.10)	0.21	0.81	5.2 to 7.3	2.5 to 41
	All	77	-3.22(0.27)	0.69(0.04)	0.22	0.89	5.2 to 8.1	1.3 to 432
M = a+b × log(RLD)	SS	93	4.33(0.06)	1.49(0.05)	0.24	0.96	4.8 to 8.1	1.5 to 350
	R	50	4.49(0.11)	1.49(0.09)	0.26	0.93	4.8 to 7.6	1.1 to 80
	N	24	4.34(0.23)	1.54(0.18)	0.31	0.88	5.2 to 7.3	3.8 to 63
	All	167	4.38(0.06)	1.49(0.04)	0.26	0.94	4.8 to 8.1	1.1 to 350
log(RLD)= a+b × M	SS	93	-2.57(0.12)	0.62(0.02)	0.15	0.96	4.8 to 8.1	1.5 to 350
	R	50	-2.42(0.21)	0.58(0.03)	0.16	0.93	4.8 to 7.6	1.1 to 80
	N	24	-1.88(0.37)	0.50(0.06)	0.17	0.88	5.2 to 7.3	3.8 to 63
	All	167	-2.44(0.11)	0.59(0.02)	0.16	0.94	4.8 to 8.1	1.1 to 350
M= a+b × log(RW)	SS	87	3.80(0.17)	2.59(0.18)	0.45	0.84	4.8 to 8.1	1.5 to 350
	R	43	4.37(0.16)	1.95(0.15)	0.32	0.90	4.8 to 7.6	1.1 to 80
	N	23	4.04(0.29)	2.11(0.28)	0.31	0.86	5.2 to 7.3	3.8 to 63
	All	153	4.06(0.11)	2.25(0.12)	0.41	0.84	4.8 to 8.1	1.1 to 350
log(RW) = a + b × M	SS	87	-0.76(0.12)	0.27(0.02)	0.14	0.84	4.8 to 8.1	1.5 to 350
	R	43	-1.61(0.20)	0.41(0.03)	0.15	0.90	4.8 to 7.6	1.1 to 80
	N	23	-1.14(0.28)	0.35(0.05)	0.12	0.86	5.2 to 7.3	3.8 to 63
	All	153	-1.01(0.10)	0.32(0.02)	0.15	0.84	4.8 to 8.1	1.1 to 350
M= a+b × log(RA)	SS	83	3.98(0.07)	1.02(0.03)	0.23	0.96	4.8 to 7.9	3 to 5,184
	R	43	4.33(0.12)	0.90(0.05)	0.25	0.94	4.8 to 7.6	2.2 to 2,400
	N	22	3.93(0.23)	1.02(0.10)	0.25	0.92	5.2 to 7.3	19 to 900
	All	148	4.07(0.06)	0.98(0.03)	0.24	0.95	4.8 to 7.9	2.2 to 5,184
log(RA) = a + b × M	SS	83	-3.42(0.18)	0.90(0.03)	0.22	0.96	4.8 to 7.9	3 to 5,184
	R	43	-3.99(0.36)	0.98(0.06)	0.26	0.94	4.8 to 7.6	2.2 to 2,400
	N	22	-2.87(0.50)	0.82(0.08)	0.22	0.92	5.2 to 7.3	19 to 900
	All	148	-3.49(0.16)	0.91(0.03)	0.24	0.95	4.8 to 7.9	2.2 to 5,184

* SRL- surface rupture length (km); RLD- subsurface rupture length (km); RW- downdip rupture width (km), RA – rupture area (km^2).
† SS – strike slip; R-reverse; N-normal.

TABLE 8. RELATIONS BETWEEN DISPLACEMENT AND MOMENT MAGNITUDE [78]

Equation*	Slip type†	Number of events	Coefficients and (Standard Errors)		Standard Deviation s	Correlation Coefficient r	Magnitude Range	Length\Width Range (km)
			a(sa)	b(sb)				
$M_W = a + b \times \log(MD)$	SS	43	6.81(0.05)	0.78(0.06)	0.29	0.90	5.6 to 8.1	0.01 to 14.6
	{R‡	21	6.52(0.11)	0.44(0.26)	0.52	0.36	5.4 to 7.4	0.11 to 6.5}
	N	16	6.61(0.09)	0.71(0.15)	0.34	0.80	5.2 to 7.3	0.06 to 6.1
	All	80	6.69(0.04)	0.74(0.07)	0.40	0.78	5.2 to 8.1	0.01 to 14.6
$\log(MD) - a + b \times M_W$	SS	43	- 7.03(0.55)	1.03(0.08)	0.34	0.90	5.6 to 8.1	0.01 to 14.6
	{R	21	- 1.84(1.14)	0.29(0.17)	0.42	0.36	5.4 to 7.4	0.11 to 6.5}
	N	16	- 5.90(1.18)	0.89(0.18)	0.38	0.80	5.2 to 7.3	0.06 to 6.1
	All	80	-5.46(0.51)	0.82(0.08)	0.42	0.78	5.2 to 8.1	0.01 to 14.6
$M_W = a + b \times \log(AD)$	SS	29	7.04(0.05)	0.89(0.09)	0.28	0.89	5.6 to 8.1	0.05 to 8.0
	{R	15	6.64(0.16)	0.13(0.36)	0.50	0.10	5.8 to 7.4	0.06 to 1.5}
	N	12	6.78(0.12)	0.65(0.25)	0.33	0.64	6.0 to 7.3	0.08 to 2.1
	All	56	6.93(0.05)	0.82(0.10)	0.39	0.75	5.6 to 8.1	0.05 to 8.0
$\log(AD) - a + b \times M_W$	SS	29	- 6.32(0.61)	0.90(0.09)	0.28	0.89	5.6 to 8.1	0.05 to 8.0
	{R	15	- 0.74(1.40)	0.08(0.21)	0.38	0.10	5.8 to 7.4	0.06 to 1.5}
	N	12	- 4.45(1.59)	0.63(0.24)	0.33	0.64	6.0 to 7.3	0.08 to 2.1
	All	56	- 4.80(0.57)	0.69(0.08)	0.36	0.75	5.6 to 8.1	0.05 to 8.0

* MD-maximum displacement (m); AD- average displacement (m)
† SS- strike slip; R-reverse; N-normal
‡ Regression for reverse slip relationships shown in italics and brackets are not significant at a 95% probability

However, there are common limitations to the above empirical regressions, including:

- a large standard deviation;
- data are obtained from shallow crustal earthquakes and therefore the regressions cannot be applied to all tectonic environments.

Based on Wells and Coppersmith's regressions, various authors have attempted to avoid these issues by integrating the database and by adjusting the deviations to arrive at the most objective result possible.

3.1.1.2 Mohammadioun and Serva in 2001 [28]: stress drop and moderate magnitude earthquake issues

Mohammadioun and Serva [28] conducted a critical review of the theoretical relationships between certain source parameters: seismic moment, magnitude, stress drop, rupture length, and fault displacement, and more specifically, the variation in stress drop for different slip types and corresponding scaling laws.

Furthermore, the authors proposed new correlations between the more available M_s (and not the moment magnitude as in the case of Wells and Coppersmith [78]; this is because M_s does not depend from an assumed value of stress drop), the source parameters and the stress drop (that can be estimated both from geologic observations and from characteristics of near-field spectra), and its estimate and variability on the basis of data from the fault slip, rupture length, slip type and fault width.

The proposed relationship links M_S to L and $\Delta\sigma$:

$$M_S = \log L + 1.33 \log \Delta\sigma + 1.66 \quad (2)$$

Where, M_S is the surface wave magnitude, L is the rupture length in km and $\Delta\sigma$ is the stress drop in bars.

Earthquake data from all over the world, and in particular those collected in Wells and Coppersmith [78] described above, were used in order to compute stress drop values. The obtained results show that stress drop values increase with fault width down to approximately 15 km (corresponding perhaps to the brittle-ductile boundary). This increase is more pronounced in the case of reverse faults than it is for strike-slip or normal fault mechanisms.

Furthermore, the authors have highlighted the limits of regression developed by Wells and Coppersmith in certain types of tectonic environment (as visible, for instance, in Fig. 44, which shows the example of surface faulting earthquakes from the Apennines of Italy and M. Etna volcano).

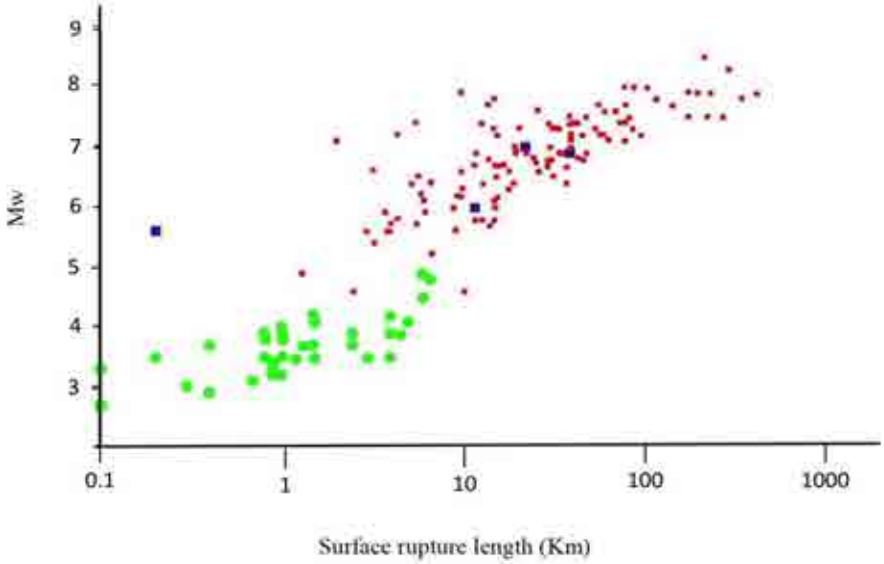

FIG. 44. Magnitude plotted versus surface rupture length: seismic events from Etna volcano (Green) and Apennines regions in Italy (Blue) compared with the data from Wells and Coppersmith (1994) [78] (dots), reproduce with permission of Mohammadioun and Serva in 2001 [28].

It is notable that data from normal faulting earthquakes in the Apennine region correlate with the data accumulated in the rest of the world, even if they show that the threshold for surface faulting in extensional settings is around M_w 5.5–6 (or lesser magnitude values as in the case of Mount Etna, Fig. 44), which challenges the idea that earthquakes of Magnitude 6 or less do not lead to surface faulting. The authors underline that the magnitude value over which surface faulting can occur is a function of the context in which the fault is present. In other words, it depends on the rheology of the material and on the typology of the stress environment at hypocentral depths. This is clearly demonstrated in volcanic environments; for example, data collected on Mt. Etna volcano (Italy) show that modest tectonic earthquakes may also generate surface faulting.

3.1.1.3 Stirling et al. in 2002 [314]: pre-instrumental data

Stirling et al. [314] show that the estimation of the rupture of surface faults (in particular for crustal earthquakes) caused by pre-instrumental (pre-1900) earthquakes, obtained using traditional methods (e.g. [315, 316]), tends to give values that are greater than estimates derived from Wells and Coppersmith's [74] regression.

These discrepancies have been ascribed to:

- uncertainties inherent in the pre-instrumental data;
- artefact of data selection in the dataset of Wells and Coppersmith.

In order to verify the error hypothesis, the authors have:

- integrated the dataset used by Wells and Coppersmith in 1994 [78] with the new earthquake data (post-1994) and instrumental data originally excluded in their analysis;
- collected data for the pre-instrumental period (pre-1900) and developed regressions on this basis;
- compared and contrasted the two new sets of regressions with each other and with Wells and Coppersmith's original dataset in order to evaluate the differences (Fig. 45).

The new regressions (see Table 9) that have been developed seem to have succeeded in reducing the amount of discrepancies but have not eliminated them completely. The hypothesis is that these differences are linked to the erosive process on traces of the pre-instrumental earthquakes characterized by modest surficial ruptures.

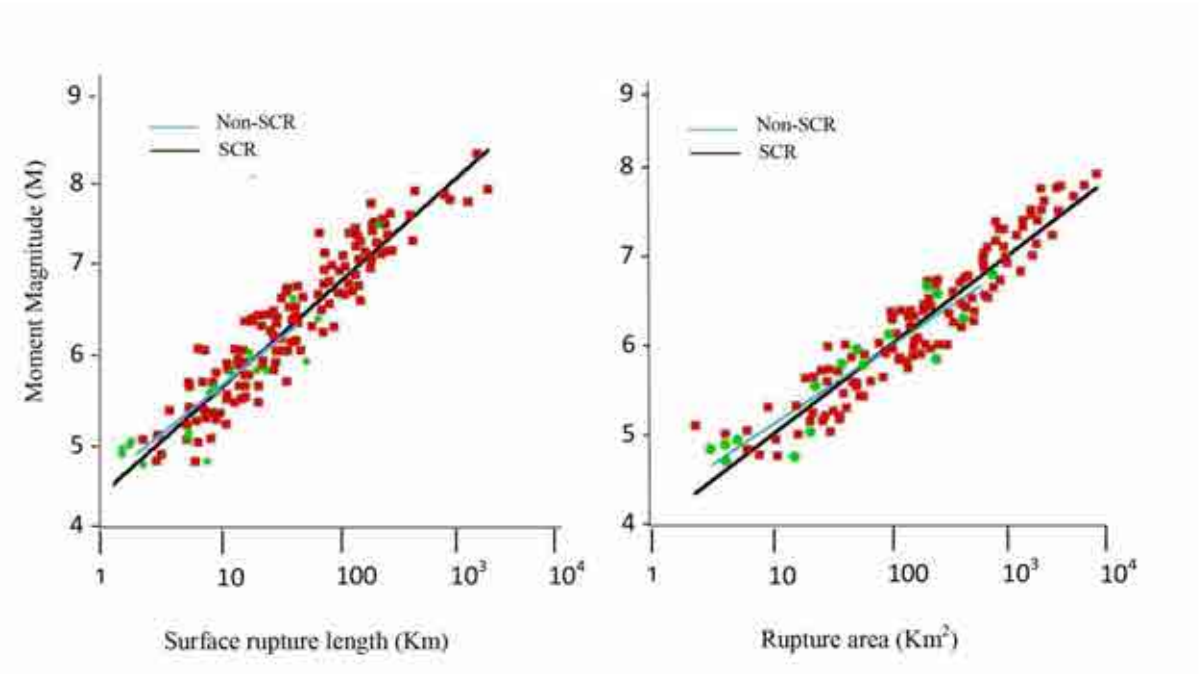

FIG. 45. Regressions of magnitude versus surface rupture length for our worldwide instrumental dataset, the worldwide pre-1900 pre-instrumental dataset and the original regression of Wells and Coppersmith (Based on Stirling et al. in 2002 [314]). SCR=Stable Continental Region.

TABLE 9. REGRESSIONS DEVELOPED BY STIRLING ET AL. IN 2002 [313]

Regressions of M_w on surface rupture length (L)				
Subset	N	a(sa)	b(sb)	RSD
M_w=a+b log(L)				
Instrumental	167	5.45(0.08)	0.95 (0.06)	0.37
Pre-instrumental	59	5.89(0.11)	0.79(0.06)	0.21
W and C	77	5.08(0.10)	1.16(0.07)	0.28

Regressions of M_w on an approximation of fault area (A) (A = surface rupture length X estimated rupture width)				
Subset	N	a(sa)	b(sb)	R.s.d
M_w=a+b log(A)				
Instrumental	108	4.54(0.12)	0.89(0.05)	0.31
Pre-instrumental	30	4.95(0.19)	0.78(0.06)	0.16
W and C	148	4.07(0.06)	0.98(0.03)	0.24
Rupture areas are approximated by surface length X estimated rupture width in our study, and by this method and from the spatial extent of aftershocks in Wells and Coppersmith's study. This latter therefore shows more data (148 events) than Stirling's instrumental dataset (108 events).				

Regression of average surface displacement (D) on surface rupture length (L)				
Subset	N	a(sa)	b(sb)	R.s.d
Log (D) = a+b log(L)				
Instrumental	95	-0.81(0.13)	0.56(0.08)	0.32
Pre-instrumental	30	-0.09(0.17)	0.35(0.10)	0.33
W and C	66	-1.43(0.18)	0.88(0.11)	0.36

Range of Data				
Subset	N	LL(km)	AA($km^{2)}$	D(m)
Instrumental	-4.6–8.1	-1–400	-3–7,000	-0.05–15
Pre-instrumental	-6.2–8.2	-2–400	-100–20,000	-1–10
W and C	-4.8–8.1	-1.3–432		-0.01–14.6
N is the number of data entries used in regression; a and b are the parameters of the regression, with associated standard errors sa and sb in parentheses; RSD is the residual standard deviation for the dependent variable; Mw is moment magnitude; L is surface rupture length; A is rupture area; and D is average surface displacement.				

3.1.1.4 Stirling et al in 2013 [317]: tectonic regime and fault slip type

This work was performed for the implementation of the GEM (Global Earthquake Model) project. As already discussed by Mohammadioun and Serva [28], Stirling et al in 2013 [317] and Stirling and Goded in 2012 [318] discuss the issues linked to the union of data from different tectonic environments in historical earthquake databases, and the consequent different forms of the regression equations that can result in large differences in magnitude for a given fault rupture.

Starting with the example of the significant underestimation of the M_w 7.1, 4 September 2010 Darfield (New Zealand) earthquake by the most used regressions worldwide (in particular Wells and Coppersmith [78], relations), they criticize the use of these relations with little or no consideration as to their applicability to a particular environment.

In order to provide a useful tool for choosing the most suitable regression to use in seismic hazard modeling, they have compiled a set of 72 existing empirical relations. The authors group these relations by their grade of applicability in different tectonic regimes and fault slip types, mainly on the basis of the characteristics of the earthquake contained in the dataset used for the development of the single regressions (Table 10).

TABLE 10. TECTONIC REGIMES, SUB REGIMES, AND MECHANISM (SLIP TYPES) USED AS A BASIS FOR SORTING REGRESSION FOR APPROPRIATE USE IN SEISMIC HAZARD STUDIES BASED ON STIRLING ET AL IN 2013 [317]

Tectonic regime	Sub regime	Mechanism
A-Plate Boundary crustal	Fast Plate Boundary Faults (> 10mm\year) (A1) Slow Plate Boundary faults (<10 mm\year) (A2)	Strike-slip dominated (A11) All faults (A21) Strike-slip (A22) Normal (A23) Reverse (A24)
B-Stable continental		Reverse (B1) Strike-slip (B2)
C-Subduction	Continental Marine Intraslab	Thrust (C1) Thrust (C2) Normal (C3)
D-Volcanic	Thin Crust (<10km) Thick (>10 Km)	Normal (D1) Normal (D2)

The compilation is limited to regressions of moment magnitude M_w, or seismic moment, on source area or length (Table 11).

TABLE 11. MOST RECOMMENDED REGRESSIONS, GROUPED ACCORDING TO TECTONIC REGIMES, SUB REGIMES, AND MECHANISM (SLIP TYPES); BASED ON STIRLING ET AL IN 2013 [317]

Tectonic regime	Name	Relationship	Units	Quality score	Comments
A11	Hanks and Bakun(2008) [319] - A ≤ 537 km² Hanks and Bakun(2008) [319] - A > 537 km² UCERF2 Wesnousky (2008) [320] - strike slip Leonard (2010) [321]	M_w = LogA + (3.98 ± 0.03) M_w = 4/3LogA + (3.07 ± 0.04) M_w = 4.2775 + 0.0726logA M_w = 5.56 + 0.87logL sig = 0.24 (in M_w) $W = C_1L^{\beta}$ $\dot{D} = C_2 \sqrt{A}$ Mo = uLWD $Mo = A^{1.5}$ (See below for Leonard coefficient/explanation)	A: Area (km²) L: surface rupture length (km) (*)	1 1 1 1 1	Best represented by Hanks & Bakun regressions. Regresseion datasets are dominated by fast-slipping plate boundary faults. Regression should be chosen according to the relevant fault area range.

A21	Yen and Ma (2011) [322] – all	Log A_e = -13.79 + 0.87LogM_o sig = 0.41 (in A_e) Log M_o = 16.05 + 1.5M	A: effective area (km²)	1	Best represented by Yen and Ma regression as datasets contain a mix of plate boundary earthquakes of strike-slip and dip-slip mechanisms
A22	Hanks and Bakun (2008) [319] - A ≤ 537 km² Stirling et al.(2008) [323] (New Zealand oblique-slip) Wesnousky (2008) [320] - strike slip yen and Ma (2011) [322] - strike slip	M_w = LogA + (3.98 ± 0.03) M_w = 4.18 + 2/3logW + 4/3logL sig = 0.18(in M_w) M_w = 5.56 + 0.87LogL sig = 0.24 (in M_w) LogA_e = -14.77 + 0.92LogM_o sig = 0.41 (in A_e) LogM_o = 16.05 + 1.5 M_w	A: Area (km²) W: Width (km) L: subsurface rupture length (km) L: surface rupture length (km) A: effective area (km²)	1 1 1 1	Larger magnitudes produced by Stirling et al. Than by others (larger D-L scaling)
A23	Wesnousky (2008) [320]- normal	M_w = 6.12 + 0.47LogL sig = 0.27 (in M_w)	L: surface rupture length (km)	1	Basin & Range-rich normal dip-slip earthquake dataset
A24	Stirling et al.(2008) [323] (New Zealand oblique-slip) Wesnousky (2008) [320] (New Zealand oblique-slip) Yen and Ma (2011) [322] - dip slip	M_w = 4.18 + 2/3logW + 4/3logL sig = 0.18 (in M_w) M_w = 4.11 + 1.88LogL sig=0.24 (in M_w) Log A_e = -12.45 + 0.80LogM_o sig = 0.43 (in A_e) Log Mo = 16.05 + 1.5M_w	W: Width (km) L: subsurface rupture length (km) L: surface rupture length (km) A: effective area (km²)	1 1 1	Yen and Ma sip-slip dataset dominated by reverse and thrust-slip earthquakes from wide area (Taiwan and east Asia)
B1	Anderson et al. (1996) [324] Nuttli (1983) [325]	M_w = 5.12 + 1.16LogL - 0.20LogS sig=0.26 (in M_w) Log M_o = 3.65LogL + 21.0 Log M_o = 16.05 + 1.5M_w	L: surface fault length (km) S: slip rate(mm/yr) M_o: seismic moment (dynes-cm) L: subsurface fault length (km)	2 3	Equal priority to Nuttli and Anderson et al. Regressions. Nuttli regression is developed exclusively for stable continental regions (>500km fromplate boundaries), but dataset includes stable continental earthquakes, and negative coefficient on slip rate has a major influence on Mw

B2	Anderson et al. (1996) [323] Nuttli (1983) [325]	M_w = 5.12 + 1.16LogL - 0.20LogS sig = 0.26 (in M_w) Log M_o = 3.65LogL + 21.0 Log M_o = 16.05 + 1.5Mw	L: surface fault length (km) S: slip rate(mm/yr) M_o: seismic moment (dynes-cm) L: subsurface fault length (km)	2 3	As for B1
C1	Strasser et al. (2010) [323] interface events	M_w = 4.441 + 0.846log10(A) sig = 0.286 (in M_w)	A: Rupture Area (km²)	1	Diverse dataset and Mw dependance on interface area makes the Strasser et al. Regression the most suitable for using on a wide variety of subduction 'magnitude'
C2	Strasser et al. (2010) [323] interface events Blaser et al. (2010) [327] Oceanic/subduction Reverse	M_w = 4.441 + 0.846log10(A) sig = 0.286 (in M_w) $Log_{10}L$ = -2.81 + 0-62M_w Sxy = 0.16 (orthogonal standard deviation)	A: Rupture Area (km²) L: subsurface fault length (km)	1 1	As for C1
C3	Ichinose et al. (2006) [328]	Log_{10} (A_a) = 0.57 (±0-06)M_o - 13.5(±1.5) sig = 16.1 (in A_a)	A_a = combined area of asperities M_o = seismic moment (dyne - cm)	1	Only regression of relevance to intraslab earthquakes
D1	Villmor et al. (2001) [329] (New Zealand - normal)	M_w = 3.39 + 1.33LogA sig = 0.195 (in Mw)	A: Area (km²)	1	Only regression of relevance to volcanic-normal earthquakes in thin crust (rift environments)
D2	Wesnousky (2008) [320] - normal	M_w = 6.12 + 0.47LogL sig = 0.27 (in M_w)	L: surface fault length (km)	1	Basin & Range-rich normal-slip dataset

3.1.2. Uncertainties in empirical relationships

Uncertainty is, perhaps, the most important issue in SHA. In particular, methods using empirical regressions are in an early stage of development as evidenced by the wide variety of approaches proposed in the literature. The immaturity of these models leads to greater uncertainty in the Seismic Hazard Analysis and, consequently, it is important that a formal treatment of uncertainty be incorporated into the hazard characterization.
In general, uncertainties can be classified as either 'aleatory' or 'epistemic'.

1) Aleatory uncertainties: these are the uncertainties due to the random variables that are derived from the large environmental anisotropy existing in natural processes. Assessment of future ruptures may be difficult because the potential seismic source may be hidden or have variable rupture characteristics, both in space and in time. Random uncertainty can be also introduced by the difficulty in defining the location of fault rupture from one earthquake to the next one.

2) Epistemic uncertainties: they can be caused by followings [201]:
   - *regressions and relationships*: the model used in the Seismic Hazard Analysis can introduce uncertainties by the approximations, the assumption and the intrinsic error in computing;
   - *database*: the largest uncertainty arises mainly because of the limited datasets that are available for characterizing potential seismic sources, i.e. the availability and the reliability of the parameters required in empirical relationships. In fact, studies on surface faulting are few in number and in most cases poor in information and precision. This is particularly true for distributed and triggered seismicity and in general for secondary effects (such as liquefaction, landslides, tsunamis). Moreover, coseismic environmental effects like centimeter scale displacements and ground failure effects, which are often the major cause of human and economic losses, may also occur several kilometers from the primary seismic source, and they are often not indicated in survey reports (complete and reliable data were collected only after great earthquakes, i.e. rarely and in only a few countries such as Japan, California U.S.A and Italy); the example of the Muzaffarabad earthquake, with an epicentral area in the Kashmir mountain region at the border between Pakistan and India, is very illustrative, as discussed in Section 2.1;
   - *geologic interpretation and geologic mapping*: the geologic interpretation of a fault trace connecting surface expression and environment features often has an uncertainty of at least several meters. Additionally, even if a fault trace could be well mapped, the rupture in a later earthquake may not precisely follow the previous trace.

3.1.3. Empirical relationships and paleoseismology

One of the main approaches in the field of earthquake size estimation for seismic hazard assessment involves paleoseismic investigation. Although data obtained from paleoseismic investigations could have large uncertainties (for example, due to difficulties in the identification of paleoearthquake evidence), paleoseismic data are fundamental in order to extend the past earthquake record further beyond the historical era, and a longer history of large earthquakes can, therefore, be analyzed.
Paleoseismic studies have to be performed through the accurate analysis and interpretation of trench data with the aim to define a complete and reliable seismic landscape (as well illustrated in the Section 2.1), after which the SHA can then be undertaken.

Primary fault-zone evidence (i.e. primary evidence such as rupture length, rupture area, average displacement) are traditionally used more than secondary evidence (such as liquefaction, landslides, tsunamis) in the estimation of paleoearthquake magnitudes. Sometimes, only secondary evidence is available. In these cases, the earthquake magnitude

can be estimated from the length or the area of the zone enclosing the coseismic secondary effects.

For these reasons, the best approach is generally to estimate paleomagnitudes using several methods, including both empirical regressions based on primary effects and other evaluation means (such as intensity scales; see next paragraph) also based on secondary effects (see Sections 2.1, 2.2, 2.3).

In the SHA, it is of extreme importance to undertake an extensive characterization of seismic sources that could cause an earthquake (for an example see Section 4.1).

For this reason, despite their key role in SHA, the empirical methods must be considered as a starting point and not the concluding point. That is to say that they must constitute the basis to give a rough idea of the outcomes of an event, and they have to be studied along with the values used to determine seismic recurrence.

As the collection of instrumental data is expanded, the correlations obtained display increasing levels of scatter. This is mainly due to the heterogeneity of the tectonic environment (aleatory uncertainty) together with the incompleteness of the database (epistemic uncertainty). In order to reduce scatter, records should be classified according to a number of characteristics such as, tectonic regimes, geologic environment and source mechanism. As a consequence, and in order to estimate the most probable paleoearthquake magnitude, fault parameters inferred for the event studied should only be compared to worldwide data of historic earthquakes (of known magnitude) that occurred in a similar tectonic setting.

Nevertheless, uncertainties must always be considered and as many aspects as possible should be analyzed before arriving at a conclusion: it is always of extreme importance, above all in SHA, to evaluate all uncertainties present at every step of earthquake parameters estimation.

However, thanks to the progress of technology in the collection of data and its diffusion, database accuracy is rapidly increasing. This enables the creation of a more comprehensive and reliable database together with the intention to improve the SHA thanks to a vision which is increasingly more precise and objective regarding the seismic path.

In this regard paleoseismology plays a decisive role because only through the study of pre-historical earthquakes, and the application of such obtained data in empirical relationships, it is possible to reach a more complete and reliable characterization of the seismic landscape at a specific site, both in space and in time.

3.2. THE ESI INTENSITY SCALE AND THE EEE GLOBAL CATALOGUE: TOOLS TO COMPARE PALEO, HISTORICAL AND MODERN EARTHQUAKES[1]

3.2.1 Environmental Seismic Intensity scale - ESI 2007

3.2.1.1 Introduction

Earthquake intensity is based on a classification of a seismic event's effects on man, man-made structures (buildings and infrastructures) and natural environment (environmental or geologic effects). It provides a measure of earthquake severity both at a site (local intensity) and at the epicenter (maximum and epicentral intensities), taking into account the effects in the whole range of frequencies of vibratory motion as well as static deformations (e.g. Reiter, [332]).

All the intensity scales (Rossi-Forel, Mercalli, MCS, MSK, Mercalli Modified) and the earlier researchers (e.g. [333]) consider the effects on the natural environment as diagnostic elements for the degree of intensity evaluation. However, the modern practice of macroseismic investigation (e.g. [334–336]) tends to only focus on the effects on man and man-made structures, overlooking the environmental effects, based on the assumption that they are too variable and aleatory. This is especially the case for the European Macroseismic Scale (EMS) (Grunthal, [336], Musson et al., [337]).

Nevertheless, many studies (e.g. [76, 147, 338–341]) have provided clear evidence that the characteristics of geologic and environmental effects, which nowadays are widely retrievable from historical and paleoseismic sources, are an essential piece of information for the scaling of earthquake size. To this end, the Environmental Seismic Intensity scale (ESI 2007) (Michetti et al., [77]; see Appendix 2 in this publication) was built based only on the environmental effects linked to the earthquake. Its use, alone or integrated with the macroseismic *traditional* scales and offering a more comprehensive picture of the earthquake's scenario and impact, allows a more complete estimate of intensity and, therefore, a better comparison of earthquakes can be undertaken. This occurs both:

- *in time*: effects on the natural environment are comparable for a time-window (recent, historic and paleo-seismic events) much larger than the period of instrumental record (last century). As the impact of an earthquake on the artificial environment depends on the distribution of urbanized areas, a comparison based on damage form two or more seismic events that occurred in the same area but at very different times may not be representative. Furthermore, this approach extends the time coverage of earthquake catalogs to prehistoric times. In fact, local evidence of surface faulting and the size of secondary effects (i.e. liquefaction) pertaining to pre-historic events can be evaluated via detailed paleoseismic investigations.

- *in different geographic areas*: environmental effects do not depend on peculiar socio-economic conditions or different building practices. In other words, they are uninfluenced by cultural and technological aspects, which may differ significantly from region to region. Moreover, earthquake-prone areas can be located completely or partially in sparsely populated regions, where the effects on the natural environment might be the only evidence available to estimate intensity.

[1] This section is largely based, in some parts abridged and slightly changed, on Michetti et al. [77], Guerrieri et al. [330] and Guerrieri et al. (in press) [331].

In particular, the ESI scale complements/replaces traditional seismic scales:

a) for earthquake intensity degrees larger or equal to X, when damage-based assessments are extremely difficult because the built environment is practically totally destroyed (so that any assessment based on it is not significant), while environmental effects are still diagnostic;
b) in sparsely populated areas, where man-made structures are absent or rare, so that only the environmental effects allow intensity estimates.

The definition of the intensity degrees has been the result of a revision conducted by an International Working Group formed of geologists, seismologists and engineers focused on the effects caused by a large number of earthquakes throughout the globe. Many papers have already been devoted to its illustration and application in specific cases, e.g. [17, 62, 80, 342–361].

The ESI 2007 has been ratified by INQUA (International Union for Quaternary Research) at the XVII INQUA Congress (Cairns, Australia) in 2007.

3.2.1.2 Primary and secondary effects of earthquakes

Earthquake Environmental Effects (EEEs) are all the phenomena generated in the natural environment by a seismic event. They can be categorized into two main types:

- ***primary effects:*** i.e. the surface expression of the seismogenic tectonic source (including surface faulting, surface uplift and subsidence), typically observed for crustal earthquakes over a certain threshold value of magnitude. Being directly linked to the size, hence the energy of the earthquake, these effects in principle do not suffer saturation, although there is a physical limit to their dimensions (included in the XII degree). The size of primary effects is typically expressed in terms of two parameters: i) Total Surface Rupture Length (SRL), and ii) Maximum Displacement (MD). The amount of tectonic surface deformation (uplift, subsidence) is also considered in the assessment.

The focal depth and the stress environment of an earthquake obviously control the occurrence and the size of the observed effects. Two crustal earthquakes with the same energy but very different focal depths and stress environment can produce a very different range of environmental effects and, therefore, their respective local intensity values can significantly differ. Especially in volcanic areas, earthquakes of very shallow focus (in the order of 3–4 km) and low magnitude can be associated with the manifestation of primary effects (e.g. Azzaro, [362]). To take this into account, the threshold for surface faulting in volcanic areas has been set at intensity VII, whereas for typical crustal earthquakes (focal depth 5–15 km) primary effects start from intensity VIII.

- ***secondary effects:*** phenomena generally induced by the ground shaking. Their occurrence is commonly observed in a specific range of intensities. The ESI 2007 intensity scale describes the characteristics and size of each type of secondary effect as a diagnostic feature in a range of intensity degrees. In some instances, it is only possible to establish a minimum intensity value. The total distribution area of secondary effects grows with the size of the event, without saturation: therefore, it can be used as an independent tool for the assessment of the epicentral intensity I_0.

In the ESI scale, EEEs are classified into eight main categories: 1) Hydrological anomalies; 2) Anomalous waves/tsunamis; 3) Ground cracks; 4) Slope movements; 5) Tree shaking; 6) Liquefaction; 7) Dust clouds; and 8) Jumping stones.

EEEs are more commonly observed and characterized from intensity IV. Some types of environmental effects (hydrological anomalies) may be observed even at lower degrees, but in general they are not sufficiently diagnostic. The evaluation accuracy increases towards the highest degrees, particularly in the range where primary effects occur (typically from intensity VIII with preserved resolution up to intensity XII). Indeed, effects on man and man-made structures saturate the area (i.e. buildings are often completely destroyed) starting from intensity X of traditional scales, so that a reliable intensity becomes difficult to assess. Instead, in the same range, EEEs still provide reliable evidence for an intensity appraisal.

3.2.1.3 Application of the ESI 2007 intensity scale

The ESI 2007 intensity scale (see Appendix 2) is structured in twelve degrees and is consistent with the Modified Mercalli macroseismic scale (MM-56 [363]) and the MSK-64 (Medvedev-Sponheuer-Karnik scale), since these are the most applied scales worldwide and include explicit references to environmental effects (especially in the highest degrees, X to XII).

The ESI intensity scale is an independent tool for intensity assessment. So, it can be used alone when only environmental effects are diagnostic features; this is the case when effects on man and man-made structures are too scarce or have saturated an area. Other than these cases, it is advisable to estimate two independent intensity fields, one for damage-based scales and one for ESI. Their subsequent comparison and merging, based on expert's judgment, will lead to the best intensity scenario and the most reliable intensity estimate.

Generally, the epicentral region encloses the area where the highest values of intensity are observed. The epicentral intensity (I_0) is commonly close and usually corresponds to the highest estimated value. Surface faulting parameters and the total spatial distribution of secondary effects (landslides and/or liquefactions) are two independent tools for assessing an ESI I_0, starting from intensity VII (Table 12).

Specific care has to be paid when surface faulting parameters are at the boundaries between two different degrees. In this case, the intensity value more consistent with the characteristics and areal distribution of the secondary effects should be selected. Moreover, in the evaluation of the total area, it is recommended that isolated effects which occurred in the far field are not included. This evaluation also requires judgment from experts.

TABLE 12. RANGES OF SURFACE FAULTING PARAMETERS (PRIMARY EFFECTS) AND TYPICAL EXTENTS OF TOTAL AREA (SECONDARY EFFECTS) FOR EACH INTENSITY DEGREE

I_0	PRIMARY EFFECTS		SECONDARY EFFECTS
	SURFACE RUPTURE LENGTH	MAX SURFACE DISPLACEMENT/DEFORMATION	TOTAL AREA
IV	-	-	-
V	-	-	-
VI		-	-
VII	(*)	(*)	10 km^2
VIII	Several hundred meters	a few cm	100 km^2
IX	1–10 km	5–40 cm	1000 km^2
X	10–60 km	40–300 cm	5000 km^2
XI	60–150 km	300–700 cm	10000 km^2
XII	> 150 km	> 700 cm	> 50000 km^2

(*) Limited surface fault ruptures, tens to hundreds meters long with centimeter-wide offset may occur in volcanic areas, generally associated to very shallow earthquakes.

Local intensity is generally evaluated through the description of secondary effects which have occurred in different 'Sites' included within a specific Locality. This type of intensity has to be comparable with the corresponding traditional local intensity based on damage. It must be noted that a 'Locality' can be referred to an inhabited area (a village, a town), but also to natural areas without human settlements. When only primary effects are present the local evidence of surface faulting in terms of maximum observed displacement can be used.

The ESI 2007 intensity scale starts at intensity IV, where environmental effects become regularly observed in favorable conditions (see Table 13).

TABLE 13. DIAGNOSTIC RANGE OF INTENSITY DEGREES FOR EACH CLASS OF ENVIRONMENTAL EFFECTS

	Environmental effects	Diagnostic range of intensity degrees	
	Surface Faulting And Deformation	VIII (*)	XII
A	Hydrological Anomalies	IV	X
B	Anomalous Waves/Tsunamis	IV	XII
C	Ground Cracks	IV	X
D	Slope Movements	IV	X
E	Tree Shaking	IV	XI
F	Liquefactions	V	X
G	Dust Clouds	VIII	VIII
H	Jumping Stones	IX	XII

(*) For intensity degree VII, limited surface fault ruptures, tens to hundreds meters long with several centimeters offset may occur essentially associated to very shallow earthquakes in volcanic areas.

3.2.2 The EEE Catalogue: a global database of Earthquake Environmental Effects

Nowadays, a significant amount of data about Earthquake Environmental Effects is available for a very large number of recent, historical and paleo-earthquakes. However, available

information is located in several different sources (scientific papers, historical documents, professional reports), and often difficult to access.

The EEE Catalogue is a database designed to collect information about the characteristics, size and spatial distribution of Earthquake Environmental Effects in a standard way from modern, historical and paleo-earthquakes. It has been promoted with the aim to properly retrieve the available information about EEE at a global level and archive it into a unique database, in order to facilitate their use for seismic hazard purposes. Its implementation has been endorsed at a global level by the INQUA TERPRO Project #0811, through a Working Group coordinated by ISPRA - Geological Survey of Italy.

For each event the information is collected at three levels of increasing detail (Earthquake, Locality, Site). Also, available imagery documentation (photographs, videos, sketch maps, stratigraphic logs) can be stored in the database. Moreover, within the EEE Catalogue the epicentral and local intensity values based on EEE data through the ESI 2007 scale (see Section 3.2.1) are recorded. This allows an objective comparison of earthquake intensity for events which occurred in different areas and/or in different periods.

The quality of the database in terms of completeness, reliability, and location resolution is strongly time-dependent and, therefore, is expected to be very variable according to the age of the earthquake. Nevertheless, even where the information is less accurate (historical earthquakes), the documented effects are typically the most relevant i.e. most diagnostic for intensity assessment. Similarly, the information from paleoseismic investigations, although poorly representative of the entire scenario, still includes significant data (i.e. local coseismic fault displacements) which are very helpful in estimating a minimum size for the earthquake. A first official release of the EEE Catalogue was done in the frame of the XVIII INQUA Congress, held in Bern in July 2011.

Data can be explored on a public interface based on Google Earth at:
http://www.eeecatalog.sinanet.apat.it/terremoti/index.php, (Fig. 46).
However, the implementation of the EEE catalogue is always in progress at:
http://www.eeecatalog.sinanet.apat.it/login.

FIG. 46. Screenshot of the public interface of the EEE Catalogue, developed in Google Earth http://www.eeecatalog.sinanet.apat.it/terremoti/index.php Reproduced with permission from ISPRA.

The collection of Earthquake Environmental Effects provided by the EEE Catalogue aims at identifying the natural areas most vulnerable to earthquake occurrence. In fact, through the EEE Catalogue it is possible to explore the scenarios of environmental effects induced by past earthquakes and, therefore, identify the areas where anthropic settlements and infrastructure are more exposed to this source of potential hazard. To this end, the spatial accuracy of EEEs becomes crucial.

Moreover, based on EEE characteristics, size and spatial distribution it is possible to: i) assess the earthquake intensity through the ESI scale, and ii) objectively compare the earthquake intensity of events which occurred in different areas and/or in different periods. This information must be integrated into the traditional seismic hazard assessment.

The EEE Catalogue is available on the IAEA ISSC portal (https://issc.iaea.org/home.php, Fig. 47) for use and dissemination within the worldwide nuclear engineering community. To this end, a new database infrastructure has been developed by the adaptation and customization of the EEE Catalogue to the specific ISSC standard requirements (e.g. content, reliability, magnitude thresholds, geographic priorities, IPR, security policies, etc.).

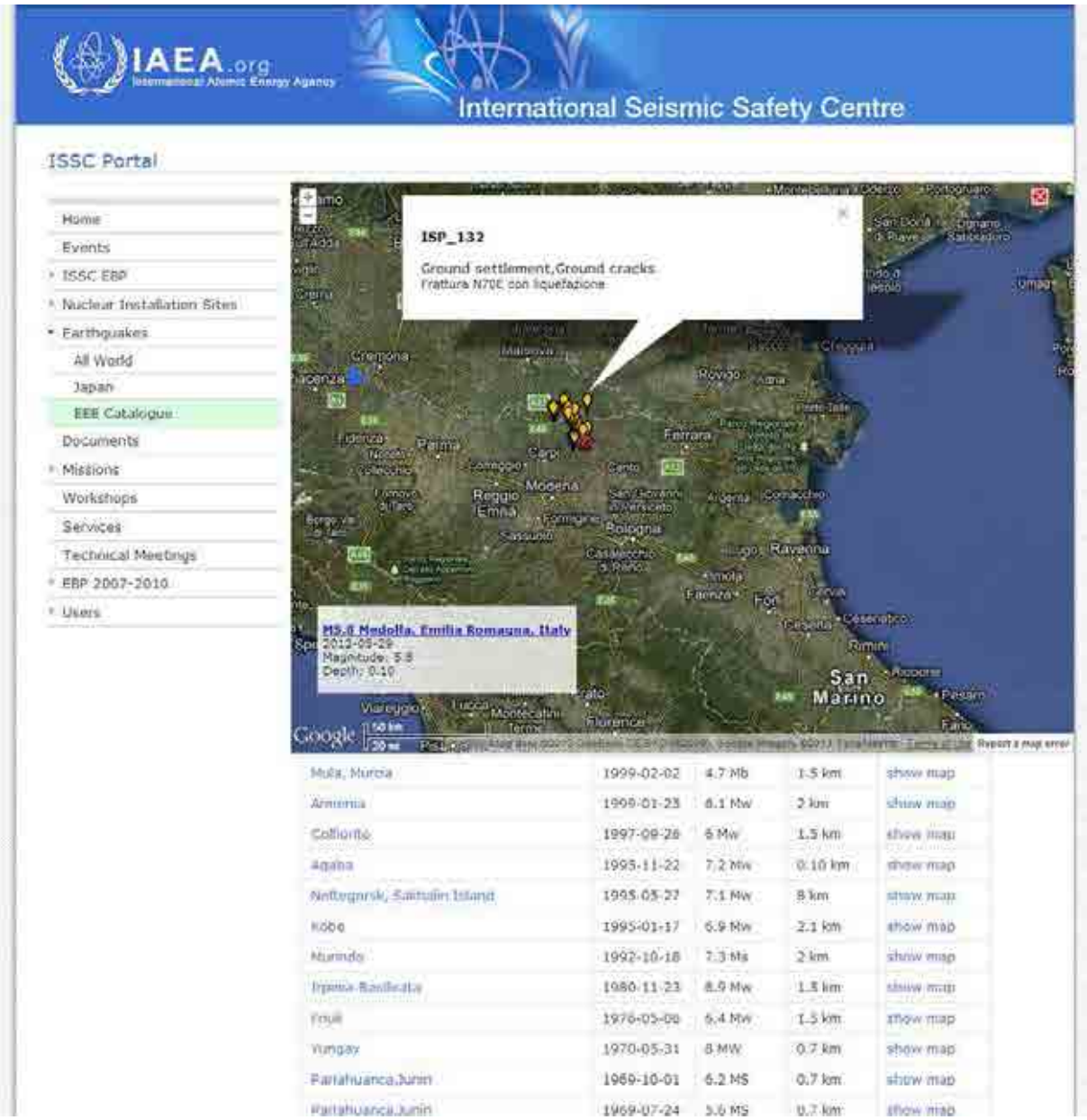

FIG. 47. Screenshot of the EEE data available on the ISSC portal, https://issc.iaea.org.

3.3. PALEOSEISMIC AND FAULT DATABASES

This Section aims at providing an overview of the online paleoseismic database resources available worldwide. The main scope is to illustrate the modern practice of implementing paleoseismic data and information into the public domain, and therefore acts as a transparent guideline for the collection and storage of diffuse information. Some outstanding examples of publicly available databases are presented and their structures commented on. Furthermore, a list is provided of the typical information and data that a paleoseismic database should include in order to be suitable for seismic hazard assessments, according to the requirements of IAEA/SSG-9 [1].

3.3.1 Introduction

Formally, a paleoseismic database is a container of geologic evidence of active faults, past earthquakes (usually pre-historic), and secondary earthquake effects that allow information about the location, size and timing of seismic events to be inferred. Information should be used for the construction of the seismotectonic model and to derive seismic parameters for seismic hazard assessment.
A tentative list of the typical content needed for a paleoseismic database includes (but is not limited to): i) displacements of the ground, as surface faulting [364, 365]; ii) paleoliquefaction evidence [366, 367]; iii) paleolandslides related to earthquakes [368, 369]; iv) paleotsunami deposits [370]; and v) other geologic effects.

There are, in practice, very few examples of paleoseismic databases, and most of them are included in or part of more general fault databases set up for the construction of seismotectonic models. Hereinafter, the content and structure of the main paleoseismic databases that are publicly available (available as an on-line resource that allows searching and queries to be carried out in an interactive way) are presented. They are divided up according to relevant information and the target of their content, through which the different sets of information and their usefulness for seismic hazard assessments are illustrated.

3.3.2 Active and capable fault databases

Such databases also contain information on active faults that may or may not be related to surface faulting and displacements, meaning, at least in part, they are related to capable faults. The most relevant databases are summarized below:

Quaternary Fault and Fold Database of the United States
The U.S. paleoseismic database [371], which is publicly available at the URL http://earthquake.usgs.gov/hazards/qfaults/, contains information on faults and folds that are believed to be sources of M>6 earthquakes during the Quaternary (the past 2.6 Ma). The database primarily includes information from paleoseismic studies such as trenching and archeological analyses to infer data on fault geometry, slip per event, slip-rate and the time elapsed from the most recent event on a fault. It represents the primary source of data for the seismotectonic models used for the National Seismic Hazard Maps (http://earthquake.usgs.gov/hazards/).

The database structure is quite flexible, allowing for static or interactive fault mapping, based on the speed connection of the user, as well as the possibility to download the entire database as Google Earth files or GIS Shapefiles. The Database Search is particularly powerful since it allows users access to a variety of data and information that are necessarily condensed in the viewer interfaces, while they are fully available in plain text formats with some of them several pages long with references. Amongst others, detailed information about paleoseismic studies, geomorphic expressions, faulting of surficial deposits and pre-historic deformations, are provided.

The database includes active faults of the conterminous United States and Hawaiian faults. As far as Alaska active faults are concerned [372], these are available as an independent database at the URL: http://www.dggs.alaska.gov/pubs/id/24956.

The paleoseismic information from the database is retrieved by selecting either the fault trace or the symbol of paleosites.

Active fault database of Japan
The Japan paleoseismic database [373, 374] is publicly available at the URL http://riodb02.ibase.aist.go.jp/activefault/index_e.html. It contains information on faults ascertained on the basis of the concept of 'behavioral segments' according to McCalpin [375] and includes parameters such as slip rates, slip per event, recurrence intervals and conditional probabilities of future ruptures derived from geologic and paleoseismic studies. The database is supplemented with data coming from investigations such as seismic tomography and gravimetry. Data are shown in both maps and vertical profiles.

The wealth of information collected in the database comes from the different approach to seismic hazard in Japan compared to that in other countries. In Japan seismic hazard is usually carried out by modeling the earthquake rupture at the source and then propagating seismic waves from the source to the site taking into account the physical properties of the medium, rather than using empirical attenuation relationships as commonly practiced in western countries. This requires a lot of supplementary information that usually comes from geophysical investigations and monitoring systems rather than from common paleoseismic studies, whose role is nevertheless fundamental in driving geophysical surveys to recognize active faults. Data for each fault includes the age of last faulting as inferred from the historical seismicity or paleoseismic evidence, along with rupture probability in next 30 years.

The database is structured into two main layers of information; layer one is for mapping active faults and fault parameters (geometry, mechanism, slip rate, displacement, among many others) and layer two allows access to geologic information and subsurface properties (body-waves velocity, Poisson ratio, and others) along pre-defined vertical profiles. The first layer is mainly devoted to the model of seismic sources, and the second to characterize the travel-path of the seismic waves.

New Zealand Active Faults Database
The New Zealand paleoseismic database, [376] is publicly available at the URL http://data.gns.cri.nz/af/. It collects data and information on active faults resulting from field surveys, trenching, direct and indirect investigations and dating. Raw data and interpretations such as inferred magnitudes, recurrence rates and dates of past earthquakes, are clearly separated and readily available.

The database structure is composed of an interactive map linked to the database through which information about fault mechanism, recurrence interval, timing of the last event, slip rate and slip per event can be retrieved once the fault has been selected. Selections can be done in different ways; either selecting the area or structure of interest on an interactive map, by directly selecting the fault from a drop-down menu, or by queries using different search parameters. Each fault page contains a small inset map of the fault overlaying the DEM and fault pictures can be viewed as well. A comprehensive list of references with abstracts is also available for each fault, allowing the retrieval of the source information regarding paleoseismic studies to be carried out.

Quaternary Active Faults Database of Iberia (QAFI)
The paleoseismic database of the Iberia Region [377] is publicly available at the URL http://www.igme.es/infoigme/aplicaciones/qafi/. The database contains information on faults with geologic evidence for activity during the Quaternary (last 2.6 Ma). The Spanish database, along with the French one (see subsequent text), are examples of paleoseismic

repositories for regions of low to moderate seismicity. A specific feature included in the Spanish database is the quantification of parameter uncertainty such as measurement errors (e.g. radiocarbon dating), upper and lower limits of parameters (e.g. slip per event), and the standard deviations for empirical relations (e.g. scaling laws inferring magnitude from fault size).

Italian database of capable faults (ITHACA)
In order to respond to the need for specific knowledge regarding Fault Displacement Hazard, the Italian Agency for Environmental Protection (ANPA, later APAT, now ISPRA) in the second half of the 1990s started the project ITHACA (ITaly HAzard from CApable faults).

The project is aimed at building a tool to summarize capable faults and to make the information easily available based on published sources, field checks and ad hoc studies (for more details, see [378]).

The Italian database of Capable Faults, ITHACA [379], is available through the geo-map server of the Italian Geological Survey at the URL:
http://sgi1.isprambiente.it/GeoMapViewer/index.html

Currently, the catalogue contains about 2000 records including faults that exhibit at least one piece of evidence of capability among the following: (a) historical coseismic surface faulting, (b) creep or surficial tectonic deformation, (c) Late Pleistocene-Holocene paleoseismic evidence of ground rupture, and (d) displacement of Quaternary deposits/landforms. Moreover, the faults are classified according to the age of the last ascertained movement.
The ITHACA database finds its application in the microzonation studies, as already acknowledged by some regional building codes.

3.3.3 Neotectonic Features Database

These databases are aimed at supplying information about neotectonic features that provide evidence of recent tectonic activity related to earthquakes, but, due to the nature of the fault ruptures, the evidence is not able to be directly related to active faults or surface displacements. These databases are developed in countries of moderate to occasionally strong seismicity, such as stable continental regions or intraplate regions. Hereinafter, the most relevant publicly available databases of this type are presented.

French Database of Recent Deformations and Paleoseismicity (NEOPAL)
The paleoseismic database of France, which is publicly available at the URL http://www.neopal.net/ contains information on geologic indications of deformations which occurred in the last 2 Ma, termed as 'Neotectonic Index'. The presentation of the database clearly states that the identification of active faults in France is very difficult owing to the moderate seismicity both recorded and historically documented.

The database collects geomorphic evidence for active tectonics such as topographic fault scarps, river planform patterns, offset landforms, and offset geologic layers. These features allow the state of activity to be ascertained on a relative basis by empirically dating the last movements; this provides a relative index of neotectonic activity. Main access to the database is through a map where areas of different size can be selected (Region/Prefecture, Department or Municipality). For these areas the assessed 'Neotectonic Index' is reported and explained by a commentary as well as by references to the studies carried out.

Australia Neotectonic Features Database
An outstanding example of database for intraplate regions is given by the Australia database [380]: URL:
http://www.ga.gov.au/earthquakes/staticPageController.do?page=neotectonics).
Despite the moderate seismic potential (around M6.5), approximately one-hundred faults and folds are mapped and the geomorphic features and state of activity of each one is reported.

3.3.4. Seismogenic sources databases

Databases of seismogenic sources contain information about seismic source zones and seismic source structures (either capable or active faults) inferred from multiple sources of data, including paleoseismicity, historical and instrumental seismicity, geomorphology, structural geology, etc. They are devoted to highlighting potential seismogenic sources of relevant earthquakes for seismic hazard assessment.

Italian Database of Individual Seismogenic Sources (DISS)
Some databases available for Europe are introduced in the following sections. The Italian composite database of faults and seismogenic sources [381], which is available at the URL http://diss.rm.ingv.it/diss/, is a repository of tectonic (e.g. folds), fault and paleoseismic data. It fully integrates information of various nature, from geologic evidence to seismologic observations in order to provide data finalized to seismic hazard studies (3D-geometry, slip rate, slip per event, recurrence interval, characteristic magnitude, last event). Data is complemented by commentary, references and pictures. Each fault is supplemented with its earthquake history. The database is available in a map view through a web-browser or downloadable as a Google Earth file. It can be queried through an interface which allows data to be accessed through user defined selection criteria (e.g. geologically detected sources, macroseismic sources, and so on).

GEM (Global Earthquake Model) Active Fault Database
Some global projects regarding fault and seismogenic source databases at over-regional scales were recently developed or are under development. The most comprehensive one is the GEM (Global Earthquake Model) Active Fault Database (URL: www.globalquakemodel.org/what/global-projects/active-faults-database/).

The database is formally a collector from other databases (such as those described above) aimed at making worldwide data on active faults available in a homogenous format. Once completed it will be a repository of virtually all Earth's faults (from continental to subduction zones up to mid-ocean ridges) reputed to be active under the current tectonic regime and responsible for the release of the major earthquakes (above M6.5). As a part of the GEM program the book Active Faults of the World [7] has been recently published showing and discussing the tectonic settings of all active regions of the Earth.

Earthquake Model of the Middle-East (EMME)
GEM also promotes the development of over-regional databases of active faults and seismogenic sources for seismic hazard assessments throughout the world, as is the case of EMME (URL: http://www.emme-gem.org/), the Earthquake Model of the Middle-East [382].

The project is structured into several work-packages, one of them (WP2) aimed to highlight seismic sources on the basis of a thorough knowledge of active tectonics derived from the

implementation of all kinds of seismic data, from the instrumentally recorded to the historically documented, up to the geologically (i.e. paleoseismic) inferred.

Seismic Hazard Harmonization in Europe (SHARE)
A European-wide program is SHARE (Seismic Hazard Harmonization in Europe, URL: http://www.share-eu.org/) which aims to provide a community-based seismic hazard model for the Euro-Mediterranean region including: the Central Mediterranean, Northern Africa, Iberia, Central Europe, Eastern Europe, Greece and Turkey. Within the framework of the SHARE-project, work package 3 (sub-task 3.2) is devoted to the compilation of the European Database of Seismogenic Faults [383]; URL: http://diss.rm.ingv.it/share-edsf/), which includes faults that are deemed to be capable of generating earthquakes greater than M5.5 and whose database structure is quite similar to that of the Italian DISS (see above).

3.3.5 Composite databases

The list of paleoseismic databases reported above, even if not exhaustive, provides an overview of the information usually contained into such repositories. In fact, many references can be found in literature addressing paleoseismic databases, often in the form of repositories of active faults, even if not always supported by an open access data container. For instance, this is the case for the Greek database GreDaSS [384] which is part of the SHARE project, and also the German paleoseismic database.

Another case is the availability of sub-regional databases (already included in more general regional scale databases) that focus on the information about the inventoried seismotectonic features at a smaller scale. An example of this is the Colorado State database (http://geosurvey.state.co.us/hazards/Earthquakes/Pages/Maps.aspx) which includes research on faults that were determined to have ruptured due to earthquakes and extends back to the Late Cenozoic (last 23 Ma).

Other important paleoseismic evidence are included in paleotsunami databases: for example, the Cascadia Tsunami Deposit Database (http://geopubs.wr.usgs.gov/open-file/of03-13/) encompasses information and data regarding the age, thickness, layering, grain-size, and other sedimentological characteristics of tsunami deposits formed during earthquakes which occurred in the Cascadia subduction zone. Another is the Euro-Mediterranean Paleotsunami Database (http://paleotsunami.rm.ingv.it/) which is still in progress under the grant from the European Commission through the TRANSFER project (http://www.transferproject.eu/).

A different kind of paleoseismic database is given by repositories of secondary effects such as liquefaction and landslides; they are still useful for the identification of paleoearthquakes when a seismic origin of such effects can be proved. They are complementary databases with respect to classical fault paleoseismic databases or paleotsunami deposit databases. The most outstanding example of a paleoliquefaction database is given by the seismic source characterization for nuclear installations in the Central and Eastern United States (http://www.ceus-ssc.org/Report/AppendixE.html) as described in section 2.2.2 of this publication. This database gives us the opportunity to clarify the use of ground failure databases in paleoseismic studies. Paleoseismic studies are primarily aimed to complement seismic hazard analysis, which means not only the characterization of seismic sources but also the assessment of ground motion. In areas where fault exposures are rare or absent but where earthquakes are known to have occurred, analysis of earthquake-triggered ground failures, especially liquefaction and landslides, may often be the only paleoseismic tool available.

Moreover, dating geologic material coming from ground effects may be easier than dating movement along faults, owing to the large amount of material suitable for such a purpose and to the larger dating methods available. Another benefit in using ground failures is that they deal with the effects of earthquakes, whose assessment is ultimately the aim of seismic hazard. Therefore, ground failure is a good proxy for the seismic shaking or, in other words, of the magnitude-distance couple that has likely triggered it.

Once a variable (i.e. magnitude or distance) can be inferred from an independent analysis, the other can be obtained from the relation between magnitude and distance such as those provided by Ambraseys [114] and Keefer [119] for liquefaction and landslides respectively, or those shown in section 2.2 of this publication.

Historically paleoseismic databases have mainly focused on geologic evidence useful for the seismic source characterization; however, in recent times there has been a growing interest for databases of geologic evidence that may improve ground shaking estimates, which strictly speaking ultimately represents the seismic hazard. We have, therefore, moved from databases of ground failures triggered by specific earthquakes (e.g. [385]), to databases encompassing earthquakes that struck an entire region or country.

Such an example is given by CEDIT, the Italian Catalogue of Earthquake-Induced Ground-Failures [386], which is accessible through the web-server of the Research Centre for the Geologic Hazards (CERI: http://www.ceri.uniroma1.it/) at the University of Rome 'Sapienza', which lists the ground effects (landslide, ground-cracks, liquefaction, surface faulting, ground level changes) triggered by earthquakes that occurred during the last millennium. The database preserves the original source of information from which earthquake-induced ground failures have been inferred, thus allowing the retrieval of the original information for any further updating, revision and interpretation of the phenomena.

Still, more generally, the catalogue of Earthquake Environmental Effects (http://www.eeecatalog.sinanet.apat.it/) described in section 3.2.2 of the publication, is aimed at collecting data and information on a worldwide basis encompassing all geologic evidence of past earthquakes.

3.3.6. Guidelines for building a Paleoseismic Database: structure and content

The variability in terms of structure and content of the paleoseismic databases shown above outlines the different approaches used to represent geologic evidence of past earthquakes and active faults. A common denominator is given by the interpreted parameters, such as the inferred magnitude, slip per event, slip-rates and recurrence intervals, according to the physics of the earthquake process which is exhaustively described by the parameter of seismic moment and its time derivative (i.e. seismic moment rate).

Unfortunately, the distinction between data and interpretations is not always clear, and this is a bias that may generate confusion or lack of credibility. Moreover, technology evolves continuously, thus new techniques of investigation, sampling and analysis are continually proposed and applied; therefore, paleoseismic databases should be under constant revision, sufficiently flexible to allow the retrieval of data and easily updatable.

Figure 48 shows a tentative proposal for a database structure that could be used as a blueprint for the buildup of databases in other regions or countries.

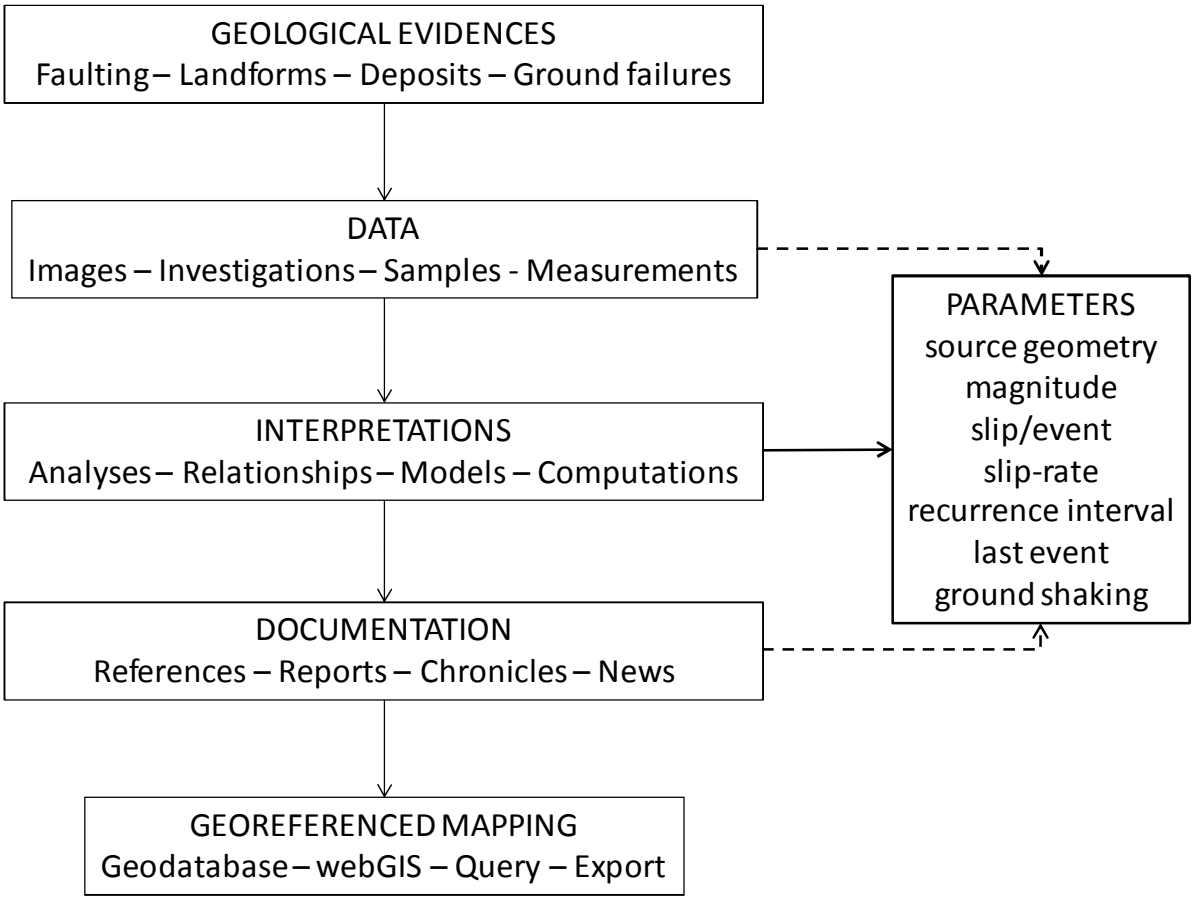

FIG. 48. Suggested structure and content of a paleoseismic and fault database.

The database is centered on the interpretation of data because a paleoseismic database should be aimed to provide information useful for seismic hazard analysis. The main relevant parameters for that purpose are listed in the right-hand box. Data should always indicate the approximation and range of the information provided, in order to be able to quantify the inherent variability of the detected or observed quantities; in turn, interpretations should always specify errors and assumptions in order to quantify the modeling uncertainty. Parameters should be expressed in terms of best estimate, along with uncertainty (aleatory + epistemic), either given in terms of standard deviation (for ascertained distributions) or upper and lower limits.

Documenting all the data acquired or the interpretations inferred as thoroughly as possible is a crucial point, since it allows users to retrieve the original source of information for all the operations carried out.

Lastly, the way the data are presented and made available is as important as the previous sections of the database. Transparent and easy access to all the information is the basis of a successful database and an effective implementation into the whole chain of the seismic hazard analysis. The best way is to provide online GIS tools to manage the database, namely making queries, selections and exporting data and information.

4. THE APPLICATION OF PALEOSEISMOLOGY TO NPP SEISMIC HAZARD ASSESSMENT

Practical examples of comprehensive procedures from paleoseismic investigations used in seismic hazard evaluation are introduced in this Section. The aim is to provide ideas by showing how paleoseismic investigations are beneficial in terms of hazard assessment.

Paleoseismic investigations are usually conducted at the initial stage of the hazard evaluation process. The practices are quite site specific; therefore, the procedures used in case-studies illustrated here might need substantial adjustments and refocusing if applied to other sites.
Regarding paleotsunami investigations, the inundation area of ancient tsunamis can be estimated by archeological or tsunami deposit investigations, as detailed in Section 2.3. However, it must be noted that suitable investigation sites are infrequent because tsunami traces are only rarely preserved in the stratigraphic record.

4.1 APPLICATIONS OF PALEOSEISMOLOGY TO NPP SEISMIC AND TSUNAMI HAZARD ASSESSMENT IN JAPAN

4.1.1 Onagawa NPP's Investigations

4.1.1.1 Paleoseismic Investigations around Onagawa NPP

Onagawa NPP is located in northeast Japan. It lies on an overriding plate, the North American plate, and is characterized by east-west compressive stress field.
The Japan Trench, approximately 200 km to the east of Onagawa NPP, is an interfacial boundary where the Pacific plate moves beneath the North American plate.
Because of that, three types of earthquake can occur at the NPP site: crustal intraplate, subduction interface and intra-slab earthquakes. In this Section we will only deal with crustal intraplate earthquakes.

Geologic and Geophysical Database
Because of its geodynamic context and according to the regulatory requirements, a regional crustal intraplate capable fault survey was carried out for the area less than 100 km in radius from the NPP (shown in Fig. 49), based on published documents (secondary data). Ad hoc data (primary data) were collected through detailed geologic and geophysical surveys in the Near Region (30 km in radius) and in the Site Vicinity area of the NPP site (5 km in radius). These surveys were carried out on the basis of the seismic landscape as defined in Section 2.1.

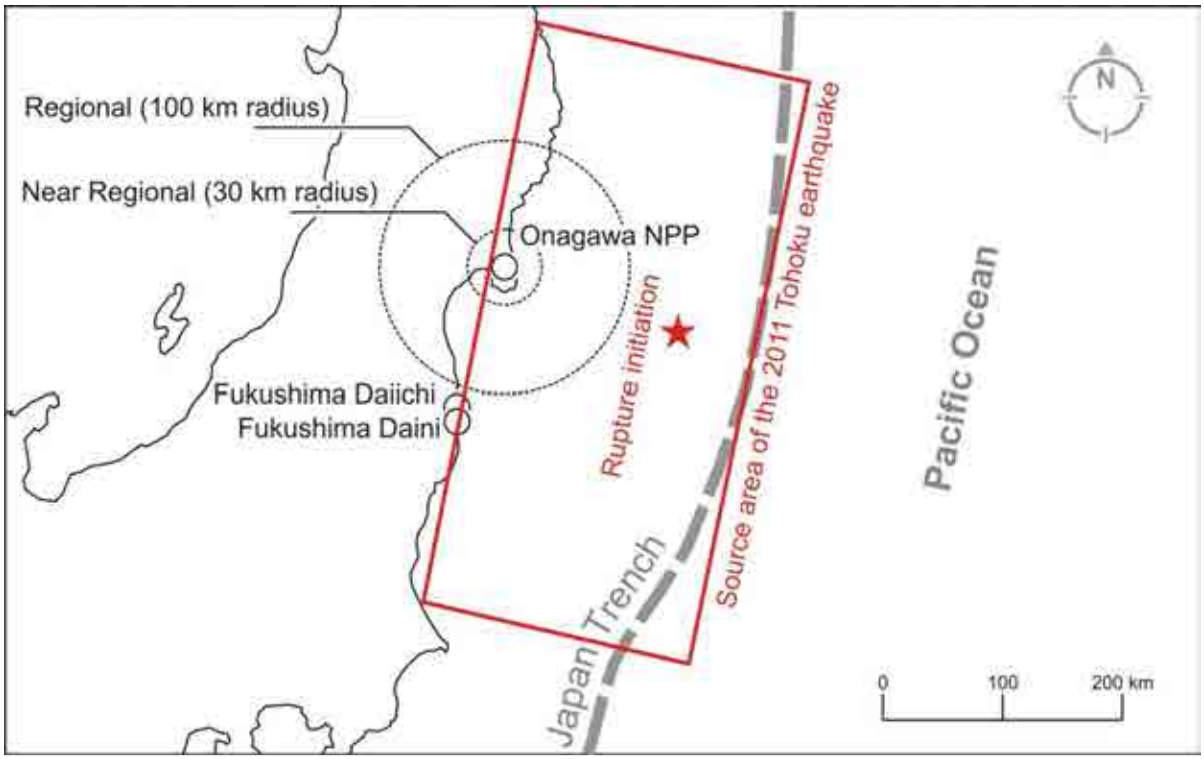

FIG. 49. Locality map of Onagawa NPP and spatial scales of geologic and geophysical investigations.

The secondary data consisted of the databases 'Active Faults in Japan' [387] and 'Digital Active Fault Map of Japan' [388], and various other geologic maps published by Geological Survey of Japan.
A summary of the performed investigations to get the primary data are listed in Table 14.

TABLE 14. INVESTIGATION LIST UNDERTAKEN FOR ONAGAWA NPP ASSESSMENT

Investigation List
Collection of existing data (published and unpublished analyses)
Aerial photograph interpretation at different scales
Geological field survey at different scales
Drilling survey
Trenching
High resolution seismic reflection profiles
Others; e.g.: aftershock distribution of the 2003 Miyagiken-chubu earthquake

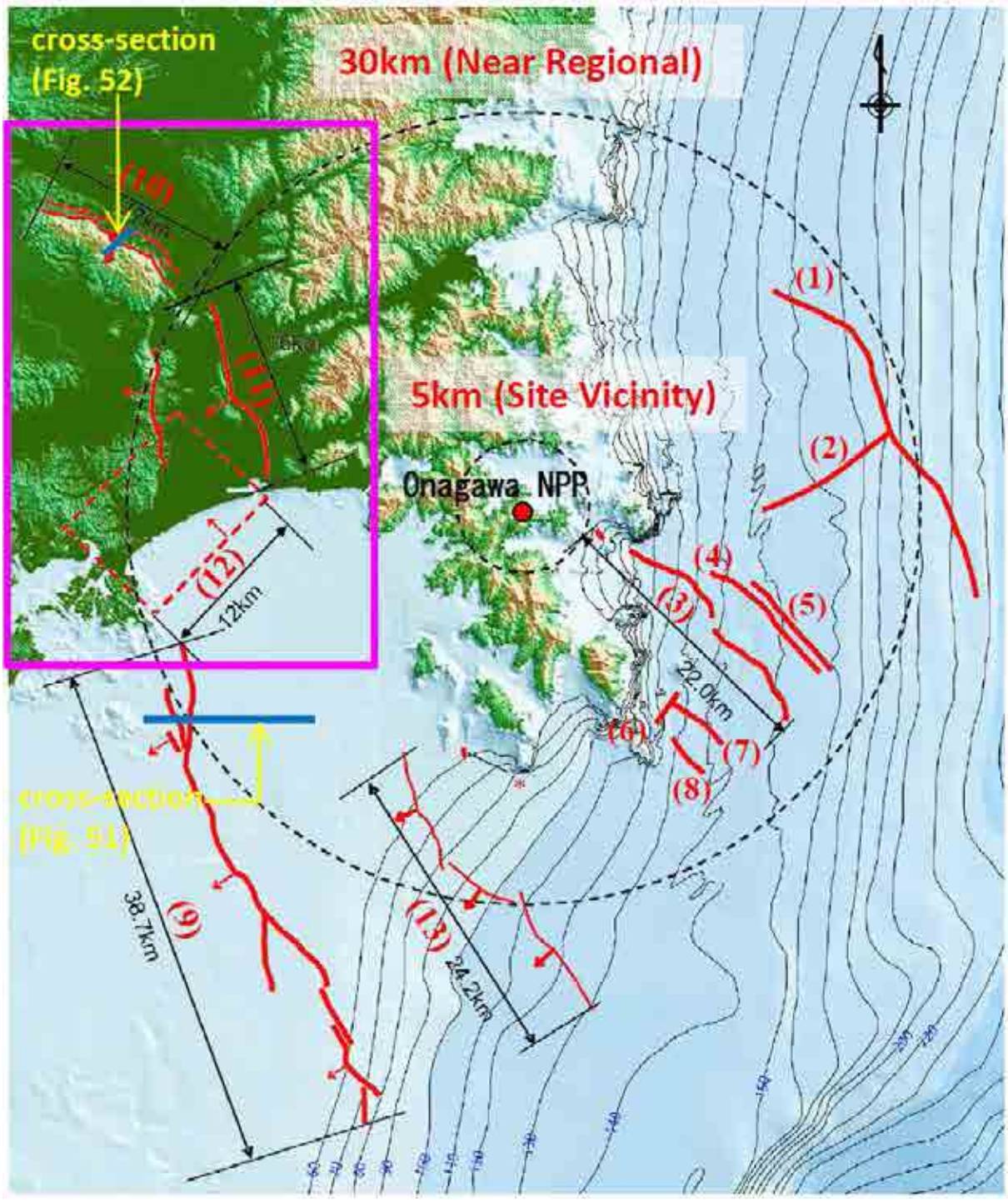

FIG. 50. Investigated faults in 30km radius (Blue line shows position of seismic profile line of FIGS. 51 and 52).

As a result of the geologic investigations at Onagawa NPP, 13 faults have been identified as capable faults. The NPP seismic design is based on this evaluation. These 13 faults are shown in Fig. 50 and are listed in Table 15. Especially in off-shore areas, activity, location and length of faults have been conservatively determined on the basis of high resolution seismic reflection profiles; an example is shown in Fig. 51, where a profile was acquired in order to confirm the deformation of Quaternary sediments.

For the 13 identified faults, the maximum potential earthquake was evaluated mainly on the rupture length parameters of each fault (see Section 3.1). The obtained values are also given in the Table 15. Considering their proximity to the NPP site, the given magnitude, and their structural relationship, an event on either fault 3, 4 or 5 would have the biggest influence on the NPP among the crustal intraplate earthquakes.

TABLE 15. SCREENED FAULTS

Fault	Profile		Existing documents
	L (km)	M_w	
(1)	27.9	7.2	
(2)	11.2	6.7	
(3)	22 in total	7.1	
(4)			
(5)			
(6)	3.3	6.7	
(7)	5.1	6.7	
(8)	3.7	6.7	
(9)	38.7	7.5	
(10)	45 in total	6.6	✓
(11)			✓
(12)			
(13)	24.2	7.1	

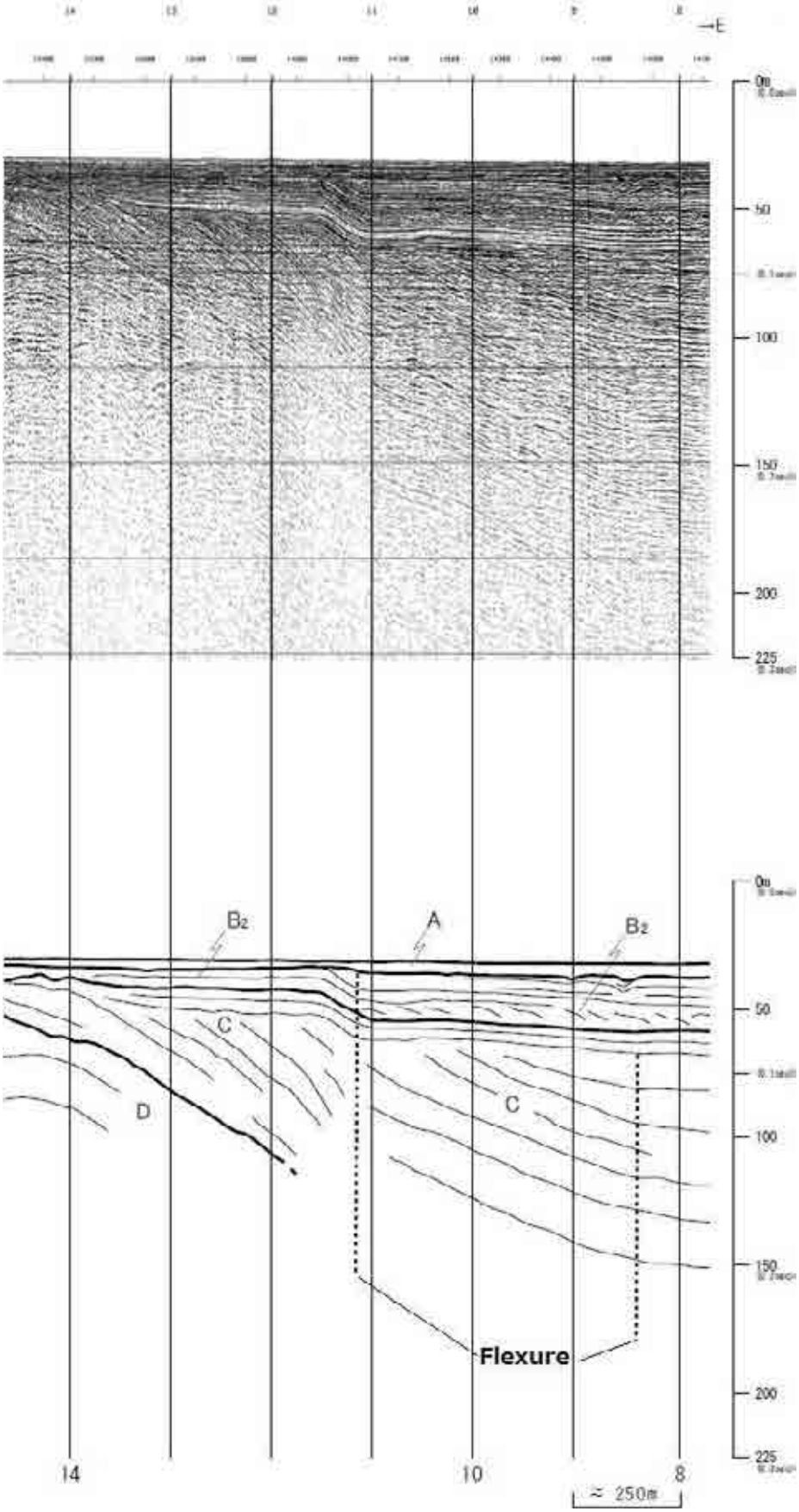

FIG. 51. Example of seismic reflection profile of (9) in Table 15, fault in ocean area (Blue line in Fig. 50). Reproduced with the permission of Tohoku EPCO.

The possibility that some fault segments could rupture together in the deterministic approach was also considered for a conservative evaluation. In particular, this was done for faults 10, 11 and 12, because of their close tectonic (structural) relationships (Fig. 50, area in magenta). Faults 10 and 11 were already mapped by the Research Group for Active Faults of Japan [387] and Nakata and Imaizumi [388]; however, for faults 10 and 11 the Asahiyama flexure was re-investigated through aerial-photo interpretation and some lineaments were recognized in close proximity to them. In addition, detailed field mapping was carried out to investigate the surrounding geologic structures, and detailed data were collected from identification of fault outcrops; however, these outcrops were not enough to identify the precise fault position.

The obtained data (lineaments and outcrops) were unfortunately not enough to locate the fault's latest rupture. Therefore, seismic reflection surveys were conducted around faults 10 and 11 to verify the subsurface structure and to identify the geometry of the faults and their activity, and drilling surveys were then undertaken in order to correlate seismic reflections with strata and their geologic age (shown in Fig. 52). At the end, the capability of these faults was confirmed.

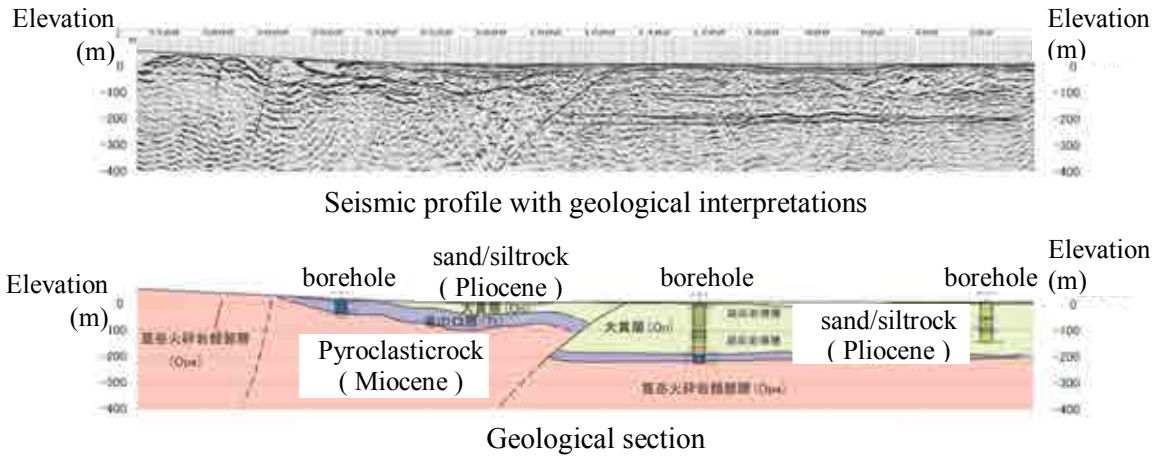

FIG. 52. Seismic reflection of fault 10 and geologic cross-section with borehole data. Reproduced with the permission of Tohoku EPCO.

Moreover, interpretation regarding the 2003 Miyagiken-chubu earthquake, in particular the foreshock's epicenter and the aftershock cluster's distribution, suggested the existence of the southern Segment Fault 12. This avoided new *ad hoc* geologic and geophysical investigations at fault 12, as this segment was evaluated as a capable fault. The close relationship between the three faults was confirmed by foreshock, mainshock and the largest aftershock of the 2003 Miyagiken-chubu earthquake since they occurred at all the three faults.

Considering the simultaneous movement of the three segments, they became the controlling structure for the seismic design of the NPP in the deterministic approach. In the next paragraph the models that were used for estimation of the input ground motion for seismic design are explained.

Strong motion evaluation using fault models

The ground motion evaluation was carried out with ground motion simulation using both fault models and the GMPE (see Noda et al., [389]; The Headquarters for Earthquake Research Promotion, [390]). As shown in Fig. 53, based on the results of the survey and tectonic regime

surrounding Onagawa NPP, the fault model is assumed to be a reverse fault reflecting the 2003 event and the results of the geologic/geophysical investigations. Still, uncertainties remain in some parameters even after considering the detailed survey results; therefore, several models were considered in parametric study and the most conservative case was introduced in the figure for deterministic approach. Total cumulative length of the three fault segments is 45 km and the evaluated M_w was 6.6. The three individual rectangles are the modeled segments. The segments are also indicated in plane projection in yellow balloons, where the A-A', B-B' and C-C' are vertical from down to up. A fault width of 13 km was estimated based on crustal thickness in this region. The segments were divided into finite elements less than 2 km both in horizontal and vertical directions. The ends of the segments are overlapped, at blue lines in the balloons and red broken lines in the map, and these overlapped areas are eliminated in the simulation of the ground motion as indicated with the gray color. Ground motion can be generated mainly from elements in magenta known as asperities; these are where significant dislocations were evaluated due to large geomorphic deformation. Rupture initiation was investigated by several case studies and the most conservative case for the site was taken into account as indicated by the yellow star. Of course there is always uncertainty within the model; physical parameters for the ground motion simulation were assumed based on methodology introduced in the draft Safety Report on Fault Rupture modeling. Evaluated ground motions are indicated with black solid and broken lines for GMPE and the model respectively.

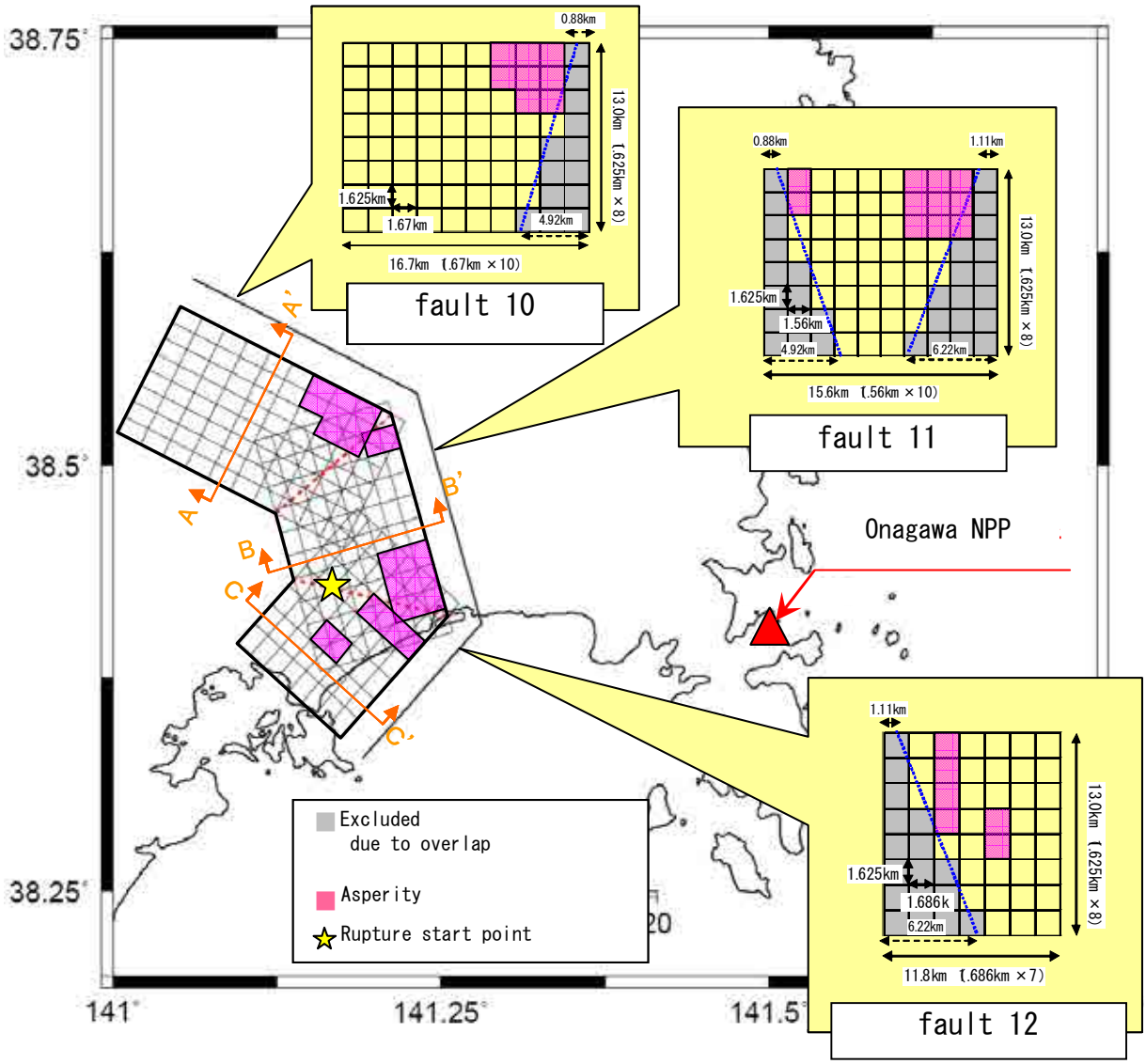

FIG. 53. Merged Fault Rupture Model of (10), (11), and (12) Faults as segments.

'Ground motion without specific source location' in Fig. 54 means an evaluated ground motion from a diffused seismicity model stipulated by Regulatory Guide for Reviewing Seismic Design of Nuclear Power Reactor Facilities (2006) in Japan (see The nuclear safety commission of Japan, [391]; Mitzutani et al., [392]). This motion has no specific magnitude and distance definition but envelops observed motions. Considering historical earthquakes, massive earthquakes occurred frequently in/off the Miyagi region over an approximate 40-year cycle; therefore, ground motions from those seismic sources were also evaluated by both the GMPE and the fault model indicated with blue lines. Observed ground motions from the 2011 Tohoku Earthquake off the Pacific coast is also indicated with green lines. In the short period range, ground motion levels were almost equivalent to the diffuse seismicity, historical based earthquakes and the 2011 Tohoku Earthquake off the Pacific coast. Evaluated ground motions from the model of fault 10, 11, and 12 were relatively lower than the others, although the conservative assumption of segmentation was taken into account.

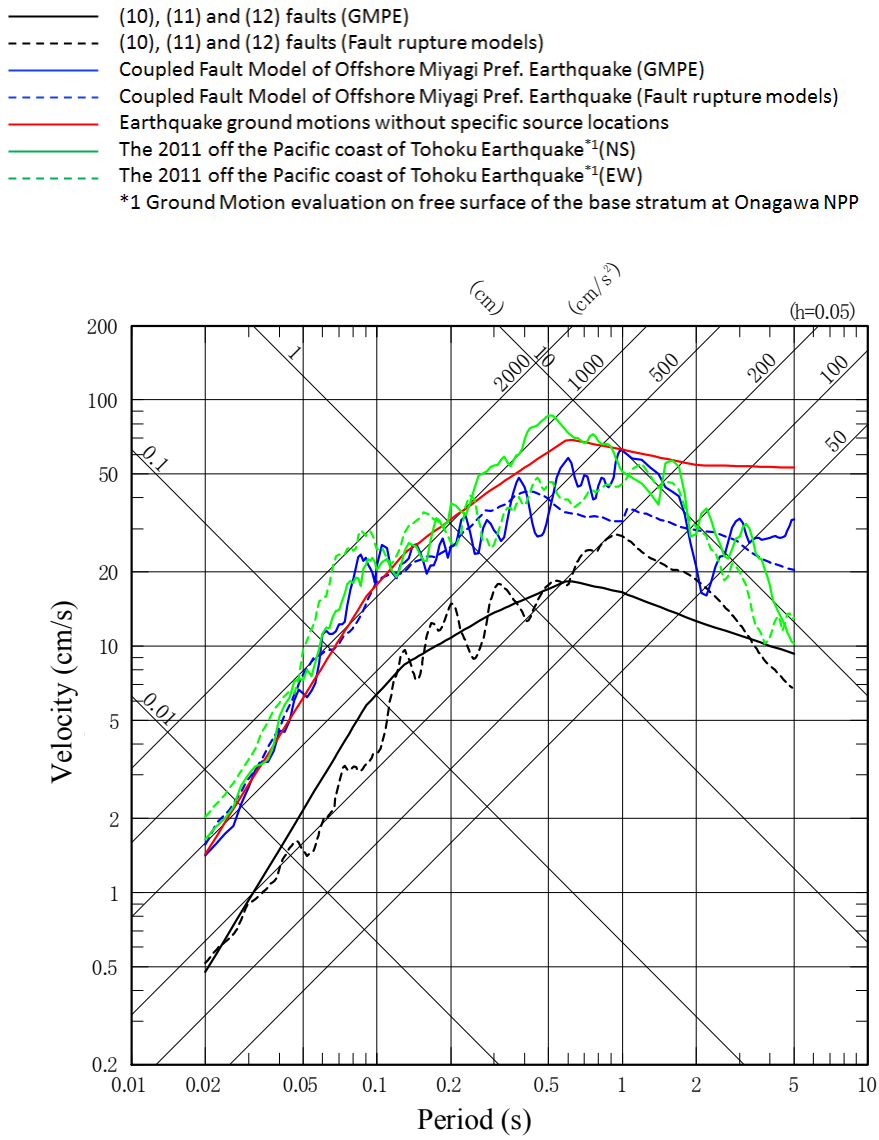

FIG. 54. Horizontal Response Spectrum (Evaluation Result of ground motion of each earthquake by GMPE and Fault Rupture Model). Reproduced with the permission of Tohoku EPCO.

4.1.1.2 Paleotsunami Investigations around Onagawa NPP

In Japan tsunamis are investigated from the viewpoints of (1) historical tsunami records, (2) active faults at bottom of the ocean/sea, and (3) paleotsunami studies. Based on findings from these investigations, numerical simulations of the tsunamis are performed, and the influence of the tsunami hazard on the nuclear power plant is examined.

There are tsunamis from a near-by origin caused by the earthquakes along the Japan Trench, and tsunamis from a distant origin. In this section, the focus will be on tsunamis from a near-by origin because the influence of this type of tsunami is relatively larger than tsunamis from a distant origin. In addition, tsunamis caused by active faults (F-2, F-4, F-6 - F-9 faults) were estimated by using a simple predictive expression, which was proposed by Abe [393]. The results were, however, quite low compared to historical tsunamis. Historical tsunamis that took place around Onagawa NPP (Fig. 55) include: (1) AD 869 Jogan tsunami, (2) AD 1611 Keicho Sanriku tsunami, (3) AD 1896 Meiji Sanriku tsunami, and (4) AD 1933 Showa Sanriku tsunami.

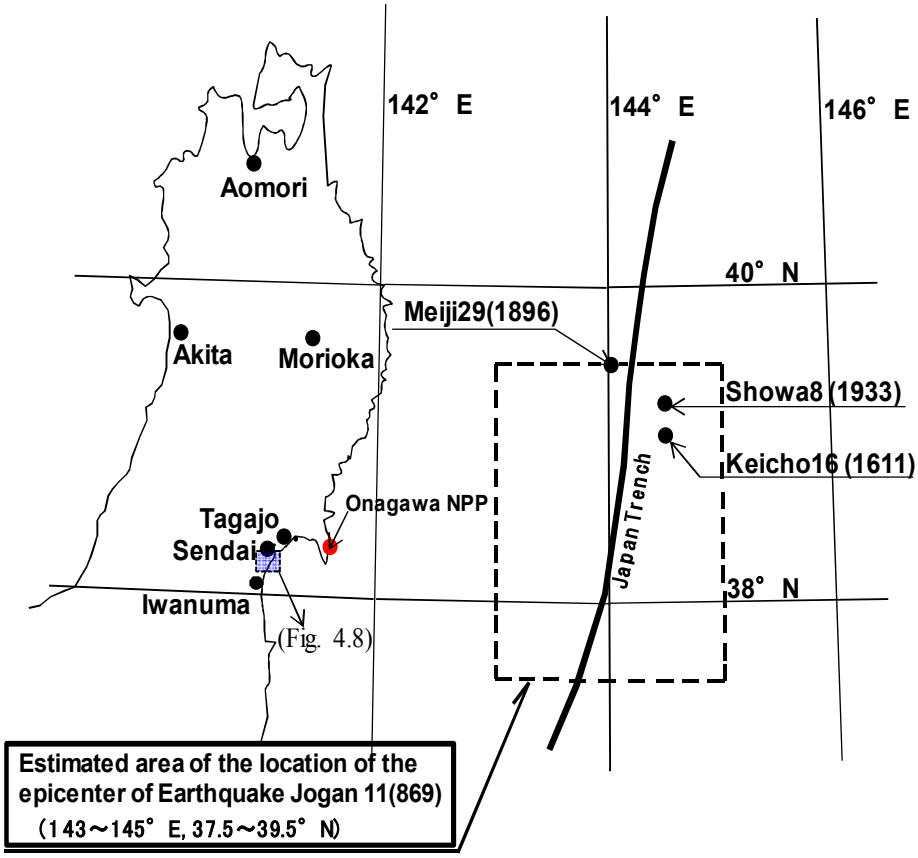

FIG. 55. Epicenters of the great tsunamigenic earthquakes which occurred of the Sanriku Coast.

Among tsunamis (2), (3) and (4) at the Onagawa NPP, it can be estimated that the AD 1611 Keicho Sanriku tsunami was the most influential through literature research and numerical simulations. However, clear information on tsunami height had not been obtained about (1) AD 869 Jogan tsunami and it is very hard to determine which tsunami ((1) Jogan or (2) Keicho) was more influential on Onagawa NPP.

Therefore, Tohoku EPCO estimated the tsunami height and inundation area of the Jogan tsunami by paleotsunami investigations. These used tsunami deposit investigations together with an archeological investigation for planning the Onagawa unit 2. The tsunami deposit investigation used here is an example of the technique discussed in the section 2.3.

The outline of paleotsunami investigation is as follows [394], and Fig. 56 shows location of the investigation.

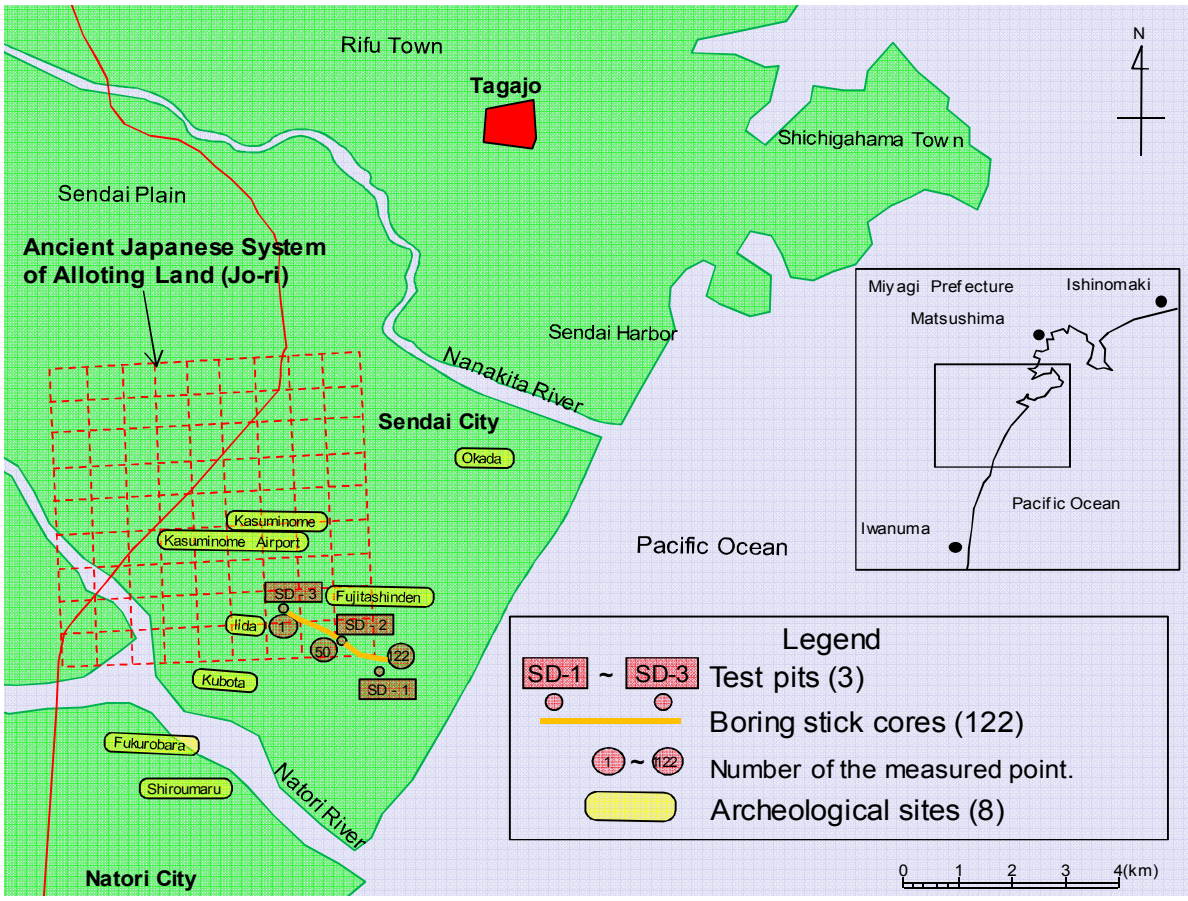

FIG. 56. Location of investigation of AD 869 Jogan tsunami. Reproduced with the permission of Tohoku EPCO.

1. Archeological investigations

As a result of the archeological investigation at eight locations, no tsunami evidence was discovered.

2. Tsunami deposit investigation

Test pit surveys (SD-1 to SD-3, Fig. 57) and simple soil observations (122 locations, Fig. 58) using a soil research stick were carried out. Evidence which was thought to be from the Jogan tsunami was confirmed at the location of soil research stick No. 50 and test pit SD-2. However, in test pit SD-3, approximately 3km from the shore, no evidence was observed as shown in Fig. 59.

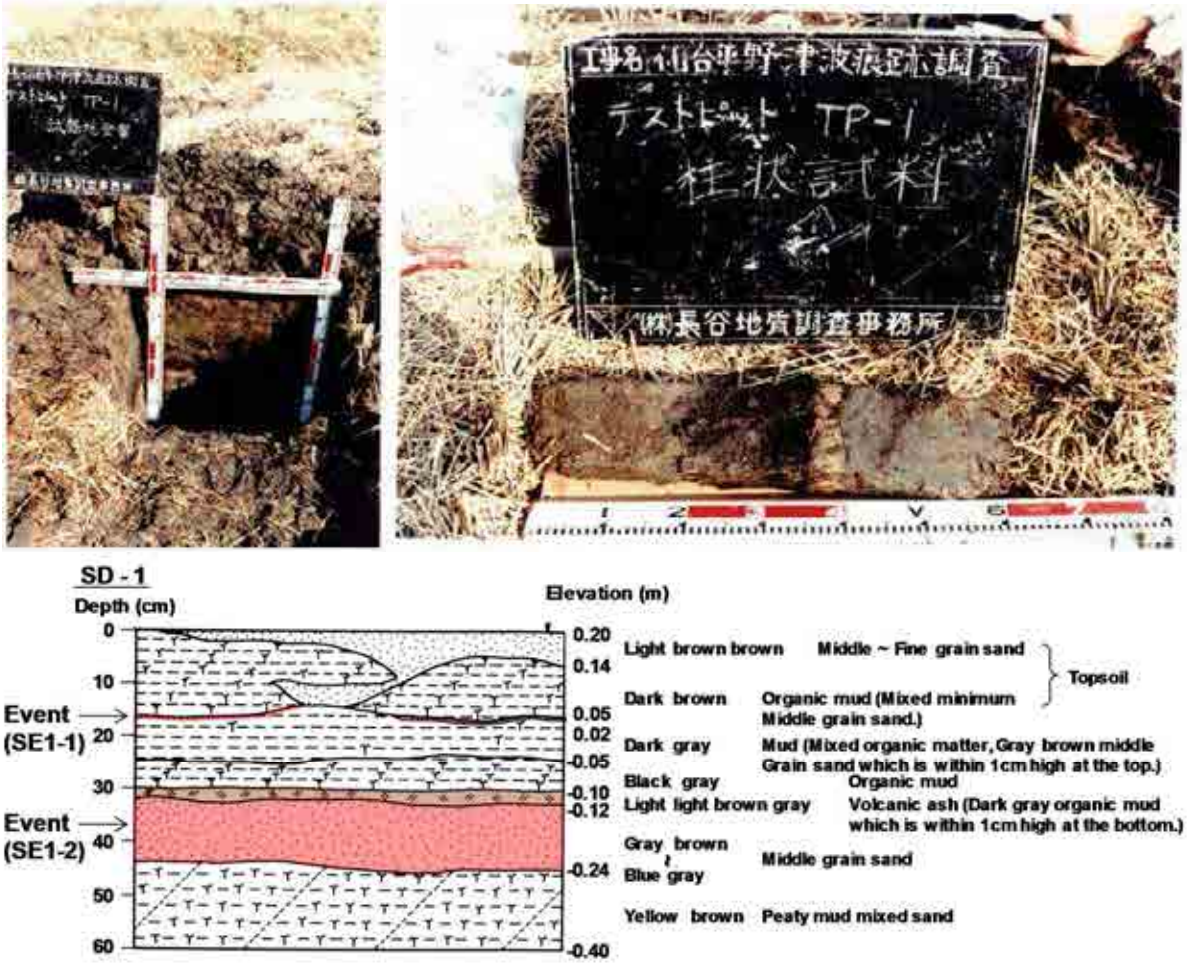

FIG. 57. Photos of Test Pit Investigation at Sendai Plains (SD-1). Reproduced with the permission of Tohoku EPCO.

FIG. 58. Photos of Soil Research Stick Investigation at Sendai Plains. Reproduced with the permission of Tohoku EPCO.

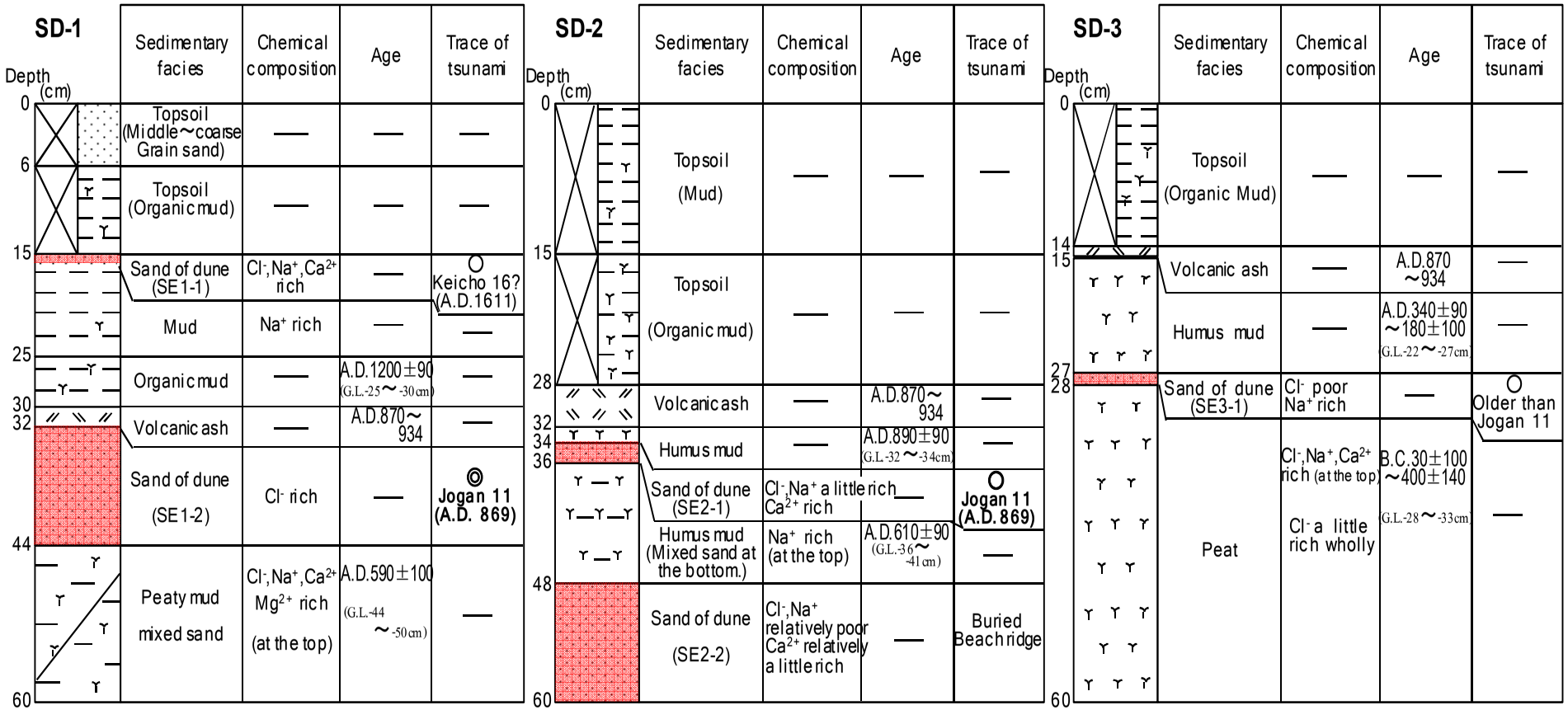

FIG. 59. Judgment of the tsunami traces. Reproduced with the permission of Tohoku EPCO.

As for the tsunami caused by the AD 869 Jogan earthquake, the damage records such as "A tsunami attacked the Tagajo, and approximately 1,000 people were drowned." were described in 'Nihon Sandai Jitsuroku', which is one of Japan's imperial historical records. This damage record does not to contradict the Jogan tsunami run up height and inundation area which were estimated by paleotsunami investigations. A possible tsunami trace was confirmed in test pit SD-3, but the ^{14}C generation of the humus mud right above it was dated between AD 340 ±90y and AD180 ±100y; therefore, it was estimated that this trace is older than AD 869 Jogan tsunami.

The tsunami run-up height at the Sendai plains was estimated to be 2.5–3 m as a result of the paleotsunami investigation for the AD 869 Jogan tsunami. On the other hand, Hatori [395] stated that for the AD 1611 Keicho tsunami, the run-up height was 6–8 m at Iwanuma in the southern part of the Sendai plains. Comparing these two tsunamis, as shown in Fig. 60, although the epicenter of Keicho tsunami is assumed to have occurred farther from the Sendai plains than that of Jogan tsunami, the tsunami trace of Keicho tsunami is higher than that of Jogan tsunami. Therefore, the scale of Keicho tsunami is thought to be larger than Jogan tsunami. For both these two tsunamis, the Onagawa NPP is approximately located on the spread courses of the waves, from the source area to the Sendai plains; thus, it was thought that the tsunami characteristics in Sendai plains were similar to the tsunami at Onagawa NPP site. Therefore, at the Onagawa NPP site, it was estimated that AD 1611 Keicho tsunami was bigger than AD 869 Jogan tsunami. This was later confirmed by numerical simulations using simulation models of the Jogan tsunami suggested by Satake et al. [396].

Regarding the AD 1611 Keicho tsunami, numerical simulations using a fault model (KC-3) suggested by Aida [397] were carried out. The tsunami height at the Onagawa NPP site was calculated to be approximately 9.1 m (at the time of a high tide). In contrast, it was confirmed that the site level (14.8 m) was high enough to allow for the tsunami water, and Onagawa NPP was deemed safe from a similar size tsunami (Fig. 60).

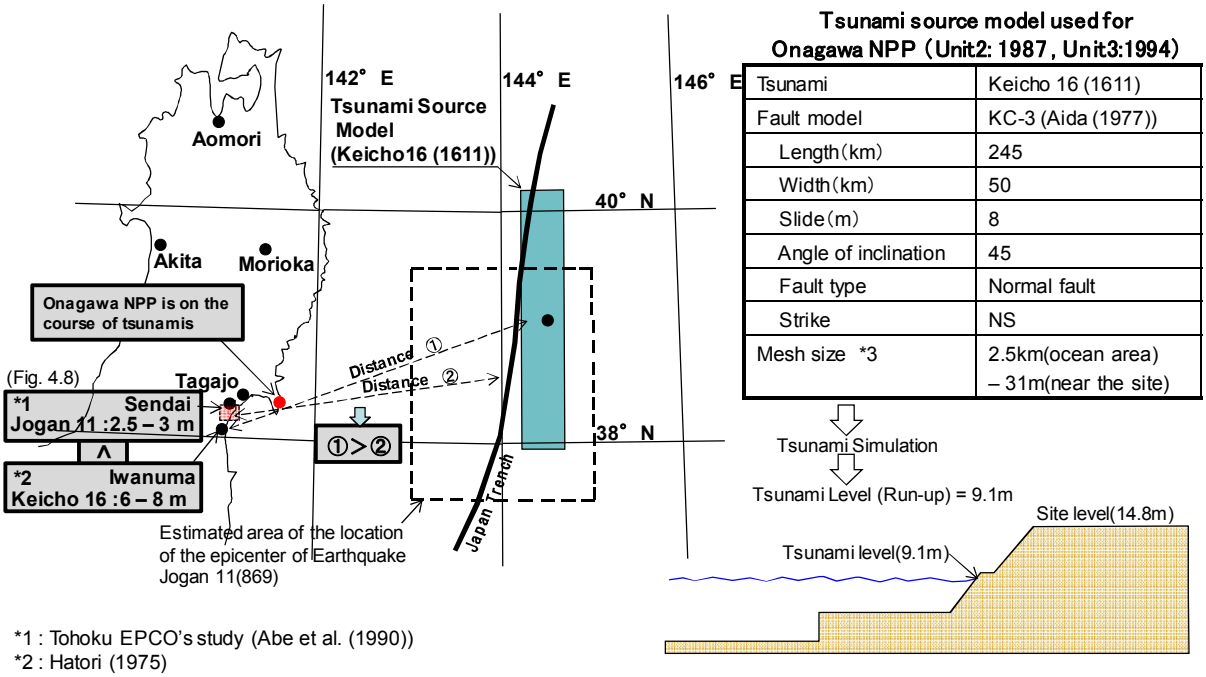

Tsunami	Keicho 16 (1611)
Fault model	KC-3 (Aida (1977))
Length(km)	245
Width(km)	50
Slide(m)	8
Angle of inclination	45
Fault type	Normal fault
Strike	NS
Mesh size *3	2.5km(ocean area) – 31m(near the site)

*1 : Tohoku EPCO's study (Abe et al. (1990))
*2 : Hatori (1975)
*3 : Mesh size near the site is about 5m or less in recent tsunami simulations.

FIG. 60. Comparison of the scale of tsunamis, and the Keicho 16 tsunami model. Reproduced with the permission of Tohoku EPCO.

The inundation area of ancient tsunamis that are not listed in historical documents can be estimated by archeological or tsunami deposit investigations. However, it is necessary to be careful regarding the limited investigation localities, and also how tsunami traces not consistently preserved in the geologic record.

After the Great East Japan Earthquake on March 11, 2011, paleotsunami investigation technology including tsunami deposit survey has been rapidly progressing; the scale or the frequency of the past big tsunamis will be clarified and utilized for the design of Nuclear Power Plants.

4.1.2 Paleotsunami Investigations around the Fukushima area

In the application document for establishment permit of the Fukushima Dai-ichi NPP, the subject tsunami source was the 1960 Chile Earthquake (M 9.5) and the design basis tsunami water level was 3.1 m. In 2002, TEPCO evaluated the design tsunami height based on the 'Tsunami Assessment Method for Nuclear Power Plants in Japan' (Japan Society of Civil Engineers [399]) voluntarily assessing the 1938 Fukushima offshore earthquake (M 7.9) as M 8.0, and the highest water level of each Unit was set to levels between 5.4 and 5.7 m. At the 32nd Joint Working Group for Earthquake, Tsunami, Geology, and Foundations under the Seismic and Structural Design Subcommittee (June 24, 2009), held in order to conduct examinations related to earthquakes, it was pointed out that although the investigation on tsunamis caused by the Jogan earthquake in AD 869 was reported by National Institute of Advanced Industrial Science and Technology (AIST) and Tohoku University, the earthquake causing the tsunami was not dealt with. Regarding this, Nuclear and Industrial Safety Agency requested TEPCO at the 33rd Joint Working Group (July 13th, 2009) to take into account the Jogan earthquake for evaluating design tsunami height when new knowledge on this tsunami is obtained. The survey reports by AIST and Tohoku University were summarized by HERP [399]. Several examples of them follow below.

Summarized history of the Jogan paleotsunami survey

The history of the Jogan paleotsunami survey is summarized from Sugawara et al. [193]. Until the late 1980s, the written record 'Nihon Sandai Jitsuroku' was the exclusive information source for the Jogan event. The sand layer deposited by the Jogan tsunami has been used to estimate its alongshore extent and inundation since the late 1980s. The geologic record of the Jogan tsunami was a focus of the early paleotsunamis investigations in Japan. A number of field surveys to detect traces of the Jogan and other past tsunamis were conducted in the coastal areas of Iwate, Miyagi and Fukushima prefectures. To date, research teams have surveyed 30 different sites, with more than one group studying several sites. Before 2000, field surveys of the Jogan tsunami deposit were limited to sites on the Sendai Plain and in Soma, which is in northern Fukushima prefecture. The number of field surveys increased in the early 2000s, with a large increase since 2006. This is mainly caused by the start of the 'High-priority Observation and Survey on Miyagi-oki Earthquakes' research program in 2005, managed by HERP [373].

Example of the Jogan paleotsunami survey

The Iwaki Coast area is located from near the mouth of the Abukuma River to Soma City, and has a Holocene geomorphic surface (alluvial plain). In the Matsukawaura region, the Towada tephra (volcanic ash) (dated to AD 915) is found at depth of tens of centimeters and a tsunami deposit was identified directly beneath this tephra [400–401]). It was believed that this tsunami deposit was likely formed by the historical Jogan tsunami (AD 869). Considering

these results, at the 3 points in lowland area along the Nikkeshi River, event deposits supposed to be Jogan and former tsunami deposits were sampled using the special technique which directly pulls out the cross section sample of the strata from the ground, and depositional ages of each event deposits are determined. In this survey, a volcanic glass condensed layer directly beneath the surface was observed with a sand layer directly underneath. The grain size of this sand layer is homogeneous, and contains blocks of clay. Tephra analysis confirmed that this tephra is the Towada-a tephra (AD 915) on the basis of shape and refractive index of volcanic glass. Considering these stratigraphic and chronologic results, the sand layer directly beneath this tephra is very likely a tsunami deposit formed during the Jogan tsunami.

Tsunami events before the Jogan tsunami

At the survey points where the event deposit corresponding to the Jogan tsunami was observed, several event deposits pre-dating the Jogan tsunami were also observed. Comparing the results along the Iwaki coast area south of Sendai plain, at least 4 event deposits since ca. 4,000 years ago were observed before the Jogan tsunami event deposit. Focusing on the period following the Jogan tsunami, at least 2 event deposits are recognized in the Sendai plain, Ishinomaki plain and Matsukawaura area. HERP [399], however, maintained that it is necessary to carry out further studies of the tsunami deposits to better constrain the age of paleotsunami deposits, to geologically validate the range of tsunami impacts, to verify whether the wide-range correlation between the Sanriku coastal area and Sendai plain-Iwaki coastal area is comparable to the Jogan event.

Availability of paleotsunami investigations for Tsunami Hazard Analysis

It is reasonable to state that the role of paleotsunami investigation will increase more and more with time, considering that geologic evidence of the Jogan tsunami was detected by means of paleotsunami investigation already well before the 2011 Tohoku Earthquake. However, many deposits were merely recognized as candidates for tsunami deposits because of the limited extent of the investigation and/or lack of standard procedures for characterizing tsunami deposits. As mentioned above, it has taken about 20 years to apply the results of tsunami deposit investigations to disaster prevention through the verification of potential evidence by many specialists. There are three main factors leading to such a long time: (1) limited availability of researchable area, (2) lack of verification by different research groups, and (3) lack of objective verification by many specialists. In order to apply paleotsunami data to Tsunami Hazard Analysis, it is necessary not just to accumulate data, but to also have a technical and political framework resolving the above factors.

4.2. APPLICATION OF PALEOSEISMOLOGY TO SEISMIC HAZARD ANALYSIS IN THE CENTRAL AND EASTERN UNITED STATES (CEUS)

Paleoseismology techniques have been applied across the CEUS (Central and Eastern United States) to augment seismic data and to improve seismic hazard analyses. Considering paleoseismic data along with historic data may increase the number of events and their maximum magnitudes (Mmax), which may decrease the recurrence time of seismic events included in hazard calculations. More importantly, paleoseismic studies extend the length of the earthquake record often by 1000s–10,000s of years and reduce uncertainties related to sources, magnitude, and recurrence times of earthquakes. The CEUS Seismic Source Characterization (Technical Report, [108]) uses a lot of paleoseismic data in building the source model for seismic hazard analyses. Most of these data are derived through study of paleoliquefaction features. Appendix E of the Technical Report [108] compiles data from ten

distinct regions in eastern North America where paleoliquefaction features have been used to improve knowledge of regional seismic history. These regions are shown in Fig. 61. Paleoliquefaction data can significantly impact seismic hazard calculations by better defining earthquake sources, Mmax for those sources, and recurrence rates of large earthquakes.

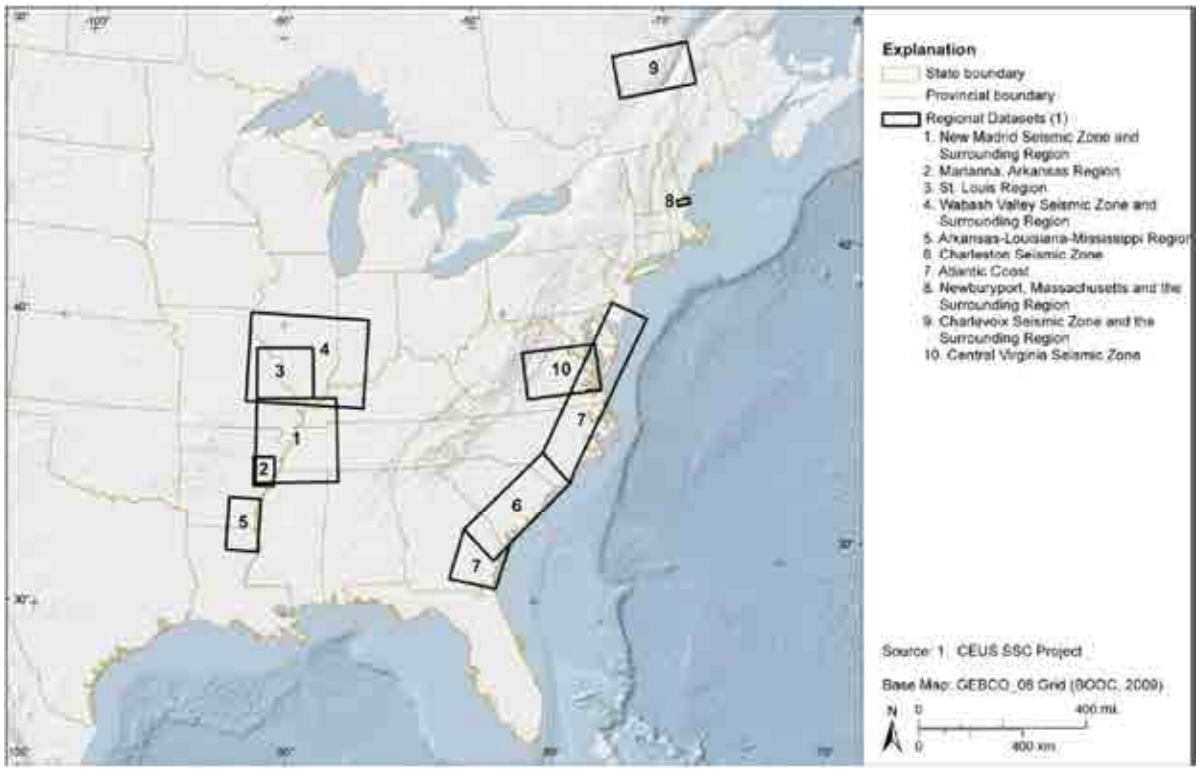

FIG. 61. Map of CEUS showing locations of regional data sets in the CEUS-SSC project paleoliquefaction database. Figure reproduced with permission from Tuttle and Hartleb in 2012 [109].

At the request of the U.S. Nuclear Regulatory Commission, all NPP operators in the CEUS are required to recalculate their site hazard using the new source model by 2014. The Technical Report [108] does provide example hazard comparisons between the new model and the two older source models. Comparisons are made with the U.S. Geological Survey model developed for the National Seismic Hazard Mapping Project [402] and an unpublished model known as the 'COLA' model used for NPP license applications in the CEUS since 2003. The 'COLA' model is the EPRI-SOG [403] model updated with more recent source characterizations for the Charleston Seismic Zone (CSZ) and New Madrid Seismic Zone (NMSZ). These models pre-date the CEUS-SSC model by less than a decade, so they do consider some of the paleoliquefaction data from the CSZ and NMSZ. Early seismic hazard analyses that were used to license many operating NPPs in the CEUS considered little or no paleoliquefaction data. Comparisons of those analyses to the new hazard analyses using the CEUS-SSC model will be completed by NPP operators in 2014. Those comparisons will better illustrate the impact on hazard results from the paleoliquefaction data.

The Technical Report [108] defines one type of seismic source zone as a location of repeated large magnitude earthquakes (RLME), which receives special consideration in the hazard analysis. An RLME is defined as a seismic source that has generated more than one earthquake with $M \geq 6.5$ in the historical or paleoearthquake record. Eleven unique RLME sources are described in Section 6 of the Technical Report [108], and several of them would not be defined as such if not for paleoliquefaction and other paleoseismic data revealing

multiple large earthquakes. Three RLMEs, the CSZ in the Southeastern U.S., and the Wabash Valley Seismic Zone, and the Marianna Seismic Zone in the Central U.S., rely on paleoliquefaction data to define more than one large earthquake, and thus establish their status as RLMEs. Paleoliquefaction data collected from the CSZ and the NMSZ in the central U.S have revealed several large earthquakes over the past few thousand years, increasing recurrence rates in these two source zones. As a result, the greatest impacts from paleoliquefaction data on CEUS seismic hazard calculations occur in the areas encompassing these seismic sources.

The CSZ provides an excellent example of the impact that paleoliquefaction data can have on seismic hazard calculations through earthquake recurrence estimates. The largest earthquake to affect the Eastern U.S. in historic time was the Charleston earthquake of 1886. Moment magnitude estimates for this event range from high-6 to mid-7, but most recently Bakun and Hopper [404] estimated the magnitude at M 6.9, with a 95 percent confidence interval of M 6.4–7.1, and Talwani [405] made a best estimate of M 7.0. The Charleston earthquake produced many sand-blow craters in the area (see Figure 19 as an example). No fault surface rupture was noted during the 1886 event, and a causative fault for the Charleston earthquake has not been definitively identified. The Charleston area is located in the Coastal Plain of the Atlantic passive margin, which lacks the landforms and topography typically observed in interplate regions with high rates of seismicity. The topography and the modest instrumental seismic record suggest that the 1886 earthquake could have been a rare, isolated event; however, paleoliquefaction data reveals that it was not.

In the 1980s, researchers began identifying paleoliquefaction features, mostly sand blows, in the Charleston region that pre-date the 1886 event, indicating strong, prehistoric ground motions. Documentation of these features, including age data, is provided by Talwani and Cox [406], Obermeier et al. [407], Weems and Obermeier [408], Amick et al. [409, 410], Talwani and Schaeffer [411], and Talwani et al. [412]. Unfortunately, none of these studies considered the relative size of historical and prehistoric liquefaction features as has been done for other seismic zones. The CSZ studies and the Technical Report [108] found that paleoliquefaction features are confined to the Charleston area, with spatial distribution similar to that of the liquefaction features generated in 1886. Such a spatial distribution suggests the magnitudes of the paleoearthquakes were no larger than the 1886 event, and epicentral areas were similar. This conclusion is supported by analyses of the geotechnical properties of the sediments that liquefied in the prehistoric earthquakes (Hu et al., [413, 414]). The Hu et al. [413, 414] analysis, as well as refinements by Leon [415] and Leon et al. [416] that considered aging of the sediments since the time of liquefaction, derived earthquake magnitude estimates from the mid-5 to mid-7 range. Gassman et al. [417] narrowed the estimates to M 6.7–7.0 for the prehistoric events and the 1886 event. As a result, paleoliquefaction data did not affect estimates of Mmax for the CSZ in the Technical Report [108].

The Technical Report [108] compiled available paleoliquefaction data for the CSZ, including numerous ages of paleoliquefaction features. Most of these are believed to be contemporary ages, derived from radiocarbon dating of organic material collected from sand blow deposits or deposited within sand-blow craters shortly after they formed. Other ages are derived from sediments either underlying or overlying sand blow deposits providing maximum and minimum constraining ages (see section 2.2.2.2 for a discussion of dating paleoliquefaction features). The data can be displayed in a space-time diagram, enabling easier interpretation of unique earthquakes based on age estimates of PL features, as seen in Fig. 62.

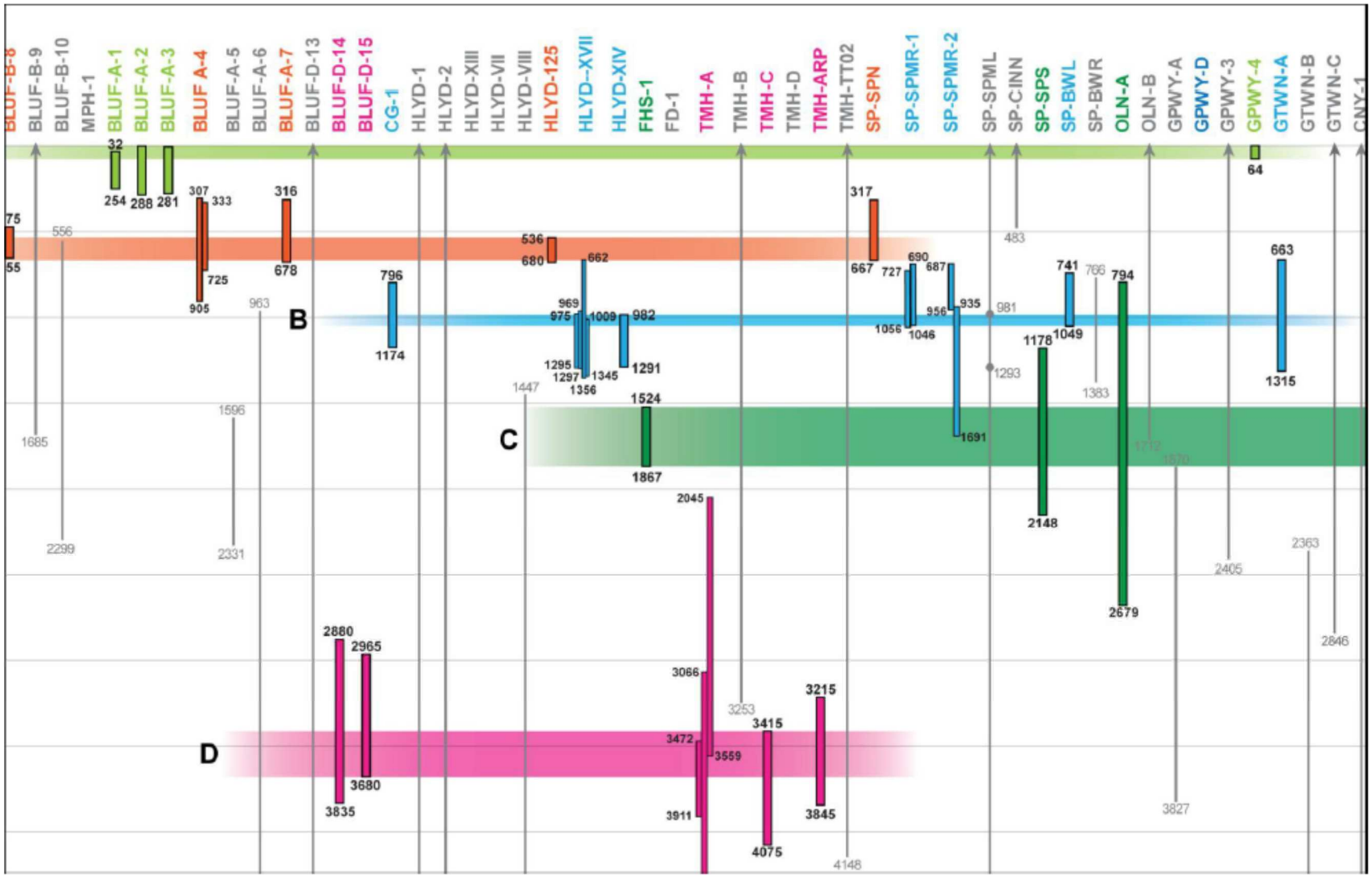

FIG. 62. Space-time diagram of paleoliquefaction feature ages and interpreted earthquakes in the CSZ. This figure uses only paleoliquefaction ages that are believed contemporaneous with formation of the paleoliquefaction feature. Vertical bars represent age ranges for individual sand blows, and colored bands represent inferred earthquake times based on intersection of overlapping age estimates. Figure reproduced with permission from Technical Report in 2012 [108].

Talwani and Schaeffer [411] first combined the available paleoliquefaction age data to derive a CSZ recurrence interval of approximately 550 to 1000 years. The Technical Report [108] considered additional data, recalculated the radiocarbon ages following the technique of Tuttle [31], and concluded that, including the 1886 event, four liquefaction-inducing earthquakes have occurred in approximately the last 2000 years. One or two additional earthquakes likely occurred between 2000 and 5500 years ago. This information was used to bound earthquake recurrence rates for the CSZ, which served as input to the hazard model. The uncertainties in the recurrence rate and other parameters are incorporated into the hazard model through a logic tree for the CSZ, described in Section 6.1.2 of the Technical Report [108]. The logic tree considers several options for the number of earthquakes and recurrence rate, source zone geometry, as well as the possibility that CSZ earthquakes cluster in time.

Paleoseismic data are important to recurrence rate calculations within all RLMEs in the CEUS-SSC model, and in some they impact Mmax as well. The CSZ is highlighted here because the paleoseismic data have such a clear impact on large earthquake recurrence rate.

A similar case has been made for the NMSZ in the Central U.S. for repeating earthquake sequences including very large earthquakes of $M \geq 7$ (Tuttle et al., [117]; Tuttle and Hartleb, [109]). To gain a qualitative appreciation for the impact that paleoliquefaction data have on the seismic hazard near the CSZ, consider that without PL data, the seismic history of this region would contain only one M 6.9 event in 1886 and modest seismicity since instrumental recordings began in the mid-1900s. A typical Gutenberg-Richter, frequency-magnitude distribution would have an anomalous point representing the M 6.9 1886 event, but this would likely elevate the local seismic hazard only modestly compared to areas with similar instrumental records without an historic M 6.9 earthquake. With a more complete seismic history provided by the PL data, hazard models consider, with high probability, a recurrence of M ~6.9 earthquakes approximately every 500 years. Although a quantitative comparison of these two scenarios is not available at this time, the impact is apparent.

In summary, the CEUS seismic hazard analysis, documented in the Technical Report [108], demonstrates that collection of paleoseismic data (especially paleoliquefaction data), when available, can greatly improve completeness of the seismic record. This leads to improved hazard estimates with lower uncertainties.

4.3. PREHISTORIC SEISMIC RUPTURES REVEALED BY PALEOSEISMIC STUDIES IN THE SIERRAS PAMPEANAS, ARGENTINA

4.3.1. Nature of the problem

Earthquakes in intraplate settings are less frequent than in interplate areas, but they can produce substantial damage to structures because they are not generally designed to withstand strong ground motions.

The recurrence time for major earthquakes on individual faults is much longer than records of historical seismicity, which sometimes results in damaging earthquakes occurring in unexpected locations. This issue becomes even more critical in America, where historic seismicity encompasses a time span no longer than 500 years. Therefore, these regions are very challenging for understanding earthquake occurrence in space and time and for assessing the seismic capability of fault sources.

The Sierras Pampeanas (Pampean Ranges) constitute the broken foreland of the Andes above the flat-slab subducting segment of the Nazca Plate between 27°30'S and 33°00'S [418–420] (Fig. 63). They are characterized by mountain blocks emerging at the westernmost part of the Chaco-Pampean plain in western Argentina and are bounded by reverse faults with evidence of Quaternary activity [421].

This region provides an excellent example of the challenges for gathering paleoseismic data and also illustrates how this information could help to better understand the seismic capability of an area or structure.

The historical seismicity of the Sierras Pampeanas is characterized by crustal earthquakes with magnitudes $M_s \leq 6.4$ and the instrumentally recorded events do not illuminate the subsurface geometry of the main crustal morphogenic structures. There are no records of crustal earthquakes producing either primary coseismic surface ruptures, or secondary related phenomena. The only exception is the 1977 M_w 7.4 Caucete earthquake (19 km depth), but this event was located at the junction with the Andean orogenic front. This important event related to a compressive rupture [422] produced extensive damage, but just led to secondary submetric ruptures at the surface (bending-moment faults?).

Based on the seismologic information, the Sierras Pampeanas have traditionally been considered as an area with a seismic capability considerably lower than the Andean belt, with maximum expected PGA of 0.18g [423]. However, a lot of earthquake-related evidence has been found along neotectonic faults during the last years. They account for primary surface ruptures, large rock-avalanches and paleoliquefaction. These phenomena have no historical analogs in the region and bear witness for the occurrence of crustal prehistoric earthquakes larger than previously thought.

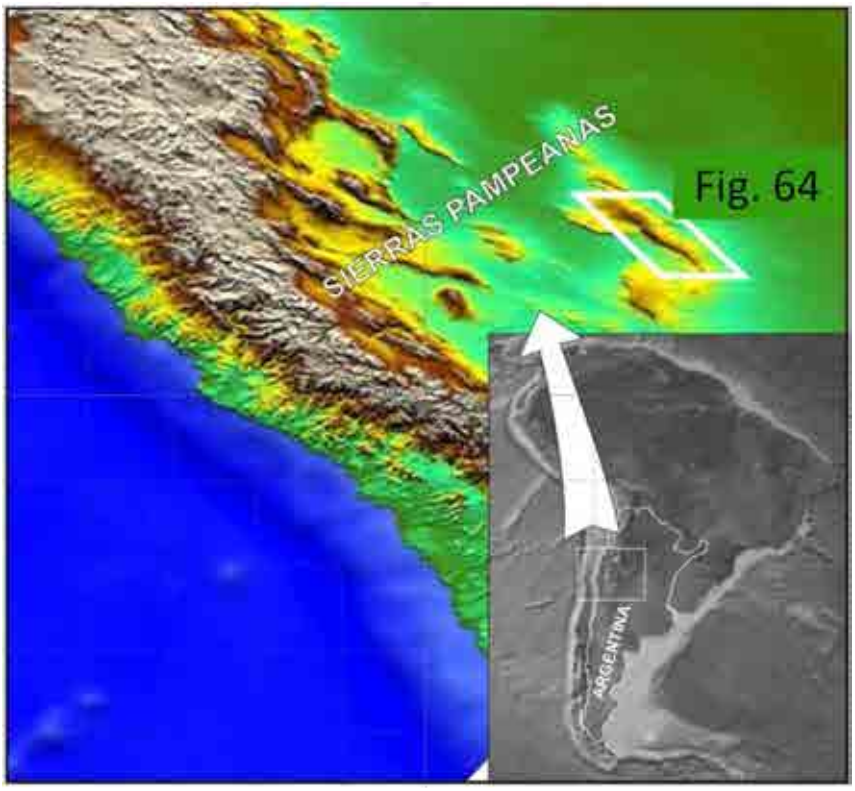

FIG. 63. Location of the Sierras Pampeanas mountain blocks. The white rectangle indicates the location of the Comechingones range.

4.3.2. Paleoseismic studies at El Molino fault

The Comechingones fault limits the western slope of the Comechingones range (Fig. 64) [81, 424–425]. However, no faults deforming young alluvial deposits have been found along the main hillslope break. Instead, an incipient piedmont foreland [308] can be recognized to the West of the main slope break from aligned scarps (Fig. 64). No primary fault-related landforms are present along this piedmont belt, but detailed field surveys have demonstrated that evidence of recent tectonic activity is exposed at the western margin of these basement-cored hillocks.

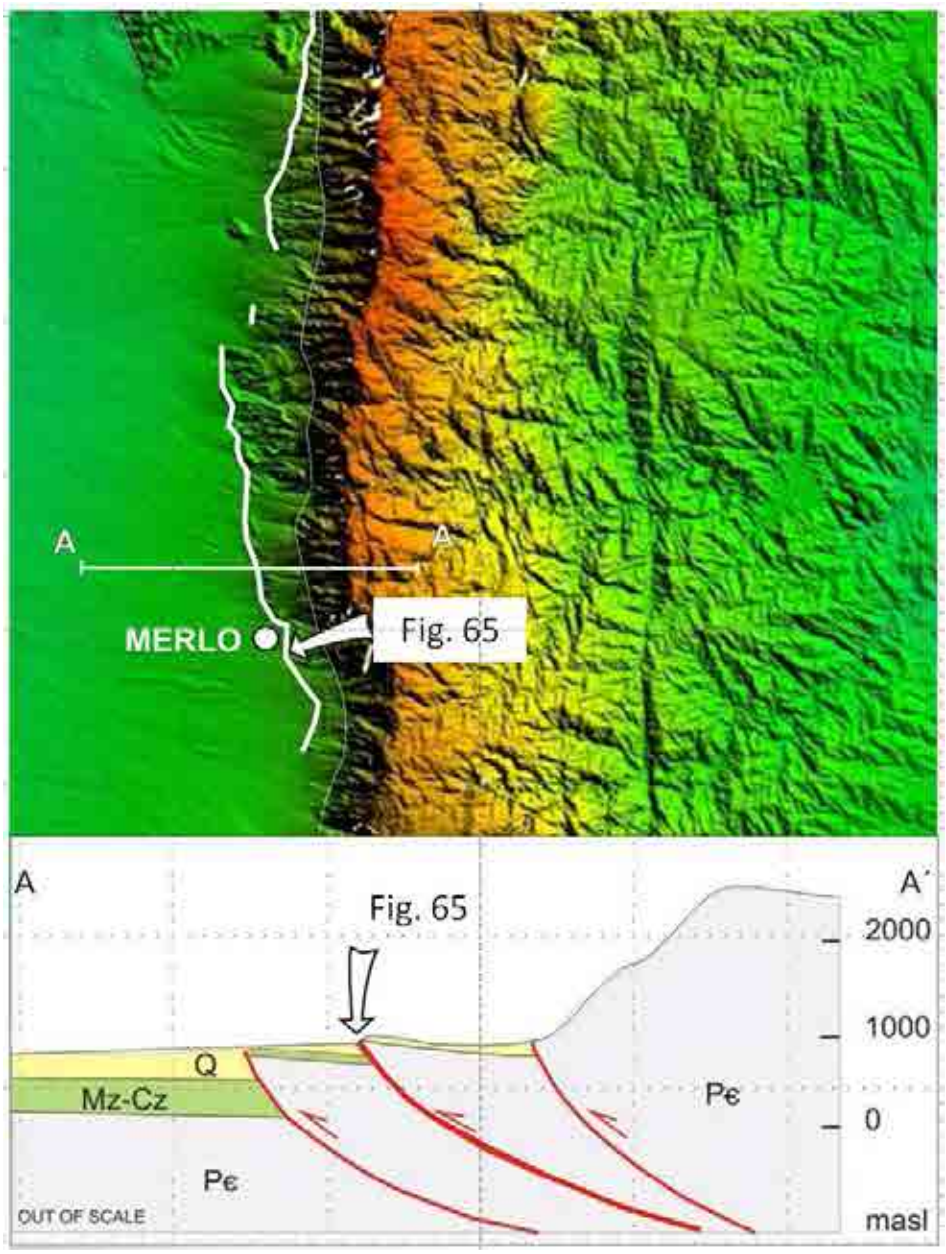

FIG. 64. Digital elevation model of the Comechingones range. The thin solid line shows the main bounding fault (Comechingones fault). The thick solid lines points out to the Quaternary-active footwall shortcut of the main thrust, where evidence of Holocene deformation has been located. A simplified cross-section (A-A') sketches the shallow structure, where another Quaternary-active structure without surface signature is located to the West of the study area, as suggested by subsurface information.

Trenches excavated near Merlo village across the El Molino fault, a footwall shortcut of the main Comechingones fault (32°21'30,75'S-64°58'57,77'W), have revealed two opposing-verging thrusts deforming the Holocene cover (Fig. 65). The eastern branch or main fault emplaces Precambrian basement over proximal scarp-derived deposits, whereas the western thrust results in an east-directed fault-propagation fold that deforms wash-slope and fluvio-aeolian deposits.

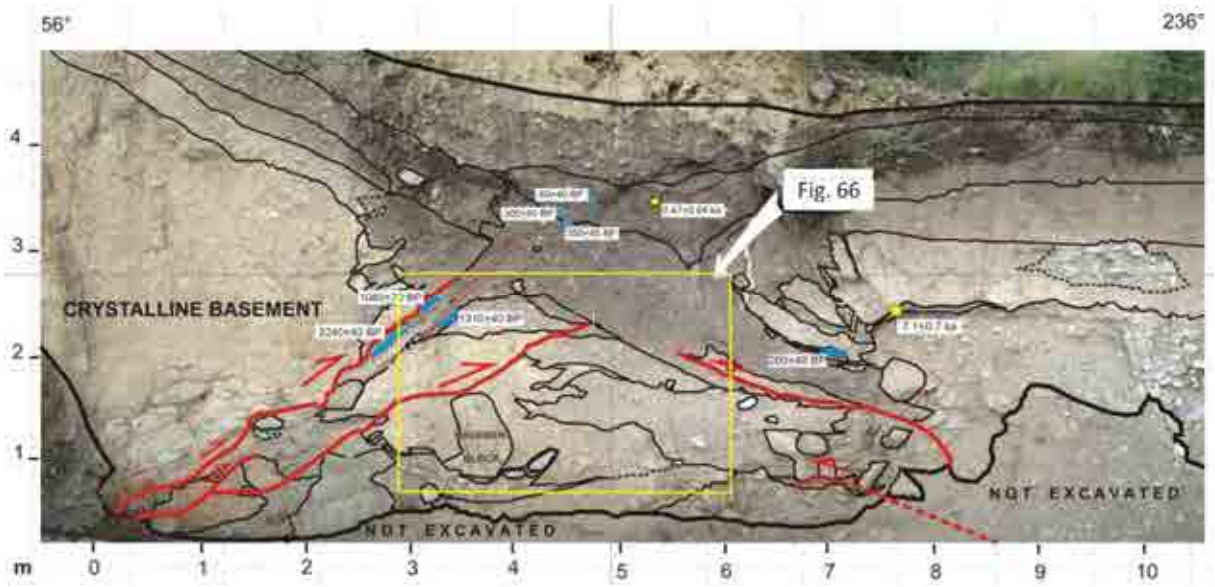

FIG. 65. Simplified trench log of the El Molino fault trench site, after Costa et al. (2010) [426]. The Precambrian crystalline basement (sheared migmatites) overrides alluvial and scarp-derived deposits. Blue dots correspond to radiocarbon samples and yellow dots to OSL samples with the corresponding ages. Based on Costa et al in 2010 [426].

According to Costa et al., in 2010 [426],

> "the ages of the fault-related deposits have been reasonably defined through radiocarbon and optically stimulated luminescence methods which provide ages ranging from 7.1+0.4 ka to 350+40 cal yr BP. Evidences of surface deformation are related to multiple-events with colluvial wedges and filling wedges derived from bending-moment ruptures at the fold hinge zone" (Fig. 66). See also [424–425].

Figure 66 provides an example of clear evidence for prehistoric ruptures and also sheds light on the possible height of the related coseismic scarps. It depicts a multiple event colluvial wedge, where the light colored units are gravitational deposits collapsed from the hanging-wall. They derive from the sudden rise of the hanging-wall during each coseismic rupture and are entirely made up by basement debris. The basement boulder identified in Fig. 66, with a long axis of 0.62 m according to the orientation of the trench wall, should have been derived from a coseismic scarp with at least that height (0.62 m). But plotting a Fault Slip Component diagram [427] with the slickenlines measured on the fault surface, it turns out that the vertical slip (V) contributes from 15% to 36% of the total slip vector (D). Therefore, a single coseismic slip of 2.13 m could be interpreted for one of those events. This scarp should have been related to a prehistoric earthquake much larger than those recorded by seismicity.

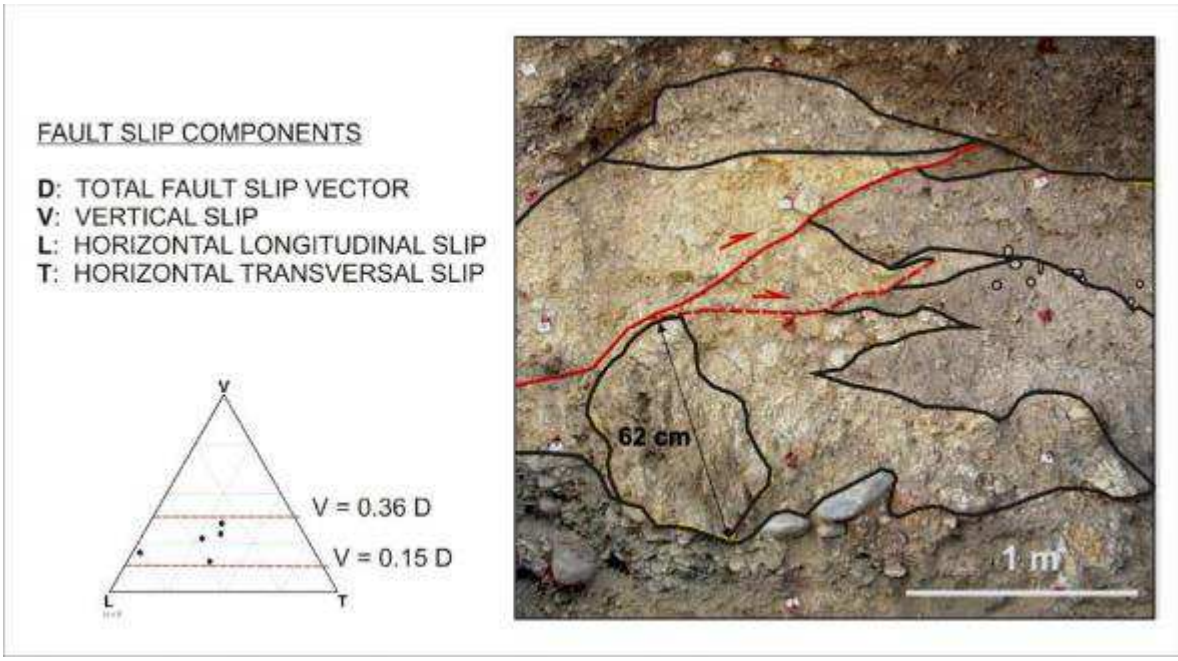

FIG. 66. Detail of the trench log shown in FIG. 65. The colluvial wedges derived from the sheared migmatites of the hanging-wall show dominant yellowish colors. They indicate primary coseismic scarps related to the main west-directed thrust. The other gray to brownish units are dominantly made up by a mix of wash slope and aeolian deposits including paleosoils. Colluvial wedges are faulted indicating several rupturing events. A single boulder collapsed from the thrust hanging-wall is also highlighted with solid black line. Dip and rake angles of slickenlines plotted in the Fault Slip Components diagram on the left, indicate that the vertical slip (V) represents a percentage of the total slip vector ranging from 15% to 36%. Based on Costa et al. in 2010 [426].

According to Costa et al. (2010) [426],

> "It has not been possible to unravel whether these structures slipped in simultaneous or separated events which of course impacts in the discrimination of the number of earthquakes recorded in this sequence record. Accordingly, a minimum of four and a maximum of nine surface ruptures younger than 7.1+0.4 ka can be preliminarily interpreted at this trench site, where the elapsed time since the last rupture event is > 350+40 calibrated years BP. Estimated recurrence intervals vary according to different approaches from 0.8 to 3.0 ka (preferred 1.0–2.5 ka), whereas by retrodeforming the total shortening exposed in the trenches, a maximum slip rate of 1.13 mm/year was obtained".

These slip rates appear to be high for an intraplate and may suggest that there has been a peak in fault activity with associated surface deformation during the past 7 ka, resulting in a clustering of crustal earthquakes rupturing at surface (M > 7.0).

4.3.3. Some lessons learned from the Sierras Pampeanas case

Reverse faults and blind thrusts are troublesome, because they commonly bear no diagnostic landforms to recognize the causative underlying structure. Terrain analysis is less dependable than in other settings, highlighting that 'the absence of evidence is not necessarily the evidence of absence'.

According to historical seismicity data, the threshold magnitude for crustal earthquakes to produce surface rupture in this tectonic setting is considered to be at least $M_s \geq 7.0$ [428]. It is interpreted that primary coseismic rupture took place along the study fault and a related

coseismic slip up to ~ 2m should account for prehistoric earthquakes with magnitudes M ≥ 7.5. This makes a significant difference with the data provided by the seismic catalog (M ≤ 6.4).

When estimating the Maximum Credible Earthquake (MCE) according to worldwide used empirical relationships based on rupture length, rupture area and coseismic slip, the obtained results fall below the threshold earthquake estimated for the Sierras Pampeanas [428]. This would lead to interpreted events with little or no chance of rupturing at the surface, and therefore, an underestimation of the real paleomagnitudes. There are few proxies for understanding the correspondence between the seismogenic potential of capable structures at these crustal settings, their signature at surface and seismogenic parameters derived from paleoseismic studies. Therefore, caution is needed when estimating paleomagnitudes from main parameters used by most accepted empirical relationships.

The short time period provided by the seismic catalog data may underestimate the seismic capability of sources; therefore, supplementing the historical record with paleoseismic data is necessary for more realistic hazard assessments. Due to the activity rate of faults, deep trenches and/or a significant number of them may be required at these settings for deriving parameters such as slip rate and recurrence interval.

APPENDIX 1 - SEISMIC VS. ASEISMIC FAULTS (CREEPING): SOME CRITERIA FOR DISCRIMINATION

Surface faulting characterized by creeping falls beyond the scope of the SSG9 guidelines. However, creeping faults can sometimes cause severe earthquakes and result in sudden surface deformation. Accordingly, these faults would therefore be investigated with paleoseismic techniques.

Creep is generally attributed to low frictional strength on faults. This can be due to the geologic properties of faults or due to low values of normal stress (for example due to high pore pressure) (e.g. Irwin and Barnes, [429]; Gratier et al., [430]). Recently, after the Tohoku megathrust earthquake, Noda and Lapusta [431] proposed that physical changes in the fault zone could be responsible for the coseismic slip of previously creeping patches. Chang et al. [432] also mention that a seasonal change could have been responsible for the coseismic brittle ruptures at the surface during the 2003 earthquake caused by the Chihshang fault (Taiwan), instead of its usual aseismic slip. Along a single fault, this frictional state can vary in space and time.

Aseismic slip along faults is a well-established fact along subduction zones (e.g. [433–436]), as well as along crustal faults. Regarding crustal faults, the best documented examples are perhaps portions of the San Andreas Fault System (i.e. the Hayward and Calaveras faults) in California, the Longitudinal Valley Fault in Taiwan or of the North-Anatolian Fault in Turkey. Earthquake hazard along the Hayward fault is especially difficult to assess because, besides the occurrence of damaging earthquakes (1836, 1868) along several segments, it currently releases a significant fraction of strain by creeping (5 mm/a). By pointing out the discrepancy between the current creep rate and the Holocene slip rate (8 mm/a), Lienkaemper and Borchardt [437] conclude that the Hayward fault is now accumulating strain at depth for future earthquakes. Later, the same team (e.g. Lienkaemper et al., [438]) proved, thanks to trenching surveys, that this 'creeping' fault actually experienced a tenth of all the surface rupturing earthquakes on the San Andreas over the last 2000 years. The Longitudinal Valley fault (Taiwan) is another crustal creeping fault along which surface rupturing earthquakes occurred in 1951 and 2003. Lee et al. [439] measured along its Chihshang segment a steady creeping rate of about 20 mm/a, just before this active segment generated the earthquake of 2003 (M=6.5) which caused surface deformation (folding and minor faulting both on primary and secondary faults). In Turkey, the Ismetpasa segment is a well-studied creeping portion of the North Anatolian Fault, where creep rate seems to change with time in relation with stress changes and earthquake sequence [440, 441].

> *"Coseismic or aseismic slip? What are their morphologic signals and how to discriminate them in the stratigraphic record?"*

As mentioned by McCalpin [379], the degree to which creep and rapid slip can be distinguished is not just a function of their relative importance, but also depends on the relative rate of local external processes which may blur or erase any reliable evidence (erosion, sedimentation).

Many geomorphic markers are indicative of tectonic displacements along capable faults [413]. Most of them (e.g. the scarp profile) are the product of tectonic and external processes and the offset variations with time (if existing) may be smoothed, especially over long time

periods. They thus can only reveal cumulative displacements and are not emblematic of aseismic or seismic behavior. However, in certain conditions, the morphologic features can be used to discard creeping and validate sudden episodes of deformation:

1. The most striking example is perhaps the Wairarapa fault in New Zealand, where Rodgers and Little [442] used the space between successive entrenched and beheaded streams to infer successive coseismic offsets (>12 m). Increasing displacement of older and older terrace risers is also common useful evidence of successive earthquakes along strike-slip faults displacing alluvial channels. However, similar morphologic features can be generated with a steady fault displacement as well, if strong incision phases alternate.
2. Stepped marine terraces and wave-cut platforms or notches have also been attributed to large subduction earthquakes inducing coastline uplift, but similar uplifted features are also recognized at longer time spans and cannot be interpreted in terms of aseismic/seismic faulting.
3. The topographic analysis of fault scarps can reveal their coseismic origin and relative age [443]. However, the scarp free-face degradation and the debris accumulation tend to smooth the initial profile [444], erasing the coseismic signal and giving then a 'classical' wash-slope shape.

The stratigraphic record of displacement sequence across a fault may be the most interesting tool to explore fault behavior. Definitive discrimination between coseismic and aseismic character of faulting is often a difficult task. Many stratigraphic markers are used to determine this distinction, but most of them taken alone are unequivocal proof of an earthquake. The main evidence for earthquakes includes:

1. Sudden changes in deformation between deposit units, for instance leading to drastic unconformities between discrete packages with conformable layers.
2. Liquefaction, which can be the result of shaking during earthquakes, but may be triggered by remote faults.
3. Multiple fault traces close to the surface and a complex branching pattern leading to anastomosing geometry (in plain view) or pop-up or flower structures (in section), because they suggest a recurrent character of shearing [445]. However, these geometries may also only be due to the effect of the 'free ground surface' during upward fault propagation.

Perhaps the best evidence in stratigraphic record of a succession of quiescence and abrupt deformation are the following:

1. The preservation of colluvial wedges or blocky scarp colluvium, which are made of local deposits derived from the free-face of the coseismic scarp, interbedded within background sedimentation (especially for dip-slip faults) (e.g. [2, 446]). However, high creep rates may create steep slopes and change erosion/sedimentation rates and potentially create pinching-out layers of colluvium, above the fault trace. This kind of feature may look like colluvial wedges.
2. Along pure strike-slip faults, surficial fault breccia or collapsed void with a basal rubble zone may be regarded as equivalent of colluvial wedges (e.g. [447]).
3. The fissuring of the ground surface (fissure fills in geologic record, for example with syn- to post-event soils) in the close area of active faults, either extensional, compressive, or strike-slip.
4. The upward terminations of fault strands beneath an undeformed sedimentary unit [448]. This criteria may be ambiguous because fault strands naturally die out upward

and it should be used as a coseismic evidence only when these terminations are numerous at a given strata level.

In fact, demonstrating that a fault is creeping is a hard task at the macroscopic scale (i.e. at the trench scale) and is often inferred from the absence of coseismic indices. However, several pieces of evidence can allow aseismic behavior to be deduced. Creeping dip-slip faults tend to produce slight thickening of layers across faults or lead to growth-fault geometries. This is because their activity is likely to balance with the erosional/depositional processes. Creeping faults can generate unconformities, but when creep occurs during sedimentation, each successive layer is incrementally more folded or tilted (progressive unconformity). Because they do not create a scarp with a free face, creeping faults are free from actual colluvial wedges or other free-face derived deposits (like collapse features). Likewise, creeping faults are prone to create closed fractures in unconsolidated surface sediments, instead of open cracks with different in-fill deposits, because aseismic creep is generally too slow to create long-lived fissures.

Some interesting investigation markers also exist in microscopic analyses of fault planes and gouges, even in surficial loose sediments. Aseismic and coseismic slip may, therefore, be inferred from the sediment fabric. For instance, Cashman et al. [449] observe that coseismic slip along the 1906 San Francisco earthquake led to gouge cataclasis, grain rotation, grain breakage and localized porosity variations, whereas aseismic slip along a creeping portion of the San Andreas fault is marked by distributed deformation within the fabric of the fault-gouge sediment.

As stated by McCalpin (2009) [2], a critical issue in future paleoseismology is to:

"develop methods for distinguishing seismogenic from non-seismogenic faults"

and

"paleoseismologists need to educate themselves about deformation phenomena that resemble coseismic deformation, but are produced by non-seismic mechanisms".

Surface deformation (discrete displacement, but also ground tilting or bending), associated with the activity of a capable fault, may be hazardous for nuclear installations (pipelines, basement slabs, etc.) whether or not it is a creeping feature. Moreover, according to the examples quoted above, a creeping fault may generate significant earthquakes and coseismic surface faulting at any time, and it has to be considered as a potential capable fault.

Appropriate paleoseismic techniques must thus be performed to characterize them. Regarding the ground motion issue of seismic hazard assessment, the creep rate of a fault may be accounted for because it tends to lower the seismic hazard.

APPENDIX 2 - ENVIRONMENTAL SEISMIC INTENSITY SCALE - ESI 2007

In this Appendix the definition of intensity degrees according to the ESI 2007 intensity scale [77] is reported. More details are in Section 3.2.

DEFINITION OF INTENSITY DEGREES

From I to III: There are no environmental effects that can be used as diagnostic.

IV Largely observed/First unequivocal effects in the environment

Primary effects: are absent.

Secondary effects:

a) Rare small variations of the water level in wells and/or of the flow-rate of springs are locally recorded, as well as extremely rare small variations of chemical-physical properties of water and turbidity in springs and wells, especially within large karstic spring systems, which appear to be most prone to this phenomenon.
b) In closed basins (lakes, even seas) seiches with height not exceeding a few centimeters may develop, commonly observed only by tidal gauges, and only exceptionally by the naked eye. These typically occur in the far field of strong earthquakes. Anomalous waves are perceived by all people on small boats, few people on larger boats, and most people on the coast. Water in swimming pools swings and may sometimes overflow.
c) Hair-thin cracks (millimeter-wide) might occasionally be seen where lithology (e.g. loose alluvial deposits, saturated soils) and/or morphology (slopes or ridge crests) are most prone to this phenomenon.
d) Exceptionally, rocks may fall and small landslides may be (re)activated along slopes where the equilibrium is already near the limit state, e.g. steep slopes and cuts, with loose and generally saturated soil.
e) Tree limbs shake feebly.

V Strong/Marginal effects in the environment

Primary effects: are absent.

Secondary effects:

a) Rare variations of the water level in wells and/or of the flow-rate of springs are locally recorded, as well as small variations of chemical-physical properties of water and turbidity in lakes, springs and wells.
b) In closed basins (lakes, even seas) seiches with height of decimeters may develop, sometimes noted also by naked eye. These typically occur in the far field of strong earthquakes. Anomalous waves up to several tens of cm high are perceived by all people on boats and on the coast. Water in swimming pools overflows.
c) Thin cracks (millimeter-wide and several cms to one meter in length) are locally seen where lithology (e.g. loose alluvial deposits, saturated soils) and/or morphology (slopes or ridge crests) are most prone to this phenomenon.
d) Rare small rockfalls, rotational landslides and slump earth flows may take place, often along slopes where equilibrium is near the limit state but not necessarily steep - mainly

loose deposits and saturated soil. Underwater landslides may be triggered, which can induce small anomalous waves in coastal areas of seas and lakes.

e) Tree limbs and bushes shake slightly, very rare cases of fallen dead limbs and ripe fruit.
f) Extremely rare cases are reported of liquefaction (sand boil), small in size and in areas most prone to this phenomenon (highly susceptible, recent, alluvial and coastal deposits, near-surface water table).

VI Slightly damaging/Modest effects in the environment

Primary effects: are absent.

Secondary effects:

a) Significant variations of the water level in wells and/or of the flow-rate of springs are locally recorded, as well as small variations of chemical-physical properties of water and turbidity in lakes, springs and wells.
b) Anomalous waves up to many tens of cm high flood very limited areas near the shore. Water in swimming pools and small ponds and basins overflows.
a) *Occasionally, millimeter-centimeter wide and up to several meters long fractures are observed in loose alluvial deposits and/or saturated soils; along steep slopes or riverbanks they can be 1–2 cm wide. A few minor cracks develop in paved (either asphalt or stone) roads.*
b) Rockfalls and landslides with volume reaching ca. 10^3 m^3 can take place, especially where equilibrium is near the limit state, e.g. steep slopes and cuts, with loose saturated soil, or highly weathered/fractured rocks. Underwater landslides can be triggered, occasionally provoking small anomalous waves in coastal areas of sea and lakes, commonly seen by instrumental records.
c) Trees and bushes shake moderately to strongly; a very few tree tops and unstable-dead limbs may break and fall, also depending on species, fruit load and state of health.
d) *Rare cases are reported of liquefaction (sand boil), small in size and in areas most prone to this phenomenon (highly susceptible, recent, alluvial and coastal deposits, near surface water table).*

VII Damaging/Appreciable effects in the environment

Primary effects: observed very rarely, and almost exclusively in volcanic areas. Limited surface fault ruptures tens to hundreds of meters long and with several cm of offset may occur, which are essentially associated to very shallow earthquakes.

Secondary effects: The total affected area is in the order of 10 km^2.

a) Significant temporary variations of the water level in wells and/or of the flow-rate of springs are locally recorded. Seldom, small springs may temporarily run dry or appear. Weak variations of chemical-physical properties of water and turbidity in lakes, springs and wells are locally observed.
b) Anomalous waves even higher than a meter may flood limited near-shore areas and damage or wash away objects of variable size. Water overflows from small basins and watercourses.
c) *Fractures up to 5–10 cm wide and up to one hundred meters long are commonly observed, in loose alluvial deposits and/or saturated soils; rarely in dry sand, sand-clay, and clay soil, fractures up to 1 cm wide can occur. Centimeter-wide cracks are common in paved (asphalt or stone) roads.*

d) Scattered landslides occur in prone areas, where equilibrium is unstable (steep slopes of loose/saturated soils), while modest rock falls are common on steep gorges, cliffs). Their size is sometimes significant (10^3–10^5 m^3); in dry sand, sand-clay, and clay soil, the volumes are usually up to 100 m^3. Ruptures, slides and falls may affect riverbanks and artificial embankments and excavations (e.g. road cuts, quarries) in loose sediment or weathered/fractured rock. Significant underwater landslides can be triggered, provoking anomalous waves in coastal areas of sea and lakes, directly felt by people on boats and ports.
e) Trees and bushes shake vigorously; especially in densely forested areas, many limbs and tops break and fall.
f) *Rare cases are reported of liquefaction, with sand boils up to 50 cm in diameter, in areas most prone to this phenomenon (highly susceptible, recent, alluvial and coastal deposits, near surface water table).*

VIII Heavily damaging/Extensive effects in the environment

Primary effects: observed rarely.

Ground ruptures (surface faulting) may develop, up to several hundred meters long, with offsets not exceeding a few cm, particularly for very shallow focus earthquakes such as those common in volcanic areas. Tectonic subsidence or uplift of the ground surface with maximum values on the order of a few centimeters may occur.

Secondary effects: The total affected area is in the order of 100 km^2.

a) Springs may change, generally temporarily, their flow-rate and/or outcrop elevation. Some small springs may even run dry. Variations in water level are observed in wells. Weak variations of chemical-physical properties of water, most commonly temperature, may be observed in springs and/or wells. Water turbidity may appear in closed basins, rivers, wells and springs. Gas emissions, often sulphureous, are locally observed.
b) Anomalous waves up to 1–2 meters high flood near-shore areas and may damage or wash away objects of variable size. Erosion and dumping of waste is observed along the beaches, where some bushes and even small weak-rooted trees can be eradicated and drifted away. Water violently overflows from small basins and watercourses.
c) *Fractures up to 50 cm wide are and up to one hundred meters long are commonly observed in loose alluvial deposits and/or saturated soils; in rare cases fractures with widths up to 1 cm can be observed in competent dry rocks. Decimetric cracks common in paved (asphalt or stone) roads, as well as small pressure undulations.*
d) Small to moderate (103–105 m^3) landslides are widespread in prone areas; rarely they can also occur on gentle slopes; where equilibrium is unstable (steep slopes of loose/saturated soils; rock falls on steep gorges, coastal cliffs) their size is sometimes large (105–106 m^3). Landslides can occasionally dam narrow valleys causing temporary or even permanent lakes. Ruptures, slides and falls affect riverbanks and artificial embankments and excavations (e.g. road cuts, quarries) in loose sediment or weathered/fractured rock. Frequent occurrence of landslides under the sea level in coastal areas.
e) *Trees shake vigorously; branches may break and fall, even uprooted trees, especially along steep slopes.*
f) *Liquefaction may be frequent in the epicentral area, depending on local conditions; sand boils up to ca. 1 m in diameter; apparent water fountains in still waters; localized lateral spreading and settlements (subsidence up to ca. 30 cm), with fissuring parallel to waterfront areas (river banks, lakes, canals, seashores).*
g) *In dry areas, dust clouds may rise from the ground in the epicentral area.*

h) Stones and even small boulders and tree trunks may be thrown in the air, leaving typical imprints in soft soil.

IX Destructive/Effects in the environment are a widespread source of considerable hazard and become important for intensity assessment

Primary effects: observed commonly.

Ground ruptures (surface faulting) develop, up to a few km in length, with offsets generally in the order of several cm. Tectonic subsidence or uplift of the ground surface with maximum values in the order of a few decimeters may occur.

Secondary effects: *The total affected area is in the order of 1000 km^2.*

a) Springs can change, generally temporarily, their flow-rate and/or location to a considerable extent. Some modest springs may even run dry. Temporary variations of water level are commonly observed in wells. Water temperature often changes in springs and/or wells. Variations of chemical-physical properties of water, most commonly temperature, are observed in springs and/or wells. Water turbidity is common in closed basins, rivers, wells and springs. Gas emissions, often sulphureous, are observed, and bushes and grass near emission zones may burn.

b) Meter high waves develop in still and running waters. In flood plains water streams may even change their course, also because of land subsidence. Small basins may appear or be emptied. Depending on shape of sea bottom and coastline, dangerous tsunamis may reach the shores with run-ups of up to several meters flooding wide areas. Widespread erosion and dumping of waste is observed along the beaches, where bushes and trees can be eradicated and drift away.

c) Fractures up to 100 cm wide and up to hundreds of meters long are commonly observed in loose alluvial deposits and/or saturated soils; in competent rocks they can reach up to 10 cm in width. Significant cracks common in paved (asphalt or stone) roads, as well as small pressure undulations.

d) Landsliding is widespread in prone areas, also on gentle slopes; where equilibrium is unstable (steep slopes of loose/saturated soils; rock falls on steep gorges, coastal cliffs) their size is frequently large (105 m^3), sometimes very large (10^6 m^3). Landslides can dam narrow valleys causing temporary or even permanent lakes. Riverbanks, artificial embankments and excavations (e.g. road cuts, quarries) frequently collapse. Frequent large landslides under the sea level in coastal areas.

e) Trees shake vigorously; branches and thin tree trunks frequently break and fall. Some trees might be uprooted and fall, especially along steep slopes.

f) Liquefaction and water upsurge are frequent; sand boils up to 3 m in diameter; apparent water fountains in still waters; frequent lateral spreading and settlements (subsidence of more than ca. 30 cm), with fissuring parallel to waterfront areas (river banks, lakes, canals, seashores).

g) In dry areas, dust clouds commonly rise from the ground.

h) Small boulders and tree trunks may be thrown in the air and move away from their site for meters, also depending on slope angle and roundness, leaving typical imprints in soft soil.

X Very destructive/Effects on the environment become a leading source of hazard and are critical for intensity assessment

Primary effects: become leading.

Surface faulting can extend for few tens of km, with offsets from tens of cm up to a few meters. Gravity grabens and elongated depressions develop; for very shallow focus earthquakes in

volcanic areas rupture lengths might be much lower. Tectonic subsidence or uplift of the ground surface with maximum values in the order of few meters may occur.

Secondary effects: *The total affected area is in the order of 5000 km^2.*

a) Many springs significantly change their flow-rate and/or outcrop elevation. Some springs may run temporarily or even permanently dry. Temporary variations of water level are commonly observed in wells. Even strong variations of chemical-physical properties of water, most commonly temperature, are observed in springs and/or wells. Often water becomes very muddy in even large basins, rivers, wells and springs. Gas emissions, often sulphureous, are observed, and bushes and grass near emission zones may burn.
b) *Several-meter high waves develop, even in big lakes and rivers, which overflow their banks. In flood plains rivers may also change their course, temporary or even permanently, because of widespread land subsidence. Basins may appear or be emptied. Depending on shape of sea bottom and coastline, tsunamis may reach the shores with run-ups exceeding 5 m flooding flat areas for thousands of meters inland. Small boulders can be dragged for many meters. Widespread deep erosion is observed along the shores, with noteworthy changes of the coastline profile. Near-shore trees are eradicated and drift away.*
c) *Open ground cracks up to and over 1 m wide and up to hundreds of meters long are frequent, mainly in loose alluvial deposits and/or saturated soils; in competent rocks widths reach several decimeters. Wide cracks develop in paved (asphalt or stone) roads, as well as pressure undulations.*
d) *Large landslides and rock-falls (> 10^5–10^6 m^3) are frequent, practically regardless of the slopes' equilibrium state, causing temporary or permanent barrier lakes. River banks, artificial embankments, and sides of excavations typically collapse. Levees and earth dams may even incur serious damage. Frequent large landslides under the sea level in coastal areas.*
e) *Trees shake vigorously; many branches and tree trunks break and fall. Some trees might be uprooted and fall.*
f) *Liquefaction, with water upsurge and soil compaction, may change the aspect of wide zones; sand volcanoes with more than 6 m in diameter; vertical subsidence > 1m; large and long fissures due to lateral spreading are common.*
g) *In dry areas, dust clouds may rise from the ground.*
h) *Boulders (diameter in excess of 2–3 meters) can be thrown in the air and move away from their site for hundreds of meters down even gentle slopes, leaving typical imprints in soil.*

XI Devastating/Effects on the environment become decisive for intensity assessment, due to saturation of structural damage

Primary effects: are dominant

Surface faulting extends from several tens of km up to more than one hundred km, accompanied by offsets reaching several meters. Gravity graben, elongated depressions and pressure ridges develop. Drainage lines can be seriously offset. Tectonic subsidence or uplift of the ground surface with maximum values in the order of numerous meters may occur.

Secondary effects: *The total affected area is in the order of 10,000 km^2.*

a) Many springs significantly change their flow-rate and/or outcrop elevation. Many springs may run temporarily or even permanently dry. Temporary or permanent variations of water level are generally observed in wells. Even strong variations of chemical-physical properties of water, most commonly temperature, are observed in springs and/or wells. Often water becomes very muddy in even large basins, rivers, wells and springs. Gas

emissions, often sulphureous, are observed, and bushes and grass near emission zones may burn.

b) *Large waves develop in big lakes and rivers, which overflow their banks. In flood plains rivers can change their course, temporary or even permanently, also because of widespread land subsidence and landsliding. Basins may appear or be emptied. Depending on shape of sea bottom and coastline, tsunamis may reach the shores with run-ups reaching 15 meters and more devastating flat areas for kilometers inland. Even meter-sized boulders can be dragged for long distances. Widespread deep erosion is observed along the shores, with noteworthy changes of the coastal morphology. Near-shore trees are eradicated and drift away.*

c) Open ground cracks up to several meters wide are very frequent, mainly in loose alluvial deposits and/or saturated soils. In competent rocks they can reach 1 m. Very wide cracks develop in paved (asphalt or stone) roads, as well as large pressure undulations.

d) *Large landslides and rock-falls (> 10^5–10^6 m^3) are frequent, practically regardless of the slopes' equilibrium state, causing many temporary or permanent barrier lakes. River banks, artificial embankments, and sides of excavations typically collapse. Levees and earth dams incur serious damage. Significant landslides can occur at 200 – 300 km distance from the epicenter. Frequent large landslides under the sea level in coastal areas.*

e) *Trees shake vigorously; many branches and tree trunks break and fall. Many trees are uprooted and fall.*

f) *Liquefaction changes the aspect of extensive zones of lowland, determining vertical subsidence possibly exceeding several meters, numerous large sand volcanoes, and severe lateral spreading features.*

g) In dry areas dust clouds arise from the ground.

h) Big boulders (diameter of several meters) can be thrown in the air and move away from their site for long distances down even gentle slopes, leaving typical imprints in soil.

XII Completely devastating/Effects in the environment are the only tool for intensity assessment

Primary effects: are dominant.

Surface faulting is at least several hundred km long, accompanied by offsets reaching several tens of meters. Gravity graben, elongated depressions and pressure ridges develop. Drainage lines can be seriously offset. Landscape and geomorphic changes induced by primary effects can attain extraordinary extent and size (typical examples are the uplift or subsidence of coastlines by several meters, appearance or disappearance from sight of significant landscape elements, rivers changing course, origination of waterfalls, formation or disappearance of lakes).

Secondary effects: *The total affected area is in the order of 50,000 km^2 or more.*

a) Many springs significantly change their flow-rate and/or outcrop elevation. Temporary or permanent variations of water level are generally observed in wells. Many springs and wells may run temporarily or even permanently dry. Strong variations of chemical-physical properties of water, most commonly temperature, are observed in springs and/or wells. Water becomes very muddy in even large basins, rivers, wells and springs. Gas emissions, often sulphureous, are observed, and bushes and grass near emission zones may burn.

b) *Giant waves develop in lakes and rivers, which overflow their banks. In flood plains rivers change their course and even their flow direction, temporary or even permanently, because of widespread land subsidence and landsliding. Large basins may appear or be emptied. Depending on shape of sea bottom and coastline, tsunamis may reach the shores*

with run-ups of several tens of meters devastating flat areas for many kilometers inland. Big boulders can be dragged for long distances. Widespread deep erosion is observed along the shores, with outstanding changes of the coastal morphology. Many trees are eradicated and drifted away. All boats are tore from their moorings and swept away or carried onshore even for long distances. All people outdoors are swept away.

c) Ground open cracks are very frequent, up to one meter or more in width within bedrock, up to more than 10 m wide in loose alluvial deposits and/or saturated soils. These may extend up to several kilometers in length.

d) *Large landslides and rock-falls (> 10^5–10^6 m^3) are frequent, practically regardless of the slopes' equilibrium state, causing many temporary or permanent barrier lakes. River banks, artificial embankments, and sides of excavations typically collapse. Levees and earth dams incur serious damage. Significant landslides can occur at more than 200 – 300 km distance from the epicenter. Frequent very large landslides occur on the sea bed in coastal areas*

e) Trees shake vigorously; many branches and tree trunks break and fall. Many trees are uprooted and fall.

f) *Liquefaction occurs over large areas and changes the morphology of extensive flat zones, determining vertical subsidence exceeding several meters, widespread large sand volcanoes, and extensive severe lateral spreading features.*

g) In dry areas dust clouds arise from the ground.

h) Also very big boulders can be thrown in the air and move for long distances even down very gentle slopes, leaving typical imprints in soil.

DEFINITIONS

(in this publication)

Active fault
A tectonic structure that moved in the recent geologic past and that is expected to move within a future time span of concern for the safety of a nuclear installation. In highly active (e.g. *interplate*) areas with short earthquake recurrence intervals, periods of the order of tens of thousands of years (e.g. Upper *Pleistocene* to present) may be appropriate for defining a fault as active. In less active areas (e.g. *intraplate*) much longer periods (e.g. *Pliocene – Quaternary* to present) may be appropriate. In the conservative perspective of NPP siting, any fault within the Earth's crust might need to be reassessed for potential re-activation. In fact, it is impossible to exclude that an earthquake of low magnitude may occur along any fault (Modified from IAEA SSG-9 [1], 8.4).

Age dating
Assessment of the age of a sediment using biostratigraphic, physical or chemical age dating techniques.

Age dating, cosmogenic
Physical age dating technique based on the production of certain isotopes due to the exposure of rock to cosmogenic radiation; dating the time of the exposure of the rock surface to radiation.

Age dating, geochronologic
Physical age dating of mineral or rock samples using the decay rate of unstable isotopes that are measured by mass spectrometry.

Age dating, lichometric
Age dating technique based on the growth of lichens on fresh-broken rock surfaces or bedrock fault scarps dating the time of the exposure of the rock surface by applying (usually) known lichen growth rates in the studied zone (upper age limit usually does not reach a thousand years).

Age dating, luminescence
Age dating technique based in the background ionizing radiation absorbed by quartz or feldspar particles of detritic sediments exposed to sunlight before burial. The luminescence signal increases with burial time and date the last exposure of the sediment to the sunlight (see OSL).

Age dating, radiocarbon
Physical age dating of organic material using ^{14}C carbon isotope ratios (upper age limit c. 60 thousand years).

Aleatory uncertainty
Uncertainty inherent in a phenomenon. Aleatory uncertainty is taken into account by representing the phenomenon in terms of a probability distribution model (IAEA SSG-9 [1]).

Alluvium
Loose, unconsolidated (not cemented together into a solid rock) sediments, which have been eroded, reshaped by water in some form, and re-deposited in a non-marine setting. The term

should not be used in situations where the formation of the sediment can clearly be attributed to a geologic process, e.g. for lake sediments (lacustrine), river sediments (fluvial), or glacially-derived sediments (glacial till).

Archeoseismology
The study of earthquake effects displayed in archeological remains/sites or historical buildings. Archeoseismology mostly reveals evidence of unknown ancient earthquakes or helps to refine the data of known historical events. Additional evidence is necessary, but extracted data may be classified in terms of intensity.

Arias intensity
Measure of the strength of a ground motion determining the intensity of shaking by measuring the acceleration of transient seismic waves. The Arias intensity is used to describe earthquake shaking necessary to trigger landslides or mass movements.

Attenuation
Diminution of the energy with which an earthquake affects a location depending on the distance between the *hypocenter* and the site of interest.

Blind fault
Buried *fault* not reaching up to the ground surface when it was last active. Usually applied to buried reverse or thrust faults.

Capable fault
An *active fault* that has a significant potential for displacement at or near the ground surface (IAEA SSG-9 [1]).

Colluvium
A general name for loose, unconsolidated sediments that have been deposited at the base of hillslopes or scarps by either rainwash, sheetwash, slow continuous downslope creep, unconcentrated surface runoff, or a variable combination of these processes.

Colluvial wedge
Colluvium that has been deposited at the base of a *single-event fault scarp* after a surface-breaking earthquake. The colluvial wedge results from the re-deposition of sediment during the erosive degradation of the scarp. Besides pure 'colluvium' deposits, it also can include gravity-driven deposits that collapsed from the free-face at toe of the scarp.

Composite fault scarp
Fault scarp formed a succession of several surface-breaking earthquakes.

Coseismic
An event that occurs contemporaneously with an earthquake (e.g. fault surface rupture/displacement). Primary and secondary earthquake environmental effects considered in the ESI-07 scale.

Creep
Steady and rather continuous deformation that do not produce (significant) earthquakes. 'Creeping' is thus usually used as a synonymous for aseismic behavior.

Deformation rate
Average velocity of the tectonic deformation of a geologic material (see stress rate).

Dendrochronology
Age dating of wood using tree ring growth patterns (upper age limit usually several hundreds of years).

Diffuse seismicity
Areas where *seismogenic structures* cannot be clearly identified because their geomorphic and/or structural evidence are absent and the correlation between seismicity and the causative structures is difficult or impossible.

Earthquake environmental effects (EEE)
Effects in the natural environment produced during an earthquake affecting the ground surface, subsurface, slopes, water bodies and vegetation. They are classified as primary effects (on-fault effects; fault surface rupture or surface uplift) and secondary effects (off-fault effects; e.g. liquefaction, slope movements, tsunamis, etc.). During past earthquakes EEE can be incorporated in the geologic record, being subject of paleoseismic evidence and paleoseismic research.

Earthquake effects, Primary
The surface expression of seismogenic tectonic source (including surface faulting, surface uplift and subsidence). Primary effects gave place to characteristic tectonic landforms (*e.g. fault scarps, pressure ridges*) and eventually, particular landform assemblages of seismic origin (*i.e. seismic landscapes*).

Earthquake effects, Secondary
Phenomena generally induced by seismic ground shaking, including e.g. liquefaction, mass movements and tsunamis. (See *earthquake environmental effects*). Exclude coseismic displacement on the earthquake source (main/primary) fault and on the structurally associated secondary structures.

Environmental Seismic Intensity Scale (ESI)
Intensity scale aimed at evaluating the severity of an earthquake based only on the characteristics and size of Earthquake Environmental Effects (EEE). Its use, alone or integrated with the macroseismic damage-based scales, allows a more complete estimate of intensity and, therefore, a better comparison among earthquakes both in time and in space.

Epicentral intensity (I_0)
Intensity of an earthquake at its *epicenter* (usually equal to the maximum intensity).

Epicenter
The point on the Earth's surface directly above the focus (i.e. *hypocenter*) of an earthquake (IAEA SSG-9 [1]).

Epistemic uncertainty
Uncertainty attributable to incomplete knowledge about a phenomenon, which affects the ability to model it. Epistemic uncertainty is reflected in a range of viable models, multiple expert interpretations and statistical confidence (IAEA SSG-9 [1]).

Fault
A planar or gently curved fracture surface or zone of the Earth across which there has been relative displacement (IAEA SSG-9 [1]).

Fault scarp
A linear or gently curved morphologic slope formed by the displacement of the ground surface by a *capable fault*. The morphology of the scarp is different for normal, reverse and strike-slip faults; and it changes (slope decrease) with time due to the acting erosive/sedimentary processes.

Fault segment
Part of a geologic *fault* that is bound by either a lithological, structural or geometrical discontinuity (e.g. fault bend, stepover or branch) or a combination of these. These bounds can act as barriers or initiation points for earthquakes [25]. The term 'segment' is thus often used by earthquake geologists as a fault portion that ruptured during a single earthquake (earthquake segment).

Flowstone
Mineral deposits that have accumulated on the floor or wall of caves.

Geomorphology
The scientific study of the landforms and related deposits that are assembled in the present landscape. It also includes the study of the operating geologic processes (e.g. surface, volcanic or tectonic processes) to decode the evolution of the Earth surface through time.

Georadar
Geophysical method providing images of the sub-surface derived from the reflection of electromagnetic waves. Reflections are produced by layers of different conductivity. Detailed investigation depths reach up to c. 10–15 m depending on electromagnetic wavelength used.

Glaciotectonism
Processes that deform unconsolidated material in relation to glacier displacements. Can produce deformation forms similar to those generated by compressional tectonics, such as reverse faults, thrusts and folds.

Ground crack (Coseismic)
Fissures, fractures or cracks formed in the ground surface during an earthquake, which are not directly related to the surface rupture of a *capable fault*. Secondary earthquake effect considered in the ESI-07 Scale.

Ground Penetrating Radar (GPR)
see *Georadar*

Hyperpycnal flow
Produced when the density of the river water entering the basin is greater than the density of the standing water in the ocean basin (or in a lake). This higher density river water will flow below the standing water in the basin because of the difference in density. A zone of mixing occurs along the outer edge of the flow. As the river water flows beneath the standing water, it erodes the previously deposited bottom sediments. Further out in the basin, the flow eventually deposits the eroded sediments as turbidites.

Holocene
Geologic epoch within the Quaternary Period which began at the end of the *Pleistocene,* after the deglaciation (around 11,700 years ago), and continues to the present [1]. Also known as 'the Present Interglacial Period'.

Hypocentre
The point (focus) within the Earth at which an earthquake is initiated (IAEA SSG-9 [1]).

Intensity
Classification of the severity of the ground shaking on the basis of observed effects in a limited area. Intensity scales quantify the effects of an earthquake on the Earth's surface, humans, objects of nature, and man-made structures in a descriptive way.

Interplate
Concerning tectonic processes at the boundaries between the lithospheric tectonic plates (IAEA SSG-9 [1]).

Interplate setting
A geologic area located at or close to a plate boundary characterized by moderate to high *deformation rates* and moderate to high seismicity. Interplate settings may include broad deformation zones such as subduction zones, orogenic belts or rifts, as well as narrow fault zones.

Intraplate
Concerning tectonic processes within the Earth's tectonic plates (IAEA SSG-9 [1]).

Intraplate setting
A geologic area located in the interior of a lithospheric plate usually characterized by low to moderate *deformation rates* and low to moderate seismicity.

Landslide
A general term covering a wide variety of mass-movement landforms and processes involving the downslope transport, under gravitational influence, of soil and rock material. Can be triggered by earthquakes or other processes.

Lateral spreading
Liquefaction induced down-slope movement of sediments that frequently lead to foundation failure. Commonly occurs at river and lake banks and magnified by seismic shaking. Common earthquake environmental effect from ESI intensity VII–VIII.

LIDAR (Light Detection and Ranging)
A remote sensing technology that measures distance by illuminating a target with a laser and analyzing the reflected light. Airborne LIDAR is a technology frequently used to make high resolution digital elevation models.

Lineament
Any linear feature on the Earth's surface shown by remote sensing data, aerial photographs, digital elevation models, or geophysical data. Lineaments may have any origin and are not necessarily tectonic.

Liquefaction
Extreme reduction of shear strength of soil and unconsolidated fine-grained sediments by the expulsion of pore water due to seismic shaking. Liquefaction can lead to water escape and fluidization of the sediment (suspended particles in water flow), generating sedimentary structures characteristic of seepage (e.g. sand boils and sand-filled dykes) that may be identified by paleoseismic techniques. Common earthquake environmental effect from ESI intensity VII–VIII, but depending of the geologic environment might occur from intensity V.

Local intensity (I)
Intensity of an earthquake at a specific site.

M_0
Seismic moment:

$$M_0 = \mu A d \tag{3}$$

where, μ: rock rigidity in dynes/cm²; A: area of fault movement (cm²); d: displacement (cm).

Used to calculate the 'M_w: moment magnitude', which is the common scale to appreciate the energy released during an earthquake.

Magnitude
Measure of the size of an earthquake relating to the energy released in the form of seismic waves. Seismic magnitude means the numerical value on a standardized scale such as, but not limited to, moment magnitude (M_w), surface wave magnitude (M_s), body wave magnitude (*mB* or *mb*), local magnitude (M_L), or duration magnitude (IAEA SSG-9 [1]). Magnitude is measured on a logarithmic scale as introduced by Richter [450]. Magnitude definitions use amplitudes of different wave types at different frequency ranges on different components from seismograms recorded at different stations, applying different calibration functions leading to the co-existence of numerous magnitude definitions.

Mass movement, coherent (C-type)
Large slope movements such as complex composite landslides. These are often, but not always, seismically induced from ESI intensity VII–VII, and therefore subject of paleoseismic research in tectonically active areas. Earthquake environmental effect considered in the ESI-07 scale.

Mass movement, disrupted (D-type)
Slope movements such as rock falls and rock/earth avalanches which generate a disorganized mass of mobilized material. These are frequently seismically induced from ESI intensity VI (less than C-type).

Maximum Credible Earthquake (MCE)
Estimate of the potential maximum size of an expected earthquake derived from historical, paleoseismic, seismic or other geologic data/information.
According to the US NRC [3]: The term 'maximum credible earthquake' means that earthquake which would cause the maximum vibratory ground motion based upon an evaluation of earthquake potential considering the regional and local geology and seismology and specific characteristics of local subsurface material.

Maximum potential magnitude
Reference value used in seismic hazard analysis characterizing the potential of a *seismic source* to generate earthquakes. The way in which it is calculated depends on the type of *seismic source* considered and the approach to be used in the seismic hazard analysis (IAEA SSG-9 [1]).

m_B,
Medium period body wave *magnitude* (Gutenberg, 1945).

m_b;
Body wave *magnitude* (S-wave). Maximum body wave amplitudes are used for intermediate and deep earthquakes.

$$m_b = \log_{10}\frac{A}{T} + Q(D,h) \tag{4}$$

Where, *A*: maximum ground amplitude in micrometers; *T*: period in second; *Q*: dept *h* (km) hand distance *D* (degree) factor.

M_L
Local *magnitude* (Richter, 1935) based on the measurement of the maximum amplitude of a Wood-Anderson seismograph.

M_s
Surface wave *magnitude* derived from the maximum amplitude of surface waves with a period of 20 s (for periods between 18 and 22 s). Used for shallow earthquakes at the distance range 20–160°.

$$M_s = \log_{10}\frac{A}{T} + 1.66\log_{10}D + 3.3 \tag{5}$$

Where, *A*: maximum ground amplitude in micrometers; *T*: period in second, and *D*: distance in degree.

M_w
Moment *magnitude*. M_w is based on the seismic moment M_0, which is proportional to the fault area that moved during an earthquake and the average displacement along the fault during the event. M_w therefore can be estimated by paleoseismic methods that quantify the size and displacement along a fault during a single earthquake.

Optically stimulated luminescence (OSL)
A physical age dating technique of quartz or feldspar grains dating the time when a grain was exposed to light prior to its burial in the sediment (upper age limit c. 150 to 300 thousand years depending on material and methodology).

Paleoliquefaction features
Liquefaction structures identified in the sedimentary record of alluvial or coastal plains (usually) that serve as indication of past strong seismic shaking if there is 'near-regional' or 'site vicinity' evidence of widespread and continuous liquefied horizons over these areas.

Paleoseismology
The study of evidence of past (typically prehistoric) earthquakes manifested as displacement on a *fault* or secondary effects such as ground deformation (i.e. liquefaction, tsunami, landslides) with geologic techniques, providing data on the timing, location, and size of these earthquakes (modified from IAEA SSG-9 [1]).

Paleosoil
A former soil preserved in the geologic record. This may be a relict soil on the surface (i.e. terrace surface) or a fossil soil buried underneath younger sediments (e.g. *alluvium, colluvium, loess*). Paleosols are one of the few unequivocal geologic evidence of an ancient ground surface and therefore valuable key-horizons in paleoseismic research.

Peak Ground Acceleration (PGA)
The maximum absolute value of ground acceleration displayed on an accelerogram; the greatest ground acceleration produced by an earthquake at a site (IAEA SSG-9 [1]).

PFDHA
Probabilistic Fault Displacement Hazard Analysis. A method that aims at assessing the probability of exceedance of a displacement value at the ground surface, both on the earthquake source (capable fault) of interest and off this main structure (distributed faulting). This method follows the same formulation as the Probabilistic Seismic Hazard Analysis used for ground shaking and also uses (fault displacement) attenuation empirical relations.

Pleistocene
First geologic epoch of the Quaternary Period. It began at the end of the *Pliocene* (around 2.588 million years ago) and continues to the *Holocene* (until 11,700 years ago) [1]. Much of the Pleistocene is commonly characterized by alternating glacial and interglacial periods.

Pliocene
Last geologic epoch of the Neogene period. The Pliocene began around 5.333 million years ago and continues to the *Pleistocene* epoch (until 2.588 million years ago).

Precariously (balanced) rocks
Large rock or boulder, sometimes of substantial size laying in equilibrium. The instability of these features is used to estimate the minimum seismic ground acceleration that may trigger their failure/falling.

Quaternary
Last period of the geological time-scale (from around 2.588 million years ago to present). It is subdivided in the *Pleistocene* and *Holocene epochs* and preceded by the Neogene Period.

Response spectrum
A curve calculated from an accelerogram that gives the value of peak response in terms of the acceleration, velocity or displacement of a damped single-degree-of-freedom linear oscillator (with a given damping ratio) as a function of its natural frequency or period of vibration (IAEA SSG-9 [1]).

Rheology
Physical laws that characterize the flow of materials, which exhibits a combination of elastic, viscous and plastic behavior. The laws usually provide a relation between material deformation (strain) to stress.

Rupture area
Area of a *fault-plane* that ruptures during a single earthquake.

Rupture length
Length of a *fault* that ruptured during a single earthquake measured along fault strike.

Sand boil
Sand extruded from the ground surface during seismic shaking caused by fluid overpressure and subsurface liquefaction. Also known as *sand blows* or *sand volcanos*. Earthquake environmental effect included in the ESI-07 scale, normally produced from intensity V-VI, but widespread from intensity VII-VIII where favorable geologic conditions exits.

Seismicity, historical
Intensity-based information on past earthquakes. For historical events earthquake *magnitude* is estimated from the *intensity* data usually applying empirical correlations. Historical catalogs typically contain data on the last centuries (2 to 10, depending on the region).

Seismicity, instrumental
Instrumental information on current earthquakes, providing direct data on the earthquake *magnitude*. Instrumental catalogs typically contain data on the last decades.

Seismic moment
See M_0

Seismite
Sedimentary beds disturbed by seismic shaking. The term describes both sedimentary beds deformed by seismic shaking and associated soft sediment deformation structures formed by shaking that may or may not remain confined to a stratigraphic layer (i.e. clastic dikes or sand volcanos).

Seismogenic structure
A structure that displays earthquake activity or that manifests historical surface rupture or the effects of paleoseismicity, and that is considered likely to generate macro-earthquakes within a time period of concern (IAEA SSG-9 [1]).

Seismotectonic model
The model that defines the characterization of seismic sources in the region around a site of interest, including the aleatory and epistemic uncertainties in the seismic source characteristics (IAEA SSG-9) [1].

Seismoturbidite
Earthquake-triggered sub-aquatic turbidite (dense and suspended flow) which might be preserved in the sedimentary record of lakes and offshore littoral zones.

Single-event fault scarp
Fault scarp formed by a single surface-breaking earthquake.

Sinter
Rock deposit formed by precipitation from natural water.

Site response
The behavior of a rock or soil column at a site under a prescribed ground motion load (IAEA SSG-9) [1].

Slip-rate
Average displacement velocity of a *fault* or other tectonic structure *(i.e. fold)* over a defined interval of time.

Soft-sediment deformation features
General term describing small-scale plastic deformations (e.g. convolute bedding) of muddy or other cohesionless sediments. Their formation does not require liquefaction and they can form under static (gravity) conditions or other non-seismic processes (under rapid sedimentation, hydrologic forcing, wave propagation).
Their utility in seismic hazard assessment may be more limited than liquefaction features [155].

Speleo-seismite
Cave sedimentary deposit (including *speleothems*) that record earthquake effects.

Speleoseismology
The detection and analysis of earthquake effects in caves from speleo-seismite evidence. Speleologic methods and techniques are usually required.

Speleothem
General term for all cave mineral deposits formed by progressive precipitation of carbonate, including *stalagmites*, *stalactites*, *flowstones,* etc.

Stalactite
Speleothem hanging from a cave roof.

Stalagmite
Speleothem growing upwards from the bottom of a cave.

Strain
Deformation of a geologic material (rock).

Strain rate
see *deformation rate*

Surface rupture
Permanent offsetting or tearing of the ground surface by differential movement across a *capable fault* (based on IAEA SSG-9 [1]). Can be seismic (i.e. during an earthquake) as well as aseismic (i.e. creeping). Primary earthquake environmental effect considered in the ESI-07 scale, starting from the VII–IX intensity degree.

Taphonomy
The study of burial and fossilization of organisms or sediments deposited on the Earth's surface.

Tectonic geomorphology
(1) The study of the interplay between tectonic and surface processes that shape the landscape in regions of active deformation. (2) Application of geomorphic principles to evaluate the

occurrence, patterns of rates of tectonics process. Especially useful in diffuse seismicity areas where other direct paleoseismic methods cannot be applied.

Tectonic landform
Geomorphic feature created by activity of faults or folds, normally affecting to Holocene or Pleistocene alluvial materials (e.g. a fault scarp, shutter ridge).

Tectonic relief
Geomorphic feature formed by tectonics. Mainly applied to rock-reliefs affecting pre-Quaternary materials.

Terrace
Inactive flat surface topping alluvial or coastal sediments, typically near an active stream (aggradation fluvial terrace) or coastline (aggradation marine terrace). A terrace can also be generated by direct river/littoral abrasion of the bedrock (strath or erosive terraces).

Thermo luminescence dating
Determination, by means of measuring the accumulated radiation dose, of the time elapsed since material containing crystalline minerals was either heated (e.g. lava, ceramics) or exposed to sunlight (*see luminescence dating or OSL*).

Trenching, paleoseismic
Geologic assessment of a *capable fault* using a man-made exposure (trench) across the fault.

Tsunami
A series of water waves caused by the displacement of a large volume/body of water, generally in oceans or large lakes by earthquakes, volcanic eruptions, landslides, glacier calvings, meteorite impacts and other disturbances above or below water. Hazardous tsunamis of tectonic origin are usually generated at subduction zones in interplate settings. Tsunamis are one of the relevant earthquake environmental effects considered in the ESI-07 scale.

Tsunami Deposit
Sediment deposited by a *tsunami*. Tsunami deposits are also known as tsunamites or tsunamiites. The areal extent and inland penetration of tsunami deposits provide evidence for the tsunami hazard. Tsunami deposits can be preserved in the sedimentary record of coastal areas (e.g. coastal plains, lagoons, estuaries) evidencing the tsunami history of that area.

Turbidites
Sediments which are transported and deposited by sediment density flow. Seismoturbidites are turbidites triggered by earthquake processes.

REFERENCES

[1] IAEA, Seismic Hazards in Site Evaluation for Nuclear Installations, IAEA Safety Standards Series No. SSG-9, IAEA, Vienna (2010).

[2] McCalpin, J.P., Paleoseismology, Elsevier, 2nd edition (2009) 613.

[3] NATIONAL RESEARCH COUNCIL, Living on an Active Earth: Perspectives on Earthquake Science, National Research Council, Board on Earth Sciences and Resources, Washington, DC (2003) 418.

[4] WALLACE, R.E., Ed., 'Impacts on society', Active Tectonics, National Academy Press, Washington, D.C. (1986) 266.

[5] VITTORI, E., SYLOS-LABINI, S., SERVA, L., Paleoseismology: review of the state of the art, Tectonophysics **193** (1991) 9–32.

[6] MICHETTI, A.M., HANCOCK, P.L., Paleoseismology: Understanding past earthquakes using Quaternary geology, Journal of Geodynamics **24** 4 (1997) 3–10.

[7] YEATS, R.S., Active faults of the World, Cambridge University Press (2012) 621.

[8] WALLACE, R.E., 'Fault scarps formed during the earthquake of October 2, 1915, in Pleasant Valley, Nevada, and some tectonic implication', Faulting Related to the 1915 Earthquakes in Pleasant Valley, Nevada, U.S. Geological Survey Prof. Paper **1274–A** (1984) 1–33.

[9] GUPTA, S., COWIE, P.A., DAWERS, N.H., UNDERHILL, J.R.U., A mechanism to explain rift-basin subsidence and stratigraphic patterns through fault array evolution, Geology **26** (1998) 595–598.

[10] AUDEMARD, F.A., 'Morpho-structural expression of active thrust fault systems in the humid tropical foothills of Colombia and Venezuela', Proc. Fourth Int. Conf. Geomorphology, Bologna 1997, Frisch, W., ed., Z. Geomorph. N.F. **118** (1999) 1–18.

[11] SERVA, L., BLUMETTI, A.M., GUERRIERI, L., MICHETTI, A.M., The Apennine intermountain basins: the result of repeated strong earthquakes over a geological time interval, Boll. Soc. Geol. It. **121** (2002) 939–946.

[12] ROBERTS, G.P., MICHETTI, A. M., Spatial and temporal variations in growth rates along active normal fault systems: an example from the Lazio-Abruzzo Apennines, central Italy, Journal of Structural Geology **26** (2004) 339–376.

[13] WESNOUSKY, S.G., BORMANN, J.M., KREEMER, C., HAMMOND, W.C., BRUNE, J.N., Neotectonics, geodesy, and seismic hazard in the Northern Walker Lane of Western North America: Thirty kilometers of crustal shear and no strike-slip?, Earth and Planetary Science Letters **329** (2012) 133–140.

[14] COWIE, P.A., SCHOLZ, C.H., ROBERTS, G.P., WALKER, J.F. STEER, P., Viscous roots of active seismogenic faults revealed by geologic slip rate variations, Nature Geoscience **6** (2013) 1036–1040, published online Nov. 3, 2013.

[15] DE POLO, C.M., C1ARK, D.G., SLEMMONS, D.B., RAMELLI, A.R., Historical surface faulting in the Basin and Range Province, Western North America: implications for fault segmentation, J. Struct. Geol. **13** (1991) 123–136.

[16] SILVA, P.G., et al., Archeoseismic record at the ancient Roman city of Baelo Claudia (Càdiz, South Spain), Tectonophysics **408** 4 (2005).

[17] SILVA, P. G., et al., Catalogacion de los efectos geologicos y ambientales de los terremotos en Espana en la Escala ESI 2007 y su aplicacion a los estudios paleosismologicos, Geotemas **6** (2008) 1063–1066.

[18] GRUETZNER, J., UENZELMANN-NEBEN, G., FRANKE, D., Seismic reflection imaging of a canyon system at the Argentine continental margin to identify changes in sediment transport und ocean circulation, EGU General Assembly, Vienna (2012).

[19] AUDEMARD, F.A., 'objectives, methods, applications, limitations and perspectives', Paleoseismology in Venezuela, Tectonophysics **408** 4 (2005) 29–61.

[20] CUSHING, M., et al., 'Paleo-earthquakes investigations in the Upper Rhine Graben in the framework of the PALEOSIS project', Workshop Proceedings: HAN2000-Evaluation of the Potential for Large Earthquakes in Regions of Present Day Low Seismic Activity in Europe, Han-sur-Lesse, Belgium (2000) 39–43.
[21] JONGMANS, D., TEERLYNCK, H., RENARDY, F., 'The use of geophysical prospecting for paleoseismology in the Rhine graben: potentiality and perspectives', Evaluation of the potential for large earthquakes in regions of present day low seismic activity in Europe (Workshop proceedings, HAN2000), Han-sur-Lesse, Belgium (2000) 83–88.
[22] MEGHRAOUI, M., CAMELBEECK, T., VANNESTE, K., BORNDEEL, M., JONGMANS, D., Active faulting and paleoseismology along the Bree fault, lower Rhine graben, Belgium, J. Geophys. Res. **105** B6 (2000) 13809–13841.
[23] NELSON, A.R., et al., Late Holocene earthquakes on the Toe Jam Hill fault, Seattle fault zone, Bainbridge Island, Washington, Geol. Soc. Am. Bull. **115** (2003) 1388–1403.
[24] GRANT, L.B., 'Paleoseismology', International Handbook of Earthquake and Engineering Seismology, LEE, W.H.K., KANAMORI, H., JENNINGS, P.C., KISSLINGER, C. Eds., IASPEI, Elsevier **81A** (2002) 475–490.
[25] YEATS, R.S., SIEH, K.E., ALLEN, C.R., GEIST, E.L., The Geology of Earthquakes, Oxford university press, New York **568** (1997).
[26] MICHETTI, A.M., BRUNAMONTE, F., SERVA, L., VITTORI, E., Trench investigations of the 1915 Fucino earthquake fault scarps (Abruzzo, Central Italy): geological evidence of large historical events, J. Geophys. Res. **101** B3 (1996) 5921–5936.
[27] MICHETTI, A.M., AUDEMARD, F.A.M., MARCO, S., Future trends in paleoseismology: Integrated study of the seismic landscape as a vital tool in seismic hazard analyses, Tectonophysics **408** 4 (2005) 3–21.
[28] MOHAMMADIOUN, B., SERVA, L., Stress Drop, Slip Type, Earthquake Magnitude and Seismic Hazard, Bull. Seism. Soc. Am. **91** 4 (2001) 694–707.
[29] SCHOLZ, C.H., The Mechanics of Earthquakes and Faulting, 2nd ed. Cambridge Univ. Press (2002) 471.
[30] TUTTLE, M.P., Late Holocene Earthquakes and Their Implications for Earthquake Potential of the New Madrid Seismic Zone, Central United States, Ph.D. dissertation, University of Maryland (1999) 250.
[31] TUTTLE, M.P., The use of liquefaction features in paleoseismology: Lessons learned in the New Madrid seismic zone, central United States, Journal of Seismology **5** (2001) 361–380.
[32] ALLEN, C.R., Geologic criteria for evaluating seismicity, Geological Society of America Bulletin **86** (1975) 1041–1056.
[33] SLEMMONS, D.B., DePOLO, C.M., 'Evaluation of active faulting and associated hazard', Active Tectonics, WALLACE, R.E. (Panel Chairman), National Academy Press, Washington, D.C. (1986) 45–62.
[34] VITTORI, E., et al., Ground effects and surface faulting in the September-October 1997 Umbria-Marche (Central Italy) seismic sequence, Journal of Geodynamics **29** (2000) 535–564.
[35] JACKSON, J.A., et al., Seismicity, normal faulting and the geomorphological development of the Gulf of Corinth (Greece): The Corinth earthquakes of February and March 1981, Earth and Planetary Science Letters **57** (1982) 377–397.
[36] WESTAWAY, R., JACKSON, J.A., Surface faulting in the southern Italian Campania-Basilicata earthquake of 23 November 1980, Nature **312** (1984) 436–438.
[37] STEWART, I.S., HANCOCK, P.L., Normal fault zone evolution and fault scarp degradation in the Aegean region, Basin Research **1** (1988) 139–154.

[38] MICHETTI, A.M., et al., Ground effects during the 9 September 1998, Mw=5.6, Lauria earthquake and the seismic potential of the 'aseismic' Pollino region in Southern Italy, Seismological Research Letters **71** (2000) 31–46.
[39] GALADINI, F., GALLI, P., Active tectonics in the central Apennines (Italy): input data for seismic hazard assessment, Natural Hazard **22** (2000) 225–270.
[40] PORFIDO, S., et al., Areal distribution of ground effects induced by strong earthquakes in the southern Apennines (Italy), Surveys in Geophysics **23** (2002) 529–562.
[41] MOREWOOD, N.C., ROBERTS, G.P., Surface observations of active normal fault propagation: implications for growth, Journal of the Geological Society **159** 3 (2002) 263–272.
[42] PAPANIKOLAOU, I., ROBERTS, G., MICHETTI, A.M., 'Fault scarps and deformation rates in Lazio–Abruzzo, Central Italy: comparison between geological fault slip-rate and GPS data', Paleoseismology, Integrated Study of the Quaternary Geological Record for Earthquake Deformation and Faulting, MICHETTI, A.M., AUDEMARD, F., MARCO, S. Eds., Special Issue, Tectonophysics **408** 4 (2005) 147–176.
[43] SERVA, L., 'Il terremoto del 1694 in Irpinia e Basilicata', Volume Speciale Della Commissione ENEA-ENEL: Contributo Alla Caratterizzazione Della Sismicità Del Territorio Italiano, CNR, Convegno annuale Geodinamica, Udine (1981) 183–208.
[44] GALLI, P., PERONACE, E., New paleoseismic data from the Irpinia fault. A different seismogenic perspective for southern Apennines (Italy). Earth-Science Reviews, **136** (2014) 175–201.
[45] PANTOSTI, D., D'ADDEZIO, G., CINTI, F.R., Paleoseismological evidence of repeated large earthquakes along the 1980 Irpinia earthquake fault, Annali di Geofisica, **36** (1993a) 321–330.
[46] PANTOSTI, D., SCHWARTZ, D.P., VALENSISE, G., Paleoseismology along the 1980 Irpinia earthquake fault and implications for earthquake recurrence in the southern Apennines, J. Geophys. Res. **98** (1993b) 6561–6577.
[47] SALVI, S., NARDI, A., Contribution of Landsat synthetic stereopair to morphotectonic analysis in the Irpinia area (Southern Italy), Il Quaternario Italian Journal of Quaternary Sciences **4** (1991) 107–120.
[48] CINQUE, A., LAMBIASE, S., SGROSSO, I., Su due faglie nell'alta valle del Selelegate al terremoto del 23.11.1980, Rend. Soc. Geol. It. **4** (1981) 127–129.
[49] BLUMETTI, A.M., et al., 'New data and reinterpretation on the November 23, 1980, M 6.9 Irpinia - Lucania earthquake (Southern Apennines) coseismic surface effects', International Workshop (Large-Scale Vertical Movements and Related Gravitational Processes), Dramis, F., Farabollini, P., Molin, P., eds., Studi Geologici Camerti, Numero Speciale (2003) 19–27.
[50] VITTORI, E., et al., Surface faulting of the April 6, 2009, Mw 6.3 L'Aquila earthquake in Central Italy, Bull. Seism. Soc. Am. **101** 4 (2011) 1507–1530.
[51] GUERRIERI, L., et al., InSAR data as a field guide for mapping minor earthquake surface ruptures: ground displacements along the Paganica Fault during the April 6th, 2009, L'Aquila earthquake, J. Geophys. Res. **115** B12331 (2010).
[52] SERVA, L., BLUMETTI, A.M., MICHETTI, A.M., Gli effetti sul terreno del terremoto del Fucino (13/1/1915), tentativo di interpretazione della evoluzione tettonica recente di alcune strutture, Mem. Soc. Geol. It. **35** (1988) 893–907.
[53] BLUMETTI, A.M., DRAMIS, F., MICHETTI, A.M., Fault-generated mountain fronts in Central Apennines (Central Italy): geomorphological features and seismotectonic implications, Earth Surface Processes and Landforms **18** (1993) 203–223.

[54] PANTOSTI, D., D'ADDEZIO, G., CINTI, F., Paleoseismicity of the Ovindoli-Pezza fault, central Apennines, Italy: a history including a large previously unrecorded earthquake in the Middle Ages (860-1300 A.D.), J. Geoph. Res. **101** (1996) 5937–5960.
[55] GALADINI, F., GALLI, P., GIRAUDI, C., MOLIN, D., Il terremoto del 1915 e la sismicità della piana del fucino (Italia Centrale), Boll. Soc. Geol. It. **115** (1995).
[56] GALADINI, F., GALLI, P., GIRAUDI, C., Geological investigations of Italian earthquakes: new paleoseismological data from the Fucino Plain (Central Italy), Journal of Geodynamics **24** (1997a) 87–103.
[57] GALADINI, F., GALLI, P., GIRAUDI, C., Paleosismologia della Piana del Fucino (Italia Centrale), Il Quaternario **10** 1 (1997b) 27–64.
[58] GALADINI, F., GALLI, P., The Holocene paleoearthquakes on the 1915 Avezzano earthquake faults (central Italy): implications for active tectonics in the central Apennines, Tectonophysics **308** (1999) 143–170.
[59] GALLI, P., GALADINI, F., PANTOSTI, D., Twenty years of paleoseismology in Italy, Earth Science Reviews **88** (2008) 89–117.
[60] CAVINATO, G.P., CARUSI, C., DALL'ASTA, M., MICCADEI, E., PIACENTINI, T., Sedimentary and tectonic evolution of Plio–Pleistocene alluvial and lacustrine deposits of Fucino Basin (central Italy), Sedimentary Geology **148** 1 (2002) 29–59.
[61] SALVI, S., NARDI, A., 'The Ovindoli fault: a segment of a longer, active fault zone in Central Abruzzi, Italy', Perspectives in Paleoseismology, SERVA, L., SLEMMONS, D.B. Eds., Bulletin of the Association of Engineering Geologists, Special Publication **6** (1995) 101–113.
[62] ODDONE, E., Gli elementi fisici del grande terremoto marsicano-fucense del 13 gennaio 1915, Le osservazioni macrosismiche, Società tipografica modenese (1915).
[63] NIJMAN, W., Tectonics of the Velino-Sirente area, Abruzzi, central Italy: Modification of compressional structures by subsequent dilatatation and collapse, Koninkl. Ned. Ak. Von Weten, S.B. **74** (1971) 156–184.
[64] KANEDA, H., et al., Surface rupture of the 2005 Kashmir, Pakistan, earthquake and its active tectonic implications, Bull. Seism. Soc. Am. **98** 2 (2008) 521–557.
[65] ALI, Z., et al., The Muzzaffarabad, Pakistan earthquake of 8 October 2005: Surface faulting environmental effects and macroseismic intensity, Geol. Soc. London Spec. Publ. **316**, (2009) 155–172.
[66] AVOUAC, J.P., AYOUB, F., LEPRINCE, S., KONCA, O., HELMBERGER, D.V., The 2005, Mw7.6 Kashmir earthquake: Sub-pixel correlation of ASTER images and seismic waveforms analysis, Earth and Planetary Science Letters **249** 3 (2006) 514–528.
[67] KONDO, H., et al., Long recurrence interval of faulting beyond the 2005 Kashmir earthquake around the northwestern margin of the Indo-Asian collision zone, Geology **36** (2008) 731–734.
[68] FANTONI, R., BERSEZIO, R., FORCELLA, F., Alpine structure and deformation chronology at the Southern Alps-Po Plain border in Lombardy, Bollettino della Societa` Geologica Italiana **123** (2004) 463–476.
[69] BURRATO, P., CIUCCI, F., VALENSISE, G., An inventory of river anomalies in the Po Plain, Northern Italy: evidence for active blind thrust faulting, Annals of Geophysics **46** 5 (2003) 865–882.
[70] LIVIO, F., et al., Quaternary capable folds and seismic hazard in Lombardia (Northern Italy): the Castenedolo structure near Brescia, Boll. Soc. Geol. It. (Italian Journal of Geoscience) **128** 1 (2009a) 191–200.
[71] LIVIO, F., et al., Active fault related folding in the epicentral area of the December 25, 1222 (Io = IX MCS) Brescia earthquake (Northern Italy): seismotectonic implications, Tectonophysics **476** 2 (2009b) 320–335.

[72] LIVIO, F.A., et al., Progressive offset and surface deformation along a seismogenic blind thrust in the Po Plain foredeep (Southern Alps, Northern Italy), J. Geophys. Res., Solid Earth **119** 10 (2014) 7701–7721.
[73] ZERBONI, A., et al., The loess-paleosoil sequence at Monte Netto: a record of climate change in the Upper Pleistocene of the central Po Plain, northern Italy, Journal of Soils and Sediments (2014) 22.
[74] DESIO, A., I rilievi isolati della Pianura Lombarda ed i movimenti tettonici del Quaternario. Rend. Istituto Lombardo, Rendiconti Scienze A, Milano **99** (1965) 881–894.
[75] MICHETTI, A.M., et al., Active compressional tectonics, Quaternary capable faults, and the seismic landscape of the Po Plain (N Italy), Annals of Geophysics **55** 5 (2012) 969–1001.
[76] SERVA, L., Ground effects in intensity scales, Terra Nova **6** (1997) 414–416.
[77] MICHETTI, A.M., et al., 'Intensity Scale ESI 2007, Servizio Geologico d'Italia in Mem. Descr. Carta Geologica d'Italia', GUERRIERI, L., VITTORI, E., Eds., Dipartimento Difesa del Suolo, APAT, Rome, Italy (2007) 74.
[78] WELLS, D.L., COPPERSMITH, K.J., New empirical relationships among magnitude, rupture length, rupture width, rupture area and surface displacement, Bull. Seism. Soc. Am. **84** (1994) 974–1002.
[79] SERVA, L., Il ruolo delle scienze della terra nelle analisi di sicurezza di un sito per alcune tipologie di impianti industriali: il terremoto di riferimento per il sito di Viadana (MN) (Role of Earth sciences in the safety analysis of the site of a particular typology of an industrial plant: the reference earthquake at Viadana), Boll. Soc. Geol. It. **109** 2 (1990) 375–411.
[80] DI MANNA, P., et al., Ground effects induced by the 2012 seismic sequence in Emilia: implications for seismic hazard assessment in the Po Plain, Annals of Geophysics **55** 4 (2012) 697–703.
[81] COSTA, C., GARDINI, C., DIEDERIX, H., CORTÉS, J., The Andean thrust front at Sierra de Las Peñas, Mendoza, Argentina, Journal of South American Earth Sciences **13** (2000a) 287–292.
[82] ALVARADO, P., BECK, S., Source characterization of the San Juan (Argentina) crustal earthquakes of 15 January 1944 (Mw 7.0) and 11 June 1952 (Mw 6.8), Earth and Planetary Science Letters **243** (2006) 615–631.
[83] COSTA, C., AHUMADA, E., GARDINI, C., VAZQUEZ, F., DIEDERIX, H., Quaternary shortening at the orogenic front of the Central Andes of Argentina (32°15'-32°40'S): A field survey of the Las Peñas Thrust System, Geol. Soc. Sp. Publ. (2013).
[84] MOREIRAS, S.M., PÁEZ, M.S., 'Historical damages and earthquake environmental effects related to shallow intraplate seismicity of Central-Western Argentina', Geodynamic Processes in the Andes of Central Chile and Argentina, SEPULVEDA, S., Ed., Geological Society, London, Special Publications, **399** (2013).
[85] VOLANT, P., et al., The South Eastern Durance fault permanent network: preliminary results, J. Seism. **4** (2000) 175–189.
[86] BAIZE, S., et al., Inventaire Des Indices De Rupture Affectant Le Quaternaire En Relation Avec Les Grandes Structures Connues, En France Métropolitaine Et Dans Les Régions Limitrophes, Soc. Géol. Fr., **175** (2002) 142.
[87] SÉBRIER, M., GHAFIRI, A., BLÈS, J.L., Paleoseismicity in France: Fault trench studies in a region of moderate seismicity, J. Geodynamics **24** (1997) 207–217.
[88] CHARDON, D., HERMITTE, D., NGUYEN, F., BELLIER, O., First paleoseismological constraints on the strongest earthquake in France (Provence) in the twentieth century, Geology **33** (2005) 901–904.

[89] CUSHING, E.M., et al., A multidisciplinary study of a slow-slipping fault for seismic hazard assessment: the example of the Middle Durance Fault (SE France), Geophys. J. Int. **172** (2008) 1163–1178.
[90] BAROUX, E., PINO, N.A., VALENSISE, G., SCOTTI, O., CUSHING, M., Source parameters of the 11 June 1909, Lambesc (Provence, southeastern France) earthquake: A reappraisal based on macroseismic, seismological and geodetic observations, J. Geophys. Res. **108** (2003).
[91] CHARDON, D., BELLIER, O., Geological boundary conditions of the 1909 Lambesc (Provence, France) earthquake: structure and evolution of the Trévaresse ridge anticline, Bull. Soc. géol. Fr. **174** (2003) 497–510.
[92] AOCHI, H., CUSHING, E.M.., SCOTTI, O., BERGE-THIERRY, C., Estimating rupture scenario likelihood based on dynamic rupture simulations: the example of the segmented Middle Durance fault, southeastern France, Geophys. J. Int. **165** (2006) 436–446.
[93] THOUVENOT, F., et al., The Ml=5.3 Epagny (French Alps) earthquake of 1996 July 15: a long-awaited event on the Vuache Fault, Geophys. J. Int., **135** (1998) 876–892.
[94] BAIZE, S., et al., Contribution to the seismic hazard assessment of a slow active fault, the Vuache fault in the southern Molasse basin (France), Bull. Soc. Géol. Fr. **182** (2011) 347–365.
[95] SEILACHER, A., Fault-graded beds interpreted as seismites, Sedimentology **13** (1969) 15–159.
[96] MONTENAT, C., BARRIER, P., OTTD´ESTEVOU, P., HIBSCH, C., Seismites: An attempt at critical analysis and classification, Sed. Geol. **196** (2007) 5–30.
[97] BECKER, A., FERRY, M., MONECKE, K., SCHNELLMANN, M., GIARDINI, D., Multiarchive paleoseismic record of late Pleistocene and Holocene strong earthquakes in Switzerland, Tectonophysics **400** 4 (2005) 153–177.
[98] KEEFER, D.K., Investigating landslides caused by earthquakes: a historical review, Surveys in Geophysics **23** 6 (2002) 473–510.
[99] MÖRNER, N.A., Paleoseismicity of Sweden: A novel paradigm, Paleogeophysics and Geodynamics, Stockholm University (2003), 320.
[100] GALLI, P., New empirical relationships between magnitude and distance for liquefaction, Tectonophysics **324** 3 (2000) 169–187.
[101] REICHERTER, K., et al., Active basins and neotectonics: morphotectonics of the Lake Ohrid Basin (FYROM and Albania), Z. Dt. Ges. Geowiss. **162** 2 (2011) 217–234.
[102] OBERMEIER, S.F., 'Using liquefaction-induced features for paleoseismic analysis', Paleoseismology, McCALPIN, J.P. Ed., Academic Press, San Diego, CA (1996) 331–396.
[103] BOULANGER, R.W., IDRISS, I.M., Liquefaction susceptibility criteria for silts and clays, J. Geotechnical and Geoenvironmental Engineering **132** (2006) 1413-1426.
[104] ANDRUS, R.D., STOKOE, K. H., Liquefaction resistance of soils from shear-wave velocity, J. Geotechnical and Geoenvironmental Engineering **126** (2000) 1015–1025.
[105] ISHIHARA, K., 'Stability of natural deposits during earthquakes', Proc. 11th International Conference on Soil Mechanics and Foundation Engineering, San Francisco **2** (1985) 321–376.
[106] ISHIHARA, K. Liquefaction and flow failure during earthquakes, Geotechnique **43** (1993) 351–415.
[107] MARTO, A., SOON, T.C., Short Review on liquefaction susceptibility, International Journal of Engineering Research and Applications (IJERA) **2** 3 (2012) 2115–2119.
[108] TECHNICAL REPORT, Central And Eastern United States Seismic Source Characterization For Nuclear Facilities, EPRI, Palo Alto, CA, U.S. DOE and U.S. NRC (2012).

[109] TUTTLE, M.P., HARTLEB, R., 'Central and eastern U.S. paleoliquefaction database, uncertainties associated with paleoliquefaction data, and guidance for seismic source characterization', The Central and Eastern U.S. Seismic Source Characterization for Nuclear Facilities (Appendix E.), Technical Report, EPRI, Palo Alto, CA, U.S. DOE, and U.S. NRC (2012) 135 (plus database).
[110] SIMS, J. D., Determining earthquake recurrence intervals from deformational structures in young lacustrine sediments, Tectonophysics **29** (1975) 141–153.
[111] WOLF, L. W., TUTTLE, M. P., BROWNING, S., PARK, S., Geophysical surveys of earthquake induced liquefaction deposits in the New Madrid seismic zone, Geophysics **71** 6 (2006) B223–B230.
[112] Al-SHUKRI, H., MAHDI, H., TUTTLE, M., Three-dimensional imaging of earthquake induced liquefaction features with ground penetrating radar near Marianna, Arkansas, Seismological Research Letters **77** (2006) 505–513.
[113] TUTTLE, M. P., BARSTOW, N., Liquefaction-related ground failure: A case study in the New Madrid seismic zone, Central United States, Bull. Seism. Soc. Am. **86** (1996) 636–645.
[114] AMBRASEYS, N. N., 'earthquake engineering and structural dynamics', Engineering Seismology, Journal of the International Association of Earthquake Engineering **17** (1988) 1–105.
[115] CASTILLA, R.A., AUDEMARD, F.A., Sand blows as a potential tool for magnitude estimation of pre-instrumental earthquakes, Journal of Seismology **11** (2007) 473–487.
[116] KELSON, K.I., et al., Multiple Holocene earthquakes along the Reelfoot fault, central New Madrid seismic zone, J. Geophys. Res. **101** (1996) 6151–6170.
[117] TUTTLE, M.P., et al., The earthquake potential of the New Madrid seismic zone, Bull. Seism. Soc. Am. **92** 6 (2002) 2080–2089.
[118] TUTTLE, M.P., SCHWEIG, E.S., CAMPBELL, J., THOMAS, P.M., SIMS, J.D., LAFFERTY, R.H., Evidence for New Madrid earthquakes in AD 300 and 2350 B.C., Seismological Research Letters **76** 4 (2005) 489–501.
[119] KEEFER, D. K., Landslides caused by earthquakes, Bull. Seism. Soc. Am. **95** (1984) 406–421.
[120] RODRÍGUEZ, C.E., BOMMER, J.J., CHANDLER, R.J., Earthquake-induced landslides: 1980–1997, Soil Dynamics and Earthquake Engineering **18** (1999) 325–346.
[121] BOMMER, J., RODRÍGUEZ, C.E., Earthquake-induced landslides in Central America, Engineering Geology **63** (2002)189–220.
[122] DELGADO, J., GARRIDO, J., LOPEZ-CASADO, C., MARTINO, S., PELAEZ, J.A., On far field occurrence of seismically induced landslides, Engineering Geology **123** (2011a) 204–213.
[123] RODRÍGUEZ-PECES, M.J., et al., Applicability of Newmark method at regional, sub-regional and site scales: seismically induced Bullas and La Paca rock-slide cases (Murcia, SE Spain), Natural Hazards **59** (2011a) 1109–1124.
[124] BECKER, A., DAVENPORT, C.A., Rockfalls triggered by the AD 1356 Basle earthquake, Terra Nova **15** (2003) 258–264.
[125] JIBSON, R.W., HARP, E.L., SCHULZ, W., KEEFER, D.K., Large rock avalanches triggered by the M 7.9 Denali fault, Alaska, earthquake of 3 November 2002, Engineering Geology **83** (2006) 144–160.
[126] KEEFER, D.K., WARTMAN, J., NAVARRO OCHOA, C., RODRÍGUEZ-MAREK, A., WIECZOREK, G.F., Landslides caused by the M 7.6 Tecomán, Mexico earthquake of January 21, 2003, Engineering Geology **86** (2006) 183–197.
[127] MAHDAVIFAR, M.R., SOLAYMANI, S., JAFARI, M.K., Landslides triggered by the Avaj, Iran earthquake of June 22, 2002, Engineering Geology **86** (2006) 166–182.

[128] MICCADEI, E., PIACENTINI, T., SCIARRA, N., 'Seismically induced landslides caused by the earthquake of 6 April 2009 in Abruzzo Region (Central Italy)', Geologically Active (Proceedings of 'Geologically Active' 11th IAEG Congress, Auckland, New Zealand, 2010), Taylor and Francis Group, London (2010) 127–141.
[129] ALFARO, P., et al., Seismic induced landslides in Spain: A review 7ª Asamblea Hispano-Portuguesa de Geodesia y Geofísica, AHPGG, San Sebastian (2012) 1–7.
[130] TANG, C., ZHU, J., QI, X., DING, J., Landslides induced by the Wenchuan earthquake and the subsequent strong rainfall event: A case study in the Beichuan area of China, Engineering Geology **122** (2011).
[131] UGAI, K., YAGI, H., WAKAI, A. Eds., Earthquake-Induced Landslides, Proceedings of the International Symposium on Earthquake-Induced Landslides, Kiryu, Japan 2012 Springer Series **18** (2013) 996.
[132] DELGADO, J., et al., Seismically-induced landslides in the Betic Cordillera (S Spain), Soil Dynamics and Earthquake Engineering **31** (2011) 1203–1211.
[133] HARP, E.L., KEEFER, D.K., SATO, H.P., YAGI, H., Landslide inventories: The essential part of seismic landslide hazard analyses, Engineering Geology **122** 2 (2011) 9–21.
[134] YAMADA, M., WANG, G., MUKAI, K., 'The classification and features of earthquake-induced landslides in the world', Earthquake-Induced Landslides, Proceedings of the International Symposium on Earthquake-Induced Landslides, Kiryu, Japan, 2012, (2013) 117–124.
[135] JIBSON, R.W., 'Using landslides for paleoseismic analysis'. Paleoseismology, 2nd Edition (McCalpin, J. Ed.,), Second edition Academic Press, London (2009) 397– 438.
[136] HAMMOND, C.M., MEIER, D., DARREN BECKSTRAND, D., Paleo-landslides in the Tyee Formation and highway construction, central Oregon Coast Range, GSA Field Guides **15** (2009) 481–494.
[137] SUTINEN R., HYVÖNEN, E., Paleo-landslides in the Suasselkä fault-zone, Finnish Lapland, derived from LiDAR data, 12th International Circumpolar Remote Sensing Symposium. Levi, Finland (2012). <http://alaska.usgs.gov/science/geography/CRSS2012/presentations/SutinenHyvonen.pdf>
[138] JIBSON, R.W., HARP, E.L., MICHAEL, J.A., A method for producing digital probabilistic seismic landslide hazard maps, Engineering Geology **58** (2000) 271–289.
[139] GARCÍA-RODRÍGUEZ, M.J., MALPICA, J.A., BENITO, B., DÍAZ, M., Susceptibility assessment of earthquake-triggered landslides in El Salvador using logistic regression, Geomorphology **95** (2008) 172–191.
[140] STROM, A., 'Use of indirect evidence for the prehistoric earthquake-induced landslides identification', Earthquake-Induced Landslides, UGAI, K., et al. Ed., Springer Series **18** (2013) 21–30.
[141] SÁNCHEZ-GÓMEZ M., et al., Evidence for a 4700-2100 BC palaeoearthquake recorded in a fluvial-archaeological sequence of the Segura River, SE Spain, Quaternary International **112** (2011).
[142] CARRACEDO, J.C., DAY, S., GUILLOU, H., PÉREZ-TORRADO, F.J., Giant Quaternary landslides in the evolution of La Palma and El Hierro, Canary Islands, Journal of Volcanology and Geothermal Research **94** (1999) 169–190.
[143] OTA, Y., CHAPPELL, J., BERRYMAN, K., OKAMOTO, Y., Late Quaternary paleolandslides on the coral terraces of Huon Peninsula, Papua New Guinea, Geomorphology **19** (1997) 55–76.
[144] MORA, S., MORA, R., Los deslizamientos causados por el terremoto de Limón: Factores de control y comparación con otros eventos en Costa Rica, Revista Geologica de America Central. Vol. Especial Terremoto de Limón (1994) 139–152.

[145] PAPADOPOULOS, G.A., PLESSA, A., Magnitude-distance relations for earthquake–induced landslides in Greece, Engineering Geology **58** (2000) 377–386.
[146] PRESTININZI, A., ROMEO, R., Earthquake-induced ground failures in Italy, Engineering Geology **58** (2000) 387–397.
[147] HANCOX, G.T., PERRIN, N.D., DELLOW, G.D., Recent studies of historical earthquake induced landsliding, ground damage, and MM intensity in New Zealand, Bulletin of the New Zealand Society for Earthquake Engineering **35** 2 (2002) 59–95.
[148] CEREIS 2010, Catálogo de intensidades, Centro Regional de Sismología para América del Sur (2010), http://www.cereis.org/portal/catal_inten.php.
[149] ROMEO, R. Seismically induced landslide displacements: a predictive model, Engineering Geology **58** (2002) 337–351.
[150] JIBSON, R.W. Regression models for estimating coseismic landslide displacement, Engineering Geology **91** (2007) 209–218.
[151] VOLLMERT, A., et al., Seismic landslide hazard assessment for the city of Carmona (SW–Spain), Ann. Geophysics (2013).
[152] OTA, Y., AZUMA, T., NINA LIN, Y.S., 'Application of INQUA environmental seismic intensity scale to recent earthquakes in Japan and Taiwan', Paleoseismology: Historical and Prehistorical records of earthquake ground effects, REICHERTER, K., MICHETTI, A.M., SILVA, P.G. Eds., Geological society of London Special Publication, London (UK) **316** (2009) 55–71.
[153] NEWMARK, N.M., Effects of earthquakes on dams and embankments, Geotechnique **15** (1965) 139–160.
[154] RODRÍGUEZ-PECES, M.J., GARCÍA-MAYORDOMO, J., AZAÑÓN, J.M., INSUA-ARÉVALO J.M., JIMÉNEZ PINTOR J., Constraining pre-instrumental earthquake parameters from slope stability back-analysis: Paleoseismic reconstruction of the Güevéjar landslide during the 1st November 1755 Lisbon and 25th December 1884 Arenas del Rey earthquakes, Quaternary International **242** (2011b) 76–89.
[155] GOLDFINGER, C., Sub-aqueous paleoseismology, In: Paleoseismology, MCCALPIN, J. Eds., International Geophysics 95 (2009) 119–170.
[156] BECK, C., Late Quaternary lacustrine paleo-seismic archives in north-western Alps: Examples of earthquake-origin assessment of sedimentary disturbances, Earth-Science Reviews **96** 4 (2009) 327–344.
[157] STRASSER, M., et al., Quantifying subaqueous slope stability during seismic shaking: Lake Lucerne as model for ocean margins, Mar. Geol. **240** (2007) 77–97.
[158] STRASSER, M., MONECKE, K., SCHNELLMANN, M., ANSELMETTI, F.S., Lake sediments as natural seismographs: A compiled record of Late Quaternary earthquakes in Central Switzerland and its implication for Alpine deformation, Sedimentology **60** (2013) 319–341.
[159] MARCO, S., STEIN, M., AGNON, A., ROC, H., Long term earthquake clustering: A 50,000 year paleoseismic record in the Dead Sea graben, J. Geophys. Res. **101** (1996) 6179–6191.
[160] MARCO, S., AGNON, A., High-resolution stratigraphy reveals repeated earthquake faulting in the Masada Fault Zone, Dead Sea Transform, Tectonophysics **408** (2005) 101–112.
[161] KAGAN, E., STEIN, M., AGNON, A., NEUMANN, F., Intrabasin paleoearthquake and quiescence correlation of the late Holocene Dead Sea, J. Geophys. Res., B: Solid Earth **116** 4 (2011).
[162] GARDUNO-MONROY et al., Evidence of tsunami events in the Paleolimnological record of Lake Pátzcuaro, Michoacán, Mexico, Geofísica Internacional **50** 2 (2011) 147–161.

[163] NAKAJIMA, T., KANAI, Y., Sedimentary features of seismoturbidites triggered by the 1983 and older historical earthquakes in the eastern margin of the Japan Sea, Sedimentary Geology **135** (2000) 1–19.
[164] KAWAGUCCI et al., Disturbance of deep-sea environments induced by the M9.0 Tohoku Earthquake, Nature, Scientific Reports **2** (2012).
[165] SÉGURET, M., LABAUME, P., MADARIAGA, R., Eocene seismicity in the Pyrénées from megaturbidites of the South Pyrenean basin (Spain), Mar. Geol **55** (1984) 117–131.
[166] MONECKE, K., et al., Earthquake-induced deformation structures in lake deposits: A Late Pleistocene to Holocene paleoseismic record for Central Switzerland. Eclogae geol. Helv. **99** (2006) 343–362.
[167] HIBSCH, C., ALVARADO, A., YEPES, H., PEREZ, H., SEBRIER, M., Holocene liquefaction and soft-sediment deformation in Quito (Ecuador): a palæosismic history recorded in lacustrine sediments, J. Geodyn. **24** 4 (1994) 259–280.
[168] RODRIGUEZ-PASCUA, M.A., DE VICENTE, G., CALVO, J.P., PEREZ-LOPEZ, R., Similarities between recent seismic activity and paleoseismites during the Late Miocene in the external Betic Chain (Spain): relationship between 'b' value and the fractal dimension, J. Struct. Geol. **25** (2003) 749–763.
[169] ALLEN, J.R.L., Earthquake magnitude–frequency, epicentral distance, and soft-sediment deformation in sedimentary basins, Sediment. Geol. **46** (1986) 67–75.
[170] PEDERNEIRAS, R. G. G., Paleosismicidade e sedimentaçao — Evidências no compartimento Sul da Bacia do Recôncavo, Bahia, Geoci. PETROBRAS **5** 4 (1991) 39–68.
[171] AUDEMARD, F., DE SANTIS, F., Survey of liquefaction structures induced by recent moderate earthquakes, Bull. Intern. Assoc. Eng. Geol. **44** (1991) 5–16.
[172] POSTPISCHL, D., AGOSTINI, S., FORTI, P., QUINIF, Y. Paleoseismicity from karst sediments: the 'Grotta del Cervo' cave case study (Central Italy), Tectonophysics **193** (1991) 33–44.
[173] LEMEILLE, F., et al., Co-seismic ruptures and deformations recorded by speleothems in the epicentral zone of the Basel earthquake, Geodinamica Acta **12** (1999) 179–191.
[174] GILLI, E., LEVRET, A., SOLLOGOUB, P., DELANGE, P., Research on the February 18, 1996 earthquake in the caves of Saint-Paul-de-Fenouillet area, (eastern Pyrenees, France), Geodinamica Acta **12** (1999) 143–158.
[175] KAGAN, E.J., AGNON, A., BAR-MATTHEWS, M., AYALON, A., Dating large, infrequent earthquakes by damaged cave deposits, Geology **33** (2005) 261–264.
[176] GILLI, E., Review on the use of natural cave speleothems as paleoseismic or neotectonics indicators, Comptes Rendus, Geoscience **337** 13 (2005) 1208–1215.
[177] BECKER, A., et al., Speleoseismology: a critical perspective, Journal of Seismology **10** 3 (2006) 371–388.
[178] LACAVE, C., LEVRET, A., KOLLER, M.G., 'Measurements of natural frequencies and damping of speleothems', Proc. 12th World Conference on Earthquake Engineering, Auckland, New-Zealand (2000) Paper No. 2118.
[179] LACAVE, C., KOLLER, M.G., EGOZCUE, J.J., What can be concluded about seismic history from broken and unbroken speleothems? Journal of Earthquake Engineering **8** 3 (2004) 431–455.
[180] VOLANT, P., et al., An archaeo-seismological study of the Nîmes Roman aqueduct, France: indirect evidence for an M6 seismic event?, Natural Hazards **49** (2009) 53–77.
[181] PASSCHIER, C.W., WIPLINGER, G., SÜRMELIHINDI, G., KESSENER, P., GÜNGÖR, T., 'Roman aqueducts as indicators of historically active faults in the Mediterranean basin', Earthquake Geology (Proc. 2nd INQUA-IGCP-567 International Workshop on Active Tectonics), Archaeology and Engineering Corinth, Greece (2011).

[182] BAKER, J.W., ABRAHAMSON, N.A., WHITNEY, J.W., BOARD, M.P., HANKS, T.C., Use of fragile geologic structures as indicators of unexceeded ground motions and direct constraints on probabilistic seismic hazard analysis, Bull. Seism. Soc. Am. **103** 3 (2013) 1898–1911.
[183] BRUNE, J.N., ANOOSHEHPOOR, A., PURVANCE, M.D., Band of precariously balanced bocks between the Elsinore and San Jacinto, California fault zones: Constraints on ground motion for large earthquakes, Geology **34** (2006) 137–140.
[184] LACAVE, C., SADIER, B., DELANNOY, J.J., NEHNE, C., ECOZCUE, J.J., 'The use of speleothems to better constrain long return period seismic hazard in Libanon', Proc. 15th World Conference on Earthquake Engineering, Lisboa, Portugal (2012) Paper No. 354.
[185] ATWATER, B.F., NELSON, A.R., CLAGUE, J.J., et al., Summary of coastal geologic evidence for past great earthquakes at the Cascadia subduction zone, Earthquake Spectra **11** (1995) 1–19.
[186] YEATS, R.S. (Ed.), The Geology of Earthquakes, 2nd Edition, Oxford University Press, New York (2013) 534.
[187] ATWATER, B.F., et al., The orphan tsunami of 1700 – Japanese clues to a parent earthquake in North America, U.S. Geological Survey Professional Paper **1707** (2005) 133.
[188] NANAYAMA, F., et al., Unusually large earthquakes inferred from tsunami deposits along the Kuril trench, Nature **424** (2003) 660–663.
[189] SAWAI, Y., NAMEGAYA, Y., OKAMURA, Y., SATAKE, K., SHISHIKURA, M., Challenges of anticipating the 2011 Tohoku earthquake and tsunami using coastal geology, Geophysical Research Letters **29** (2012).
[190] DAWSON, A.G., SHI, S., Tsunami deposits, Pure and Applied Geophysics **157** (2000) 875–897.
[191] BOURGEOIS, J., 'The geologic effects and records of tsunamis', in Bernard, E.N., and Robinson, A.R., eds., The Sea, Vol. 15 Tsunamis, Cambridge, Massachusetts, Harvard University Press (2009) 53–91.
[192] PENEGINA, T.K., BOURGEOIS, J., BAZANOVA, L.I., MELEKESTEV, I.V., BRAITSEVA, O.A., A millennial-scale record of Holocene tsunamis on the Kronotskiy Bay coast Kamchatka, Russia, Quatern. Res. **59** (2003) 36–47.
[193] SUGAWARA, D., GOTO, K., IMAMURA, F., MATSUMOTO, H., MINOURA, K., Assessing the magnitude of the 869 Jogan tsunami using sedimentary deposits: Prediction and consequence of the 2011 Tohoku-oki tsunami, Sedimentary Geology **282** (2012) 14–26.
[194] ATWATER, B.F., Evidence for great Holocene earthquakes along the outer coast of Washington state, Science **236** (1987) 942–944.
[195] PETERS, B., JAFFE, B., GELFENBAUM, G., PETERSON, C., Cascadia Tsunami Deposit Database, U. S. Geological Survey Open-File Report 03–13, (2003) 24. Electronic database and GIS coverage [URL: http://geopubs.wr.usgs.gov/open-file/of03-13/].
[196] PETERS, R., JAFFE, B.E., GELFENBAUM, G., Distribution and sedimentary characteristics of tsunami deposits along the Cascadia margin of western North America, Sedimentary Geology **200** (2007) 372–386.
[197] PRIEST, G.R., et al., Confidence levels for tsunami-inundation limits in northern Oregon inferred from a 10000-year history of great earthquakes at the Cascadia subduction zone, Natural Hazards **54** (2010) 27–73.
[198] GOLDFINGER, C., et al., 'Turbidite event history: Methods and implications for Holocene paleoseismicity of the Cascadia subduction zone', U.S. Geological Survey Professional Paper **1661–F** (2012).

[199] ATWATER, B., GRIGGS, G., Deep-Sea Turbidites as Guides to Holocene Earthquake History at the Cascadia Subduction Zone: Alternative views for a Seismic-Hazard Workshop, U.S. Geological Survey Open-File Report (2012) 2012–1043.
[200] PETERSON, C.D., CRUIKSHANK, K.M., JOL, H.M., SCHLICHTING, R.B., Minimum runup heights of paleotsunami from evidence of sand ridge overtopping at Cannon Beach, Oregon, Central Cascadia Margin, U.S.A, Journal of Sedimentary Research **78** 6 (2008) 390–409.
[201] PETERSON, C.D., et al., Evaluation of the use of paleotsunami deposits to reconstruct inundation distance and runup heights associated with prehistoric inundation events, Crescent City, southern Cascadia margin, Earth Surface Processes and Landforms **36** 7 (2011) 967–980.
[202] WITTER, R.C., JAFFE, B.E., ZHANG, Y., PRIEST, G., Reconstruction hydrodynamic flow parameters of the 1700 tsunami at Cannon Beach, Oregon, USA, Natural Hazards **63** (2012) 223–240.
[203] GONZALEZ, F.I., et al., Probabilistic tsunami hazard assessment at Seaside, Oregon, for near- and far-field seismic sources, J. Geophys. Res. **114** C11023 (2009).
[204] WALSH, T.J., et al., Tsunami hazard map of the southern Washington coast: Modeled tsunami inundation from a Cascadia subduction zone earthquake, Washington Division of Geology and Earth Resources, Geologic Map GM–49 (2000).
[205] GEIST, E.L., PARSONS, T., Probabilistic analysis of tsunami hazards, Natural Hazards **37** (2006) 277–314.
[206] MACINNES, B.T., WEISS, R., BOURGEOIS, J., PINEGINA, T.K., Slip distribution of the 1952 Kamchatka great earthquake based on near-field tsunami deposits and historical records, Bull. Seism. Soc. Am. **100** (2010) 1695–1709.
[207] REICHERTER, K., et al., The sedimentary inventory of tsunamis along the southern Gulf of Cadiz (southwestern Spain), Zeitschriff für Geomorphologie **54** (2010) 147–173.
[208] SCHEFFERS, A., KELLETAT, D., Tsunami relics on the coastal landscape west of lisbon, Portugal, Science Of Tsunami Hazard **23** (2005) 3–16.
[209] COSTA, P.J.M., et al., A tsunami record in the sedimentary archive of the central Algarve coast, Portugal: Characterizing sediment, reconstructing sources and inundation paths, The Holocene **22** (2012) 899–914.
[210] BAPTISTA, M.A., MIRANDA, P.M., MIRANDA, J.M., MENDES, V.L. Constrains on the source of the 1755 Lisbon tsunami inferred from numerical modeling of historical data, Journal of Geodynamics **25** (1998) 159–174.
[211] BAPTISTA, M.A., MIRANDA, J.M., CHIERICI, F., ZITELLINI, N., New study of the 1755 earthquake source based on multi-channel seismic survey data and tsunami modeling, Natural Hazards and Earth System Sciences **3** (2003) 333–340.
[212] VILANOVA, S.P., NUNES, C.F., FONSECA, J.F.B.D., Lisbon 1755: A Case of triggered onshore rupture? Bull. Seism. Soc. Am. **93** (2003) 2056–2068.
[213] BARKAN, R., TEN BRINK, U.S., LIN, J., Far field tsunami simulations of the 1755 Lisbon earthquake: Implications for tsunami hazard to the U.S. East Coast and the Caribbean, Marine Geology **264** (2010) 109–122.
[214] ROGER, J., et al., The 1755 Lisbon tsunami in Guadeloupe Archipelago: Source sensitivity and investigation of resonance effects, The Open Oceanography Journal **4** (2010) 58–70.
[215] RUIZ, F., et al., Evidence of high-energy events in the geological record: Mid-holocene evolution of the southwestern Doñana National Park (SW Spain), Palaeogeography Palaeoclimatology Palaeoecology **229** (2005) 212–229.
[216] LUQUE, L., et al., Tsunami deposits as paleoseismic indicators: examples from the Spanish coast, Acta Geologicahispanica **36** (2001) 197–211.

[217] MORALES, J.A., BORREGO, J., SAN MIGUEL, E.G. LÓPEZ-GONZÁLEZ, N., CARRO, B., Sedimentary record of recent tsunamis in the Huelva Estuary (south-western Spain), Quaternary Science Reviews **27** (2008) 734–746.
[218] NISHIMURA, Y., MIYAJI, N., Tsunami deposits from the 1993 southwest Hokkaido earthquake and the 1640 Hokkaido Komagatake eruption, northern Japan, Pure and Applied Geophysics **144** (1995) 719–733.
[219] MOORE, A.L., NISHIMURA, Y., GELFENBAUM, G., TAKANOBU, K., TRIV, R., Sedimentary deposits of the 26 December 2004 tsunami on the northwest coast of Aceh, Indonesia, Earth Planets Space **58** (2006) 253–258.
[220] MORTON, R.A., GELFENBAUM, G., JAFFE, B.E., Physical criteria for distinguishing sandy tsunami and storm deposits using modern examples, Sedimentary Geology **200** (2007) 184–207.
[221] PETERS, R., JAFFE, B.E., Identification of Tsunami Deposits in the Geologic Record: Developing Criteria Using Recent Tsunami Deposits, US Geological Survey Open-File Report 2010–1239, (2010) 39. [URL: http://pubs.usgs.gov/of/2010/1239/].
[222] CLARK, K., et al., Characteristics of the 29th September 2010 South Pacific tsunami as observed at Niuatoputapu Island, Tonga, Earth-Science Reviews **107** (2011) 52–65.
[223] PUTRA, P. S., NISHIMURA, Y., AND YULIANTO, E., Sedimentary features of tsunami deposits in carbonate-dominated beach environments: a case study from the 25 October 2010 Mentawai tsunami, Pure and Applied Geophysics **170** (2013) 1583–1600.
[224] MOORE, A., MCADOO, B.G., RUFFMAN, A., Landward fining from multiple sources in a sand sheet deposited by the 1929 Grand Banks tsunami, Newfoundland, Sedimentary Geology **200** (2007) 336–346.
[225] GOTO, K., MIYAGI, K., KAWAMATA, H., IMAMURA, F., Discrimination of boulders deposited by tsunamis and storm waves at Ishigaki Island, Japan, Marine Geology **269** (2010) 34–45.
[226] SWITZER, A.D., BURSTON, J.M., Competing mechanisms for boulder deposition on the southeast Australian coast, Geomorphology **114** (2010) 42–54.
[227] ETIENNE, S., et al., The use of boulders for characterising past tsunamis: Lessons from the 2004 Indian Ocean and 2009 South Pacific tsunamis, Earth Science Reviews **107** 2 (2011) 76–90.
[228] PARIS, R., NAYLOR, L.A., STEPHENSON, W.J., Boulders as a signature of storms on rock coasts, Marine Geology **283** 4 (2011) 1–11.
[229] HIGMAN, B., BOURGEOIS, J., 'Deposits of the 1992 Nicaragua tsunami', Tsunamites Features and Implications, SHIKI, T., TSUJI, Y., MINOURA, K., YAMAZAKE, T. Eds., Elsevier Publications (2008) 81–103.
[230] BOURGEOIS, J., MACINNES, B., Tsunami boulder transport and other dramatic effects of the 15 November 2006 central Kuril Islands tsunami on the island of Matua, Zeitschrift für Geomorphologie, Supplementary Issues **54** (2010) 175–195.
[231] LAMARCHE, G., PELLETIER, B., GOFF, J., Impact of the 29 September 2009 South Pacific tsunami on Wallis and Futuna, Marine Geology **271** (2010) 297–302.
[232] RICHMOND, B.M., et al., Recent storm and tsunami coarse-clast deposit characteristics, southeast Hawaii, Marine Geology **283** (2011) 79–89.
[233] MORTON, R.A., BARRAS, J.A., Hurricane impacts on coastal wetlands: a half-century record of storm-generated features from southern Louisiana, Journal of Coastal Research **27** (2011) 27–43.
[234] SPISKE, M., BAHLBURG, H., A quasi-experimental setting of coarse clast transport by the 2010 Chile tsunami (Bucalemu, Central Chile), Marine Geology **289** (2011) 72–85.
[235] GOTO, K., et al., New insights of tsunami hazard from the 2011 Tohoku-oki event, Marine Geology **290** (2012) 46–50.

[236] WOODWARD, S.M., Principal Component Analysis of Sediment Deposited in the Village of Titiana from the Solomon Islands Tsunami of April 2, 2007, MSc thesis, Kent State University (2009) 55.
[237] NICHOL, S.L., KENCH, P.S., Sedimentology and preservation potential of carbonate sand sheets deposited by the December 2004 Indian Ocean tsunami, South Baa Atoll, Maldives, Sedimentology **55** (2008) 1173–1187.
[238] GOFF, J., CHAGUÉ-GOFF, C., NICHOL, S., JAFFE, B.E., DOMINEY-HOWES, D., Progress in paleotsunami research, Sedimentary Geology **243–244** (2012) 70–88.
[239] GOTO, K., MIYAGI, K., KAWAMATA, H., AND IMAMURA, F. Discrimination of boulders deposited by tsunamis and storm waves at Ishigaki Island, Japan, Marine Geology **269** (2011) 34-45.
[240] TAKAHASHI, T., IMAMURA, F., SHUTO, N., Numerical Simulation of Topography Change Due to Tsunamis, Proceedings IUGG/IOC International Tsunami Symposium, Wakayama (1993) 243–255.
[241] TAKAHASHI, T., SHUTO, N., IMAMURA, F., ASAI, D., A movable bed model for tsunami with exchange rate between bed load layer and suspended layer, Annual Journal of Coastal Engineering **46** (1999) 606–610 (in Japanese).
[242] TAKAHASHI, T., SHUTO, N., IMAMURA, F., ASAI, D., Modeling Sediment Transport Due to Tsunamis with Exchange Rate between Bed Load Layer and Suspended Load Layer, Proceedings International Conference on Coastal Engineering, ASCE (2000) 1508–1519.
[243] JAFFE, B.E., GELFENBAUM, G., A simple model for calculating tsunami flow speed from tsunami deposits, Sedimentary Geology **200** (2007) 347–361.
[244] SOULSBY, R.L., SMITH, D.E., RUFFMAN, A., Reconstructing tsunami run-up from sedimentary characteristics: A simple mathematical model, Coastal Sediments ’07 **2** (2007) 1075–1088.
[245] JAFFE, B.E., et al., Flow speed estimated by inverse modeling of sandy tsunami deposits: results from the 11 March 2011 tsunami on the coastal plain near the Sendai Airport, Honshu, Japan, Sedimentary Geology **282** (2012) 90–109.
[246] LARIO, et al., Tsunami vs. storm surge deposits: a review of the sedimentological and geomorphological records of extreme wave events (EWE) during the Holocene in the Gulf of Cadiz, Spain, Zeitschrift Fuer Geomorphologie **54** 3 (2010) 301–316.
[247] MORTON, R.A., RICHMOND, B.M., JAFFE, B.E., GELFENBAUM, G., ‘Reconnaissance investigation of Caribbean extreme wave deposits: preliminary observations, interpretations, and research directions’, Report U.S. Geological Survey Open-File Report 2006-1293, **45** (2006), http://pubs.usgs.gov/of/2006/1293/.
[248] ENGEL, M., et al., Shoreline changes and high-energy wave impacts at the leeward coast of Bonaire (Netherlands Antilles), Earth Planets and Space **64** (2012) 905–921.
[249] ATWATER, B.F., et al., Geomorphic and stratigraphic evidence for an unusual tsunami or storm a few centuries ago at Anegada, British Virgin Islands, Natural Hazards **63** (2012) 51–84.
[250] COX, R., ZENTNER, D.B., KIRCHNER, B.J., COOK, M.S., Boulder ridges on the Aran Islands (Ireland): recent movements caused by storm waves, not tsunamis, The Journal of Geology **120** (2012) 249–272.
[251] WEISS, R., The mystery of boulders moved by tsunamis and storms, Marine Geology **295–298** (2012) 28–33.
[252] TUTTLE, M.P., RUFFMAN, A., ANDERSON, T., JETER, H., Distinguishing tsunami from storm deposits in Eastern North America: the 1929 Grand Banks tsunami versus the 1991 Halloween storm, Seismological Research Letters **75** (2004) 117–131.
[253] MONECKE, K., et al., A 1000-year sediment record of tsunami recurrence in northern Sumatra, Nature **455** (2008) 1232–1234.

[254] JANKAEW, K., et al., Medieval forewarning of the 2004 Indian Ocean tsunami in Thailand, Nature **455** (2008) 1228–1231.
[255] OVENSHINE, A.T., LAWSON, D.E., BARTSCH-WINKLER, S.R., The Portage river Silt: an intertidal deposit caused by the 1964 Alaska earthquake, Journal of Research of the U.S. Geological Survey **4** (1976) 151–162.
[256] ATWATER, B.F., et al., Rapid resetting of an estuarine recorder of the 1964 Alaska earthquake, Geological Society of America Bulletin **113** (2001) 1193–1204.
[257] WITTER, R.C., KELSEY, H.M., HEMPHILL-HALEY, E., Pacific storms, El Nino and tsunamis: competing mechanisms for sand deposition in a coastal marsh, Euchre Creek, Oregon, Journal of Coastal Research 17 (2001) 563–583.
[258] SZCZUCIŃSKI, W., The post-depositional changes of the onshore 2004 tsunami deposits on the Andaman Sea coast of Thailand, Natural Hazards **60** (2012) 115–133.
[259] NAKAMURA Y., NISHIMURA, Y., PUTRA, P. S., Local variation of inundation, sedimentary characteristics, and mineral assemblages of the 2011 Tohoku-oki tsunami on the Misawa coast, Aomori, Japan, Sedimentary Geology **282** (2012) 216–227.
[260] OKAMURA, M., MATSUOKA, H., Nankai Earthquake recurrences from tsunami sediment, Kagaku **82** (2012) 182–191 (in Japanese).
[261] MATSUMOTO, D., et al., Thickness and grain-size distribution of the 2004 Indian ocean tsunami deposits in Periya Kalapuwa Lagoon, eastern Sri Lanka, Sedimentary Geology **230** (2010) 95–104.
[262] JAFFE, B., et al., 'Tsunami deposits: Identification and interpretation of tsunami deposits from the June 23, 2001 Peru tsunami', Proceedings of the International Conference on Coastal Sediments 2003, CD-ROM Published by World Scientific Publishing Corp and East Meets West Productions, Corpus Christi, TX, USA. 13.
[263] SUGAWARA, D., GOTO, K., JAFFE, B.E., Numerical models of tsunami sediment transport: Current understanding and future directions, Marine Geology **352** (2014) 295–320.
[264] APOTSOS, A.A., et al., Tsunami sediment transport and deposition in a sediment limited embayment on American Samoa, Earth Science Reviews **10**7 (2011) 1–11.
[265] MOORE, A., JAFFE, B., 'Geologic evidence of tsunamis', Scientific and Technical Issues in Tsunami Hazard Assessment of Nuclear Power Plant Sites, Science Review Working Group 2007, NOAA Tech. Memo. OAR PMEL-136, (2007) 15–21.
[266] WALKER, M.J.C., Quaternary Dating Methods, John Wiley & Sons Ltd. (2005) 286.
[267] NOLLER, J.S., SOWERS, J.M., LETTIS, W.R., (Eds.), Quaternary Geochronology: Methods and Application, AGU, Reference Shelf Series **4** (2000) 582. Wiley.
[268] HUYBERS, P., Glacial variability over the last two million years: An extended depth-derived age model, continuous obliquitiy pacing, and the Pleistocene progression, Quat. Sci. Rev., **26** (2007) 37–55.
[269] SHACKLETON, N.J., SÁNCHEZ-GOÑI, M.F., PALLIER, D., LANCELOT, Y., Marine Isotope Substage 5e and the Eemian Interglacial, Global and Planet Change **36** (2003) 151–155.
[270] BENEDETTI, L., et al., Postglacial slip history of the Sparta Fault (Greece) determined by 36Cl cosmogenic dating: evidence for non-periodic earthquakes, Geophys. Res. Lett. **29** (2002) 8701–8704.
[271] BENEDETTI, L., et al., Motion on the Kaparelli fault (Greece) prior to the 1981 earthquake sequence determined from 36Cl cosmogenic dating, Terra Nova **15** (2003) 118–124.
[272] PALUMBO, L., BENEDETTI, L., BOURLES, D., CINQUE, A., FINKEL, R., Slip history of the Magnola fault (Apennines, Central Italy) from 36Cl surface exposure dating: evidence for strong earthquakes over the Holocene, Earth Planet. Sci. Lett. **225** (2004) 163–176.

[273] NASH, D. B., Morphological dating of degraded normal fault scarps, J. Geol. **88** (1980) 353–360.
[274] NASH, D.B., A general method for morphologic dating of hillslopes, Geology **33** (2005) 693–695.
[275] COOK, E.R., KAIRIUKSTIS, L.A. (Eds.), Methods of Dendrochronology: Application in the Environmental Sciences, Kluwer Academic Publications (1992) 340.
[276] STOFFEL, M., BOLLSCHWEILER, M., BUTLER, D.R., LUCKMAN, B.H. (Eds.), Tree Rings and Natrual Hazards, A State of the art, Advances in global change research **41** (2010) 502., Springer.
[277] RINK, W.J., THOMPSON, J. (Eds.), Encyclopedia of Scientific Dating Methods, 1000. (2015). Springer, http://www.springer.com/earth+sciences +and+geography/geochemistry/book/978-94-007-6303-6
[278] ARNOLD, J.R., LIBBY, W.F., Age determinations by radiocarbon content: checks with samples of known age, Science **110** 2869 (1949) 678–680.
[279] LIBBY, W.L., Radiocarbon Dating, University of Chicago Press, Chicago (1952).
[280] BRONK RAMSEY, C., Radiocarbon calibration and analysis of stratigraphy: The OxCal program, Radiocarbon **37** 2 (1995) 425–430.
[281] STUIVER, M., van der Plicht, J. (Eds.), IntCal 98: Calibration Issue, Radiocarbon **40** 3 (1998).
[282] REIMER, P.J., et al., INTCAL 09 and MARINE09 radiocarbon age calibration curves, 0-50000 years Cal BP, Radiocarbon **51** 4 (2009) 1111–1150.
[283] GREILICH, S., GLASMACHER, U.A., WAGNER, G.A., Spatially resolved detection of luminescence: a unique tool for archaeometry, Naturwissenschaften **89** (2002) 371–375.
[284] PREUSSER, F., et al., Luminescene dating: basic, methods and applications, Eiszeitalter und Gegenwart, QSJ **57** 2 (2008) 95–149, Hannover.
[285] ZREDA, M., NOLLER, J.S., Ages of prehistoric earthquakes revealed by cosmogenic Chlorine-36 in a bedrock fault scarp at Hebgen Lake, Science **282** (1998) 1097–1099.
[286] SCHLAGENHAUF, A., et al., Using in situ Chlorine-36 cosmonuclide to recover past earthquake histories on limestone normal fault scarps: a reappraisal of methodology and interpretations, Geophys. Jour. Int. **182** (2010) 36–72.
[287] SCHLAGENHAUF, A., et al., Earthquake Supercycles in Central Italy, Inferred from ^{36}Cl Exposure Dating, Earth Planet. Sci Letters **307** (2011) 487–500.
[288] CARCAILLET, J., MANIGHETTI, I., CHAUVEL, C., SCHLAGENHAUF, A., NICOLE, J.M., Identifying Past Earthquakes on an Active Normal Fault (Magnola, Italy) from the Chemical Analysis of Its Exhumed Carbonate Fault Plane, Earth Planet. Sci. Letters **271** (2008) 145–158.
[289] RITZ, J.F., et al., Slip rates along active faults estimated with cosmic-ray-exposure dates, Application to the Bogd fault, Gobi Altaï, Mongolia, Geology **23** (1995) 1019–1022.
[290] VAN DER WOERD, J., et al., Holocene left-slip rate determined by cosmogenic surface dating on the Xidatan segment of the Kunlun fault (Qinghai, China), Geology **26** (1998) 695–698.
[291] IVY-OCHS, S., KOBER, F., Surface exposure dating with cosmogenic nuclids, Eiszeitalter und Gegenwart (Quaternary Science Journal) **57** 2 (2008) 179–209.
[292] GOSSE, J.C., PHILLIPS, F.M., Terrestrial in situ cosmogenic nuclides: theory and application, Quat. Sci. Rev. **20** (2001) 1475–1560.
[293] DUNAI, T.J., Cosmogenic Nuclides: Principles, Concepts and Applications in the Earth Surface Sciences, Cambridge University Press, Cambridge, MA (2010) 198.

[294] RENNE, P.R., SHARP, W.D., DEINO, A.L., ORSI, G., CIVETTA, L., $^{40}Ar/^{39}Ar$ dating into the Historical Realm: calibration against Pliny the Younger, Science **277** (1996) 1279–1280.
[295] WAGNER, B., et al., Possible earthquake trigger for 6th century mass wasting deposit at Lake Ohrid (Macedonia/Albania), Clim. Past **8** (2013) 2069–2078.
[296] SHARP, W.D., LUDWIG, K.R., CHADWICK, O.A., AMUNDSON, R., GLASER, L.I., Dating fluvial terraces by 230Th/U on pedogenic carbonate, Wind River Basin, Wyoming, Quat. Research **59** (2003) 139–150.
[297] BAILLIE, M.G.L., Tree-ring Dating and Archaeology, Croom Helm, London (1982) 272.
[298] ESPER, J., COOK, E.R., SCHWEINGRUBER, F.H., Low-frequency signals in long tree-ring chronologies and the reconstruction of past temperature variability, Science **295** (2002) 2250–2253.
[299] JACOBY, G.C., Application of tree ring analysis to paleoseismology, Reviews Geophysics **35** (1997) 109–124.
[300] DE GEER, G., A geochronology of the last 12000 years. Compte Rendu 11 Congrès Géologique International, 11th International Geological Congress 1910, Stockholm, Sweden, **1** (1912) 241–253.
[301] MÖRNER, N.A., Liquefaction and varve disturbance as evidence of paleoseismic events and tsunamis: the autumn 10,430 BP event in Sweden, Quat. Sci. Rev. **15** (1996) 939–948.
[302] BESCHEL, R.E., Ecology and growth of lichens, PhD Thesis, University of Insbruck, Austria (1950).
[303] BULL, W.B., Dating San Andreas fault earthquakes with lichenometry, Geology **24** (1996) 111–114.
[304] BULL, W.B., Tectonic Geomorphology of Mountains: A New Approach to Paleoseismology, Blackwell Publishing (2007).
[305] ZACHARIASEN, J., SIEH, K., TAYLOR, F.W., EDWARDS, R.L., HANTORO, W.S. Submergence and uplift associated with the giant 1833 Sumatran subduction earthquake: Evidence from coral microatolls, J. Geophys. Res. **104** (1999) 895–919.
[306] NATAWIDJAJA, D.H., et al., Interseismic deformation above the Sunda Megathrust recorded in coral microatolls of the Mentawai islands, West Sumatra, J. Geophys. Res. **112** B02404 (2007).
[307] ROCKWELL, T.K., 'Use of soil geomorphology in fault studies', Quaternary Geochronology: Methods and Applications, Noller, J.S., SOWERS, J.M., LETTIS, W.R., Eds., AGU Reference Shelf 4, American Geophysical Union, Washington D.C. (2000) 273–292.
[308] TUTTLE, M.P., COLLIER, J., WOLF, L. W., LAFFERTY, R.H., New evidence for a large earthquake in the New Madrid seismic zone between AD 1400 and 1670, Geology **27** 9 (1999) 771–774.
[309] SILVA, P. G., et al., 'Geological and archaeological record of the 1504 AD Carmona Earthquake (Guadalquivir Basin, South Spain): A Review after Bonsor (1918) based on the ESI-2007 Scale', Earthquake Archaeology and Palaeoseismology in the Alpine-Himalaya Collision Zone, PÉREZ-LÓPEZ, R., et al. Eds., Proceeding 1st INQUA-IGCP-567 Workshop (2009) 139–142.
[310] GENTY, D., et al., Calculation of past dead carbon proportion and variability by the comparison of AMS 14C and TIMS U/Th ages on two Holocene stalagmites, Radiocarbon **41** 3 (1999) 251–270.
[311] GENTY, D., BAKER, A., VOKAL, B., (2001). Intra- and inter- annual growth rate of modern stalagmites, hemical Geology **176** (2001) 193–214.

[312] WOODHEAD, J., PICKERING, R., Beyond 500ka: Progress and prospects in the UPb chronology of speleothems, and their application to studies in paleoclimate, human evolution, biodiversity and tectonics, Chemical Geology **322–323** (2012) 290–299.
[313] PONS-BRANCHU, E., HAMELIN, B., BRULHET, J., BRUXELLES, L., Speleothem rupture in karst: tectonic or climatic origin? U-Th dating of rupture events in Salamandre Cave (Gard, South-Eastern France), Bulletin de la Société Géologique de France **175** (2004) 473–479.
[314] STIRLING, M.W., RHOADES, D., BERRYMAN, K., Comparison of earth scaling relations derived from data of the instrumental and preinstrumental Era, Bull. Seism. Soc. Am. **92** 2 (2002) 812–830.
[315] HANKS, T.C., KANAMORI, H., A moment magnitude scale, J. Geophys. Res. **84** (1979) 2348–2350.
[316] AKI, K., RICHARD, P.G., 'Theory and methods', Quantitative Seismology, Freeman, W.H., San Francisco, California (1980).
[317] STIRLING, M., GODED, T., BERRYMAN, K., LITCHFIELD, N., Selection of earthquake scaling relationships for seismic hazard analysis, Bull. Seism. Soc. Am. **103** 6 (2013) 2993–3011.
[318] STIRLING, M., GODED, T., 'Magnitude scaling relationships', Report Produced for the GEM Faulted Earth & Regionalisation Global Componets, GNS Science Miscellaneous Series **42** (2012) 35.
[319] HANKS, T.C., BAKUN, W.H., M-logA observations for recent large earthquakes, Bull. Seism. Soc. Am. **98** (2008) 490–494.
[320] WESNOUSKY, S.G., Displacement and geometrical characteristics of earthquake surface ruptures: Issues and implications for seismic hazard analysis and the process of earthquake rupture, Bull. Seism. Soc. Am. **98** 4 (2008) 1609–1632.
[321] LEONARD, M., Earthquake fault scaling: Relating rupture length, width, average displacement and moment release, Bull. Seism. Soc. Am. **100** 5A (2010) 1971–1988.
[322] YEN, Y.T., MA, K.F., Source scaling relationship for M 4.6-8.1 earthquakes, specifically for earthquakes in the collision zone of Taiwan, Bull. Seism. Soc. Am. **101** 2 (2011) 464–481.
[323] STIRLING, M. et al., Seismic hazard of the Canterbury region, New Zealand: New earthquake source model and methodology, Bull. New Zeal. Natl. Soc. Earthq. Eng. **41** (2008) 51–67.
[324] ANDERSON, J.G., WESNOUSKY, S.G., STIRLING, MARK, W., Earthquake size as a function of fault slip rate, Bull. Seism. Soc. Am. **86** 3 (1996) 683–690.
[325] NUTTLI, O., Average seismic source-parameter relations for mid-plate earthquakes, Bull. Seism. Soc. Am. **73** 2 (1983) 519–535.
[326] STRASSER, F.O., ARANGO M.C., BOMMER J.J., Scaling of the source dimensions of interface and intraslab subduction-zone earthquakes with moment magnitude, Seism. Res. Lett. **81** 6 (2010) 941–950.
[327] BLASER, L., KRUGER, F., OHRNBERGER, M., SCHERBAUM, F., Scaling relations of earthquake source parameter estimates with special focus on subduction environment, Bull. Seism. Soc. Am. **100** 6 (2010) 2914–2926.
[328] ICHINOSE, G.E., THIO, H.K., SOMERVILLE, P.G., Moment tensor and rupture model for the 1949 Olympia, Washington, earthquake and scaling relations for Cascadia and global intraslab earthquakes, Bull. Seism. Soc. Am. **96** 3 (2006) 1029–1037.
[329] VILLAMOR, P., et al., Waikato Seismic Loads: Revision of Seismic Source Characterisation, GNS Client Report, 2001/59 (2001).

[330] GUERRIERI, L., et al., The INQUA TERPRO Project No. 0811 Working Group, 'Earthquake environmental effects, intensity and seismic hazard assessment: the EEE catalogue (INQUA Project #0418)', Earthquake Geology (Proceedings of the 2nd INQUA - IGCP 567 Workshop on Active Tectonics), Archaeology and Engineering, Corinto (Greece) 18–25 September (2011) 62–65.
[331] GUERRIERI, L., et al., Earthquake environmental effects for seismic hazard assessment: the ESI intensity scale and the EEE Catalogue, Mem. Descr. Carta Geologica d'Italia 95. (in press). http://www.isprambiente.gov.it/en/projects/soil-and-territory/inqua-scale/documents.
[332] REITER. L., Earthquake Hazard Analysis: Issues and insights, Columbia University Press, New York (1990) 254.
[333] BARATTA, M., 'I terremoti d'Italia. Saggio di storia', Geografia e Bibliografia Sismica Italiana, Arnaldo Forni Editore, Torino (1901) 952.
[334] ESPINOSA, A.F., HUSID, R., QUESADA, A., 'Intensity distribution and source parameters from field observations', The Guatemalan Earthquake of February 4, 1976: a Preliminary Report, Espinosa, A.F. ed., U.S. Geological Survey Professional Paper 1002, U.S. Govt. Print. Off., Washington (1976) 52–66.
[335] ESPINOSA, A.F., HUSID, R., ALGERMISSEN, S.T., DE LAS CASAS, J., The Lima earthquake of October 3, 1974, intensity distribution, Bull. Seism. Soc. Am. **67** (1976) 1429–1440.
[336] GRUNTHAL, G., European Macroseismic Scale 1998 (EMS-98), European Seismological Commission, Subcommission on Engineering Seismology, Working Group Macroseismic Scales. Conseil de l'Europe, Cahiers du Centre Européen de Géodynamique et de Séismologie, 15, Luxembourg (1998) 99.
[337] MUSSON, R., GRÜNTHAL, G., STUCCHI, M., The comparison of macroseismic intensity scales, Journal of Seismology **14** 2(2010) 413–428.
[338] DENGLER, L., MCPHERSON, R., The 17 August 1991 Honeydew earthquake North Coast California: a case for revising the Modified Mercalli Scale in sparsely populated areas, Bull. Seism. Soc. Am. **83** (1993) 108–1094.
[339] DOWRICK, D. J., The Modified Mercalli earthquake intensity scale- revisions arising from recent studies of New Zealand earthquakes, Bull. NZ Nat. Soc. for Earthq. Eng. **29** 2 (1996) 92–106.
[340] ESPOSITO, E., PORFIDO, S., MASTROLORENZO, G., NIKONOV, A.A., SERVA, L., 'Brief review and preliminary proposal for the use of ground effects in the macroseismic intensity assessment', Proc. 30th Int. Geol. Congr., Beijing, China **5** (1997) 233–243.
[341] MICHETTI, A.M., et al., 'The INQUA scale: an innovative approach for assessing earthquake intensities based on seismically-induced ground effects in the environment', Special Paper, VITTORI, E., COMERCI, V., Eds., Memorie Descrittive Della Carta Geologica d'Italia **67** (2004) 120.
[342] AZUMA, T., OTA, Y., 'Comparison between seismic ground effects and instrumental seismic intensity–an example from a study on the 2004 Chuetsu earthquake in Central Japan', EGU 2006, Geophysical Research Abstracts **8** 01004 (2006).
[343] BERZHINSKII, Yu.A., et al., Application of the ESI_2007 scale for estimating the intensity of the Kultuk earthquake, August 27, 2008 (South Baikal), Seismic Instruments Allerton Press Inc. **46** 4 (2010) 307–324.
[344] FOKAEFS, A., PAPADOPOULOS, G., Testing the new INQUA intensity scale in Greek earthquakes, Quaternary International **173/174** (2007) 15–22.
[345] GOSAR, A., Application of environmental seismic intensity scale (ESI 2007) to Krn mountains 1998 Mw = 5.6 earthquake (NW Slovenia) with emphasis on rockfalls, Nat. Hazards Earth Syst. Sci. **12** (2012) 1659–1670.

[346] GUERRIERI, L., et al., 'Earthquake environmental effects (EEE) and intensity assessment: the INQUA scale project', Special Section: Tectonic Geomorphology, Dramis, F., Galadini, F., Galli, P., Vittori, E. Eds., Boll. Soc. Geol. It. **126** 2 (2007) 375–386.
[347] GUERRIERI, L., et al., Capable faulting, environmental effects and seismic landscape in the area affected by the 1997 Umbria-Marche (Central Italy) seismic sequence, Tectonophysics **476** 2 (2008) 269–281.
[348] GUERRIERI, L., et al., Earthquake environmental effects induced by the 2012 seismic sequence in Emilia: implications for seismic hazard assessment in Northern Italy, 3rd INQUA-IGCP-567 International Workshop on Active Tectonics, Paleoseismology and Archaeoseismology, Morelia, Mexico (2012) 6.
[349] LALINDE, C. P., SANCHEZ, J.A., Earthquake and environmental effects in Colombia in the last 35 years, INQUA Scale Project, Bull. Seism. Soc. Am. **97** 2 (2007) 646–654.
[350] LEKKAS, E.L., The 12 May 2008 Mw 7.9 Wenchuan, China, Earthquake: Macroseismic Intensity Assessment Using the EMS-98 and ESI 2007 Scales and Their Correlation with the Geological Structure, Bull. Seism. Soc. Am. **100** (2010) 2791–2804.
[351] LIVIO, F., et al., 'Macroseismic investigation of the 2012 Po Plain sequence using the ESI 2007 scale, and comparison with the MCS scale', Proceedings 31° Convegno Nazionale Gruppo Nazionale Geofisica della Terra Solida, In: SLEJKO, D., REBEZ, A., ARGNANI, A., DEL PEZZO, E., GALLI, P., PETRINI, R., SERPELLONI, E., SOLARINO, S., Tema 1: Geodinamica (2012)70–75.
[352] MOSQUERA-MACHADO, S., LALINDE-PULIDO, C., SALCEDO-HURTADO, E., MICHETTI, A.M., Ground effects of the October 18, 1992, Murindo Earthquake (NW Colombia), using the Environmental Seismic Intensity Scale (ESI 2007) for the assessment of the intensity, Geol. Soc. London Spec. Publ. **316** (2009) 123–144.
[353] OTA, Y., CHEN, Y.G., CHEN, W.S., Review of paleoseismological and active fault studies in Taiwan in the light of the Chichi earthquake of September 21, 1999, Tectonophysics **408** 4 (2009).
[354] PAPANIKOLAOU, I.D., PAPANIKOLAOU, D.I., LEKKAS, E.L., 'Advances and limitations of the Environmental Seismic Intensity scale (ESI 2007) regarding near-field and far-field effects from recent earthquakes in Greece: implications for the seismic hazard assessment', In Paleoseismology: Historical and Prehistorical Records of Earthquake Ground Effects for Seismic Hazard Assessment, REICHERTER, K., MICHETTI, A.M., SILVA BARROSO, P.G. Eds., Geol. Soc. London Spec. Publ. **316** (2009) 11–30.
[355] PAPANIKOLAOU, I., Uncertainty in intensity assignment and attenuation relationships: How seismic hazard maps can benefit from the implementation of the Environmental Seismic Intensity scale (ESI 2007), Quaternary International **242** (2011) 42–51.
[356] PAPATHANASSIOU, G., VALKANIOTIS, S., PAVLIDES, S., Applying the INQUA Scale to the Sofaeds 1954, Central Greece earthquake, Bull. Geol. Soc. of Greece **37** (2007) 1226–1233.
[357] PAPATHANASSIOU, G., PAVLIDES, S., Using the INQUA Scale for the Assessment of Intensity: Case Study of the 2003 Lefkada (Ionian Islands), Greece Earthquake, Quaternary International **173–174** (2007) 4–14.
[358] PORFIDO, S., et al., Seismically induced ground effects of the 1805, 1930 and 1980 earthquakes in the Southern Apennines, Italy, Ital. J. Geosci. (Boll. Soc. Geol. It.) **126** (2007) 333–346.

[359] SERVA, L., et al., Environmental effects from some historical earthquakes in Southern Apennines (Italy) and macroseismic intensity assessment, Contribution to INQUA EEE scale project, Quaternary International **173–174** (2007) 30–44.
[360] SINTUBIN, M., STEWART, I., A logical methodology for archaeoseismology: a proof of concept at the archaeological site of Sagalassos, Southwest Turkey, Bull. Seism. Soc. Am. **98** (2008) 2209–2230.
[361] TATEVOSSIAN, R.E., The Verny 1887 Earthquake in Central Asia: Application of the INQUA Scale based on Coseismic Environmental Effects, Dark Nature: Rapid Environmental Change and Human Response, Quaternary International **173–174** (2007) 23–29.
[362] AZZARO, R., Earthquake surface faulting at Mount Etna Volcano (Sicily) and implications for active tectonics, Journal of Geodynamics **28** (1999)193–213.
[363] RICHTER, C.F., Elementary Seismology, FREEMAN, W.H., and Co, San Francisco (1958) 768.
[364] BONILLA, M. G., Evaluation of Potential Surface Faulting and Other Tectonic Deformation, U.S. Geol. Surv. Open File Rep 82-0732 (1982) 1–91.
[365] ZIONY, J.I., YERKES, R.F., 'Evaluating earthquake and surface-faulting potential', Evaluating Earthquake Hazards in the Los Angeles Region: An Earth-Science Perspective, ZIONY, J. I. Ed., U.S. Geol. Surv. Prof. Pap. **1360** (1985) 43–92.
[366] TUTTLE, M.P., The liquefaction method for assessing paleoseismicity, U.S. Nucl. Regul. Comm., NUREG/CR **6258** (1994) 1–38.
[367] OBERMEIER, S.F. (Ed.), Paleoliquefaction and Appraisal of Earthquake Hazards, Engineering Geology **76** (2005) 177–320.
[368] CROZIER, M. J., 'Determination of paleoseismicity from landslides', In Landslides (Glissements de terrain), , Proceedings of the 6th International Symposium, Christchurch, New Zealand (Bell, D.H. Ed.,), A. A. Balkema, Rotterdam **2** (1992) 1173–1180.
[369] JIBSON, R.W., 'Using landslides for paleoseismic analysis', Paleoseismology, (McCalpin, J. Ed.), Academic Press, London (1996) 397– 438.
[370] DOMINEY-HOWES, T.M., HUMPHREYS, G.S., HESSE, P.P., Tsunami and paleotsunami depositional signatures and their potential value in understanding the late-Holocene tsunami record, Holocene **16** 88 (2006) 95–107.
[371] MACHETTE, M., HALLER, K., WALD, L., Quaternary Fault and Fold Database for the Nation, USGS Fact Sheet 2004-3033, (2004).
[372] KOEHLER, R.D., FARRELL, R.E. BURNS, P.A.C., COMBELLICK R.A., Quaternary faults and folds in Alaska: A digital database, Alaska Division of Geological & Geophysical Surveys Miscellaneous Publication **141** (2012).
[373] AIST, ACTIVE FAULT DATABASE OF JAPAN, DECEMBER 13, 2008 VERSION (Research Information Database DB095), National Institute of Advanced Industrial Science and Technology (2008).
[374] YOSHIOKA, T., AWATA, Y., SHIMOKAWA, Y., FUSEJIMA, Y., Explanatory text of the Rupture Probability Map of Major Active Faults in Japan, Tectonic Map Series 14, Geological Survey of Japan, AIST, Japan (2005).
[375] McCALPIN, J.P., Paleoseismology, Academic Press, New York (1996) 588.
[376] JONGENS, R., DELLOW, G., The Active Faults Database of New Zealand: Data Dictionary, Institute of Geological and Nuclear Sciences, Science Report **17** (2003).
[377] GARCÍA-MAYORDOMO, J., et al., The Quaternary active faults database of Iberia (QAFI v.2.0), Journal of Iberian Geology, **38** (2012) 285–302.
[378] COMERCI, V., et al., 'ITHACA Project and Capable Faults in the Po Plain (Northern Italy)', Ingegneria Sismica: Special Issue, Seismic risk in the Po Plain, 1-2 (2013) 36–50.

[379] MICHETTI, A.M., SERVA, L., VITTORI, E., ITHACA (Italy Hazard from Capable Faulting), A Database of Active Capable Faults of the Italian Onshore Territory, Internal Report of Agenzia Nazionale Protezione Ambiente, Rome (2000), CD-ROM.
[380] CLARK, D., MCPHERSON, A., COLLINS, C.D.N., Australia's Seismogenic Neotectonic Record: A Case for Heterogeneous Intraplate Deformation, Geoscience Australia Record 2011/11, GeoCat No. 70288 (2011b) 95.
[381] BASILI, R., et al., The Database of Individual Seismogenic Sources (DISS), version 3: Summarizing 20 Years of Research on Italy's Earthquake Geology, Tectonophysics **453** 1(2007) 20–43.
[382] SESETYAN, K., Earthquake Model of the Middle East Region(EMME): Hazard, Risk Assessment, Economics & Mitigation, A GEM Regional Project, GEM Outreach Meeting, Beijing, China (2011).
[383] BASILI, R., KASTELIC, V., 'Database of active faults and seismogenic sources', Seismic Hazard Harmonization in Europe Deliverable Report D3.4, National Institute of Geophysics and Volcanology, Italy (2011).
[384] CAPUTO, R., CHATZIPETROS, A., PAVLIDES, S., SBORAS, S., The Greek Database of Seismogenic Sources (GreDaSS): state of the art for Northern Greece, Annals of Geophysics **55** 5 (2012) 859–894.
[385] HARP, E.L., JIBSON, R.W., Landslides triggered by the 1994 Northridge, California, earthquake, Bull. Seism. Soc. Am. **86** (1996) 319–332.
[386] FORTUNATO, C., MARTINO, S., PRESTININZI, A., ROMEO, R.W., New release of the Italian catalogue of earthquake-induced ground failures (CEDIT), Italian Journal of Engineering Geology and Environment **2** (2012) 63–74, (with map).
[387] RESEARCH GROUP FOR ACTIVE FAULTS OF JAPAN, Active Faults in Japan: Sheet Maps and Inventories, University of Tokyo Press (1991).
[388] NAKATA, T., IMAIZUMI, T., (Eds.), Digital active fault map of Japan, University of Tokyo Press (2002).
[389] NODA, S., et al., 'Response spectra for design purpose of stiff structures on rock sites', Proc. of the OECD-NEA Workshop on the Relations Between Seismological Data and Seismic Engineering Analysis, Istanbul (2002) 16–18.
[390] THE HEADQUARTERS FOR EARTHQUAKE RESEARCH PROMOTION, Strong Ground Motion Prediction Method ('Recipe') for Earthquakes with Specified Source Faults (2009b).
[391] THE NUCLEAR SAFETY COMMISSION OF JAPAN, Regulatory Guide for Reviewing Seismic Design of Nuclear Power Reactor Facilities (2006).
[392] MITZUTANI, H., YASHIRO, K., KATO, K., TAKEMURA, M., DAN, K., Response spectra by blind faults for design purpose of stiff structures on rock sites, SMiRT 18-K03-1, (2005) 3016–3018.
[393] ABE, K., Estimate of Tsunami heights from magnitudes of earthquake and tsunami, Bull. Earthq. Res. Inst., Univ. Tokyo **64** (1989) 51–69 (in Japanese).
[394] ABE, H., SUGENO, Y., CHIGAMA, A., Estimation of the height of the Sanriku Jogan 11 earthquake-tsunami (A.D. 869) in the Sendai plain, Zisin 2nd **43** 4 (1990) 513–525 (in Japanese).
[395] HATORI, T., Tsunami magnitude and wave source regions of historical Sanriku tsunamis in Northeast Japan, Bulletin of the Earthquake Research Institute **50** (1975) 397–414 (in Japanese)[with English abstract].
[396] SATAKE, K., NAMEGAYA, Y., YAMAKI, S., Numerical Simulation of the AD869 Jogan Tsunami in Ishinomaki and Sendai plains, Annual Report on Active Fault and Paleoearthquake Researches, Geological Survey of Japan **8** (2008) 71–89. (in Japanese).

[397] AIDA, I., Simulations of large tsunamis occurring in the past off the Coast of the Sanriku district, Bulletin of the Earthquake Research Institute **52** (1977) 71–101 (in Japanese) [with English abstract].
[398] JAPAN SOCIETY OF CIVIL ENGINEERS, Tsunami Assessment Method for Nuclear Power Plants in Japan (2002). http://committees.jsce.or.jp/ceofnp/node/5
[399] (HERP) THE HEADQUARTERS FOR EARTHQUAKE RESEARCH PROMOTION, Multidisciplinary research project for earthquake off the coast of Fukushima Prefecture, 2005-2009 fiscal year final report (2009a). (in Japanese) http://www.jishin.go.jp/main/chousakenkyuu/miyagi_juten/h17_21/index.htm
[400] MINOURA, K., Tsunami Deposits, Gekkan Chikyu **17** (1995) 541–547. (in Japanese).
[401] SUGAWARA, D., MINOURA, K., IMAMURA, F., Field survey on deposits corresponded to AD 869 Jogan tsunami, Gekkan Chikyu, especial edition **28** (2002) 110-117 (in Japanese).
[402] PETERSEN, M.D., et al., Documentation for the 2008 Update of the United States National Seismic Hazard Maps, U.S. Geological Survey Open-file Report 2008-1128, (2008) 60.
[403] ELECTRIC POWER RESEARCH INSTITUTE (EPRI), Seismic Hazard Methodology for the Central and Eastern United States, 10 vol, EPRI-NP-4726, Palo Alto, California (1988).
[404] BAKUN, W.H., HOPPER, M.G., Magnitudes and locations of the 1811-1812 new Madrid, Missouri, and 1886 Charleston, South Carolina, earthquakes, Bull. Seism. Soc. Am. **94** (2004) 64–75.
[405] TALWANI, P., The Source and Magnitude of the Charleston Earthquakes, presentation at CEUS-SSC Project Workshop No. 2, February 18–20, Palo Alto, CA, USA (2009).
[406] TALWANI, P., COX, J., Paleoseismic evidence for recurrence of earthquakes near Charleston, South Carolina, Science **228** (1985) 379–381.
[407] OBERMEIER, S.F., WEEMS, R.E., JACOBSON, R.B., GOHN, G.S., Liquefaction evidence for repeated Holocene earthquakes in the coastal region of South Carolina, Annals of the New York Academy of Sciences **558** (1989) 183–195.
[408] WEEMS, R.E., OBERMEIER, S.F., The 1886 Charleston earthquake: An overview of geological studies, Proceedings of the U.S. Nuclear Regulatory Commission Seventeenth Water Reactor Safety Information Meeting, NUREG/CP-0105, **2** (1990) 289–313.
[409] AMICK, D., GELINAS, R., MAURATH, G., CANNON, R., MOORE, D., BILLINGTON, E., KEMPPINEN, H., Paleoliquefaction Features along the Atlantic Seaboard, U.S. Nuclear Regulatory Commission, NUREG/CR-5613 RA (1990) 146.
[410] AMICK, D., MAURATH, G., GELINAS, R., Characteristics of seismically induced liquefaction sites and features located in the vicinity of the 1886 Charleston, South Carolina earthquake, Seismological Research Letters **61** (1990) 117–130.
[411] TALWANI, P., SCHAEFFER, W., Recurrence rates of large earthquakes in the South Carolina Coastal Plain based on paleoliquefaction data, J. Geophys. Res. **106** (2001) 6621–6642.
[412] TALWANI, P., DURA-GOMEZ, I., GASSMAN, S., HASEK, M., CHAPMAN, A., Studies related to the discovery of a prehistoric sandblow in the epicentral area of the 1886 Charleston SC earthquake: Trenching and geotechnical investigations, Programs and Abstracts, Eastern Section of the Seismological Society of America (2008) 50.
[413] HU, K., GASSMAN, S.L., TALWANI, P., In-situ properties of soils at paleoliquefaction sites in the South Carolina Coastal Plain, Seismological Research Letters **73** (2002) 964–978.
[414] HU, K., GASSMAN, S.L., TALWANI, P., Magnitudes of prehistoric earthquakes in the South Carolina coastal plain, Seismological Research Letters **73** (2002) 979–991.

[415] LEON, E., Effect of aging of sediments on paleoliquefaction evaluation in the South Carolina Coastal Plain, unpublished Ph.D. dissertation, University of South Carolina (2003) 181.
[416] LEON, E., GASSMAN, S.L., TALWANI, P., Effect of soil aging on assessing magnitudes and accelerations of prehistoric earthquakes, Earthquake Spectra **21** (2005) 737–759.
[417] GASSMAN, S., TALWANI, P., HASEK, M., 'Magnitudes of Charleston, South Carolina earthquakes from In Situ geotechnical data' in: presentation given at meeting of CEUS Earthquake Hazards Program, U.S. Geological Survey, October 28-29, Memphis, Tennessee (2009).
[418] JORDAN, T., et al., Andean tectonics related to geometry of subducted Nazca plate, Bull. Seism. Soc. Am. **94** (1983) 341–361.
[419] JORDAN, T., ALLMENDINGER, R., The Sierras Pampeanas of Argentina: A modern analogue of Rocky Mountains foreland deformation, American Journal of Science **286** (1986) 737–764.
[420] RAMOS, V., CRISTALLINI, E., PÉREZ, D., The Pampean flat-slab of the Central Andes, Journal of South American Earth Sciences **15** (2002) 59–78.
[421] COSTA, C.H., et al., Map and Database of Quaternary Faults and Folds in Argentina, USGS Open-File Report 00-0108 (2000).
[422] LANGER, C., HARTZELL, S., Rupture distribution of the 1977 western Argentina earthquake, Phys. Earth Planet. Inter. **94** (1996) 121–132.
[423] INPRES, Microzonificacion sismica del valle de Tulum, Provincia de San Juan: Resumen Ejecutivo, San Juan, Instituto Nacional de Prevención Sísmica, (1982) 120.
[424] COSTA, C., VITA-FINZI, C., Late Holocene intraplate faulting in the SE Sierras Pampeanas, Argentina, Geology **24** (1996) 1127–1130.
[425] COSTA, C., MURILLO, V., SAGRIPANTI, G., GARDINI, C., Quaternary intraplate deformation in the southeastern Sierras Pampeanas, Argentina, Journal of Seismology **5** (2001) 399–409.
[426] COSTA, C., et al., 'Holocene paleoearthquake clustering along a Sierras Pampeanas (Argentina) bounding fault?' AGU, San Francisco, Calif., 13–17 Dec. 2010 (Abstract T42A05-8107 presented at 2010 Fall Meeting).
[427] COSTA, C., CESCO, J., MORÁN, R., A simple graphical method for estimating the components of the fault-slip vector, Journal of Structural Geology **19** (1997) 1245–1247.
[428] COSTA, C., 'The seismogenic potential for large earthquakes at the southern most Pampean flat-slab (Argentina) from a geologic perspective', Proceedings V International Symposium on Andean Geodynamics (2005) 211–214.
[429] IRWIN, W.P., BARNES, I., Effect of geologic structure and metamorphic fluids on seismic behavior of the San Andreas fault system in central and northern California, Geology **3** (1975) 713–716.
[430] GRATIER, J.P., et al., Geological control of the partitioning between seismic and aseismic sliding behaviours in active faults: Evidence from the Western Alps, France, Tectonophysics **600** (2013) 226–242.
[431] NODA, H., LAPUSTA, N., Stable creeping fault segments can become destructive as a result of dynamic weakening, Nature **493** (2012).
[432] CHANG et al., Modelling temporal variation of surface creep on the Chihshang fault in eastern Taiwan with velocity-strengthening friction, Geophys. J. Int. **176** (2009) 601–613.
[433] KANAMORI, H., 'Seismic and aseismic slip along subduction zones and their tectonic implications'. Island Arcs, Deep Sea Trenches and Back-Arc Basins, Maurice Ewing Series, vol. 1 (TALWANI, M., PITMAN, W.C. Eds.), Am. Geophys. Union, Washington, DC (1977) 163–174.

[434] IGARASHI et al., Repeating earthquakes and interplate aseismic slip in the northeastern Japan subduction zone, J. Geophys. Res. **108** (2003), 2249.
[435] CHLIEH, M., et al., Heterogeneous coupling of the Sumatran megathrust constrained by geodetic and paleogeodetic measurements, J. Geophys. Res. **113** (2008), B05305.
[436] PERFETTINI, H., et al., Seismic and aseismic slip on the Central Peru megathrust, Nature 465 (2010) 78–81.
[437] LIENKAEMPER, J.J., BORCHARDT, G., Holocene slip rate of the Hayward fault at Union City, California, J. Geophys. Res. **101** (1996) 6099–6108.
[438] LIENKAEMPER, J.J., et al., Evidence for a twelfth large earthquake on the Southern Hayward Fault in the Past 1900 Years, Bull. Seism. Soc. Am. **10** (2010) 2024–2034.
[439] LEE et al., Continuous monitoring of an active fault in a plate suture zone: a creepmeter study of the Chihshang Fault, eastern Taiwan, Tectonophysics **333** (2001) 219-240.
[440] KANEKO Y., FIALKO, Y., SANDWELL, D.T., TONG, X., FURUYA, M., Interseismic deformation and creep along the central section of the North Anatolian Fault (Turkey): InSAR observations and implications for rate-and-state friction properties, J. Geophys. Res., Solid Earth **118** (2013) 316–331.
[441] KUTOGLU, et al., Can a creeping segment become a monitor before destructive major earthquakes? Natural Hazards **65** (2013) 2161–2173.
[442] BURBANK, D.W., ANDERSON, R.S., Tectonic Geomorphology, John Wiley and Sons (2011).
[443] WALLACE, R.E., Profiles and ages of young fault scarps, north-central Nevada, Bull. Geol. Soc. Am. **88** (1977) 1267–1281.
[444] AVOUAC J.P., Analysis of scarp profiles: Evaluation of errors in morphologic dating. J. Geophys. Res.: Solid Earth, **98** B4 (1993) 6745–6754.
[445] LIENKAEMPER, J.J., WILLIAMS, P.L., A record of large earthquakes on the Southern Hayward fault for the past 1800 years, Bull. Seism. Soc. Am. **97** (2007) 1803–1819.
[446] LIENKAEMPER, J.J., et al., A record of large earthquakes on the Southern Hayward fault for the past 500 years, Bull. Seism. Soc. Am. **92** 7 (2002) 2637–2658.
[447] DAWSON, et al., Irregular recurrence of paleoearthquakes along the central Garlock fault near El Paso Peaks, California, J. Geophys. Res. **108** (2003), 2356.
[448] NELSON, et al., Multiple large earthquakes in the past 1500 years on a fault in metropolitan Manila, the Philippines, Bull. Seism. Soc. Am. **90** (2000) 73–85.
[449] CASHMAN et al., Microstructures developed by coseismic and aseismic faulting in near surface sediments, San Andreas fault, California, Geology **35** (2007) 611–614.
[450] RICHTER, C.F., An instrumental earthquake magnitude scale, Bull. Sesim. Soc. Am. **25** (1935) 1–32

CONTRIBUTORS TO DRAFTING AND REVIEW

Baize, S.	Institut de radioprotection et de sûreté nucléaire, IRSN, France
Blumetti, A.M.	Instituto Superiore per la Protezione e la Ricerca Ambientale, ISPRA, Italy
Costa, C.	University of San Juan, Argentina
Cushing, E.M.	Institut de radioprotection et de sûreté nucléaire, IRSN, France
Decker, K.	University of Vienna, Austria
Fukushima, Y.	International Atomic Energy Agency
Guerrieri, L.	Istituto Superiore per la Protezione e la Ricerca Ambientale, ISPRA, Italy
Hintersberger, E.	University of Vienna, Austria
Hirata, K.	Tohoku EPC, Japan
Itoh, G.	Tohoku EPC, Japan
Jaffe, B.	US Geological Survey, United States of America
Mason, J.	University of Aachen, Germany
Mc Duffie, S.	US Department of Energy, United States of America
Michetti, A.M.	University of Insubria, Italy
Nishimura, Y.	University of Hokkaido, Japan
Perez Lopez, R.	Instituto Geologico y Minero de Espana, IGME, Spain
Pervaiz, K.	Pakistan Atomic Energy Commission, PAEC, Pakistan
Reicherter, K.	RWTH Aachen University, Germany
Romeo, R.	University of Urbino, Italy
Roncoroni, M.	University of Insubria, Italy
Sanchez-Cabanero J.	Consejo de Seguridad Nuclear, CSN, Spain
Schlittenhardt, J.	Federal Institute for Geosciences and Natural Resources, BGR, Germany
Serva L.	Professional Consultant, Italy
Silva Barroso P.	University of Salamanca, Spain
Spies, T.	Federal Institute for Geosciences and Natural Resources, BGR, Germany
Tuttle, M.	Tuttle & Associates, United States of America
Uchida, J.	Japan Nuclear Energy Safety Organization, JNES, Japan
Vittori, E.	Istituto Superiore per la Protezione e la Ricerca Ambientale, ISPRA, Italy

Consultants Meetings

Modena, Italy: 2-4 October 2012
Vienna, Austria: 22-23 January 2013
Roma, Italy: 17-19 June 2013
Aachen, Germany: 9 October 2013
Vienna, Austria: 1-2 December 2014

IAEA
International Atomic Energy Agency

No. 23

ORDERING LOCALLY

In the following countries, IAEA priced publications may be purchased from the sources listed below or from major local booksellers.

Orders for unpriced publications should be made directly to the IAEA. The contact details are given at the end of this list.

AUSTRALIA
DA Information Services
648 Whitehorse Road, Mitcham, VIC 3132, AUSTRALIA
Telephone: +61 3 9210 7777 • Fax: +61 3 9210 7788
Email: books@dadirect.com.au • Web site: http://www.dadirect.com.au

BELGIUM
Jean de Lannoy
Avenue du Roi 202, 1190 Brussels, BELGIUM
Telephone: +32 2 5384 308 • Fax: +32 2 5380 841
Email: jean.de.lannoy@euronet.be • Web site: http://www.jean-de-lannoy.be

CANADA
Renouf Publishing Co. Ltd.
5369 Canotek Road, Ottawa, ON K1J 9J3, CANADA
Telephone: +1 613 745 2665 • Fax: +1 643 745 7660
Email: order@renoufbooks.com • Web site: http://www.renoufbooks.com

Bernan Associates
4501 Forbes Blvd., Suite 200, Lanham, MD 20706-4391, USA
Telephone: +1 800 865 3457 • Fax: +1 800 865 3450
Email: orders@bernan.com • Web site: http://www.bernan.com

CZECH REPUBLIC
Suweco CZ, spol. S.r.o.
Klecakova 347, 180 21 Prague 9, CZECH REPUBLIC
Telephone: +420 242 459 202 • Fax: +420 242 459 203
Email: nakup@suweco.cz • Web site: http://www.suweco.cz

FINLAND
Akateeminen Kirjakauppa
PO Box 128 (Keskuskatu 1), 00101 Helsinki, FINLAND
Telephone: +358 9 121 41 • Fax: +358 9 121 4450
Email: akatilaus@akateeminen.com • Web site: http://www.akateeminen.com

FRANCE
Form-Edit
5 rue Janssen, PO Box 25, 75921 Paris CEDEX, FRANCE
Telephone: +33 1 42 01 49 49 • Fax: +33 1 42 01 90 90
Email: fabien.boucard@formedit.fr • Web site: http://www.formedit.fr

Lavoisier SAS
14 rue de Provigny, 94236 Cachan CEDEX, FRANCE
Telephone: +33 1 47 40 67 00 • Fax: +33 1 47 40 67 02
Email: livres@lavoisier.fr • Web site: http://www.lavoisier.fr

L'Appel du livre
99 rue de Charonne, 75011 Paris, FRANCE
Telephone: +33 1 43 07 50 80 • Fax: +33 1 43 07 50 80
Email: livres@appeldulivre.fr • Web site: http://www.appeldulivre.fr

GERMANY
Goethe Buchhandlung Teubig GmbH
Schweitzer Fachinformationen
Willstätterstrasse 15, 40549 Düsseldorf, GERMANY
Telephone: +49 (0) 211 49 8740 • Fax: +49 (0) 211 49 87428
Email: s.dehaan@schweitzer-online.de • Web site: http://www.goethebuch.de

HUNGARY
Librotade Ltd., Book Import
PF 126, 1656 Budapest, HUNGARY
Telephone: +36 1 257 7777 • Fax: +36 1 257 7472
Email: books@librotade.hu • Web site: http://www.librotade.hu

INDIA
Allied Publishers
1st Floor, Dubash House, 15, J.N. Heredi Marg, Ballard Estate, Mumbai 400001, INDIA
Telephone: +91 22 2261 7926/27 • Fax: +91 22 2261 7928
Email: alliedpl@vsnl.com • Web site: http://www.alliedpublishers.com

Bookwell
3/79 Nirankari, Delhi 110009, INDIA
Telephone: +91 11 2760 1283/4536
Email: bkwell@nde.vsnl.net.in • Web site: http://www.bookwellindia.com

ITALY
Libreria Scientifica "AEIOU"
Via Vincenzo Maria Coronelli 6, 20146 Milan, ITALY
Telephone: +39 02 48 95 45 52 • Fax: +39 02 48 95 45 48
Email: info@libreriaaeiou.eu • Web site: http://www.libreriaaeiou.eu

JAPAN
Maruzen Co., Ltd.
1-9-18 Kaigan, Minato-ku, Tokyo 105-0022, JAPAN
Telephone: +81 3 6367 6047 • Fax: +81 3 6367 6160
Email: journal@maruzen.co.jp • Web site: http://maruzen.co.jp

NETHERLANDS
Martinus Nijhoff International
Koraalrood 50, Postbus 1853, 2700 CZ Zoetermeer, NETHERLANDS
Telephone: +31 793 684 400 • Fax: +31 793 615 698
Email: info@nijhoff.nl • Web site: http://www.nijhoff.nl

Swets Information Services Ltd.
PO Box 26, 2300 AA Leiden
Dellaertweg 9b, 2316 WZ Leiden, NETHERLANDS
Telephone: +31 88 4679 387 • Fax: +31 88 4679 388
Email: tbeysens@nl.swets.com • Web site: http://www.swets.com

SLOVENIA
Cankarjeva Zalozba dd
Kopitarjeva 2, 1515 Ljubljana, SLOVENIA
Telephone: +386 1 432 31 44 • Fax: +386 1 230 14 35
Email: import.books@cankarjeva-z.si • Web site: http://www.mladinska.com/cankarjeva_zalozba

SPAIN
Diaz de Santos, S.A.
Librerias Bookshop • Departamento de pedidos
Calle Albasanz 2, esquina Hermanos Garcia Noblejas 21, 28037 Madrid, SPAIN
Telephone: +34 917 43 48 90 • Fax: +34 917 43 4023
Email: compras@diazdesantos.es • Web site: http://www.diazdesantos.es

UNITED KINGDOM
The Stationery Office Ltd. (TSO)
PO Box 29, Norwich, Norfolk, NR3 1PD, UNITED KINGDOM
Telephone: +44 870 600 5552
Email (orders): books.orders@tso.co.uk • (enquiries): book.enquiries@tso.co.uk • Web site: http://www.tso.co.uk

UNITED STATES OF AMERICA
Bernan Associates
4501 Forbes Blvd., Suite 200, Lanham, MD 20706-4391, USA
Telephone: +1 800 865 3457 • Fax: +1 800 865 3450
Email: orders@bernan.com • Web site: http://www.bernan.com

Renouf Publishing Co. Ltd.
812 Proctor Avenue, Ogdensburg, NY 13669, USA
Telephone: +1 888 551 7470 • Fax: +1 888 551 7471
Email: orders@renoufbooks.com • Web site: http://www.renoufbooks.com

United Nations
300 East 42nd Street, IN-919J, New York, NY 1001, USA
Telephone: +1 212 963 8302 • Fax: 1 212 963 3489
Email: publications@un.org • Web site: http://www.unp.un.org

Orders for both priced and unpriced publications may be addressed directly to:

IAEA Publishing Section, Marketing and Sales Unit, International Atomic Energy Agency
Vienna International Centre, PO Box 100, 1400 Vienna, Austria
Telephone: +43 1 2600 22529 or 22488 • Fax: +43 1 2600 29302
Email: sales.publications@iaea.org • Web site: http://www.iaea.org/books

14-01881

International Atomic Energy Agency
Vienna
ISBN 978–92–0–105415–9
ISSN 1011–4289